

A microscopic image showing a dense network of blue and orange fibers, likely representing tissue growth or repair processes. The fibers are intertwined and form a complex, fibrous structure. The blue fibers are more numerous and form a dense mesh, while the orange fibers are fewer and appear as thicker, more distinct strands.

Mario C. Benn

TISSUE GROWTH AND
REPAIR PROCESSES
STUDIED IN
3D MICROTISSUE
PLATFORMS

Diss. ETH No. 27206

ETH zürich

DISS. ETH NO. 27206

Tissue growth and repair processes studied in 3D microtissue platforms

A thesis submitted to attain the degree of
DOCTOR OF SCIENCES of ETH ZURICH
(Dr. sc. ETH Zurich)

presented by

Mario Christian Benn

Dr. med. vet., University of Zurich

born on 04.08.1985

citizen of Germany

accepted on the recommendation of
Prof. Dr. Dr. h.c. Viola Vogel, examiner
Prof. Dr. Philip Kollmannsberger, co-examiner
PD Dr. Gertraud Orend, co-examiner

2020

"If I have seen further it is by standing on the shoulders of giants."

Isaac Newton

Abstract

Tissue growth and repair are essential for multicellular life and delicately organized like a well-orchestrated symphony by spatio-temporally controlled cell proliferation and differentiation, which is tightly linked to the production and remodelling of extracellular matrix (ECM). This is particularly relevant during embryogenic development, postnatal growth and tissue regeneration after injury. During tissue growth and repair, little is known how ECM gradients are formed and remodelled. Once homeostasis is reached, maintaining steep gradients within tissues that are tightly associated with organ function is crucial as well. As 2D cell culture approaches do not resemble the biophysical characteristics of tissues, we developed a 3D μ Tissue platform that allows to investigate tissue growth and maturation, and how this is regulated by the tensional state, cell phenotypes and ECM composition at high spatiotemporal resolution in *de novo* grown μ Tissues. Tissue growth processes occur sequentially, while the initial growth front is formed by proliferative cells that assemble a highly stretched provisional fibronectin (Fn) matrix. As the tissue matures, the provisional Fn matrix is interlaced and partially replaced by much stronger tension bearing collagen fibers in the mature inner tissue core. We identified tenascin-C (TNC) in close proximity to Fn and myofibroblasts in the growth front and in regions undergoing repair after tissue rupture events had taken place. The high transient expression of TNC at the growing front was reduced over time as the tissue matured. Crucial other players required to induce the tissue maturation process include tissue transglutaminase (TG2), broad spectrum matrix metalloproteinases (MMP), transforming growth factor beta (TGF- β) signalling, as well as the Fn strain and Fn-collagen interactions. Understanding how ECM gradients regulate tissue growth and the transition of myofibroblasts into quiescent fibroblasts behind the growth front is crucial to develop novel treatment strategies for wound healing, fibrosis and cancer.

Next, we took advantage of our μ Tissue platform to tune key parameters, i.e. tissue tension as function of cleft angle, combined with the presence of supplemented pharmaceutical inhibitors, thus parameters which are technically challenging to be tuned independently in a living system. As expected, reducing cellular contractility through myosin II inhibition reduces tissue tension and thus increases the growth front curvature. Increased cellular contractility through TGF- β 1 supplementation resulted in increased tissue volume and narrowed growth front width in all different cleft angle geometries, which underlines the prominent role of cellular contractility as regulator of tissue growth and maturation processes. Furthermore, TGF- β 1 supplementation did not prevent the reverse myofibroblast-to-fibroblast transition as the tissues matured. Inhibition of fibronectin-collagen-interaction hampered the tissue maturation processes in tissues grown in narrower clefts and subject to higher tissue tension while reducing the mechanical stability as witnessed by an increased tissue rupture probability. Taken

together, we here show that tissue tension can be tuned in *de novo* μ Tissue grown in arrays of microengineered clefts, which opens the door to systematically study how tissue tension impacts tissue growth and maturation. Our data show that tissue tension together with cellular contractility are key parameters which regulate phenotype conversion. We found that cellular contractility is essential to build sufficient tissue tension, required to allow tissue growth and maturation. Tissue tension plays a prominent role in health and disease and our findings can contribute to develop new strategies for treatment of wounds by modulating for example tissue tension and subsequently tissue growth and maturation.

To gain deeper clinical insights, we used collagenous scaffolds that are in clinical use to promote tissue regeneration, and investigated *de novo* μ Tissue growth in commercially available materials, i.e. Geistlich Mucograft® versus Geistlich Bio-Gide® in a preliminary study. As it was unknown whether Fn plays a critical role in promoting tissue growth and healing in these biomaterial scaffolds *in vivo*, we used our established protocol for *de novo* grown μ Tissues in engineered clefts and applied it to manually cut clefts using Geistlich Mucograft® and Geistlich Bio-Gide®. We demonstrated that exposure of the scaffolds to a Fn-containing cell culture medium indeed promoted its adsorption to the scaffold fibers and promoted the early onset of Fn fibrillogenesis, which in turn is suggested to promote fibroblast ingrowth. Coupled with the proof that the *de novo* μ Tissue growth technology can be applied using different biomaterial scaffolds, our work sets the stage for an advanced analytical approach and will contribute to the development of novel diagnostic and therapeutic strategies in wound healing.

Taken together, tissue growth and repair are delicately organized and plenty of different actors are required, but each of their individual actions needs to be precisely initiated and tuned in time. Our findings enabled by 3D μ Tissue platforms on how time-dependent ECM gradients are established by the residing cells, and how this spatiotemporal gradient reciprocally drives a switch in cell phenotype, i.e. from the proliferative myofibroblasts back to the more quiescent fibroblasts, is not only exciting for basic biologists. Serving the need for platforms that are positioned between 2D cell culture and animal studies, they also provide valuable information for applied biomedical researchers who are developing and testing novel therapeutic strategies to promote wound healing, or to combat fibrosis and cancer. In particular, our new insights on how tissue tension together with TGF- β -upregulated cell contractility affects tissue growth processes can contribute to develop novel topical or generalized therapeutic strategies that modulate tissue tension and subsequently tissue growth and maturation in wounds. Combined with the transferability across different scaffolds materials, our platforms allow a plethora of follow up investigations.

This thesis demonstrates the significance of the reciprocal interactions between ECM and the residing cells, which acting together enable a fast build-up of a growth front, followed by a rapid switch towards tissue maturation and mechanical stabilization required to maintain tissue integrity. We expect the presented platforms of *de novo* μ Tissue growth find intriguing new applications for applied biomedical research.

Zusammenfassung

Gewebewachstum und -reparatur ist für ein multizelluläres Leben unerlässlich und ist durch Zellproliferation und durch die Produktion extrazellulärer Matrix (ECM) wie ein gut eingespieltes Symphonieorchester delikate aufeinander abgestimmt. Dies ist besonders während der Embryogenese, des postnatalen Wachstums und der Geweberegeneration nach Verletzungen von grosser Bedeutung. Es ist wenig darüber bekannt, wie ECM-Gradienten während Wachstums- und Reparaturprozessen in Geweben gebildet und aufgelöst werden. Sobald die Homöostase erreicht wird, ist die Aufrechterhaltung steiler Gradienten innerhalb von Geweben, die eng mit Organfunktionen verbunden sind, ebenfalls von entscheidender Bedeutung. Da 2D-Zellkulturansätze den biophysikalischen Eigenschaften von Geweben nicht ähneln, haben wir eine Mikrogewebeplattform entwickelt, die es ermöglicht, die Gewebereifung, die Spannungszustände, den Zellphänotyp und die ECM-Zusammensetzung mit hoher raumzeitlicher Auflösung in *de novo* gezüchteten 3D Geweben zu untersuchen. Der Gewebewachstumsprozess verläuft hier sequentiell: Die anfängliche Wachstumsfront wird zunächst von proliferativen Zellen gebildet, die eine Matrix aus gestrecktem Fibronectin (Fn) aufbauen. Anschliessend wird während der Reifung des Gewebes die provisorische Fn-Matrix ineinander verwoben und teilweise durch viel stärkere und tragfähigere Kollagenfasern im inneren, reifen Kern des Gewebes ersetzt. Wir haben Tenascin-C (TNC) in unmittelbarer Nähe von Fn und Myofibroblasten in der Wachstumszone und in Regionen, die nach Geweberissen repariert werden, identifiziert. Die hohe transiente Expression von TNC an der Wachstumsfront wurde im Laufe der Zeit mit zunehmender Reifung des Gewebes reduziert. Zu den entscheidenden anderen Akteuren, die erforderlich sind, um den Reifungsprozess von Geweben zu induzieren, gehören die Gewebetransglutaminase (TG2), ein breites Spektrum an Matrix-Metalloproteinasen (MMP), der transformierende Wachstumsfaktor beta (TGF- β) Signalweg sowie der Fn-Streckungszustand und die Fn-Kollagen-Interaktionen. Das Verständnis darüber, wie ECM-Gradienten das Gewebewachstum und den Übergang von Myofibroblasten in ruhende Fibroblasten hinter der Wachstumsfront regulieren, ist entscheidend für die Entwicklung neuer Behandlungsstrategien bei Wundheilung, Fibrose und Krebs.

Zudem haben wir unsere Mikrogewebeplattformen genutzt, um den Einfluss von einzelnen Schlüsselparametern zu untersuchen. Im Fokus liegt vor allem die Gewebespannung als Funktion des Winkels der Spaltöffnung, in dem die Gewebe wachsen, kombiniert mit dem Einfluss ergänzender pharmazeutischer Inhibitoren, also Parameter, deren unabhängige Justierung in einem lebenden System technisch anspruchsvoll ist. Wie erwartet, verringert die Reduzierung der zellulären Kontraktilität durch die Myosin-II-Inhibition die Gewebespannung und erhöht somit die Krümmung der Wachstumsfront. Eine Steigerung der zellulären Kontraktilität durch die Supplementation mit TGF- β 1

fürte zu einem erhöhten Gewebevolumen und einer verringerten Breite der Wachstumsfront in allen verschiedenen Spaltwinkelgeometrien, was die herausragende Rolle der Zellkontraktilität für Wachstum und Reifung der Gewebe unterstreicht. Darüber hinaus wurde die Myofibroblasten-zu-Fibroblasten-Rückbildung während der Gewebereifung durch die TGF- β 1-Supplementierung nicht verhindert. Die Hemmung der Fn-Kollagen-Interaktion führte zu einer verminderten Reifung der Gewebe, die in engeren Spalten wachsen und einer höheren Gewebespannung ausgesetzt sind, während sich eine Verringerung der mechanischen Stabilität in einer erhöhten Wahrscheinlichkeit von Geweberissen niederschlug. Zusammenfassend konnten wir zeigen, dass die Gewebespannung von *de novo* gezüchteten Geweben mit mikrotechnologisch hergestellten Spaltgeometrien angepasst werden kann, was die Grundlage für weiterführende systematische Untersuchungen über das Wachstum und die Reifung von Geweben bildet. Unsere Daten zeigen, dass die Gewebespannung zusammen mit der zellulären Kontraktilität die wesentlichen Parameter sind, die die Umwandlung des Phänotyps mit der anschließenden Gewebereifung und -wachstum regulieren, ohne dass es Hinweise auf eine Beeinflussung der Sequenz gibt, in der die raumzeitliche Hochregulation von TNC und TG2 den ECM-Umbau und die Myofibroblasten-zu-Fibroblasten-Rückbildung arrangiert.

Um tiefere klinische Einblicke zu gewinnen, verwendeten wir kollagene Gerüste, die zur Förderung der Geweberegeneration im klinischen Einsatz sind, und untersuchten in einer Vorstudie *de novo* gezüchtetes Mikrogewebe in kommerziell erhältlichen Materialien, in diesem Fall Geistlich Mucograft® versus Geistlich Bio-Gide®. Da nicht bekannt war, ob Fn eine entscheidende Rolle bei der Förderung des Gewebewachstums und der Heilung in diesen Biomaterial-Gerüsten *in vivo* spielt, haben wir unser etabliertes Protokoll für *de novo* gezüchtete Mikrogewebe in mikrotechnisch hergestellten Spalten genutzt und es auf manuell geschnittene Spalte in Geistlich Mucograft® und Geistlich Bio-Gide® angewendet. Wir konnten zeigen, dass die Exposition der Gerüste mit einem Fn-haltigen Zellkulturmedium tatsächlich deren Adsorption an die Gerüstfasern fördert und den frühen Beginn der Fn-Fibrillogenese begünstigt, was wiederum das Einwachsen der Fibroblasten fördern soll. In Verbindung mit dem Nachweis, dass die Technologie *de novo* gezüchteter Mikrogewebe in verschiedenen Gerüsten aus Biomaterialien angewendet werden kann, schafft unsere Arbeit die Voraussetzung für einen zukunftsweisenden analytischen Ansatz und wird zur Entwicklung neuer diagnostischer und therapeutischer Strategien zur Förderung der Wundheilung beitragen.

Zusammengenommen sind Gewebewachstum und -reparatur äusserst delikat organisiert, weil viele verschiedene Akteure notwendig sind und deren individuellen Aktionen präzise initiiert sowie zeitlich genau aufeinander abgestimmt werden müssen. Unsere durch 3D-Gewebeplattformen ermöglichten

Erkenntnisse darüber, wie zeitabhängige ECM-Gradienten von adhärennten Zellen etabliert werden und wie dieser raumzeitliche Gradient einen reziproken Wechsel des Zellphänotyps antreibt, also von den proliferativen Myofibroblasten zurück zu den eher ruhenden Fibroblasten, sind nicht nur für Grundlagenbiologen von Interesse. Indem sie dem Bedarf an Plattformen zwischen 2D-Zellkulturen und Tierversuchen nachkommen, liefern sie auch wertvolle Informationen für angewandte biomedizinische Forscher, die neue therapeutische Strategien zur Förderung der Wundheilung oder zur Bekämpfung von Fibrose und Krebs entwickeln und erproben. Insbesondere unsere neuen Erkenntnisse darüber, wie die Gewebespannung zusammen mit der TGF- β -hochregulierten Zellkontraktilität die Gewebewachstumsprozesse beeinflusst, können dazu beitragen, neue topische oder generalisierte therapeutische Strategien zu entwickeln, die die Gewebespannung und in der Folge das Wachstum und die Reifung von Gewebe in Wunden modulieren. Dank der Übertragbarkeit auf verschiedene Gerüstmaterialien ermöglichen unsere Plattformen eine Fülle von Folgeuntersuchungen.

Diese Arbeit zeigt die Bedeutung der reziproken Interaktion zwischen der ECM und den eingebetteten adhärennten Zellen. Dieses Zusammenwirken ermöglicht den schnellen Aufbau einer Wachstumsfront, bevor der zeitlich eng getaktete Übergang zur Gewebereifung und mechanischen Stabilisierung erfolgt, was zur Aufrechterhaltung der Gewebeintegrität essentiell ist. Wir erwarten, dass die vorgestellten Plattformen des *de novo* gezüchteten Mikrogewebes faszinierende neue Anwendungen in der biomedizinischen Forschung erschliessen werden.

Contents

Abstract	v
Zusammenfassung	viii
Contents	xi
1 Scope of the thesis	1
1.1 Motivation	1
1.2 Aims and approaches	3
1.2.1 Tissue transglutaminase in fibrosis – more than an extracellular matrix cross-linker (Chapter 3)	4
1.2.2 Tenascin-C and tissue transglutaminase transiently orchestrate tissue growth enabling the transition towards tension-dependent tissue maturation (Chapter 4)	5
1.2.3 Eliciting insights how tissue tension impacts tissue growth processes (Chapter 5).....	6
1.2.4 Preliminary study: Integration of fibroblast <i>de novo</i> μ Tissue growth in Geistlich Mucograft® and Geistlich Bio-Gide® (Chapter 6)	7
1.3 References	9
2 Introduction	13
2.1 Tissue growth requires more than diffusion of soluble factors: ECM gradients are typically neglected in current <i>in vitro</i> platforms.....	13
2.2 <i>de novo</i> μ Tissue platform mimics sequential tissue growth process	14
2.3 Relevant actors in extracellular matrix (ECM) mechanobiology.....	16
2.3.1 ECM in health and disease	16
2.3.2 Myofibroblast and transforming growth factor beta (TGF- β)	17
2.3.3 Tenascin-C (TNC)	17
2.3.3.1 Time relevant aspects of TNC for ECM gradients	18
2.3.4 Tissue transglutaminase (TG2)	18
2.3.5 Significance of TG2 and TNC interplay	20
2.4 References	22
3 Tissue transglutaminase in fibrosis – more than an extracellular matrix cross-linker.....	33
3.1 Abstract	34
3.2 Introduction	34
3.3 TG2 is upregulated in the pathogenesis of a wide variety of chronic diseases.....	35
3.4 Environmental sensing through major conformational TG2 changes	36
3.5 Extra- and intracellular: Transamidation and cross-linking functions of TG2 / TGF- β 1 storage in the ECM	37
3.6 Cell membrane: TG2 regulates cell adhesion and ligand affinity.....	39
3.7 Cell membrane: TG2 as signalling protein	41
3.8 Inside the cell: Enzymatic and non-enzymatic TG2 activity	41
3.9 TG2 as major player in the development and maintenance of fibroproliferative diseases	42
3.10 Outlook: TG2 as common denominator in fibroproliferative and neoplastic diseases	43
3.11 Acknowledgements.....	43

3.12	Declarations of interest	43
3.13	References	44
4	Tenascin-C and tissue transglutaminase transiently orchestrate tissue growth enabling the transition towards tension-dependent tissue maturation	49
4.1	Abstract	50
4.2	Introduction	50
4.3	Results	54
4.4	Discussion	67
4.5	Materials and methods.....	74
4.6	Acknowledgements.....	80
4.7	References	81
5	Eliciting insights how tissue tension impacts tissue growth processes.....	91
5.1	Abstract	92
5.2	Introduction	93
5.3	Results	96
5.4	Discussion	115
5.5	Materials and methods.....	121
5.6	Acknowledgements.....	125
5.7	References	126
6	Preliminary study: Integration of <i>de novo</i> μ Tissue growth in Geistlich Mucograft® and Geistlich Bio-Gide®	131
6.1	Introduction	132
6.2	Results and discussion	132
6.2.1	Identified a technical solution to handle the fragile samples	132
6.2.2	Growth rate of <i>de novo</i> grown μ Tissues <i>in vitro</i>	133
6.2.3	Development of a biomimetic approach to promote the ingrowth of fibroblasts	134
6.2.4	Enhancing the integration of the scaffold material with the <i>de novo</i> grown μ Tissue	135
6.2.5	Can the probability of scaring be predicted?	136
6.2.6	Material shrinkage and healing capacity.....	138
6.3	Mechanobiology of wound repair: personalized wound healing.....	139
6.4	References	141
7	Significance and Outlook.....	143
8	Supplementary information	149
8.1	Supplementary Figures Chapter 4.....	150
8.2	Supplementary Figures Chapter 5.....	161
	Abbreviations	180
	Acknowledgements.....	181
	Curriculum Vitae.....	185

1 Scope of the thesis

1.1 Motivation

“That great Frenchman [Marie François Xavier Bichat, 1771 - 1802] first carried out the conception that living bodies, fundamentally considered, are not associations of organs which can be understood by studying them first apart, and then as it were federally; but must be regarded as consisting of certain primary webs or tissues, out of which the various organs -brain, heart, lungs, and so on - are compacted, as the various accommodations of a house are built up in various proportions of wood, iron, stone, brick, zinc, and the rest, each material having its peculiar composition and proportions. No man, one sees, can understand and estimate the entire structure or its parts--what are its frailties and what its repairs, without knowing the nature of the materials.”

from Middlemarch by Goerge Eliot, 1874

Tissue growth is essential for complex, multicellular life to emerge. Tissue expansion by cell proliferation and through production of extracellular matrix (ECM) occurs not only during embryogenic development, but also during post-natal growth, during tissue homeostasis and in tissue regeneration after injury. Tissues form a functional unit consisting of multiple similar cells embedded in ECM, while the dense ECM fiber network mediates both structural and signalling roles. Although the first reports of ECM date back more than 150 years [1], only the recent emergence of the field of mechanobiology allowed us to understand that ECM conveys much more to cells than simple passive structural support functions: mechanobiology describes how mechanical forces act on cells and are translated into biochemical signals (Mechanotransduction) that subsequently regulate cellular functions, and vice versa, cells stretch ECM fibers and remodel them [2]. It was shown that besides anchoring, guiding and confining of cells, the physical properties of ECM (e.g. topography, pore size, fiber size, fiber orientation, bulk- and fiber stiffness, ligand density, adhesion and cross-linking density) can regulate the cell responses [3,4]. These parameters subsequently tune tissue growth and maturation processes as well as the remodelling of tissues both in healthy and diseased conditions. Clinical and pathological investigations elucidated that ECM composition and architecture vary significantly between healthy and diseased organs [5-7]. Given the multifactorial regulation and crosstalk at the tissue level, it remains until today a great challenge to explore the reciprocity, how cells assemble and maintain a “healthy” ECM under homeostasis, and vice versa, how ECM impacts the residing cells.

The most abundant connective tissue cell type are fibroblasts, which assemble the first provisional fibronectin (Fn) matrix during growth. Over time, the provisional Fn matrix is partially replaced by fibers made from collagens and other ECM components in a process called tissue maturation. However, fundamental understanding how spatiotemporal ECM gradients are formed in health and disease is missing.

Exposure of primary fibroblasts to a combination of growth factors (most notably TGF- β) and ECM components (e.g. Fn ED-A) expressed in the wound bed and altered mechanical properties of the environment (notably tissue stress, stiffness) drives the formation of myofibroblasts. Under healthy conditions, myofibroblasts disappear from the wound site by de-differentiation into quiescent fibroblasts or by undergoing apoptosis [8]. Failed phenotype reversion and prolonged myofibroblast activity at wound sites is associated with scar tissue formation [9] since myofibroblasts incorporate an excess of collagen in the ECM and contract the fibrotic matrix into a stiff, dysfunctional tissue [9-12]. Pathological stiffening of the microenvironment further enhances myofibroblast activation and therefore leads to a vicious circle of fibrosis which ultimately results in organ dysfunction [13,14]. A better understanding of the mechanisms driving phenotype reversal is not only of fundamental interest in the biosciences, but also crucial for the development of novel therapeutical strategies. Engineered materials, micro- and nanoenvironments, as well as platform arrays, are needed to elucidate reciprocal interdependencies of cell phenotype stabilization and the surrounding ECM, and to quantify such interactions *in vitro*.

Fibroproliferative disorders cause approximately 45% of the mortality in the developed world and appear in a wide spectrum from systemic to organ-specific fibrotic diseases and myofibroblasts are the key effector cells [15-19]. Myofibroblasts that occur in the vicinity of tumor cells are called cancer-associated fibroblasts and are considered to be key drivers in tumorigenesis, angiogenesis and cancer progression via paracrine signalling and modulation of the ECM. It is therefore not surprising that close similarities between fibrotic tissue and tumor stroma were identified [19-22]. Thus, the reciprocal crosstalk between cells and their ECM, which they produce and remodel, has major implications on such wide fields of maintaining health or driving diseases. Here a better understanding might have great impact on the development of new diagnostic and therapeutic strategies. This suggests that the identification of key common ECM-dependent pathways involved in the disease pathogenesis and progression can lead to the identification of novel therapeutic targets and the development of new drugs and diagnostic methods. However, it remains not fully

understood how the time-dependent processes during ECM assembly and maturation are influencing the stabilization or clearance of myofibroblasts.

Technical advances in life science research over the last decades allowed critical and insightful studies at tissue level of organs or complete organisms. But it remains difficult to investigate the complex process of sequential tissue assembly and processing that substantially hampers our understanding of wound healing, development, fibrosis and cancer. In all these areas, extracellular matrix (ECM) gradients are relevant but in contrast to soluble gradients [23-28], fundamental understanding of how they are formed and regulate tissue development and repair is missing. In the past, most of the *in vitro* experiments were conducted in 2D cell culture. Through the recent emergence of microtissue platforms designed for *in vitro* research, it was recognized, that cellular behaviour, adhesion dynamics and matrix assembly show major differences in a 2D compared to 3D environments [29-33]. However, *in vitro* test systems are needed which mimic essential aspects of living tissues and carry a sufficient degree of inter-species transferability. This will be indispensable in order to not only follow the 3R-concept [34] (replace, reduce and refine) to enable a much more responsible use of animal experiments in the future, but further to promote the translation to novel clinical strategies. Most of the current *in vitro* systems address the third dimension, but often biomaterial scaffolds are used which do not resemble well the complexity of living ECM and, thus, fall short at the cell-scaffold and ECM-scaffold interface. While organoids have been powerful especially in combination with high-throughput 2D drug development pipelines, they have their limitations too due to significant organoid-to-organoid variabilities [35].

In this thesis, multiparameter models of *de novo* tissue growth are further developed in which spatiotemporal gradients of tissue maturation, tensional states, cell population and ECM composition can be investigated using *de novo* grown tissues. Deepening a mechanistic understanding of how ECM mechanobiology in concert with geometrical factors regulate the transition of a myofibroblast phenotype into quiescent fibroblasts is crucial to develop novel treatment strategies for wound healing, fibrosis and cancer.

1.2 Aims and approaches

This thesis is guided by the overall hypothesis that the rapid turn-over of steep spatiotemporal ECM gradients is required for tissue growth and maturation processes and enables a cell phenotype conversion. To address this hypothesis, the *de novo* tissues were either grown in microfabricated

substrates (**Chapter 4** and **5**) or commercial scaffolds (**Chapter 6**). With our study we aimed to identify factors that enable that transient ECM gradients are formed and how such gradients influence the stabilization or clearance of myofibroblast phenotype. Deepening our knowledge is highly significant as the reversal of the fibroblast-to-myofibroblast during tissue repair, and then back to fibroblasts, is the essential hallmark of reaching a pro-healing homeostasis.

To allow investigations of ECM gradients formation processes, the following tools were developed or used:

- microfabricated PDMS microtissue (μ Tissue) platform with fixed (**Chapter 4**) and altered (**Chapter 5**) geometries to tune the speed by which *de novo* tissues were grown
- phase-contrast image acquisition to document live tissue growth
- confocal and 2-photon laser scanning microscope to acquire fluorophore signals of labelled target proteins and second harmonic generation to visualize mature bundles of collagen fibers
- advanced image analysis to visualize ECM and phenotype gradients and extract relevant quantitative data

1.2.1 Tissue transglutaminase in fibrosis – more than an extracellular matrix cross-linker (**Chapter 3**)

Tissue transglutaminase (TG2) is best known for its Ca^{2+} dependent cross-linking functionality and is involved in the pathogenesis of a wide variety of diseases, most notably neoplastic and fibrotic diseases [36,37] and was suggested as treatment target [38,39].

The aim of this chapter is to review the recent literature around the versatile TG2 enzymatic and non-enzymatic functions in fibrosis and beyond. This provides the reader a detailed background to understand the extremely versatile functions of TG2. Over the time-course of this thesis our findings revealed, that enzymatic TG2 cross-linking activity is required to allow tissue maturation (see **Chapter 4**).

The review presented in **Chapter 3** is published in Current Opinion in Biomedical Engineering, Elsevier; 2019 Jun;10:156–64.

Mario C. Benn, Willi Weber, Enrico Klotzsch, Viola Vogel, Simon A. Pot. (2019) Tissue transglutaminase in fibrosis – more than an extracellular matrix cross-linker

1.2.2 Tenascin-C and tissue transglutaminase transiently orchestrate tissue growth enabling the transition towards tension-dependent tissue maturation (Chapter 4)

Wound “repair is a race against the clock” and indicates strikingly that tissue growth speed is essential for its function [40]. The purpose of tissue growth is the fast formation of tissue. To achieve this, highly dynamic and interlocking iterative processes of cellular proliferation and ECM assembly, maturation and mechanical stabilization need to be orchestrated in a timely manner. Thus, the rapid emergence of the more contractile myofibroblasts from fibroblasts, as well as of ECM gradients are of eminent importance in tissue growth processes such as in development or wound healing. However, it remains unclear how these ECM gradients are built and stabilized in a timely manner and appropriate simplified *in vitro* 3D test platforms are needed.

To address this unmet need, we developed a microfabricated PDMS platform with millimetersized clefts in which fibroblasts formed *de novo* grown μ Tissues over time. Its uniqueness is that tissue is grown in the corner of clefts, which allows to visualize along the cleft how provisional Fn ECM in the growth front is remodelled towards the cleft corner into a mechanically stabilized collagen-rich matrix as the tissue matures [41]. We thereby paid particular attention to the spatiotemporal expression, assembly and degradation of other ECM constituents such as Tenascin-C (TNC) and TG2. TNC is a matricellular glycoprotein, best known for its antiadhesive function in Fn matrices [42-47]. Both TG2 and TNC provide extremely versatile function of which many are not fully understood and both are known to be quickly upregulated in regions of mechanical stress, injury or ECM remodelling [46,48,49].

With this work described in **Chapter 4**, we aimed to answer the following questions:

1. Once a growth front has formed, what transient roles do TNC and TG2 play to initiate the onset of tissue maturation?
2. How do the spatio-temporal changes in the ECM composition contribute to the transition and stabilization of cell phenotype gradients?

We identified myofibroblasts in the Fn-rich provisional ECM of the growth front, which was enriched in TNC, as well as in regions where the tissue had spontaneously ruptured and was undergoing repair processes. Behind the growth front, the onset of the tissue maturation process is associated with a sharp transition zone of cell phenotype and ECM composition, resulting in a steep spatial gradient in between the Fn rich growth front and the collagen-rich maturing tissue. We further show a transient and spatio-temporal upregulation of TNC in the growth front, as well

as of TG2, which both disappear from the ECM in regions where second harmonic generation (SHG) positive bundles of collagen indicate tissue maturation. To further investigate the respective roles of these ECM components in orchestrating proper tissue maturation, we either supplemented the medium with TGF- β receptor inhibitor, or used broad-spectrum pharmaceutical matrix metalloproteinase activity inhibitors. We further elucidated the mechanobiological roles of Fn fiber tension, and the importance of Fn-collagen binding to initiate tissue maturation. Our data suggests a tightly timed functional complementarity between the actions of TNC and TG2 enabling the transition from the provisional to a maturing tissue never described before, where TNC conveys early ECM stabilization and is cleared over time when enzymatic cross-linking via TG2 is active. The time-dependent development of maturation gradients within the extracellular matrix (ECM) to gradually form mechanically stable tissue is of outstanding importance and enables much deeper insights into tissue growth and repair processes.

1.2.3 Eliciting insights how tissue tension impacts tissue growth processes (Chapter 5)

Mechanical signalling plays such a prominent role in health and disease [4,50-53], that many novel therapeutical approaches in the emerging field of mechanomedicine are proposed [39] and tissue tension is highly relevant especially for the treatment of skin wounds [54]. Previous work using osteoblasts showed that tissue growth depends on curvature [55] and that contractility mediates the effect of geometry on tissue growth [56-58], by using different scaffold geometries and controlled curvature. Furthermore, it was reported that increased tissue tension causes increased growth front curvature which drives tissue growth towards the open cleft [55-58]. In fibroblast tissues, a reversible fibroblast-to-myofibroblast transition with a gradient of upregulated myofibroblast characteristics of proliferation, α SMA contractility and more stretched Fn at the growth front was found to be the biological mechanism behind curvature-driven growth and is sensed by YAP-dependent mechanotransduction steering the cell phenotype [41]. The emergence of these gradients depends on TNC and TG2, which orchestrate the balance of tissue growth and tissue maturation (**Chapter 4**). The detailed mechanobiological characterization of spatiotemporal gradients was first done here for a fixed angle.

To elucidate how tissue tension overall affects tissue assembly processes, we next advanced our microfabricated PDMS platform and integrated an array of different cleft angle that allowed us to tune the growth curvature and thus tissue tension of the fibroblast *de novo* grown μ Tissues. While there is a full body of literature how tensional homeostasis is understood across length scales [59], it remains completely elusive, how tissue tension affects tissue growth and tissue maturation

processes. In our model, tissue tension can be modified via cleft angle and cell contractility. Pharmaceutical inhibitors and TGF- β 1 were used to modulating cellular contractility. Furthermore, in fixed angles we showed, that undisturbed Fn-collagen interaction is required for tissue maturation and to prevent tissue ruptures.

With this work described in **Chapter 5**, we aimed to answer the following questions:

1. How does tissue tension influence the time-dependent formation of ECM gradients and subsequently, tissue growth and maturation?
2. Upon partial inhibition of Fn-collagen interactions, how does tissue tension tune the resulting effects of hampered tissue maturation versus tissue ruptures?

By altering cleft geometries, we provide a novel μ Tissue platform allowing to tune tissue tension, tissue growth and growth front curvature. We found that sufficient tissue tension is required to allow tissue growth and maturation, whereby cellular contractility is essential. Our knowledge can contribute to the development of novel topical and generalized therapeutic strategies to modulate for example tissue tension and subsequently tissue growth and maturation in wounds.

1.2.4 Preliminary study: Integration of fibroblast *de novo* μ Tissue growth in Geistlich Mucograft® and Geistlich Bio-Gide® (Chapter 6)

In this preliminary study we used collagenous scaffolds in clinical use for tissue regeneration and investigated *de novo* μ Tissue growth in commercially available collagen scaffold materials from Geistlich Pharma AG, Wolhusen, Switzerland in collaboration with Dr. Birgit Schäfer. Tissue growth was compared in Geistlich Mucograft® and Geistlich Bio-Gide®. Both are 3D non-crosslinked collagen matrices of porcine origin of different architecture and were developed to serve as a matrix scaffold and guide tissue regeneration in surgery. However, it remains unknown how initial Fn matrix integrates into the scaffolds during first phases of tissue growth.

To address this, our established protocol for *de novo* grown μ Tissues in engineered clefts was applied by manually cut cleft using Geistlich Mucograft® and Geistlich Bio-Gide® and developing a custom built PDMS scaffold mount.

With this work in **Chapter 6**, we aimed to answer the following questions:

1. Does Fibronectin play a major role in initiating the healing process within the biomaterial scaffolds?
2. How do different scaffold materials support μ Tissue growth processes?

We found that our *in vitro* data regarding the tissue growth rate using different commercial materials provided by the Geistlich Pharma AG, Wolhusen, Switzerland reflected the differential observations made by them in the clinical practise. We further found that the preadsorption of Fn to the scaffold materials promoted Fn fibrillogenesis and tissue growth in both Geistlich Mucograft® and Geistlich Bio-Gide®, which represents a fundamentally new insight. Coupled with the proof that *de novo* grown μ Tissue can be grown not just in our engineered platforms, but also in other surgically relevant biomaterial scaffolds sets the stage for the development of novel diagnostic and therapeutic strategies in wound healing.

1.3 References

1. Piez KA. History of extracellular matrix: A personal view. *Matrix Biol*; 1997 Aug 1;16(3):85–92.
2. Schoen I, Pruitt BL, Vogel V. The Yin-Yang of Rigidity Sensing: How Forces and Mechanical Properties Regulate the Cellular Response to Materials. *Annu Rev*; 2013 Jul 5;43(1):589–618.
3. Hynes RO. The Extracellular Matrix: Not Just Pretty Fibrils. *Science*; 2009 Nov 27;326(5957):1216–9.
4. Vogel V. Unraveling the Mechanobiology of Extracellular Matrix. *Annu Rev*; 2018 Feb 12;80(1):353–87.
5. Provenzano PP, Inman DR, Eliceiri KW, Knittel JG, Yan L, Rueden CT, White JG, Keely PJ. Collagen density promotes mammary tumor initiation and progression. *BMC Med*; 2008;6(1):11.
6. Yu H, Mouw JK, Weaver VM. Forcing form and function: biomechanical regulation of tumor evolution. *Trends Cell Biol*; 2011 Jan;21(1):47–56.
7. Frantz C, Stewart KM, Weaver VM. The extracellular matrix at a glance. *J Cell Sci*; 2010 Dec 15;123(24):4195–200.
8. Van De Water L, Varney S, Tomasek JJ. Mechanoregulation of the Myofibroblast in Wound Contraction, Scarring, and Fibrosis: Opportunities for New Therapeutic Intervention. *Adv Wound Care*; 2013 May;2(4):122–41.
9. Pakshir P, Hinz B. The big five in fibrosis: Macrophages, myofibroblasts, matrix, mechanics, and miscommunication. *Matrix Biol*; 2018 Aug 1;68-69:81–93.
10. Hinz B. Matrix mechanics and regulation of the fibroblast phenotype. *J Periodontol*; 2013 Aug 11;63(1):14–28.
11. Bochaton-Piallat M-L, Gabbiani G, Hinz B. The myofibroblast in wound healing and fibrosis: answered and unanswered questions. *F1000Res*; 2016;5:752.
12. Pakshir P, Noskovicova N, Lodyga M, Son DO, Schuster R, Goodwin A, Karvonen H, Hinz B. The myofibroblast at a glance. *J Cell Sci*; 2020 Jul 10;133(13):jcs227900.
13. Cordero-Espinoza L, Huch M. The balancing act of the liver: tissue regeneration versus fibrosis. *J Clin Invest*; 2018 Jan 2;128(1):85–96.
14. Weiskirchen R, Weiskirchen S, Tacke F. Organ and tissue fibrosis: Molecular signals, cellular mechanisms and translational implications. *Mol Asp Med*; 2019 Feb;65:2–15.
15. Wynn TA. Cellular and molecular mechanisms of fibrosis. *J Pathol*; 2008 Jan;214(2):199–210.
16. Wynn TA, Ramalingam TR. Mechanisms of fibrosis: therapeutic translation for fibrotic disease. *Nat Med*; 2012 Jul 6;18(7):1028–40.
17. Piera-Velazquez S, Mendoza FA, Jimenez SA. Endothelial to Mesenchymal Transition (EndoMT) in the Pathogenesis of Human Fibrotic Diseases. *J Clin Med*; 2016 Apr 11;5(4):45.
18. Urban ML, Manenti L, Vaglio A. Fibrosis--A Common Pathway to Organ Injury and Failure. *N Engl J Med*; 2015 Jul 2;373(1):95–6.
19. Piersma B, Hayward MK, Weaver VM. Fibrosis and cancer: A strained relationship. *Biochim Biophys Acta Rev Cancer*; 2020 Apr 1;1873(2):188356.
20. Rybinski B, Franco-Barraza J, Cukierman E. The wound healing, chronic fibrosis, and cancer

- progression triad. *Physiol Genomics*; 2014 Apr 1;46(7):223–44.
21. Cox TR, Erler JT. Molecular Pathways: Connecting Fibrosis and Solid Tumor Metastasis. *Clin Cancer Res*; 2014 Jul 14;20(14):3637–43.
 22. Foster DS, Jones RE, Ransom RC, Longaker MT, Norton JA. The evolving relationship of wound healing and tumor stroma. *JCI Insight*; 2018 Sep 20;3(18):696.
 23. Ishida-Ishihara S, Akiyama M, Furusawa K, Naguro I, Ryuno H, Sushida T, Ishihara S, Haga H. Osmotic gradients induce stable dome morphogenesis on extracellular matrix. *J Cell Sci*; 2020 Jul 15;133(14):jcs243865.
 24. Shimizu A, Goh WH, Itai S, Karyappa R, Hashimoto M, Onoe H. ECM-based microfluidic gradient generator for tunable surface environment by interstitial flow. *Biomicrofluidics*; 2020 Jul;14(4):044106.
 25. Wang Y, He G, Wang F, Zhang C, Ge Z, Zheng X, Deng H, Yuan C, Zhou B, Tao X, Zhang J, Tang K. Aspirin inhibits adipogenesis of tendon stem cells and lipids accumulation in rat injury tendon through regulating PTEN/PI3K/AKT signalling. *J Cell Mol Med*; 2019 Nov 1;23(11):7535–44.
 26. Hubka KM, Carson DD, Harrington DA, Farach-Carson MC. Perlecan domain I gradients establish stable biomimetic heparin binding growth factor gradients for cell migration in hydrogels. *Acta Biomater*; 2019 Oct;97:385–98.
 27. Thotakura S, Basova L, Makarenkova HP. FGF Gradient Controls Boundary Position Between Proliferating and Differentiating Cells and Regulates Lacrimal Gland Growth Dynamics. *Front Genet*; 2019 May 28;10:543.
 28. Wu W, Tholozan FM, Goldberg MW, Bowen L, Wu J, Quinlan RA. A gradient of matrix-bound FGF-2 and perlecan is available to lens epithelial cells. *Exp Eye Res*; 2014 Mar 1;120:10–4.
 29. Doyle AD, Yamada KM. Mechanosensing via cell-matrix adhesions in 3D microenvironments. *Exp Cell Res*; 2016 Apr 10;343(1):60–6.
 30. Doyle AD, Carvajal N, Jin A, Matsumoto K, Yamada KM. Local 3D matrix microenvironment regulates cell migration through spatiotemporal dynamics of contractility-dependent adhesions. *Nat Commun*; 2015;6(1):8720.
 31. Hynes RO. Stretching the boundaries of extracellular matrix research. *Nat Rev Mol Cell Biol*; 2014 Dec;15(12):761–3.
 32. Amatangelo MD, Bassi DE, Klein-Szanto AJP, Cukierman E. Stroma-Derived Three-Dimensional Matrices Are Necessary and Sufficient to Promote Desmoplastic Differentiation of Normal Fibroblasts. *Am J Pathol*. Elsevier; 2005 Aug 1;167(2):475–88.
 33. Yamada KM, Cukierman E. Modeling tissue morphogenesis and cancer in 3D. *Cell*; 2007 Aug 24;130(4):601–10.
 34. Prescott MJ, Lidster K. Improving quality of science through better animal welfare: the NC3Rs strategy. *Lab Anim*; 2017 Mar 22;46(4):152–6.
 35. Kim J, Koo B-K, Knoblich JA. Human organoids: model systems for human biology and medicine. *Nat Rev Mol Cell Biol*; 2020 Oct 1;21(10):571–84.
 36. Katt WP, Antonyak MA, Cerione RA. Opening up about Tissue Transglutaminase: When Conformation Matters More than Enzymatic Activity. *Med one*; 2018;3(6).
 37. Nyström A, Bruckner-Tuderman L. Injury- and inflammation-driven skin fibrosis: The paradigm of

- epidermolysis bullosa. *Matrix Biol*; 2018 Aug;68-69:547–60.
38. S K, SC O, BW M, DH L. Transglutaminase 2 Regulates Self-renewal and Stem Cell Marker of Human Colorectal Cancer Stem Cells. *Anticancer Res*; 2018 Feb 1;38(2):787–94.
 39. Tschumperlin DJ, Lagares D. Mechano-therapeutics: Targeting Mechanical Signaling in Fibrosis and Tumor Stroma. *Pharmacol Ther*; 2020 Aug;212:107575.
 40. Midwood KS, Williams LV, Schwarzbauer JE. Tissue repair and the dynamics of the extracellular matrix. *Int J Biochem Cell Biol*; 2004 Jun;36(6):1031–7.
 41. Kollmannsberger P, Bidan CM, Dunlop JWC, Fratzl P, Vogel V. Tensile forces drive a reversible fibroblast-to-myofibroblast transition during tissue growth in engineered clefts. *Sci Adv*; 2018 Jan 1;4(1):eaao4881.
 42. Lightner VA, Erickson HP. Binding of hexabrachion (tenascin) to the extracellular matrix and substratum and its effect on cell adhesion. *J Cell Sci*; 1990 Feb;95 (Pt 2)(2):263–77.
 43. Chiquet-Ehrismann R. Anti-adhesive molecules of the extracellular matrix. *Curr Opin Cell Biol*; 1991 Oct 1;3(5):800–4.
 44. Prieto AL, Andersson-Fisone C, Crossin KL. Characterization of multiple adhesive and counteradhesive domains in the extracellular matrix protein cytotactin. *J Cell Biol*; 1992 Nov 1;119(3):663–78.
 45. Fischer D, Brown-Ludi M, Schulthess T, Chiquet-Ehrismann R. Concerted action of tenascin-C domains in cell adhesion, anti-adhesion and promotion of neurite outgrowth. *J Cell Sci*; 1997 Jul;110 (Pt 13)(13):1513–22.
 46. Midwood KS, Chiquet M, Tucker RP, Orend G. Tenascin-C at a glance. *J Cell Sci*; 2016 Dec 1;129(23):4321–7.
 47. Radwanska A, Grall D, Schaub S, la Forest Divonne SB-D, Ciais D, Rekima S, Rupp T, Sudaka A, Orend G, Van Obberghen-Schilling E. Counterbalancing anti-adhesive effects of Tenascin-C through fibronectin expression in endothelial cells. *Sci Rep*; 2017 Oct 6;7(1):12762.
 48. Gundemir S, Colak G, Tucholski J, Johnson GVW. Transglutaminase 2: A molecular Swiss army knife. *Biochim Biophys Acta Mol Cell Res*; 2012 Feb;1823(2):406–19.
 49. Benn MC, Weber W, Klotzsch E, Vogel V, Pot SA. Tissue transglutaminase in fibrosis — more than an extracellular matrix cross-linker. *Curr Opin Biomed Eng*; 2019 Jun 1;10:156–64.
 50. Phillip JM, Aifuwa I, Walston J, Wirtz D. The Mechanobiology of Aging. *Annu Rev Biomed Eng*; 2015;17(1):113–41.
 51. Vining KH, Mooney DJ. Mechanical forces direct stem cell behaviour in development and regeneration. *Nat Rev Mol Cell Biol*; 2017 Nov 8;18(12):728–42.
 52. Cole MA, Quan T, Voorhees JJ, Fisher GJ. Extracellular matrix regulation of fibroblast function: redefining our perspective on skin aging. *J Cell Commun Signal*; 2018 Mar 1;12(1):35–43.
 53. Hsu CK, Lin H-H, Harn HIC, Hughes MW, Tang MJ, Yang C-C. Mechanical forces in skin disorders. *J Dermatol Sci*; 2018 Jun 1;90(3):232–40.
 54. Harn HIC, Ogawa R, Hsu CK, Hughes MW, Tang MJ, Chuong CM. The tension biology of wound healing. *Exp Dermatol*; 2019 Apr 1;28(4):464–71.
 55. Rumpler M, Woesz A, Dunlop JWC, van Dongen JT, Fratzl P. The effect of geometry on three-dimensional tissue growth. *J R Soc Interface*; 2008 Oct 6;5(27):1173–80.

56. Bidan CM, Kommareddy KP, Rumpler M, Kollmannsberger P, Bréchet YJM, Fratzl P, Dunlop JWC. How Linear Tension Converts to Curvature: Geometric Control of Bone Tissue Growth. *PLOS ONE*; 2012 May 11;7(5):e36336.
57. Bidan CM, Kommareddy KP, Rumpler M, Kollmannsberger P, Fratzl P, Dunlop JWC. Geometry as a Factor for Tissue Growth: Towards Shape Optimization of Tissue Engineering Scaffolds. *Adv Healthcare Mat*; 2013 Jan 1;2(1):186–94.
58. Ehrig S, Schamberger B, Bidan CM, West A, Jacobi C, Lam K, Kollmannsberger P, Petersen A, Tomancak P, Kommareddy K, Fischer FD, Fratzl P, Dunlop JWC. Surface tension determines tissue shape and growth kinetics. *Sci Adv*; 2019 Sep;5(9):eaav9394.
59. Stamenović D, Smith ML. Tensional homeostasis at different length scales. *Soft Matter*; 2020;16(30):6946–63.

2 Introduction

2.1 Tissue growth requires more than diffusion of soluble factors: ECM gradients are typically neglected in current *in vitro* platforms

The diffusion and convection of signalling molecules are directed by classical laws [1]. To address the complex extracellular regulations, however, a deep understanding of the complex cellular and matrix dependencies is crucial. Different laws must be postulated, which direct a spatial-to-temporal diverging production and consumption or degradation, respectively, resulting in a complex environment where two or more gradients interact with each other [2]. The complex 3D environment not only influences spatial and temporal aspects of diffusion [2], but is also composed of different chemical and mechanical gradients (e.g. ECM topology, ECM molecular composition and concentration, ECM crosslinking density, ECM porosity, adhesion site density, ECM remodelling, fiber stiffness, ECM elasticity, ECM confinement of cells) that alter cellular behaviour [3].

It is well described that the culture dimensionality influences cell morphology, adhesion and mechanotransduction [4], but gradients are mostly discussed in terms of soluble factors, which are in parts immobilized by ECM, or as gradients of substrate rigidity [2]. Gradients of morphogens, ECM compositions and cell phenotypes are highly relevant in nature and a rich body of literature indicates the importance of gradients in regulating health and disease, however so far dominated by gradients of soluble molecules [5-10]. Yet neither of these models reproduce the exact architecture, composition and viscoelasticity of the native ECM [11]. Most synthetic hydrogels are nanoporous and do not reflect fibrillar structure of native ECM [12]. Further, Fn gradients even on 2D planar glass substrates indicated significant effects on cellular behaviour [13]. While phenotype heterogeneity in conventional organoid cultures may lead to false result interpretations [14], the investigation of ECM gradients in organoids is difficult due to their heterogenic morphology [15]. Many other three dimensional tissue engineering platforms (e.g. hydrogels [16-18]) do not reproduce well the architecture and composition of native ECM scaffolds. Often other methods only test single parameters, e.g. stiffness [19,20], fiber alignment [21,22], but neglect ECM composition, which makes the transferability of the results difficult. In comparison with our platform even decellularized mammalian tissues fall short, because they typically lack a standardized spatio-temporal gradient essential for investigations on tissue growth and

maturation [23]. Life quality of patients will benefit from platforms that closely mimic ECM of target tissue, which allows fundamental understanding and clinical application [24].

Taken together, ECM gradients established by varying cell phenotypes are highly important not only for tissue growth in regeneration and development, but also for the physiological functionality of vital organs [25]. However, the literature search for ECM gradients mainly yields results on soluble factors in ECM or refers to ECM bound surface density or topography in 2D planar models [26]. There is currently no model described, which allows to investigate ECM gradients during tissue growth.

2.2 *de novo* μ Tissue platform mimics sequential tissue growth process

The μ Tissue platform further developed in this thesis allows to investigate ECM and cell phenotype gradients. It is part of a technical evolution of *de novo* grown tissue platforms and based on a large number of previous studies on various similar substrates, which showed that the geometric control of tissue growth is particularly important [27-34]. Initially, pre-osteoblastic cell line (MC3T-E1) were seeded on hydroxyapatite scaffolds with fabricated pores [27]. For the first time, a collagen-rich tissue growth in pores was quantified, while the deposition was significantly increased on concave compared to flat or even convex surfaces [27,29]. Similar growth mechanics have been shown with fibroblast and mesenchymal stem cells [31,33]. As in the example of water surface tension, the Laplace equation is linking surface tension with curvature relevant in droplet formation due to intermolecular attraction. While in biology, tissue tension is created by cell generated contractile forces and the concept how tissue tension dictates shape is realized across length scales [35].

In 3D scaffolds with constant mean curvature and rotational symmetry, cell contractility is required for developing sufficient surface tension to allow tissue growth as approximated by the physics of fluids (Laplace equation) [34]. Tissue growth occurs in this model a 'layer-by-layer' manner [32]. The initial growth front is formed by myofibroblasts producing the highly stretched Fn fibers, which are partially replaced as the tissue matures by strong tension bearing collagen fibers [32,33], further demonstrating the sequential process of tissue growth.

In the following section the sequential growth process of *de novo* μ Tissue growth by primary human dermal fibroblast is described based on PDMS scaffolds that were precoated with Fn covalently cross-linked to the substrates [33]. This methodology provided the basis for the development of the platforms in **Chapter 4** and **5**.

After cell seeding, fibroblasts adhere and spread first on the 2D top surfaces and actively assemble Fn into provisional ECM fibers [36-43]. Rho-mediated cellular contractile forces are required to

stretch and partially unfold Fn [44] and thereby promoting Fn assembly by exposing cryptic binding sites [45].

Furthermore, cells initiate early growth steps with actively exerting contractile forces to assemble and align early fibronectin protofibrils [46]. To allow subsequent tissue growth, those protofibrils need to be bundled and laterally crosslinked in order to gain mechanical stability, but this process is not fully understood (see **Chapter 4**). Cell contractility is applied to maintain tissue integrity [47] and as these processes and tissue maturation progress, the assembly of stronger collagen fibers occur which take over the tissue's main load [32]. The region-specific orientation of the Fn and collagen fibers results from cellular traction forces [48,49]. Myofibroblasts are known to exert sufficient contractile forces on their microenvironment for example in wound closure [50,51]. Myofibroblasts were identified in the highly tensed growth front and were shown to direct the tissue growth by applying cytoskeletal tension, assembling highly stretched Fn fibers and cellular proliferation [33].

Fn is a provisional matrix protein [52] and provides a template for collagen and several ECM components like LTBP1, thrombospondin, fibulin and others [53] and also serves as a framework for cell adhesion and migration. Further, in the absence of Fn and Fn polymerization no $\alpha 5\beta 1$ integrin localize to cell-matrix adhesion sites [54]. The nucleation of collagen I polymerization requires fibronectin fibers, especially in relaxed conformation [55], which act as multivalent templates for collagen peptides [56-58]. Fibronectin matrix and $\alpha 2\beta 1$ -integrin are required for collagen polymerization and for dense collagen network formation [54,59]. The presence of Fn promotes procollagen cleavage and contributes to the regulation of the lysol oxidase (LOX) mediated collagen cross-linking, both is further supporting tissue maturation [60-62]. Briefly, collagen fibrillogenesis requires post-translation proteolytic processing of procollagen by distinct proteases (BMP-1 and ADAMTS-2) and Fn binds and enhances bone morphogenic protein 1 (BMP-1). Therefore, Saunders et Schwarzbauer suggested a model for nascent collagen fiber assembly through procollagen processing on Fn matrix, which however neglects the above mentioned Fn conformation dependent nucleation of collagen I polymerization [55]. Collagen fiber assembly involves multiple complex intra- and extracellular post-translational processes ranging from the translational product to a tension-bearing fibrillar structure which is capable of withstanding tensile forces [63]. Tissue maturation shifts the tensional load away from the cellular contractility towards a mechanically stable collagen matrix which is capable of carrying the main load to maintain tissue integrity [32]. At the final stage of tissue maturation, it is no longer needed for cells to exert high contractile forces to maintain tissue integrity since a mature collagen matrix

took over most of the load [32,55] and the myofibroblast transition back to fibroblast over time [33].

During this sequential process of tissue growth, it remains unclear what additional actors are relevant, how ECM gradients are built up within short time and how this affects the phenotypic changes. A thorough understanding which sequential steps are necessary to ensure early tissue stabilization is key (see **Chapter 4** and **Chapter 5**).

2.3 Relevant actors in extracellular matrix (ECM) mechanobiology

2.3.1 ECM in health and disease

Cells and ECM are the major building blocks of multicellular organisms. Biochemical and biophysical regulations are governed by reciprocal interactions of both cells influencing the ECM composition and organization as ‘inside-out’ components and ECM mediating effects on cells as ‘outside-in’ components of mechanotransduction [64]. Integrins act as bifunctional proteins representing the main link between the ECM and the cytoskeleton, thus playing a major role in cell-ECM signalling events [65,66]. Fibrillar ECM is composed of a heterogeneous network of fibrous proteins, e.g. fibronectin and collagen, and proteoglycans and forms tissue-specific microenvironments in connective tissue, muscle tissue, nervous tissue, epithelial tissue and mineralized tissue. In addition, clinical and pathological investigations at the tissue level showed that ECM composition and architecture varies also dramatically between healthy and diseased states [67-69]. As a consequence, alterations in ECM of diseased state (e.g. matrix composition, matrix crosslinking, tension, stiffness) influence cellular behaviour and vice versa [69-72]. Furthermore, the alignment of stromal collagen has been described as a novel biomarker to predict clinical outcome of human breast cancer via the ECM characterization [73].

Fibronectin provides biochemical and mechanical cues for adherent cells at the early stages of wound healing [74,75] and serves as template for the subsequent deposition of other ECM molecules, particularly type I collagens, whose presence is critical for normal progression of wound healing [54-56,60]. Fn fibers can be stretched and partially unfolded by cell-generated forces, which can open up cryptic binding sites [36,41,44,76-78]. Fn fiber stretching can thus switch Fn’s binding affinity to other matrix proteins and alter the bioavailability of cellular binding sites on the FN molecule that can be recognized by cell surface integrin receptors [44,45,47,55,79-82]. Collagen I fibers preferentially bind to structurally relaxed Fn fibers in the ECM [55]. As such, the molecular folding state of Fn fibers in the ECM directly regulates further ECM assembly and directs the behaviour of resident cells, as demonstrated in previous publications from our laboratory

[33,55,83]. A dynamic force balance called 'tensional homeostasis' exists between cells and ECM in healthy tissues [84]. Changes in either cellular contractility or ECM tension are equilibrated and cause a shift in tissue tension, which is significantly increased during the development of fibrosis [47,84]. Importantly, mechanical integrin activation and integrin clustering at focal adhesion sites results in the activation of profibrotic downstream signalling activity [85-87]. Sustained disruptions in tensional homeostasis can be caused by chronic changes in the extracellular matrix, allowing it to serve as a mechanically based memory-storage device that can perpetuate disease [88].

2.3.2 Myofibroblast and transforming growth factor beta (TGF- β)

Myofibroblasts play central roles in orchestrating wound healing processes and, if remaining activated, drive disease progression such as fibrosis and cancer. In health and disease, fibroblast differentiate in varying organs to myofibroblast upon different triggers, such as mechanical tension, TGF- β , EDA-Fn and Tenascin-C [50,51,84,89-91].

The TGF- β superfamily of multi-functional cytokines, ubiquitously present in mammals and besides conveying pro-fibrotic functions, they are associated with wide range of diseases [92-100] and serve as treatment target [101-103]. The description of paradox TGF- β functionality in cancer underlines that we are far away from complete understanding of TGF- β [104,105].

For further description of myofibroblast and TGF- β the reader is referred to the literature review in **Chapter 3**.

2.3.3 Tenascin-C (TNC)

Tenascin-C (TNC) is a large multivalent hexameric matricellular glycoprotein, each monomer can range from 220 to 280 kDA in small and large TNC isoforms, and is best known for its mainly anti-adhesive function when binding to Fn matrices [106]. TNC binds to fibronectin (Fn) via Hep I, Hep II or Hep III domain of Fn [107]. The anti-adhesive function of TNC results from it competing with cell surface syndecan-4 binding to the Fn Hep II domain [108-110]. This creates an environment promoting cell motility and tissue regeneration [111-113]. TNC directly interacts with its microenvironment through cells, growth factors and ECM maintaining tissue homeostasis [114], while it is known to be upregulated by TGF- β in a SMAD-3 dependent manner [115,116] and drive persistence in fibrosis [89]. It is highly expressed during development in various organs and in adult only present in tissues of high cell turnover or tensile stress as during wound healing, inflammation, regeneration, cancer and fibrosis [117,118]. TNC was identified as marker for fibrosis [119], cancer [120] and immature matrix [121]. Interestingly, TNC supplemented to murine skin wounds accelerated healing and reduced scarring [122]. Besides regulating cell motility, proliferation,

differentiation and survival TNC exhibits a wide number of other function (reviewed in [106,114,123]).

2.3.3.1 Time relevant aspects of TNC for ECM gradients

TNC is regulating itself by inducing a negative-feedback loop [124]. Briefly, the interaction between Fn and ubiquitous cell surface proteoglycan syndecan-4 is stabilizing the cell attachment to the ECM [125]. TNC binds to Fn and blocks the interaction of Fn and syndecan-4 and consequently RhoA / ROCK pathway is not activated resulting in no actin reorganization and in addition no further expression of TNC by cyclic strain [124]. Fn, as an early ECM component, is required for RhoA dependent and strain-induced TNC induction [124]. TNC can induce MMP-2 expression [126] and MMP2 cleaves in part depending on alternative spliced TNC, especially large isoforms contain cleavage sites [127-129]. Cleavage of TNC can lead to reduction of TNC levels, exposure of cryptic binding sites, release of domains mediating cell adhesion [130,131] and create or cover ECM binding sites (e.g. Fn) [132,133]. During the process of TNC degradation, smaller fragments with new binding sites are generated conveying in part complete opposite functionality described as “matricryptins” [132,134]. Cleavage of TNC with MMP-2 generates cryptic binding sites which permits interaction with heparan sulfated side-chains of syndecan-4 to promote β 1 integrin clustering and cell spreading [127,128,130].

Interestingly, different degradative fragments of TNC convey in part opposite functionality, ranging to promote migration, as full-length TNC, far to inhibit migration completely [134]. Furthermore, TNfn1-8 and FBG domains of TNC, but not full length TNC, inhibit the assembly of a dense FN fibrillar matrix over 22h incubation with temporally and spatially distinct effects [132].

This differentially regulated fibroblast migration might act in a concerted manner to allow a fine-tuned cellular response: After injury, induced TNC was suggested to promote fibroblast infiltration into the initial ECM and, at a later time point after TNC degradation, TNC fragments inhibits further fibroblast migration[135].

In addition to the many different functions of TNC, the novel functionalities of its fragments elucidate the complexity of its nature: “It seems that the more we learn about this extraordinary matrix glycoprotein, the more complex and intricate the story becomes.” [128].

2.3.4 Tissue transglutaminase (TG2)

In diseased ECM, enhanced cross-linking is associated with reduced ECM compliance [136-139]. Thus, in the newly emerging field of mechanomedicine targeting mechanisms that increase extracellular matrix stiffness was proposed as novel treatment strategy [140,141] (Fig. 1). Tissue

transglutaminase (TG2) and lysol oxidase (LOX) represent the most prominent ECM cross-linker, however recent reports indicated higher clinical relevance for TG2 [142]. While LOX was reported to be more required at later stages of maturation after collagen matrix is fully assembled, TG2 is prominent in early and late ECM remodelling phases [143]. Within the scope of **Chapter 4**, we focused thus on the role of TG2, since in addition there are also many non-enzymatic functions reported (see review in **Chapter 3**). TGF- β 1 activation is thought to be facilitated by TG2 since TG2 cross-links latent TGF- β binding protein (LTBP) to the ECM and can stiffen a compliant matrix via ECM cross-linking [144]. A positive feedback loop is suggested between TG2 and TGF- β [145,146] and inhibition of TG2 leads to decrease in expression of TGF- β , NF κ B and decrease of matrix deposition [147]. In **Chapter 3**, more details of enzymatic and non-enzymatic TG2 function and interaction with TGF- β are reviewed.

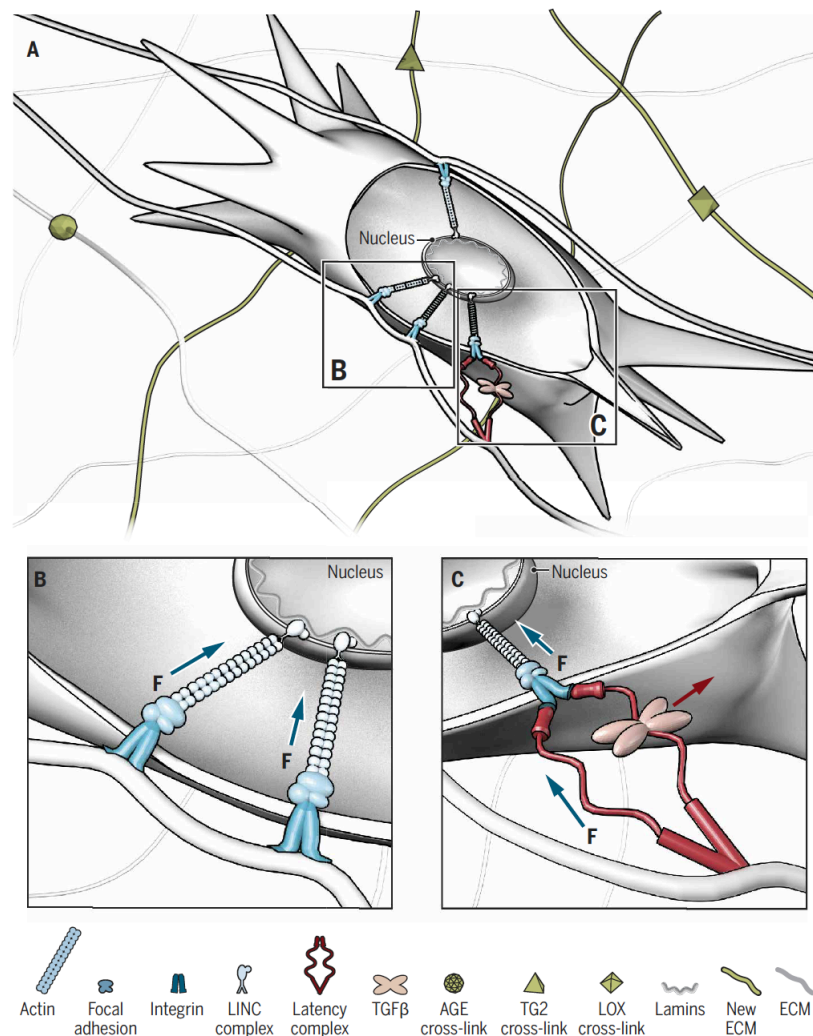


Fig. 1 Suggested mechanism of mechanical TGF- β release in a cross-linked ECM in response to increased microenvironment stiffness. *Graphic: A. KITTERMAN/SCIENCE TRANSLATIONAL MEDICINE. From Lampi and Reinhart-King, Sci. Transl. Med. 10, eaao0475 (2018) [140]. Reprinted with permission from AAAS.*

2.3.5 Significance of TG2 and TNC interplay

To our knowledge, no literature exists which describes mechanistic dependencies between TNC and TG2. However, due to their central roles in the cell-ECM interphase much effort has been expended to conduct *in vitro* studies to investigate each TG2 and TNC separately, as above mentioned. Much attention attracted us, that there is a huge overlap in binding partners which interact individually with TNC and TG2 (see above), while TNC and TG2 both achieve pleiotropic roles in diverse cellular and ECM functions [106,114,146] (see **Chapter 3** for TG2). Some of which are shaking hands like regulating cell adhesion where TNC facilitates de-adhesion and TG2 adhesion of cells to ECM [148-151]. TNC and TG2 are both reported to be quickly upregulated at the boarder of healing wounds and other sites of ECM remodelling [135,143,152], mechanical stress [153-156], as well as during embryonic development, wound healing or pathological conditions of fibrosis or cancer [89,119,157-161]. Fibronectin binds to both TNC and TG2, but at two distinct binding sites. TNC binds to Fn at Hep I, Hep II and Hep III domain [162] while the amino-terminal location of Fn Hep I domain is adjacent to the gelatin-/collagen-binding domain where TG2 binds to [163]. Both TG2 and TNC can crosslink ECM, but TG2 carries out an enzymatic crosslinking function and TNC conveys a non-enzymatic cross-linker function due to its hexameric structure [164]. Syndecan-4, a plasma membrane proteoglycan, accumulates in focal adhesions and interacts via heparan sulfate chains with the Hep2-region of Fn. TNC binds to Fn conveying its' de-adhesive function [165] through blocking the Fn-Syndecan-4-interaction, which prevents activation of the RhoA/ROCK pathway and downstream actin re-organization and TNC expression and allows TNC regulation through negative feedback [124]. Interestingly, the strain-induced induction of TNC also requires binding of TNC to Fn [124] and β 1-integrins [154,166-168].

TG2 itself clusters Fn, syndecan-4 and β 1-integrin which is suggested to promote tissue repair after damage, where TG2-Fn-syndecan-4- β 1-integrin-complex enhances adhesive and signalling functions and might therefore compensate for integrin-dependent adhesion deficiency and lack of Fn fiber assembly [169]. Another interaction partner is MMP-2, which can be induced by TNC in smooth muscle cells [126]. Cleavage of TNC by MMP2 generates cryptic binding sites which permit interaction with syndecan-4 to promote β 1-integrin clustering and cell spreading [128,130]. MMP-2 cleaves and inactivates TG2 [170]. However, there is a negative feedback loop described where TG2 is associated with the activation of MMP-2 intermediate resulting in reducing MMP-2 activity with subsequent protection of TG2 proteolysis [171]. It was shown that MMP-2 expression in fibroblast were inversely related to the α SMA expression, thus MMP-2 expression is suppressed by myofibroblast phenotype [172]. TGF- β upregulates both TNC [173] and TG2 [145].

However, only very little work can be found where observations of TG2 and TNC were reported in healthy or diseased tissue. One study identified different phenotypic subpopulations of cancer-associated fibroblasts (CAFs) in pancreatic cancer and reported high TNC levels in the matrix within the range of 100 μm of cancer cells. On the contrary, high TG2 levels were observed in healthy lobular tissue TG2, but the role of TG2 was not discussed further [174]. Both TG2 and TNC are found to be upregulated under inflammatory conditions [175]. In non-neoplastic reactive lymphoid tissue specimen removed from human patients TG2 and TNC showed similar expression patterns in close proximity of the marginal zone and T-cell area [176]. Human breast cancer biopsies were described with both high TNC and TG2 levels in invasive ductal carcinoma (IDC) compared to normal breast tissue [177]. Another *in vivo* infection study in piglets demonstrated in early (24 h post infection) and late (48 h post infection) piglets infected with *Salmonella enterica* serovar Choleraesuis that genes for TG2 were upregulated in the mesenteric lymph node in both groups, while TNC (here HXB for hexabrachion) was upregulated in late group only [178].

In summary, even though few studies identified the presence of both TG2 and TNC *in vitro* and *in vivo*, no literature is available so far describing a functional dependency between TNC and TG2.

2.4 References

1. Patrick Müller AFS. Extracellular movement of signaling molecules. *Dev Cell*; 2011 Jul 19;21(1):145–58.
2. Majumdar R, Sixt M, Parent CA. New paradigms in the establishment and maintenance of gradients during directed cell migration. *Curr Opin Cell Biol*; 2014 Oct;30:33–40.
3. Yamada KM, Sixt M. Mechanisms of 3D cell migration. *Nat Rev Mol Cell Biol*; 2019 Dec 1;20(12):738–52.
4. Baker BM, Chen CS. Deconstructing the third dimension – how 3D culture microenvironments alter cellular cues. *J Cell Sci*; 2012 Jul 1;125(13):3015–24.
5. Ishida-Ishihara S, Akiyama M, Furusawa K, Naguro I, Ryuno H, Sushida T, Ishihara S, Haga H. Osmotic gradients induce stable dome morphogenesis on extracellular matrix. *J Cell Sci*; 2020 Jul 15;133(14):jcs243865.
6. Shimizu A, Goh WH, Itai S, Karyappa R, Hashimoto M, Onoe H. ECM-based microfluidic gradient generator for tunable surface environment by interstitial flow. *Biomicrofluidics*; 2020 Jul;14(4):044106.
7. Wang Y, He G, Wang F, Zhang C, Ge Z, Zheng X, Deng H, Yuan C, Zhou B, Tao X, Zhang J, Tang K. Aspirin inhibits adipogenesis of tendon stem cells and lipids accumulation in rat injury tendon through regulating PTEN/PI3K/AKT signalling. *J Cell Mol Med*; 2019 Nov 1;23(11):7535–44.
8. Hubka KM, Carson DD, Harrington DA, Farach-Carson MC. Perlecan domain I gradients establish stable biomimetic heparin binding growth factor gradients for cell migration in hydrogels. *Acta Biomater*; 2019 Oct;97:385–98.
9. Thotakura S, Basova L, Makarenkova HP. FGF Gradient Controls Boundary Position Between Proliferating and Differentiating Cells and Regulates Lacrimal Gland Growth Dynamics. *Front Genet*; 2019 May 28;10:543.
10. Wu W, Tholozan FM, Goldberg MW, Bowen L, Wu J, Quinlan RA. A gradient of matrix-bound FGF-2 and perlecan is available to lens epithelial cells. *Exp Eye Res*; 2014 Mar 1;120:10–4.
11. Bonnans C, Chou J, Werb Z. Remodelling the extracellular matrix in development and disease. *Nat Rev Mol Cell Biol*; 2014 Dec;15(12):786–801.
12. Chaudhuri O, Cooper-White J, Janmey PA, Mooney DJ, Shenoy VB. Effects of extracellular matrix viscoelasticity on cellular behaviour. *Nature*; 2020 Aug 1;584(7822):535–46.
13. Moyes KW, Sip CG, Obenza W, Yang E, Horst C, Welikson RE, Hauschka SD, Folch A, Laflamme MA. Human Embryonic Stem Cell-Derived Cardiomyocytes Migrate in Response to Gradients of Fibronectin and Wnt5a. *Stem Cells Dev*; 2013 Aug 15;22(16):2315–25.
14. Shin W, Wu A, Min S, Shin YC, Fleming RYD, Eckhardt SG, Kim HJ. Spatiotemporal Gradient and Instability of Wnt Induce Heterogeneous Growth and Differentiation of Human Intestinal Organoids. *iScience*; 2020 Aug 21;23(8):101372.
15. Bécavin T, Kuchler-Bopp S, Kökten T, Huck O, Messaddeq N, Lesot H, Deveaux E, Benkirane-Jessel N, Laetitia K. Well-organized spheroids as a new platform to examine cell interaction and behaviour during organ development. *Cell Tissue Res*; 2016;366(3):601–15.
16. Yu S, Duan Y, Zuo X, Chen X, Mao Z, Gao C. Mediating the invasion of smooth muscle cells into a cell-responsive hydrogel under the existence of immune cells. *Biomaterials*; 2018 Oct;180:193–205.

17. Xia T, Liu W, Yang L. A review of gradient stiffness hydrogels used in tissue engineering and regenerative medicine. *J Biomed Mat Res*; 2017 Jun 1;105(6):1799–812.
18. Hadden WJ, Young JL, Holle AW, McFetridge ML, Kim DY, Wijesinghe P, Taylor-Weiner H, Wen JH, Lee AR, Bieback K, Vo B-N, Sampson DD, Kennedy BF, Spatz JP, Engler AJ, Cho YS. Stem cell migration and mechanotransduction on linear stiffness gradient hydrogels. *Proc Natl Acad Sci*; 2017 May 30;114(22):5647–52.
19. Lavrentieva A, Fleischhammer T, Enders A, Pirmahboub H, Bahnemann J, Pepelanova I. Fabrication of Stiffness Gradients of GelMA Hydrogels Using a 3D Printed Micromixer. *Macromol Biosci*; 2020 Jul 1;20(7):2000107.
20. Barber-Pérez N, Georgiadou M, Guzmán C, Isomursu A, Hamidi H, Ivaska J. Mechano-responsiveness of fibrillar adhesions on stiffness-gradient gels. *J Cell Sci*; 2020 Jun 22;133(12).
21. Morrow CM, Mukherjee A, Traore MA, Leaman EJ, Kim A, Smith EM, Nain AS, Behkam B. Integrating nanofibers with biochemical gradients to investigate physiologically-relevant fibroblast chemotaxis. *Lab Chip*; 2019;19(21):3641–51.
22. Seidi A, Sampathkumar K, Srivastava A, Ramakrishna S, Ramalingam M. Gradient nanofiber scaffolds for tissue engineering. *J Nanosci Nanotechnol*; 2013 Jul 1;13(7):4647–55.
23. Gupta SK, Mishra NC, Dhasmana A. Decellularization Methods for Scaffold Fabrication. *Decell Scaff Organogen*; 2017;1577:1-10.
24. Kim Y, Ko H, Kwon IK, Shin K. Extracellular Matrix Revisited: Roles in Tissue Engineering. *Int Neurourol J*; 2016 May;20:S23–9.
25. Reid LM, Fiorino AS, Sigal SH, Brill S, Holst PA. Extracellular matrix gradients in the space of Disse: relevance to liver biology. *Hepatology*; 1992 Jun;15(6):1198–203.
26. Park J, Kim D-H, Levchenko A. Topotaxis: A New Mechanism of Directed Cell Migration in Topographic ECM Gradients. *Biophys J*; 2018 Mar 27;114(6):1257–63.
27. Rumpler M, Woesz A, Dunlop JWC, van Dongen JT, Fratzl P. The effect of geometry on three-dimensional tissue growth. *J R Soc Interface*; 2008 Oct 6;5(27):1173–80.
28. Bidan C, Kommareddy K, Manjubala I, Rumpler M, Fratzl P, Dunlop J. Geometric Control of Tissue Growth. *Bone*; 2010 Mar;46:S47–8.
29. Bidan CM, Kommareddy KP, Rumpler M, Kollmannsberger P, Bréchet YJM, Fratzl P, Dunlop JWC. How Linear Tension Converts to Curvature: Geometric Control of Bone Tissue Growth. *PLOS ONE*; 2012 May 11;7(5):e36336.
30. Bidan CM, Kommareddy KP, Rumpler M, Kollmannsberger P, Fratzl P, Dunlop JWC. Geometry as a Factor for Tissue Growth: Towards Shape Optimization of Tissue Engineering Scaffolds. *Adv Healthcare Mat*; 2013 Jan 1;2(1):186–94.
31. Herklotz M, Prewitz MC, Bidan CM, Dunlop JWC, Fratzl P, Werner C. Availability of extracellular matrix biopolymers and differentiation state of human mesenchymal stem cells determine tissue-like growth *in vitro*. *Biomaterials*; 2015 Aug;60:121–9.
32. Bidan CM, Kollmannsberger P, Gering V, Ehrig S, Joly P, Petersen A, Vogel V, Fratzl P, Dunlop JWC. Gradual conversion of cellular stress patterns into pre-stressed matrix architecture during *in vitro* tissue growth. *J R Soc Interface*; 2016 May;13(118):20160136.
33. Kollmannsberger P, Bidan CM, Dunlop JWC, Fratzl P, Vogel V. Tensile forces drive a reversible fibroblast-to-myofibroblast transition during tissue growth in engineered clefts. *Sci Adv*; 2018 Jan

- 1;4(1):eaao4881.
34. Ehrig S, Schamberger B, Bidan CM, West A, Jacobi C, Lam K, Kollmannsberger P, Petersen A, Tomancak P, Kommareddy K, Fischer FD, Fratzl P, Dunlop JWC. Surface tension determines tissue shape and growth kinetics. *Sci Adv*; 2019 Sep;5(9):eaav9394.
 35. Kollmannsberger P, Bidan CM, Dunlop JWC, Fratzl P. The physics of tissue patterning and extracellular matrix organisation: how cells join forces. *Soft Matter*; 2011;7(20):9549–60.
 36. Singh P, Carraher C, Schwarzbauer JE. Assembly of Fibronectin Extracellular Matrix. *Annu Rev Cell Dev Biol*; 2010 Nov 10;26(1):397–419.
 37. Fernandez-Sauze S, Grall D, Cseh B, Van Obberghen-Schilling E. Regulation of fibronectin matrix assembly and capillary morphogenesis in endothelial cells by Rho family GTPases. *Exp Cell Res*; 2009 Jul 15;315(12):2092–104.
 38. Vogel V. Mechanotransduction involving multimodular proteins: converting force into biochemical signals. *Annu Rev Biophys Biomol Struct*; 2006;35(1):459–88.
 39. Mao Y, Schwarzbauer JE. Accessibility to the fibronectin synergy site in a 3D matrix regulates engagement of alpha5beta1 versus alphavbeta3 integrin receptors. *Cell Commun Adhes*; 2006 Sep;13(5-6):267–77.
 40. Geiger B, Bershadsky A, Pankov R, Yamada KM. Transmembrane crosstalk between the extracellular matrix and the cytoskeleton. *Nat Rev Mol Cell Biol*; 2001 Nov;2(11):793–805.
 41. Baneyx G, Vogel V. Self-assembly of fibronectin into fibrillar networks underneath dipalmitoyl phosphatidylcholine monolayers: Role of lipid matrix and tensile forces. *Proc Natl Acad Sci*; 1999 Oct 26;96(22):12518–23.
 42. Mosher DF. Assembly of fibronectin into extracellular matrix. *Curr Opin Structural Biol*; 1993 Apr 1;3(2):214–22.
 43. Grinnell F. Fibronectin and wound healing. *Am J Dermatopathol*; 1982 Jan 1;4(2):185–8.
 44. Baneyx G, Baugh L, Vogel V. Fibronectin extension and unfolding within cell matrix fibrils controlled by cytoskeletal tension. *Natl Acad Scs*; 2002 Apr 16;99(8):5139–43.
 45. Zhong C, Chrzanowska-Wodnicka M, Brown J, Shaub A, Belkin AM, Burridge K. Rho-mediated contractility exposes a cryptic site in fibronectin and induces fibronectin matrix assembly. *J Cell Biol*; 1998 Apr 20;141(2):539–51.
 46. Dzamba BJ, Peters DM. Arrangement of cellular fibronectin in noncollagenous fibrils in human fibroblast cultures. *J Cell Sci. The Company of Biologists Ltd*; 1991 Nov;100 (Pt 3)(3):605–12.
 47. Schoen I, Pruitt BL, Vogel V. The Yin-Yang of Rigidity Sensing: How Forces and Mechanical Properties Regulate the Cellular Response to Materials. *Annu Rev*; 2013 Jul 5;43(1):589–618.
 48. Lemmon CA, Chen CS, Romer LH. Cell Traction Forces Direct Fibronectin Matrix Assembly. *Biophys J*; 2009;96(2):729–38.
 49. Jansen KA, Licup AJ, Sharma A, Rens R, MacKintosh FC, Koenderink GH. The Role of Network Architecture in Collagen Mechanics. *Biophys J*; 2018 Jun;114(11):2665–78.
 50. Tomasek JJ, Gabbiani G, Hinz B, Chaponnier C, Brown RA. Myofibroblasts and mechano-regulation of connective tissue remodelling. *Nat Rev Mol Cell Biol*; 2002 May 1;3(5):349–63.
 51. Hinz B. Myofibroblasts. *Exp Eye Res*; 2016 Jan;142:56–70.

52. Clark RAF, Lanigan JM, DellaPelle P, Manseau E, Dvorak HF, Colvin RB. Fibronectin and Fibrin Provide a Provisional Matrix for Epidermal Cell Migration During Wound Reepithelialization. *J Invest Dermatol*; 1982 Nov;79(5):264–9.
53. Dallas SL, Sivakumar P, Jones C, Chen Q, Peters DM, Mosher DF, Humphries MJ, Kielty CM. Fibronectin regulates latent transforming growth factor-beta (TGF beta) by controlling matrix assembly of latent TGF beta-binding protein-1. *J Biol Chem*; 2005;280(19):18871–80.
54. Sottile J, Hocking DC. Fibronectin polymerization regulates the composition and stability of extracellular matrix fibrils and cell-matrix adhesions. *Mol Biol Cell*; 2002 Oct;13(10):3546–59.
55. Kubow KE, Vukmirovic R, Zhe L, Klotzsch E, Smith ML, Gourdon D, Luna S, Vogel V. Mechanical forces regulate the interactions of fibronectin and collagen I in extracellular matrix. *Nat Commun*; 2015 Aug 14;6(1):8026.
56. Kadler KE, Hill A, Canty-Laird EG. Collagen fibrillogenesis: fibronectin, integrins, and minor collagens as organizers and nucleators. *Curr Opin Cell Biol*; 2008 Oct;20(5):495–501.
57. Sottile J, Shi F, Rublyevska I, Chiang H-Y, Lust J, Chandler J. Fibronectin-dependent collagen I deposition modulates the cell response to fibronectin. *Am J Physiol Cell Physiol*; 2007 Dec;293(6):C1934–46.
58. McDonald JA, Kelley DG, Broekelmann TJ. Role of fibronectin in collagen deposition: Fab' to the gelatin-binding domain of fibronectin inhibits both fibronectin and collagen organization in fibroblast extracellular matrix. *J Cell Biol*; 1982 Jan 1;92(2):485–92.
59. Velling T, Risteli J, Wennerberg K, Mosher DF, Johansson S. Polymerization of Type I and III Collagens Is Dependent On Fibronectin and Enhanced By Integrins $\alpha 11\beta 1$ and $\alpha 2\beta 1$. *J Biol Chem*; 2002 Sep 27;277(40):37377–81.
60. Fogelgren B, Polgár N, Szauter KM, Újfaludi Z, Laczkó R, Fong KSK, Csiszar K. Cellular fibronectin binds to lysyl oxidase with high affinity and is critical for its proteolytic activation. *J Biol Chem*; 2005 Jul 1;280(26):24690–7.
61. Huang G, Zhang Y, Kim B, Ge G, Annis DS. Fibronectin binds and enhances the activity of bone morphogenetic protein 1. *J Biol Chem*; 2009;284(38):25879–88.
62. Saunders JT, Schwarzbauer JE. Fibronectin matrix as a scaffold for procollagen proteinase binding and collagen processing. *Mol Biol Cell*; 2019 Aug;30(17):2218–26.
63. Mouw JK, Ou G, Weaver VM. Extracellular matrix assembly: a multiscale deconstruction. *Nat Rev Mol Cell Biol*; 2014 Dec;15(12):771–85.
64. Hynes RO. Stretching the boundaries of extracellular matrix research. *Nat Rev Mol Cell Biol*; 2014 Dec;15(12):761–3.
65. Hynes RO. Integrins: Bidirectional, Allosteric Signaling Machines. *Cell*; 2002 Sep;110(6):673–87.
66. Campbell ID, Humphries MJ. Integrin Structure, Activation, and Interactions. *Cold Spring Harb Perspect Biol*; 2011 Mar 1;3(3):a004994–4.
67. Provenzano PP, Inman DR, Eliceiri KW, Knittel JG, Yan L, Rueden CT, White JG, Keely PJ. Collagen density promotes mammary tumor initiation and progression. *BMC Med*; 2008;6(1):11.
68. Yu H, Mouw JK, Weaver VM. Forcing form and function: biomechanical regulation of tumor evolution. *Trends in Cell Biol*; 2011 Jan;21(1):47–56.
69. Frantz C, Stewart KM, Weaver VM. The extracellular matrix at a glance. *J Cell Sci*; 2010 Dec

- 15;123(24):4195–200.
70. Hinz B. Matrix mechanics and regulation of the fibroblast phenotype. *Periodontol*; 2013 Aug 11;63(1):14–28.
 71. Hinz B, Mastrangelo D, Iselin CE, Chaponnier C, Gabbiani G. Mechanical tension controls granulation tissue contractile activity and myofibroblast differentiation. *Am J Pathol*; 2001 Sep;159(3):1009–20.
 72. Leask A. Matrix remodeling in systemic sclerosis. *Semin Immunopathol*. Springer Berlin Heidelberg; 2015 Sep;37(5):559–63.
 73. Conklin MW, Eickhoff JC, Riching KM, Pehlke CA, Eliceiri KW, Provenzano PP, Friedl A, Keely PJ. Aligned collagen is a prognostic signature for survival in human breast carcinoma. *Am J Pathol*; 2011 Mar;178(3):1221–32.
 74. Suda T, Nishida T, Ohashi Y, Nakagawa S, Manabe R. Fibronectin appears at the site of corneal stromal wound in rabbits. *Curr Eye Res*; 2009 Jul 2;1(9):553–6.
 75. Wing S To KSM. Plasma and cellular fibronectin: distinct and independent functions during tissue repair. *Fibrogen Tissue Repair*; 2011;4(1):21.
 76. Smith ML, Gourdon D, Little WC, Kubow KE, Eguiluz RA, Luna-Morris S, Vogel V. Force-Induced Unfolding of Fibronectin in the Extracellular Matrix of Living Cells. *PLOS Biol*; 2007 Oct 2;5(10):e268.
 77. Little WC, Smith ML, Ebnetter U, Vogel V. Assay to mechanically tune and optically probe fibrillar fibronectin conformations from fully relaxed to breakage. *Matrix Biol*; 2008 Jun;27(5):451–61.
 78. Schwarzbauer JE, DeSimone DW. Fibronectins, Their Fibrillogenesis, and *In vivo* Functions. *Cold Spring Harb Perspect Biol*; 2011 Jul 1;3(7):a005041–1.
 79. Klotzsch E, Smith ML, Kubow KE, Muntwyler S, Little WC, Beyeler F, Gourdon D, Nelson BJ, Vogel V. Fibronectin forms the most extensible biological fibers displaying switchable force-exposed cryptic binding sites. *Proc Natl Acad Sci*; 2009 Oct 27;106(43):18267–72.
 80. Chabria M, Hertig S, Smith ML, Vogel V. Stretching fibronectin fibers disrupts binding of bacterial adhesins by physically destroying an epitope. *Nature Commun*; 2010 Dec;1(9).
 81. Seong J, Tajik A, Sun J, Guan J-L, Humphries MJ, Craig SE, Shekaran A, García AJ, Lu S, Lin MZ, Wang N, Wang Y. Distinct biophysical mechanisms of focal adhesion kinase mechanoactivation by different extracellular matrix proteins. *Proc Natl Acad Sci*; 2013 Nov 26;110(48):19372–7.
 82. Vogel V. Unraveling the Mechanobiology of Extracellular Matrix. *Annu Rev*; 2018 Feb 12;80(1):353–87.
 83. Li B, Moshfegh C, Lin Z, Albuschies J, Vogel V. Mesenchymal stem cells exploit extracellular matrix as mechanotransducer. *Sci Rep*; 2013;3(1):2425.
 84. Pakshir P, Hinz B. The big five in fibrosis: Macrophages, myofibroblasts, matrix, mechanics, and miscommunication. *Matrix Biol*; 2018 Aug 1;68-69:81–93.
 85. Janiak A, Zemskov EA, Belkin AM. Cell surface transglutaminase promotes RhoA activation via integrin clustering and suppression of the Src-p190RhoGAP signaling pathway. *Mol Biol Cell*; 2006 Apr;17(4):1606–19.
 86. Asparuhova MB, Gelman L, Chiquet M. Role of the actin cytoskeleton in tuning cellular responses to external mechanical stress. *Scandinav J Med Sci Sports*; 2009 Aug;19(4):490–9.
 87. Morgan JT, Murphy CJ, Russell P. What do mechanotransduction, Hippo, Wnt, and TGF β have in common? YAP and TAZ as key orchestrating molecules in ocular health and disease. *Exp Eye Res*; 2013

- Oct;115:1–12.
88. DuFort CC, Paszek MJ, Weaver VM. Balancing forces: architectural control of mechanotransduction. *Nat Rev Mol Cell Biol*; 2011 May;12(5):308–19.
 89. Bhattacharyya S, Wang W, Morales-Nebreda L, Feng G, Wu M, Zhou X, Lafyatis R, Lee J, Hinchcliff M, Feghali-Bostwick C, Lakota K, Budinger GRS, Raparia K, Tamaki Z, Varga J. Tenascin-C drives persistence of organ fibrosis. *Nat Commun*; 2016 Jun 3;7(1):ncomms11703.
 90. Katoh D, Kozuka Y, Noro A, Ogawa T, Imanaka-Yoshida K, Yoshida T. Tenascin-C Induces Phenotypic Changes in Fibroblasts to Myofibroblasts with High Contractility through the Integrin $\alpha\beta 1$ /Transforming Growth Factor β /SMAD Signaling Axis in Human Breast Cancer. *Am J Pathol*; 2020 Jul 8.
 91. Pakshir P, Noskovicova N, Lodyga M, Son DO, Schuster R, Goodwin A, Karvonen H, Hinz B. The myofibroblast at a glance. *J Cell Sci*; 2020 Jul 10;133(13):jcs227900.
 92. Margadant C, Sonnenberg A. Integrin–TGF- β crosstalk in fibrosis, cancer and wound healing. *EMBO*; 2010 Feb 1;11(2):97–105.
 93. Massagué J. TGF β signalling in context. *Nat Rev Mol Cell Biol*; 2012 Oct;13(10):616–30.
 94. Weiss A, Attisano L. The TGFbeta Superfamily Signaling Pathway. *Rev Dev Biol*; 2013 Jan 1;2(1):47–63.
 95. Robertson IB, Rifkin DB. Unchaining the beast; insights from structural and evolutionary studies on TGF β secretion, sequestration, and activation. *Cytokine Growth Factor Rev*; 2013 Aug 1;24(4):355–72.
 96. Sutariya B, Jhonsa D, Saraf MN. TGF- β : the connecting link between nephropathy and fibrosis. *Immunopharmacol Immunotoxicol*; 2016 Feb 5;38(1):39–49.
 97. Meng X-M, Nikolic-Paterson DJ, Lan HY. TGF- β : the master regulator of fibrosis. *Nat Rev Nephrol*; 2016 Jun;12(6):325–38.
 98. Xu X, Zheng L, Yuan Q, Zhen G, Crane JL, Zhou X, Cao X. Transforming growth factor- β in stem cells and tissue homeostasis. *Bone Res*; 2018 Jan 31;6(1):466.
 99. Caja L, Dituri F, Mancarella S, Caballero-Diaz D, Moustakas A, Giannelli G, Fabregat I. TGF- β and the Tissue Microenvironment: Relevance in Fibrosis and Cancer. *Int J Mol Sci*; 2018 May;19(5):1294.
 100. Vander Ark A, Cao J, Li X. TGF- β receptors: In and beyond TGF- β signaling. *Cell Sign*; 2018 Dec 1;52:112–20.
 101. Yingling JM, Blanchard KL, Sawyer JS. Development of TGF- β signalling inhibitors for cancer therapy. *Nat Rev Drug Discov*; 2004 Dec 1;3(12):1011–22.
 102. Rifkin DB, Rifkin WJ, Zilberberg L. LTBP in biology and medicine: LTBP diseases. *Matrix Biol*; 2018 Oct 1;71-72:90–9.
 103. Takahashi K, Akatsu Y, Podyma-Inoue KA, Matsumoto T, Takahashi H, Yoshimatsu Y, Koinuma D, Shirouzu M, Miyazono K, Watabe T. Targeting all transforming growth factor- β isoforms with an Fc chimeric receptor impairs tumor growth and angiogenesis of oral squamous cell cancer. *J Biol Chem*; 2020 Sep 4;295(36):12559–72.
 104. Roberts AB, LM W. The two faces of transforming growth factor beta in carcinogenesis. *Proceedings of the National Academy of Sciences. Proc Natl Acad Sci*; 2003 Jul 22;100(15):8621–3.
 105. Principe DR, Doll JA, Bauer J, Jung B, Munshi HG, Bartholin L, Pasche B, Lee C, Grippo PJ. TGF- β : Duality of Function Between Tumor Prevention and Carcinogenesis. *J Natl Cancer Inst*; 2014 Jan

- 30;106(2):djt369–9.
106. Midwood KS, Chiquet M, Tucker RP, Orend G. Tenascin-C at a glance. *J Cell Sci*; 2016 Dec 1;129(23):4321–7.
 107. Van Obberghen-Schilling E, Tucker RP, Saupe F, Gasser I, Cseh B, Orend G. Fibronectin and tenascin-C: accomplices in vascular morphogenesis during development and tumor growth. *Int J Dev Biol*; 2011;55(4-5):511–25.
 108. Huang W, Chiquet-Ehrismann R, Moyano JV, Garcia-Pardo A, Orend G. Interference of Tenascin-C with Syndecan-4 Binding to Fibronectin Blocks Cell Adhesion and Stimulates Tumor Cell Proliferation. *Cancer Res*; 2001 Dec 1;61(23):8586–94.
 109. Orend G, Huang W, Olayioye MA, Hynes NE, Chiquet-Ehrismann R. Tenascin-C blocks cell-cycle progression of anchorage-dependent fibroblasts on fibronectin through inhibition of syndecan-4. *Oncogene*; 2003 Jun 19;22(25):3917–26.
 110. Williams SA, Schwarzbauer JE. A shared mechanism of adhesion modulation for tenascin-C and fibulin-1. *Mol Biol Cell*; 2009 Feb;20(4):1141–9.
 111. Murphy-Ullrich JE. The de-adhesive activity of matricellular proteins: is intermediate cell adhesion an adaptive state? *J Clin Invest*; 2001 Apr 1;107(7):785–90.
 112. Flück M, Mund SI, Schittny JC, Klossner S, Durieux A-C, Giraud M-N. Mechano-regulated tenascin-C orchestrates muscle repair. *Proc Natl Acad Sci*; 2008 Sep 9;105(36):13662–7.
 113. Mackey AL, KJÆR M. Connective tissue regeneration in skeletal muscle after eccentric contraction-induced injury. *J Appl Physiol*; 2017 Mar 1;122(3):533–40.
 114. Midwood KS, Hussenet T, Langlois B, Orend G. Advances in tenascin-C biology. *Cell Mol Life Sci*; 2011 Oct 1;68(19):3175–99.
 115. Xu H, Bai D, Ruest L-B, Feng JQ, Guo Y-W, Tian Y, Jing Y, He Y, Han X-L. Expression analysis of α -smooth muscle actin and tenascin-C in the periodontal ligament under orthodontic loading or *in vitro* culture. *Int J Oral Sci*; 2015 Sep 11;7(4):232–41.
 116. Li J, Liu Y, Wang Y, Xu W. Expression of tenascin-C in a rat vocal fold injury model and its regulation of fibroblasts. *Laryngoscope*; 2018 Sep;128(9):E316–22.
 117. Chiquet-Ehrismann R, Tucker RP. Tenascins and the importance of adhesion modulation. *Cold Spring Harb Perspect Biol*; 2011 May 1;3(5):a004960–0.
 118. Chiquet-Ehrismann R, Orend G, Chiquet M, Tucker RP, Midwood KS. Tenascins in stem cell niches. *Matrix Biol*; 2014 Jul;37:112–23.
 119. Midwood KS, Orend G. The role of tenascin-C in tissue injury and tumorigenesis. *J Cell Commun Signal*; 2009 Dec;3(3-4):287–310.
 120. Yang Z, Ni W, Cui C, Fang L, Xuan Y. Tenascin C is a prognostic determinant and potential cancer-associated fibroblasts marker for breast ductal carcinoma. *Exp Mol Pathol. Academic Press*; 2017 Apr 1;102(2):262–7.
 121. Yates CC, Bodnar R, Wells A. Matrix control of scarring. *Cell Mol Life Sci*; 2011 Mar 10;68(11):1871–81.
 122. Yates CC, Nuschke A, Rodrigues M, Whaley D, Dechant JJ, Taylor DP, Wells A. Improved Transplanted Stem Cell Survival in a Polymer Gel Supplemented with Tenascin C Accelerates Healing and Reduces Scarring of Murine Skin Wounds. *Cell Transplant*; 2017 Jan;26(1):103–13.

123. Giblin SP, Midwood KS. Tenascin-C: Form versus function. *Cell Adh Migr*; 2015;9(1-2):48–82.
124. Lutz R, Sakai T, Chiquet M. Pericellular fibronectin is required for RhoA-dependent responses to cyclic strain in fibroblasts. *J Cell Sci*; 2010 May 1;123(9):1511–21.
125. Effenbein A, Simons M. Syndecan-4 signaling at a glance. *J Cell Sci*; 2013 Aug 30;126(17):3799–804.
126. Wallner K, Li C, Shah PK, Wu K-J, Schwartz SM, Sharifi BG. EGF-Like Domain of Tenascin-C Is Proapoptotic for Cultured Smooth Muscle Cells. *Arterioscl Thromb Vasc Biol*; 2004 Aug 1;24(8):1416–21.
127. Siri A, Knäuper V, Veirana N, Caocci F, Murphy G, Zardi L. Different susceptibility of small and large human tenascin-C isoforms to degradation by matrix metalloproteinases. *J Biol Chem*; 1995 Apr 14;270(15):8650–4.
128. Giblin SP, Midwood KS. Tenascin-C: Form versus function. *Cell Adhes Migr*; 2015;9(1-2):48–82.
129. Bell SC, Pringle JH, Taylor DJ, Malak TM. Alternatively spliced tenascin-C mRNA isoforms in human fetal membranes. *Mol Hum Reprod*; 1999 Nov;5(11):1066–76.
130. Saito Y, Imazeki H, Miura S, Yoshimura T, Okutsu H, Harada Y, Ohwaki T, Nagao O, Kamiya S, Hayashi R, Kodama H, Handa H, Yoshida T, Fukai F. A peptide derived from tenascin-C induces beta1 integrin activation through syndecan-4. *J Biol Chem*; 2007 Nov 30;282(48):34929–37.
131. Ambort D, Brellier F, Becker-Pauly C, Stöcker W, Andrejevic-Blant S, Chiquet M, Sterchi EE. Specific processing of tenascin-C by the metalloprotease meprinbeta neutralizes its inhibition of cell spreading. *Matrix Biol*; 2010 Jan;29(1):31–42.
132. To WS, Midwood KS. Cryptic domains of tenascin-C differentially control fibronectin fibrillogenesis. *Matrix Biol*; 2010 Sep 1;29(7):573–85.
133. To WS, Midwood KS. Identification of Novel and Distinct Binding Sites within Tenascin-C for Soluble and Fibrillar Fibronectin. *J Biol Chem*; 2011 Apr 22;286(17):14881–91.
134. Trebaul A, Chan EK, Midwood KS. Regulation of fibroblast migration by tenascin-C. *Biochem Soci Transact*; 2007 Aug 1;35(4):695–7.
135. Midwood KS, Williams LV, Schwarzbauer JE. Tissue repair and the dynamics of the extracellular matrix. *Int J Biochem Cell Biol*; 2004 Jun;36(6):1031–7.
136. Monnier VM, Mustata GT, Biemel KL, Reihl O, Lederer MO, Zhenyu D, Sell DR. Cross-linking of the extracellular matrix by the Maillard reaction in aging and diabetes: An update on “a puzzle nearing resolution.”. *Ann N Y Acad Sci*; 2005. pp. 533–44.
137. Riching KM, Cox BL, Salick MR, Pehlke C, Riching AS, Ponik SM, Bass BR, Crone WC, Jiang Y, Weaver AM, Eliceiri KW, Keely PJ. 3D Collagen Alignment Limits Protrusions to Enhance Breast Cancer Cell Persistence. *Biophys J*; 2014;107(11):2546–58.
138. Handorf AM, Zhou Y, Halanski MA, Li W-J. Tissue Stiffness Dictates Development, Homeostasis, and Disease Progression. *Organogenesis*; 2015 Mar 2;11(1):1–15.
139. Piersma B, Hayward MK, Weaver VM. Fibrosis and cancer: A strained relationship. *Biochim Biophys Acta Rev Cancer*; 2020 Apr 1;1873(2):188356.
140. Lampi MC, Reinhart-King CA. Targeting extracellular matrix stiffness to attenuate disease: From molecular mechanisms to clinical trials. *Sci Transla Med*; 2018 Jan 3;10(422):eaao0475.
141. Tschumperlin DJ, Lagares D. Mechano-therapeutics: Targeting Mechanical Signaling in Fibrosis and

- Tumor Stroma. *Pharmacol Ther*; 2020 Aug;212:107575.
142. Delaine-Smith R, Wright N, Hanley C, Hanwell R, Bhome R, Bullock M, Drifka C, Eliceiri K, Thomas G, Knight M, Mirnezami A, Peake N. Transglutaminase-2 Mediates the Biomechanical Properties of the Colorectal Cancer Tissue Microenvironment that Contribute to Disease Progression. *Cancers*; 2019 May;11(5):701.
 143. Simon DD, Niklason LE, HUMPHREY JD. Tissue Transglutaminase, Not Lysyl Oxidase, Dominates Early Calcium-Dependent Remodeling of Fibroblast-Populated Collagen Lattices. *Acta Anatomica*; 2015 Jul 1;200(2):104–17.
 144. Greenberg CS, Birckbichler PJ, Rice RH. Transglutaminases: multifunctional cross-linking enzymes that stabilize tissues. *FASEB J*; 1991 Dec;5(15):3071–7.
 145. Ritter SJ, Davies PJ. Identification of a transforming growth factor-beta1/bone morphogenetic protein 4 (TGF-beta1/BMP4) response element within the mouse tissue transglutaminase gene promoter. *J Biol Chem*; 1998 May 22;273(21):12798–806.
 146. Gundemir S, Colak G, Tucholski J, Johnson GVW. Transglutaminase 2: A molecular Swiss army knife. *Biochim Biophys Acta Mol Cell Res*; 2012 Feb;1823(2):406–19.
 147. Telci D, Collighan RJ, Basaga H, Griffin M. Increased TG2 Expression Can Result in Induction of Transforming Growth Factor β 1, Causing Increased Synthesis and Deposition of Matrix Proteins, Which Can Be Regulated by Nitric Oxide. *J Biol Chem*; 2009 Oct 16;284(43):29547–58.
 148. Lightner VA, Erickson HP. Binding of hexabrachion (tenascin) to the extracellular matrix and substratum and its effect on cell adhesion. *J Cell Sci*; 1990 Feb;95 (Pt 2)(2):263–77.
 149. Chiquet-Ehrismann R. Anti-adhesive molecules of the extracellular matrix. *Curr Opin Cell Biol*; 1991 Oct 1;3(5):800–4.
 150. Zemskov EA. The role of tissue transglutaminase in cell-matrix interactions. *Front Biosci*; 2006;11(1):1057.
 151. Radwanska A, Grall D, Schaub S, la Forest Divonne SB-D, Ciais D, Rekima S, Rupp T, Sudaka A, Orend G, Van Obberghen-Schilling E. Counterbalancing anti-adhesive effects of Tenascin-C through fibronectin expression in endothelial cells. *Sci Rep*; 2017 Oct 6;7(1):12762.
 152. Mackie EJ, Halfter W, Liverani D. Induction of tenascin in healing wounds. *J Cell Biol*; 1988 Jan 1;107(6 II):2757–67.
 153. Huelsz-Prince G, Belkin AM, vanBavel E, Bakker ENTP. Activation of Extracellular Transglutaminase 2 by Mechanical Force in the Arterial Wall. *J Vasc Res*; 2013;50(5):383–95.
 154. Chiquet M, Renedo AS, Huber F, Flück M. How do fibroblasts translate mechanical signals into changes in extracellular matrix production? *Matrix Biol*; 2003 Mar;22(1):73–80.
 155. Fluck M, Tunc-Civelek V, Chiquet M. Rapid and reciprocal regulation of tenascin-C and tenascin-Y expression by loading of skeletal muscle. *J Cell Sci*; 2000 Oct 15;113(20):3583–91.
 156. Webb CMB, Webb CM, Zaman G, Zaman G, Mosley JR, Mosley JR, Tucker RP, Tucker RP, Lanyon LE, Lanyon LE, Mackie EJ, Mackie EJ. Expression of tenascin-C in bones responding to mechanical load. *J Bone Miner Res*; 1997 Jan;12(1):52–8.
 157. Chiquet-Ehrismann R, Mackie EJ, Pearson CA, Sakakura T. Tenascin: an extracellular matrix protein involved in tissue interactions during fetal development and oncogenesis. *Cell*; 1986 Oct 10;47(1):131–9.

158. Orend G, Chiquet-Ehrismann R. Tenascin-C induced signaling in cancer. *Cancer Lett*; 2006 Dec 8;244(2):143–63.
159. Olsen KC, Sapinoro RE, Kottmann RM, Kulkarni AA, Iismaa SE, Johnson GVW, Thatcher TH, Phipps RP, Sime PJ. Transglutaminase 2 and Its Role in Pulmonary Fibrosis. *Am J Resp Critical Care Med*; 2011 Sep 15;184(6):699–707.
160. Wang Z, Stuckey DJ, Murdoch CE, Camelliti P, Lip GYH, Griffin M. Cardiac fibrosis can be attenuated by blocking the activity of transglutaminase 2 using a selective small-molecule inhibitor. *Cell Death Dis*; 2018 Apr 27;9(6):45.
161. Eckert RL. Transglutaminase 2 takes center stage as a cancer cell survival factor and therapy target. *Mol Carcinog*; 2019 Jun 1;58(6):837–53.
162. Van Obberghen-Schilling E, Tucker RP, Saupe F, Gasser I, Cseh B, Orend G. Fibronectin and tenascin-C: accomplices in vascular morphogenesis during development and tumor growth. *Int J Dev Biol*; 2011;55(4-5):511–25.
163. Radek JT, Jeong J-M, Murthy SNP, Ingham KC, Lorand L. Affinity of human erythrocyte transglutaminase for a 42-kDa gelatin-binding fragment of human plasma fibronectin. *Proc Natl Acad Sci*; 1993 Apr 15;90(8):3152–6.
164. Lundell A, Olin AI, Mörgelin M, al-Karadaghi S, Aspberg A, Logan DT. Structural basis for interactions between tenascins and lectican C-type lectin domains: evidence for a crosslinking role for tenascins. *Structure*; 2004 Aug;12(8):1495–506.
165. Midwood KS, Valenick LV, Hsia HC, Schwarzbauer JE. Coregulation of fibronectin signaling and matrix contraction by tenascin-C and syndecan-4. *Mol Biol Cell*; 2004 Dec;15(12):5670–7.
166. Chiquet M, Tunç-Civelek V, Sarasa-Renedo A. Gene regulation by mechanotransduction in fibroblasts. *Appl Physiol Nutr Metab*; 2007 Oct;32(5):967–73.
167. Maier S, Lutz R, Gelman L, Sarasa-Renedo A, Schenk S, Grashoff C, Chiquet M. Tenascin-C induction by cyclic strain requires integrin-linked kinase. *Biochim Biophys Acta*; 2008 Jun 1;1783(6):1150–62.
168. Tucker RP, Chiquet-Ehrismann R. Tenascin-C: Its functions as an integrin ligand. *Intl J Biochem Cell Biol*; 2015 Aug;65:165–8.
169. Belkin AM. Extracellular TG2: emerging functions and regulation. *FEBS J*; 2011 Nov 21;278(24):4704–16.
170. Belkin AM, Zemskov EA, Hang J, Akimov SS, Sikora S, Strongin AY. Cell-Surface-Associated Tissue Transglutaminase Is a Target of MMP-2 Proteolysis. *Biochemistry*; 2004 Sep;43(37):11760–9.
171. Nurminskaya MV, Belkin AM. Cellular functions of tissue transglutaminase. *Int Rev Cell Mol Biol*; 2012;294:1–97.
172. Howard EW, Crider BJ, Updike DL, Bullen EC, Parks EE, Haaksma CJ, Sherry DM, Tomasek JJ. MMP-2 expression by fibroblasts is suppressed by the myofibroblast phenotype. *Exp Cell Res*; 2012 Aug 1;318(13):1542–53.
173. Chiquet M, Sarasa-Renedo A, Tunç-Civelek V. Induction of tenascin-C by cyclic tensile strain versus growth factors: distinct contributions by Rho/ROCK and MAPK signaling pathways. *Biochim Biophys Acta Mol Cell Res*; 2004 Sep 17;1693(3):193–204.
174. Nielsen MFB, Mortensen MB, Detlefsen S. Typing of pancreatic cancer-associated fibroblasts identifies different subpopulations. *World J Gastroenterol*; 2018 Nov 7;24(41):4663–78.

175. Espitia Pinzón N, Brevé JJP, Bol JGJM, Drukarch B, Baron W, van Dam A-M. Tissue transglutaminase in astrocytes is enhanced by inflammatory mediators and is involved in the formation of fibronectin fibril-like structures. *J Neuroinflam*; 2017 Dec 28;14(1):260.
176. Ohe R, Aung NY, Meng H, Kabasawa T, Suto A, Tamazawa N, Yang S, Kato T, Yamakawa M. Localization of collagen modifying enzymes on fibroblastic reticular cells and follicular dendritic cells in non-neoplastic and neoplastic lymphoid tissues. *Leukemia & Lymphoma*; 2015 Dec 24;57(7):1687–96.
177. Tomko LA, Hill RC, Barrett A, Szulcowski JM, Conklin MW, Eliceiri KW, Keely PJ, Hansen KC, Ponik SM. Targeted matrisome analysis identifies thrombospondin-2 and tenascin-C in aligned collagen stroma from invasive breast carcinoma. *Sci Rep*; 2018 Aug 28;8(1):646.
178. Wang Y, Couture OP, Qu L, Uthe JJ, Bearson SM, Kuhar D, Lunney JK, Nettleton D, Dekkers JC, Tuggle CK. Analysis of Porcine Transcriptional Response to *Salmonella enterica* serovar *Choleraesuis* suggests novel targets of NFkappaB are activated in the Mesenteric Lymph Node. *BMC Genomics*; 2008;9(1):437.

3 Tissue transglutaminase in fibrosis – more than an extracellular matrix cross-linker

The work presented in this chapter has been published and is reprinted from Current Opinion in Biomedical Engineering. Elsevier; 2019 Jun 1;10:156–64.

Mario C. Benn, Willi Weber, Enrico Klotzsch, Viola Vogel, Simon A. Pot. (2019) Tissue transglutaminase in fibrosis — more than an extracellular matrix cross-linker.

M.C.B. and S.A.P. conceptualized and designed the structure of the review manuscript and drafted the figures; V.V. and E.K. critically revised the figure drafts; W.W. and E.K. created the figures; **M.C.B.**, S.A.P., E.K. and V.V. wrote the manuscript. All authors critically revised the manuscript for important intellectual content and edited the manuscript drafts. **M.C.B.** and S.A.P. contributed equally.

3.1 Abstract

Tissue transglutaminase (TG2) is upregulated in the pathogenesis of a wide variety of chronic diseases. In this review special emphasis will be placed on fundamental mechanisms underlying the critical role of TG2 in fibroproliferative disorders. TG2 is best known for its cross-linking capacities in the extracellular space but has many critical and multifaceted roles beyond protein cross-linking, which are driven by the conformation and specific localization of the molecule.

As extracellular crosslinker TG2 promotes fibrotic disease through the storage of latent TGF- β 1 in a stiffened extracellular matrix (ECM). As membrane-bound cell adhesion cofactor and signalling protein and intracellular crosslinker or G-protein, TG2 promotes fibrotic disease through cell survival and profibrotic pathway activation on a signalling, transcriptional and translational level. Similarities between the roles that TG2 plays in scar tissue and in the tumor stroma suggest that a deeper understanding of key common pathways in disease pathogenesis and progression might lead to the identification of novel treatment targets and the development of new drugs and diagnostic methods.

3.2 Introduction

Tissue transglutaminase (TG2), also named tTG, EC 2.3.2.13, is the most studied representative of a structurally and functionally related family of proteins of which nine members have been identified in humans [1,2]. TG2 is best known for its catalytic transamidation activity, resulting in the Ca²⁺ dependent post-translational formation of covalent isopeptide bonds between glutamine and lysine residues [1]. Beyond its catalytic core, TG2 consists of an N-terminal β -sandwich and two C-terminal β -barrel domains (Figure 1, left) [3–5]. Far less understood are TG2s multiple functions at the cell membrane, in the cytoplasm and in the cell nucleus, such as adhesion, migration, growth, proliferation, survival, apoptosis, differentiation and phenotype modulation [6,7]. TG2 is an integrin and syndecan-binding adhesion co-receptor for fibronectin (Fn). Approximately 5–40% of β 1 integrins are in complex with TG2 and almost all cell-membrane bound TG2 forms 1:1 complexes with integrins [8,9], which suggests a prominent role for TG2 at the cell membrane. While the focus is often on its crosslinking capacities in the extracellular space, TG2 is also active through non-enzymatic protein–protein interactions in both the extra- and intracellular space as further highlighted below. The reader is also referred to the following comprehensive review [10].

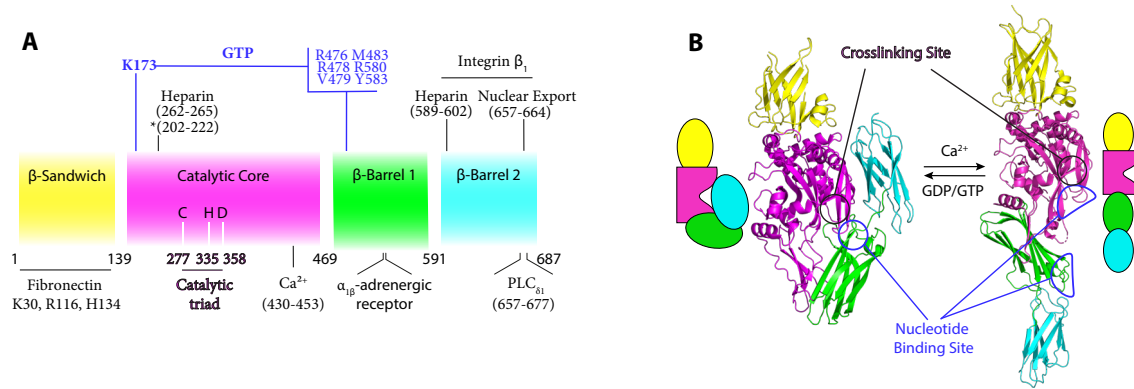


Fig. 1 Functional domains, binding sites and structure of tissue transglutaminase (TG2).

Beyond its catalytic core (140 - 454), TG2 consists of an N-terminal β -sandwich motif (1 - 139) and two C-terminal β -barrel domains (1: 469-591; 2: 592-687) [3–5]. The most relevant functional binding sites will be described briefly.

A) Recent studies identified residues K30, R116 and H134 on the N-terminal β -sandwich (yellow) as critical binding partners for the 42 kDa gelatin binding domain of Fn [5]. According to Belkin et al. TG2-integrin binding is disrupted upon deletion of C-terminal β -barrel 2 (blue), which indicates that integrin binding sites reside on that domain [4]. The catalytic core region (magenta) contains the active cross-linking site with the catalytic triad residues (C277, H335, D358). GTP (nucleotide) binding takes place on the catalytic core (K173) and β -barrel 1 (green) (R476, R478, V479, M483, R580, Y383) [70]. Heparin binding sites were identified on the catalytic core and β -barrel 2 [71]. (*) Wang et al. identified an alternative heparin binding site [9]. Ca^{2+} -binding to five of six Ca^{2+} binding sites on the catalytic core fosters allosteric catalytic site activation [72]. For information regarding further binding sites ($\alpha_{1\beta}$ -adrenergic receptor, $\text{PLC}\delta_1$, nuclear export signalling peptide) the reader is referred to the following references [70,71].

B) X-ray crystallography demonstrated that enzymatic cross-linking activity of TG2 is only possible in the Ca^{2+} -induced open-state conformation (PDB: 2Q3Z, [3]) with exposed catalytic triad residues. Nucleotide binding induces the closed-state conformation (PDB: 1KV3) with catalytic triad residues blocked by β -barrels 1 and 2 [73]. However, since TG2 has many non-enzymatic functions, “conformational state” and “activity” must be carefully distinguished [24].

Figures are adapted and modified with permission from A [70] and B [24].

3.3 TG2 is upregulated in the pathogenesis of a wide variety of chronic diseases

In most cases, the pathophysiological significance of TG2-induced modifications remains unclear. However, it is well documented that TG2 is involved in the pathogenesis of a wide variety of diseases, most notably neoplastic and fibroproliferative, including most malignant cancers and pulmonary, kidney and cardiac fibrosis [11–14]. TG2 expression is highly correlated with cancer cell survival, malignancy, metastasis and treatment resistance [13,15]. TG2 morphologically and functionally ‘shapes’ the tumor and scar tissue stroma through ECM cross-linking and binding of TGF- β 1 to the ECM, thus priming TGF- β 1, one of the most effective profibrotic stimuli, for release and activation [16,17]. Also, through its cell attachment and signalling mediator functions and its intracellular signalling and crosslinking functions, TG2 can promote tumor cell survival and the

development of fibrotic (scar) cell phenotypes [7,8,18–23]. Major attempts are thus underway to develop potent TG2 inhibitors.

3.4 Environmental sensing through major conformational TG2 changes

The biochemical functions of TG2 largely depend on its molecular conformation (Figure 1). Various environmental factors cause allosteric conformational changes and include extracellular, intracellular and intranuclear Ca^{2+} concentrations, GDP and GTP concentrations and MMP-mediated release of membrane bound TG2 into the ECM [7,9]. When bound to GTP or GDP, TG2 adopts a closed conformation with the two C-terminal β -barrel domains folded in and blocking substrate access to the catalytic site. However, with excess Ca^{2+} levels, TG2s affinity for GDP and GTP is reduced leading to a very large change in molecular shape presenting an open molecular conformation with an accessible active catalytic cross-linking site (Figure 1b) [3,24]. Low Ca^{2+} and high GDP/GTP concentrations in the cytoplasm cause TG2 to adopt a predominantly closed conformation inside the cell [25]. The conformation that TG2 adopts at the cell membrane is largely unknown. No structure has yet been solved of TG2 complexed to any binding partner even though Fn can bind to the open and closed conformations of TG2 [5]. Closed state cytosolic TG2 can bind to heparan sulfate epitopes on exosome membrane associated Syndecan-4 molecules which have a high binding affinity for the closed conformation of TG2. Syndecan-4-dependent translocation of TG2 from the cytoplasm to the extracellular space takes place by fusion of exosomes with the outer cell membrane [9,26–28]. This mechanism was identified in fibrotic kidney disease by Furini et al. [27]. Syndecan-4-associated TG2 delivered to the cell surface can interact with integrins and fibronectin to form membrane associated protein complexes exerting cell adhesion/receptor protein functions (Figure 2, 3) [7,29]. MMP2/9 activity can lead to Syndecan-TG2 shedding from the cell surface (Figure 3)[9]. Finally, TG2 predominantly adopts an open conformation in the extracellular space due to high Ca^{2+} and low GDP/GTP concentrations [24]. Formation of two disulfide bonds between cysteine residues under oxidizing conditions at the catalytic site renders TG2 catalytically inactive in its open conformation [30]. Active oxygen reduction mechanisms in the ECM therefore promote the catalytic ECM cross-linking activity of TG2 in the extracellular space [31]. Mechanical forces within the physiological range for cells have been shown to induce allosteric conformational and functional changes in proteins [32]. Also, TG2 is concentrated at focal adhesion sites [8,18] and the integrin and Fn-binding sites are located at opposite sides of the TG2 molecule with the catalytically active site and hinge region in between (Figure 1) [4]. It is therefore likely that cells that generate mechanical forces and pull at adhesion sites that are physically connected to

the extracellular matrix can induce TG2 'opening' and catalyze disulfide bond reduction, thus inducing and stabilizing an open catalytically active conformation of TG2 [3,4].

3.5 Extra- and intracellular: Transamidation and cross-linking functions of TG2 / TGF- β 1 storage in the ECM

The catalytic activity of TG2 can affect protein conformation by generating intramolecular cross-links and can catalyze the formation of covalently linked dimers, oligomers, and polymers [6]. The transamidation activity of TG2 results in protease-resistant inter- or intramolecular isopeptide bonds which effectively cross-link ECM fibrils, stiffening the ECM and protecting the ECM from proteolytic degradation [24]. A matrix reservoir of inactive TGF- β 1 is formed via TG2-mediated cross-linking of latent TGF- β 1 binding protein (LTBP-1) to the ECM (Figure 2, 3) [33,34]. ECM-bound TGF- β 1 can be activated via mechanical release (Figure 3), which is especially effective when the LTBP-1 is bound to a stiff, deformation resistant ECM that counters cell-applied forces [17,33,35,36]. As such, TGF- β 1 activation is thought to be facilitated by TG2 since TG2 cross-links LTBP to the ECM and can turn a compliant matrix into a stiffer matrix via cross-linking of various ECM components [37]. ECM prestress sensitizes latent TGF- β 1 for activation [36], which might explain increased TGF- β 1 release from stiffened fibrotic tissues. Since increased and dysregulated expression, deposition and cross-linking of ECM cause loss of vital organ function in fibrosis, TG2 and TGF- β 1 are explored as targets for the treatment of fibrotic diseases.

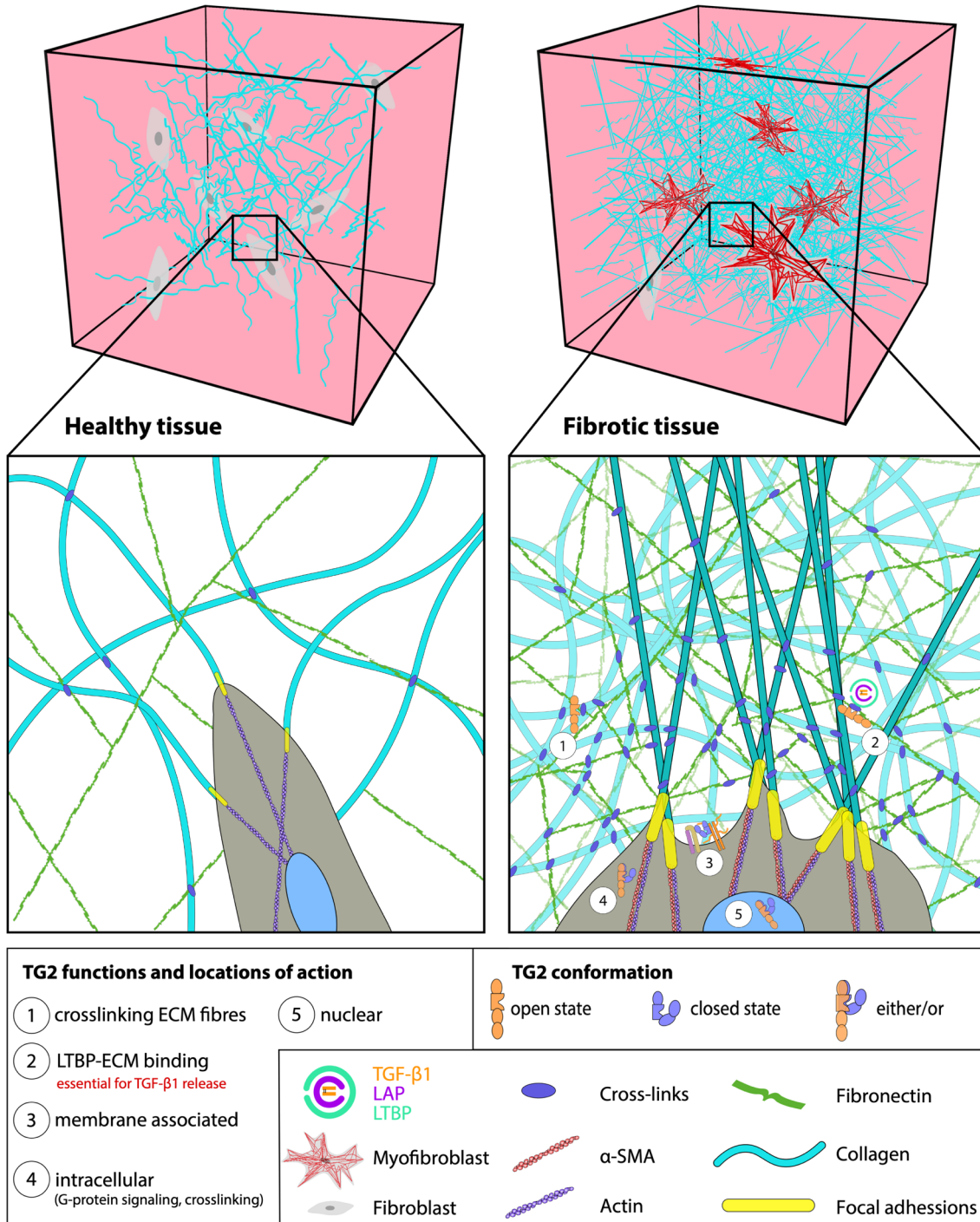


Fig. 2 TG2 functions depend on its localization, as well as its allosterically-regulated conformation as upregulated in many diseases.

Resident fibroblasts deposit and remodel the ECM in healthy tissues (top and middle left) [44], whereas α SMA expressing contractile myofibroblasts are the key players in fibrotic disease (top and middle right). Myofibroblast-dominated tissues are characterized by increased ECM fiber density and cross-linking. TG2 and TGF- β 1 are both upregulated in fibrotic tissues. The open conformation of TG2 cross-links ECM fibrils ① [1], and binds latent TGF- β 1 via LTBP-1 to the ECM ② [1,34,74]. TG2 interacts in closed or unknown conformation with cell membrane proteins ③, resulting in downstream signalling effects [9,29,41]. Cytosolic ④ and nuclear ⑤ TG2 activate intracellular signalling pathways and downstream gene expression through enzymatic (open state TG2) and non-enzymatic (closed state TG2) mechanisms.

3.6 Cell membrane: TG2 regulates cell adhesion and ligand affinity

TG2 binds to the fibronectin type I modules Fn17–9 of the collagen/gelatin binding site on the Fn molecule and interacts with cell membrane β 1, β 3 and β 5 integrins [8,38–40] and/or syndecan-4 (Figure 3) [9,28,29]. Syndecan-4 and integrin signalling is coordinated via direct complex formation of Fn-TG2, β -integrins and syndecan-4, indirect integrin cytoplasmic tail activation via Syndecan-4 activated PKC α or downstream convergence of integrin and syndecan signalling at p190RhoGAP (Figure 3) [29,41]. TG2-Fn-complexes offer cells an alternative binding site on Fn in addition to the classical integrin-Fn binding sites (e.g. RGD loop, synergy site) and facilitate RGD independent cell adhesion [28,29,42,43].

By promoting cell adhesion to Fn via cell surface integrins and syndecan-4, TG2 likely stimulates Fn fibril assembly through cell contraction-mediated Fn stretching and unmasking of Fn self-assembly sites [38,44]. Indirectly, integrin clustering and binding of TG2 at focal adhesions might concentrate TG2 catalyzed cross-linking of the dense Fn matrix at these sites as suggested by Zemskov et al. [18]. Proteolytic degradation of surface TG2 can shift cell-ECM recognition: cells cannot bind to collagen, if TG2 is bound to certain collagen-binding integrins, such as integrin α 1 β 1, likely due to steric hindrance [18]. MT1-MMP and/or MMP-2 degrade integrin-associated cell surface TG2 and restore α 1 β 1 integrin-collagen interactions, while at the same time suppressing cell adhesion and migration on fibronectin. This shift in cell-ECM recognition via dynamic regulation of surface TG2 can affect adhesion and migration of cells on various ECM ligands [7,18].

The importance of TG2 for cell adhesion is underlined by the discovery that TG2 was 1 out of only 10 proteins that consistently appeared in seven integrin adhesome datasets analyzed by Horton et al. [45].

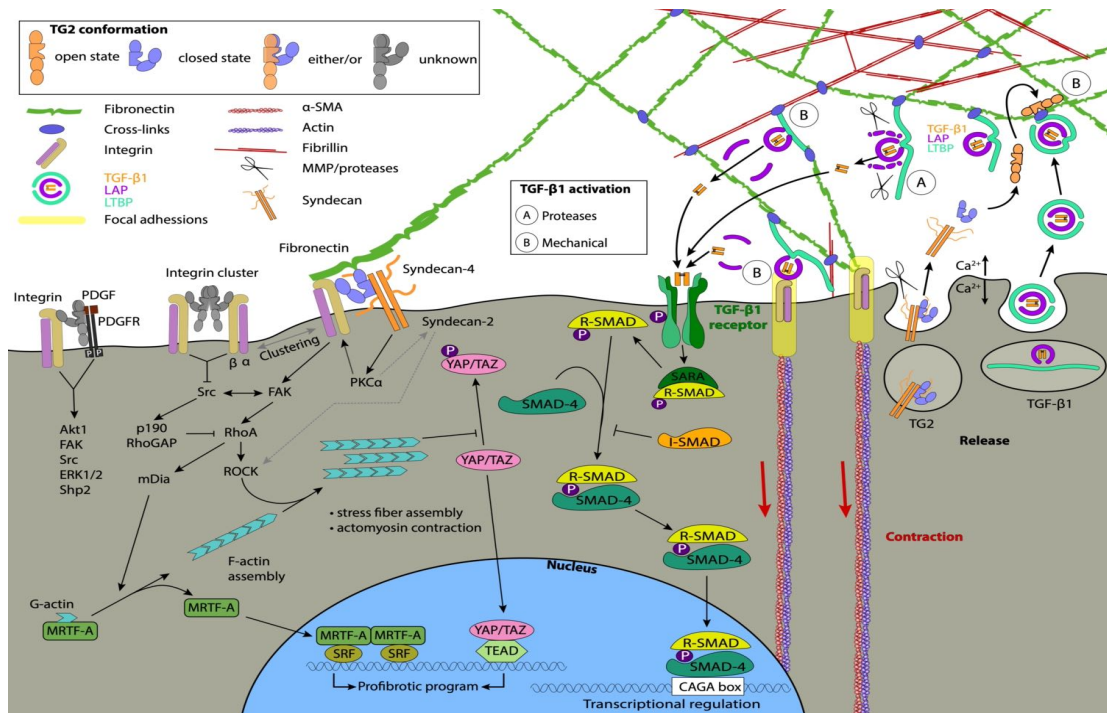


Fig. 3 Key pro-fibrotic roles of TG2 at the cell membrane and in the ECM.

The molecular sketches do not represent molecular dimensions nor potential conformational states. Unconventional cellular release and reuptake of TG2 are not depicted in this scheme. Figures are adapted and modified with permission from Belkin et al. [7] and Robertson et al. [75].

Membrane associated functions of TG2 (lower left section of figure):

TG2-integrin clusters, TG2-FN-Integrin and TG2-FN-integrin-syndecan-4 complexes are known to activate intracellular Src-FAK and inhibit p190RhoGAP through Src, with both pathways leading to RhoA-ROCK activation [7,8,19,29,41]. RhoA/ROCK pathway activation induces the assembly of cytoplasmic monomeric G-actin into F-actin fibers and the formation of stress fibers. Changes in actin dynamics are monitored by myocardin-related transcription factor A (MRTF-A), which binds to cytoplasmic G-actin, but dissociates from F-actin. Upon actin fiber assembly MRTF-A thus uncouples from G-actin and the released MRTF-A enters the nucleus. Alternatively, Rho-signalling and cytoskeletal stress drive the downregulation of YAP/TAZ phosphorylation and the subsequent nuclear translocation and activation of YAP/TAZ. Nuclear MRTF-A and YAP/TAZ both act as transcription cofactors that promote profibrotic gene expression [46,47]. RGD independent cell adhesion to Fn depends on Fn-TG2-syndecan-4 interaction and is mediated via cytoplasmic α5β1 integrin and syndecan-2 activation by Syndecan-4 activated PKCα [29]. Membrane-associated TG2 interacts with growth factor receptors (such as for PDGF, VEGF, FGF and EGF) and stimulates cell survival signalling pathways (e.g. FAK, Src, Akt, etc.) by promoting GF-receptor binding and activation [7,21].

Storage of latent TGF-β1 in the ECM and mechanoactivation of TGF-β1 (right section of figure):

TGF-β1 is secreted by cells in complex with its latency associated propeptide (LAP), which associates with latent TGF-β1 binding protein (LTBP-1) [76]. LTBP-1 facilitates secretion of TGF-β1 [77] and TG2 cross-links LTBP-1 to Fn and fibrillin ECM fibers [16,34]. As such, a matrix reservoir of inactive TGF-β1 is formed which is bound to the LTBP-1 and ECM and therefore unable to bind with its high affinity cell membrane receptor to activate the downstream SMAD-mediated signalling cascade [34,74]. Latent TGF-β1 can be activated through its release from the ECM-bound TGFβ-LAP-LTBP-1 complex by proteolysis (A) or integrin mediated cellular contraction (B) [33–35]. The N- and C-terminal matrix binding sequences of LTBP-1 [78] and integrin binding RGD sequence of LAP [79] are critical for the activation of TGF-β1. Cell membrane associated integrins bind to the RGD sequence on LAP (B) and can expose the ECM bound LTBP-1 to cellular contractile forces. This is especially effective when the LTBP-1 is bound to a stiff, deformation resistant ECM that counters cell-applied forces [17,33,35,36]. As such, TGF-β1 activation is thought to be facilitated by TG2 since TG2 cross-links LTBP to the ECM and can stiffen a compliant matrix via ECM cross-linking [37]. For a detailed review on TGF-β-LTBP interactions we refer the reader to a recent comprehensive review published by Rifkin et al. [74].

3.7 Cell membrane: TG2 as signalling protein

Almost all cell membrane-associated TG2 is bound to integrins [8], where TG2 dimers facilitate integrin clustering formation (Figure 3)[7,19]. Further ECM components (e.g. Fn) and cell membrane protein receptors that bind next to fibronectin's RGD-specific integrin binding site (e.g. Syndecan-4, PDGF, VEGF, FGF and EGF receptors) can be engaged by these TG2-integrin complexes to execute various cell adhesion (described above) and signalling functions (Figure 3) [7,9,21,29]. TG2-integrin clusters, TG2-Fn-integrin and TG2-Fn-integrin-syndecan-4 complexes are known to activate well reviewed integrin signalling cascades, resulting in RhoA-ROCK activation, actin filamentation and downstream release and nuclear translocation of MRTF-A and YAP/TAZ (Figure 3) [7,8,19,46,47]. Nuclear MRTF-A and YAP/TAZ both act as transcription cofactors that promote expression of profibrotic genes, including α SMA, Tenascin-C and CTGF, which can influence the tumor stroma and cancer development and promote fibrotic disease [17,48,49].

3.8 Inside the cell: Enzymatic and non-enzymatic TG2 activity

With low Ca^{2+} and high GDP/GTP concentrations in the cytoplasm, TG2 binds to and hydrolyzes GTP, assumes a closed conformation and acts as a G protein. For example, TG2 binds to c-Src and PI3-kinase, facilitating c-Src-dependent phosphorylation of PI3-kinase which promotes cell survival [22]. Due to fluctuations in Ca^{2+} levels, cytoplasmic open conformation cross-linking activity of TG2 can also be observed with various specific and unspecific target proteins. For example, TG2 drives the constitutive activation of NF- κ B through its cross-linking activity, which leads to increased TGF- β 1 expression (e.g. fibrotic diseases, cancer stroma), promotion of epithelial-mesenchymal transformation (increasing tumor malignancy) and cell survival [23,49]. Similarly, RhoA cross-linking and activation leads to increased stress fiber formation [50] and certain translation regulatory proteins like YB-1 can be crosslinked in a state that drives increased α SMA protein translation [20]. TG2 also regulates mitochondrial function and can initiate mitochondrial-driven apoptosis by crosslinking mitochondrial proteins in its open, catalytically active state [24,51]. At the same time, TG2 cross-linking stabilizes the structure of dying cells, prevents leakage of proteolytic enzymes and protects the environment of the cell from further damage [52]. Last, high TG2 levels increase autophagy of the tumor suppressor p53, which can help tumor cells escape apoptosis [53]. Nuclear TG2 has been shown to regulate gene expression via post-translational modification of transcriptional factors and related proteins, including Sp1, hypoxia inducible factor (HIF) 1 and histones [54]. The G-protein function of cytosolic TG2 typically enhances cell survival [22], whereas the transamidation activity of TG2 can lead to cell death or survival or even fibrotic changes

[20,23,49–51,55], depending on the target protein(s). Nuclear localization of TG2 is generally protective against cell death [56,57].

3.9 TG2 as major player in the development and maintenance of fibroproliferative diseases

Fibroproliferative disorders cause approximately 45% of the mortality in the developed world and appear in a wide spectrum from systemic to organ-specific fibrotic diseases. Besides increased mechanical tissue tension and the presence of certain ECM components like cellular fibronectin's ED-A domain, TGF- β 1 is one of the most effective profibrotic stimuli that drive the transformation of fibroblasts into myofibroblasts [17]. Myofibroblasts are the key players within fibroproliferative disorders [17,58]. They incorporate an excess of collagen and other fibrous proteins into the ECM while expressing strong contractile alpha smooth muscle actin (α SMA) positive stress fibers which contract the fibrotic matrix into a stiff, dysfunctional scar [17,33,48,59]. Interestingly, TG2 and TGF- β 1 reinforce each other in the progressive fibrotic and tumor stroma microenvironment [49]. As described in previous sections, TG2 facilitates the activation of TGF- β 1 in the ECM [16], the activation of profibrotic signalling cascades downstream from TG2- β -integrin-containing membrane signalling complexes [7] and the translation of α SMA [20]. TGF- β 1 on the other hand promotes TG2 transcription [60,61] leading to self-amplification of TG2 and TGF- β 1 in fibrotic tissues and explaining why both are upregulated in fibroproliferative disorders. The fact that TG2 knockout mice were protected against fibrosis [62,63] and that TG2 inhibition in mouse models of fibrosis significantly reduced the fibrotic phenotype [11,12,64] further underlines the critical role that TG2 plays in the pathogenesis and maintenance of fibrosis [65]. The relative contributions of catalytic and non-catalytic TG2 functions to healthy and diseased microenvironments still remain unknown. Inhibition of TG2s catalytic function can reduce cardiac fibrosis *in vivo* [11,64,66]. Wang et al. and Shinde et al. suggested further reduction of fibrosis via non-catalytic TG2-mediated mechanisms: reduced externalization of TG2 as a result of decreased interaction of intracellular TG2 with exosome membrane associated syndecan-4, decreased TGF- β 1-induced myofibroblast formation and reduced activation of fibrosis-associated genes [11,64].

3.10 Outlook: TG2 as common denominator in fibroproliferative and neoplastic diseases

The consensus in cancer research seems to mirror our descriptions of the profibrotic functions of TG2 outlined above. Extracellular TG2 in its open enzymatically active conformation promotes cancer cell malignancy through crosslinking of the tumor stroma [49,55]. Intracellular closed conformation TG2 promotes cancer cell survival and malignancy through survival pathway and EMT activation [22,49]. Stabilizing the open state of TG2 inside the cell promotes cell death and inhibits the malignant phenotype of cancer cells, thus representing a promising new avenue in the treatment of cancer [24,25]. Similarities between scar tissue and tumor stroma [67–69] suggest that the identification of key common pathways involved in the disease pathogenesis and progression might lead to the identification of novel treatment targets and the development of new drugs and diagnostic methods.

Beyond its role as ECM crosslinker, much future research is needed to understand the many roles of TG2, including cell adhesion stabilization and its nuclear functions. Also, translational research is required as just a few TG2 inhibitors are in clinical trials and none is available for clinical use [55].

3.11 Acknowledgements

This work was supported by the ETH Zurich and by Swiss National Science Foundation Grants (Grant no. 31003A_175839/1 to VV & CR32I3_156931 to VV), the Human Frontiers Science Program (Grant no. RGY0065/2017 to EK), the Volkswagenstiftung Experiment (Grant no. 95664 to EK) and by the foundation Velux Stiftung (Project n°1227 to SP).

3.12 Declarations of interest

none

3.13 References

1. Lorand L, Graham RM: Transglutaminases: crosslinking enzymes with pleiotropic functions. *Nat Rev Mol Cell Biol* 2003, 4:140–156.
2. Folk JE, Chung SI: Molecular and catalytic properties of transglutaminases. *Adv Enzymol Relat Areas Mol Biol* 1973, 38:109–191.
3. Pinkas DM, Strop P, Brunger AT, Khosla C: Transglutaminase 2 undergoes a large conformational change upon activation. *PLoS Biol* 2007, 5:e327.
4. Huelsz-Prince G, Belkin AM, VanBavel E, Bakker ENTP: Activation of extracellular transglutaminase 2 by mechanical force in the arterial wall. *J Vasc Res* 2013, 50:383–395.
5. Cardoso I, Østerlund EC, Stamnaes J, Iversen R, Andersen JT, Jørgensen TJD, Sollid LM: Dissecting the interaction between transglutaminase 2 and fibronectin. *Amino Acids* 2017, 49:489–500.
6. Nurminskaya MV, Belkin AM: Cellular functions of tissue transglutaminase. *Int Rev Cell Mol Biol* 2012, 294:1–97.
7. Belkin AM: Extracellular TG2: emerging functions and regulation. *FEBS J* 2011, 278:4704–4716.
8. Akimov SS, Krylov D, Fleischman LF, Belkin AM: Tissue transglutaminase is an integrin-binding adhesion coreceptor for fibronectin. *J Cell Biol* 2000, 148:825–838.
9. Wang Z, Collighan RJ, Pytel K, Rathbone DL, Li X, Griffin M: Characterization of heparin-binding site of tissue transglutaminase: its importance in cell surface targeting, matrix deposition, and cell signalling. *J Biol Chem* 2012, 287:13063–13083.
10. Kanchan K, Fuxreiter M, Fésüs L: Physiological, pathological, and structural implications of non-enzymatic protein-protein interactions of the multifunctional human transglutaminase 2. *Cell Mol Life Sci* 2015, 72:3009–3035.
11. Wang Z, Stuckey DJ, Murdoch CE, Camelliti P, Lip GYH, Griffin M: Cardiac fibrosis can be attenuated by blocking the activity of transglutaminase 2 using a selective small-molecule inhibitor. *Cell Death Dis* 2018, 9:613.
12. Olsen KC, Epa AP, Kulkarni AA, Kottmann RM, McCarthy CE, Johnson GV, Thatcher TH, Phipps RP, Sime PJ: Inhibition of transglutaminase 2, a novel target for pulmonary fibrosis, by two small electrophilic molecules. *Am J Respir Cell Mol Biol* 2014, 50:737–747.
13. Eckert RL: Transglutaminase 2 takes center stage as a cancer cell survival factor and therapy target. *Mol Carcinog* 2019, doi:10.1002/mc.22986.
14. Philp CJ, Siebeke I, Clements D, Miller S, Habgood A, John AE, Navaratnam V, Hubbard RB, Jenkins G, Johnson SR: Extracellular Matrix Cross-Linking Enhances Fibroblast Growth and Protects against Matrix Proteolysis in Lung Fibrosis. *Am J Respir Cell Mol Biol* 2018, 58:594–603.
15. Bagatur Y, Ilter Akulke AZ, Bihorac A, Erdem M, Telci D: Tissue transglutaminase expression is necessary for adhesion, metastatic potential and cancer stemness of renal cell carcinoma. *Cell Adh Migr* 2018, 12:138–151.
16. Troilo H, Steer R, Collins RF, Kielty CM, Baldock C: Independent multimerization of Latent TGF β Binding Protein-1 stabilized by cross-linking and enhanced by heparan sulfate. *Sci Rep* 2016, 6:34347.
17. Hinz B, McCulloch CA, Coelho NM: Mechanical regulation of myofibroblast phenocconversion and collagen contraction. *Exp Cell Res* 2019, 379:119–128.

18. Zemskov EA, Janiak A, Hang J, Waghray A, Belkin AM: The role of tissue transglutaminase in cell-matrix interactions. *Front Biosci* 2006, 11:1057–1076.
19. Janiak A, Zemskov EA, Belkin AM: Cell surface transglutaminase promotes RhoA activation via integrin clustering and suppression of the Src-p190RhoGAP signalling pathway. *Mol Biol Cell* 2006, 17:1606–1619.
20. Willis WL, Hariharan S, David JJ, Strauch AR: Transglutaminase-2 mediates calcium-regulated crosslinking of the Y-Box 1 (YB-1) translation-regulatory protein in TGF β 1-activated myofibroblasts. *Journal of Cellular Biochemistry* 2013, 114:2753–2769.
21. Zemskov EA, Loukinova E, Mikhailenko I, Coleman RA, Strickland DK, Belkin AM: Regulation of platelet-derived growth factor receptor function by integrin-associated cell surface transglutaminase. *J Biol Chem* 2009, 284:16693–16703.
22. Boroughs LK, Antonyak MA, Cerione RA: A novel mechanism by which tissue transglutaminase activates signalling events that promote cell survival. *J Biol Chem* 2014, 289:10115–10125.
23. Mann AP, Verma A, Sethi G, Manavathi B, Wang H, Fok JY, Kunnumakkara AB, Kumar R, Aggarwal BB, Mehta K: Overexpression of tissue transglutaminase leads to constitutive activation of nuclear factor- κ B in cancer cells: delineation of a novel pathway. *Cancer Res* 2006, 66:8788–8795.
24. Katt WP, Antonyak MA, Cerione RA: Opening up about Tissue Transglutaminase: When Conformation Matters More than Enzymatic Activity. *Med One* 2018, 3.
25. Katt WP, Blobel NJ, Komarova S, Antonyak MA, Nakano I, Cerione RA: A small molecule regulator of tissue transglutaminase conformation inhibits the malignant phenotype of cancer cells. *Oncotarget* 2018, 9:34379–34397.
26. Furini G, Verderio EAM: Spotlight on the Transglutaminase 2-Heparan Sulfate Interaction. *Med Sci (Basel)* 2019, 7.
27. Furini G, Schroeder N, Huang L, Boocock D, Scarpellini A, Coveney C, Tonoli E, Ramaswamy R, Ball G, Verderio C, et al.: Proteomic Profiling Reveals the Transglutaminase-2 Externalization Pathway in Kidneys after Unilateral Ureteric Obstruction. *J Am Soc Nephrol* 2018, 29:880–905.
28. Lortat-Jacob H, Burhan I, Scarpellini A, Thomas A, Imberty A, Vivès RR, Johnson T, Gutierrez A, Verderio EAM: Transglutaminase-2 interaction with heparin: identification of a heparin binding site that regulates cell adhesion to fibronectin-transglutaminase-2 matrix. *J Biol Chem* 2012, 287:18005–18017.
29. Wang Z, Collighan RJ, Gross SR, Danen EHJ, Orend G, Telci D, Griffin M: RGD-independent cell adhesion via a tissue transglutaminase-fibronectin matrix promotes fibronectin fibril deposition and requires syndecan-4/2 α 5 β 1 integrin co-signalling. *J Biol Chem* 2010, 285:40212–40229.
30. Stamnaes J, Pinkas DM, Fleckenstein B, Khosla C, Sollid LM: Redox Regulation of Transglutaminase 2 Activity. *Journal of Biological Chemistry* 2010, 285:25402–25409.
31. Plugis NM, Palanski BA, Weng C-H, Albertelli M, Khosla C: Thioredoxin-1 Selectively Activates Transglutaminase 2 in the Extracellular Matrix of the Small Intestine: implications for celiac disease. *J Biol Chem* 2017, 292:2000–2008.
32. Schoen I, Pruitt BL, Vogel V: The Yin-Yang of Rigidity Sensing: How Forces and Mechanical Properties Regulate the Cellular Response to Materials. *Annu Rev Mat Res* 2013, 43:589–618.
33. Klingberg F, Chau G, Walraven M, Boo S, Koehler A, Chow ML, Olsen AL, Im M, Lodyga M, Wells RG, et al.: The fibronectin ED-A domain enhances recruitment of latent TGF- β -binding protein-1 to the fibroblast matrix. *J Cell Sci* 2018, 131.

34. Nunes I, Gleizes PE, Metz CN, Rifkin DB: Latent transforming growth factor-beta binding protein domains involved in activation and transglutaminase-dependent cross-linking of latent transforming growth factor-beta. *J Cell Biol* 1997, 136:1151–1163.
35. Buscemi L, Ramonet D, Klingberg F, Formey A, Smith-Clerc J, Meister J-J, Hinz B: The single-molecule mechanics of the latent TGF- β 1 complex. *Curr Biol* 2011, 21:2046–2054.
36. Klingberg F, Chow ML, Koehler A, Boo S, Buscemi L, Quinn TM, Costell M, Alman BA, Genot E, Hinz B: Prestress in the extracellular matrix sensitizes latent TGF- β 1 for activation. *J Cell Biol* 2014, 207:283–297.
37. Greenberg CS, Birckbichler PJ, Rice RH: Transglutaminases: multifunctional cross-linking enzymes that stabilize tissues. *FASEB J* 1991, 5:3071–3077.
38. Akimov SS, Belkin AM: Cell-surface transglutaminase promotes fibronectin assembly via interaction with the gelatin-binding domain of fibronectin: a role in TGFbeta-dependent matrix deposition. *J Cell Sci* 2001, 114:2989–3000.
39. Mangala LS, Fok JY, Zorrilla-Calancha IR, Verma A, Mehta K: Tissue transglutaminase expression promotes cell attachment, invasion and survival in breast cancer cells. *Oncogene* 2007, 26:2459–2470.
40. Soluri MF, Boccafoschi F, Cotella D, Moro L, Forestieri G, Autiero I, Cavallo L, Oliva R, Griffin M, Wang Z, et al.: Mapping the minimum domain of the fibronectin binding site on transglutaminase 2 (TG2) and its importance in mediating signalling, adhesion, and migration in TG2-expressing cells. *FASEB J* 2019, 33:2327–2342.
41. Bass MD, Morgan MR, Roach KA, Settleman J, Goryachev AB, Humphries MJ: p190RhoGAP is the convergence point of adhesion signals from alpha 5 beta 1 integrin and syndecan-4. *J Cell Biol* 2008, 181:1013–1026.
42. Verderio EAM, Telci D, Okoye A, Melino G, Griffin M: A Novel RGD-independent Cell Adhesion Pathway Mediated by Fibronectin-bound Tissue Transglutaminase Rescues Cells from Anoikis. *Journal of Biological Chemistry* 2003, 278:42604–42614.
43. Telci D, Wang Z, Li X, Verderio EAM, Humphries MJ, Baccarini M, Basaga H, Griffin M: Fibronectin-tissue transglutaminase matrix rescues RGD-impaired cell adhesion through syndecan-4 and beta1 integrin co-signalling. *J Biol Chem* 2008, 283:20937–20947.
44. Vogel V: Unraveling the Mechanobiology of Extracellular Matrix. *Annu Rev Physiol* 2018, 80:353–387.
45. Horton ER, Byron A, Askari JA, Ng DHJ, Millon-Frémillon A, Robertson J, Koper EJ, Paul NR, Warwood S, Knight D, et al.: Definition of a consensus integrin adhesome and its dynamics during adhesion complex assembly and disassembly. *Nat Cell Biol* 2015, 17:1577–1587.
46. Asparuhova MB, Gelman L, Chiquet M: Role of the actin cytoskeleton in tuning cellular responses to external mechanical stress. *Scand J Med Sci Sports* 2009, 19:490–499.
47. Panciera T, Azzolin L, Cordenonsi M, Piccolo S: Mechanobiology of YAP and TAZ in physiology and disease. *Nat Rev Mol Cell Biol* 2017, 18:758–770.
48. Kennedy L, Shi-Wen X, Carter DE, Abraham DJ, Leask A: Fibroblast adhesion results in the induction of a matrix remodelling gene expression program. *Matrix Biol* 2008, 27:274–281.
49. Agnihotri N, Mehta K: Transglutaminase-2: evolution from pedestrian protein to a promising therapeutic target. *Amino Acids* 2017, 49:425–439.
50. Singh US, Kunar MT, Kao YL, Baker KM: Role of transglutaminase II in retinoic acid-induced activation of RhoA-associated kinase-2. *EMBO J* 2001, 20:2413–2423.

51. Pavlyukov MS, Antipova NV, Balashova MV, Shakhparonov MI: Detection of Transglutaminase 2 conformational changes in living cell. *Biochem Biophys Res Commun* 2012, 421:773–779.
52. Park D, Choi SS, Ha K-S: Transglutaminase 2: a multi-functional protein in multiple subcellular compartments. *Amino Acids* 2010, 39:619–631.
53. Kang JH, Lee J-S, Hong D, Lee S-H, Kim N, Lee W-K, Sung T-W, Gong Y-D, Kim S-Y: Renal cell carcinoma escapes death by p53 depletion through transglutaminase 2-chaperoned autophagy. *Cell Death Dis* 2016, 7:e2163.
54. Kuo T-F, Tatsukawa H, Kojima S: New insights into the functions and localization of nuclear transglutaminase 2. *FEBS J* 2011, 278:4756–4767.
55. Katt WP, Antonyak MA, Cerione RA: The diamond anniversary of tissue transglutaminase: a protein of many talents. *Drug Discov Today* 2018, 23:575–591.
56. Milakovic T, Tucholski J, McCoy E, Johnson GVW: Intracellular localization and activity state of tissue transglutaminase differentially impacts cell death. *J Biol Chem* 2004, 279:8715–8722.
57. Gundemir S, Johnson GVW: Intracellular localization and conformational state of transglutaminase 2: implications for cell death. *PLoS One* 2009, 4:e6123.
58. Van De Water L, Varney S, Tomasek JJ: Mechanoregulation of the Myofibroblast in Wound Contraction, Scarring, and Fibrosis: Opportunities for New Therapeutic Intervention. *Adv Wound Care* 2013, 2:122–141.
59. Goffin JM, Pittet P, Csucs G, Lussi JW, Meister J-J, Hinz B: Focal adhesion size controls tension-dependent recruitment of alpha-smooth muscle actin to stress fibers. *J Cell Biol* 2006, 172:259–268.
60. Ritter SJ, Davies PJ: Identification of a transforming growth factor-beta1/bone morphogenetic protein 4 (TGF- β 1/BMP4) response element within the mouse tissue transglutaminase gene promoter. *J Biol Chem* 1998, 273:12798–12806.
61. Sándor K, Daniel B, Kiss B, Kovács F, Szondy Z: Transcriptional control of transglutaminase 2 expression in mouse apoptotic thymocytes. *Biochim Biophys Acta* 2016, 1859:964–974.
62. Shweke N, Boulos N, Jouanneau C, Vandermeersch S, Melino G, Dussaule J-C, Chatziantoniou C, Ronco P, Boffa J-J: Tissue Transglutaminase Contributes to Interstitial Renal Fibrosis by Favoring Accumulation of Fibrillar Collagen through TGF- β Activation and Cell Infiltration. *Am J Pathol* 2008, 173:631–642.
63. Olsen KC, Sapinoro RE, Kottmann RM, Kulkarni AA, Iismaa SE, Johnson GVW, Thatcher TH, Phipps RP, Sime PJ: Transglutaminase 2 and its role in pulmonary fibrosis. *Am J Respir Crit Care Med* 2011, 184:699–707.
64. Shinde AV, Su Y, Palanski BA, Fujikura K, Garcia MJ, Frangogiannis NG: Pharmacologic inhibition of the enzymatic effects of tissue transglutaminase reduces cardiac fibrosis and attenuates cardiomyocyte hypertrophy following pressure overload. *J Mol Cell Cardiol* 2018, 117:36–48.
65. Szondy Z, Korponay-Szabó I, Király R, Sarang Z, Tsay GJ: Transglutaminase 2 in human diseases. *Biomedicine* 2017, 7:15.
66. Shinde AV, Frangogiannis NG: Tissue transglutaminase in the pathogenesis of heart failure. *Cell Death & Differentiation* 2018, 25:453–456.
67. Rybinski B, Franco-Barraza J, Cukierman E: The wound healing, chronic fibrosis, and cancer progression triad. *Physiol Genomics* 2014, 46:223–244.

68. Cox TR, Erler JT: Molecular pathways: connecting fibrosis and solid tumor metastasis. *Clin Cancer Res* 2014, 20:3637–3643.
69. Foster DS, Jones RE, Ransom RC, Longaker MT, Norton JA: The evolving relationship of wound healing and tumor stroma. *JCI Insight* 2018, 3.
70. Lai T-S, Greenberg CS: TGM2 and implications for human disease: role of alternative splicing. *Front Biosci* 2013, 18:504–519.
71. Scarpellini A, Germack R, Lortat-Jacob H, Muramatsu T, Billett E, Johnson T, Verderio EAM: Heparan Sulfate Proteoglycans Are Receptors for the Cell-surface Trafficking and Biological Activity of Transglutaminase-2. *Journal of Biological Chemistry* 2009, 284:18411–18423.
72. Casadio R, Polverini E, Mariani P, Spinazzi F, Carsughi F, Fontana A, Polverino de Laureto P, Matteucci G, Bergamini CM: The structural basis for the regulation of tissue transglutaminase by calcium ions. *Eur J Biochem* 1999, 262:672–679.
73. Begg GE, Carrington L, Stokes PH, Matthews JM, Wouters MA, Husain A, Lorand L, Iismaa SE, Graham RM: Mechanism of allosteric regulation of transglutaminase 2 by GTP. *Proc Natl Acad Sci U S A* 2006, 103:19683–19688.
74. Rifkin DB, Rifkin WJ, Zilberberg L: LTBP in biology and medicine: LTBP diseases. *Matrix Biol* 2018, 71-72:90–99.
75. Robertson IB, Rifkin DB: Unchaining the beast; insights from structural and evolutionary studies on TGF β secretion, sequestration, and activation. *Cytokine Growth Factor Rev* 2013, 24:355–372.
76. Öklü R, Hesketh R: The latent transforming growth factor β binding protein (LTBP) family. *Biochemical Journal* 2000, 352:601–610.
77. Miyazono K, Olofsson A, Colosetti P, Heldin CH: A role of the latent TGF- β 1-binding protein in the assembly and secretion of TGF- β 1. *The EMBO Journal* 1991, 10:1091–1101.
78. Mazzieri R, Jurukovski V, Obata H, Sung J, Platt A, Annes E, Karaman-Jurukovska N, Gleizes P-E, Rifkin DB: Expression of truncated latent TGF- β -binding protein modulates TGF- β signalling. *J Cell Sci* 2005, 118:2177–2187.
79. Yang Z, Mu Z, Dabovic B, Jurukovski V, Yu D, Sung J, Xiong X, Munger JS: Absence of integrin-mediated TGF β 1 activation *in vivo* recapitulates the phenotype of TGF β 1-null mice. *J Cell Biol* 2007, 176:787–793.

4 Tenascin-C and tissue transglutaminase transiently orchestrate tissue growth enabling the transition towards tension-dependent tissue maturation

The work presented in this chapter is currently under preparation and will be submitted for publication in the near future.

Mario C. Benn, Simon A. Pot, Jens Moeller, Tadahiro Yamashita, Charlotte M. Fonta, Sebastian Lickert, Gertraud Orend, Philip Kollmannsberger, Viola Vogel. *Tenascin-C and tissue transglutaminase transiently orchestrate tissue growth enabling the transition towards tension-dependent tissue maturation.*

M.C.B., S.A.P., J.M. and V.V. designed the research; V.V. supervised the project; S.A.P. provided preliminary experimental data on tissue transglutaminase relevant to design the study; **M.C.B.** designed the μ Tissue platform with input from P.K. and J.M.; **M.C.B.** microfabricated master structures and PDMS scaffolds; **M.C.B.** performed all cell culture experiments except WST toxicity tests; **M.C.B.** performed brightfield, confocal and 2-photon laser scanning microscopy; **M.C.B.** performed data visualization and analysis; T.Y. provided code for fiber analysis; **M.C.B.** and T.Y. analyzed the SHG fiber orientation; C.M.F. and **M.C.B.** supervised and conducted planar toxicity test (WST); C.M.F. described, plotted and analyzed planar WST tests; J.M., S.A.P., T.Y., S.L., G.O. and P.K. engaged in scientific discussions and propelled the project; **M.C.B.** and V.V. interpreted the results with input from all authors; **M.C.B.** and S.L. created and edited the figures; **M.C.B.** and V.V. wrote the manuscript with input from all authors.

4.1 Abstract

In tissue growth and maturation, little is known how the fibroblast to myofibroblast transition is regulated and whether it can be reverted. To ask whether gradients of varying extracellular matrix (ECM) compositions play a crucial role, a question that cannot be addressed in 2D cell cultures as they poorly reflect biophysical characteristics of tissues, we used *de novo* μ Tissues grown in engineered scaffold clefts. Alpha smooth muscle actin (α SMA)-expressing myofibroblasts are found in the growth front, where they first assembled tensed fibronectin fibers and express tenascin-C (TNC), which started to decorate the fibronectin (Fn) fibers just a few μ m behind the growth front. In a sharp transition zone, the signal intensities of α SMA, Fn and TNC were significantly downregulated as the tissue started to mature, while the second harmonic generation (SHG) positive signal from collagen fiber bundles was increasing. Here we show that the myofibroblast phenotype in the growth front is stabilized by the highly stretched Fn fibers and that their reversal back to quiescent fibroblasts in the maturing tissue is critically dependent on the transient activity of tissue transglutaminase (TG2) in the transition zone. Broad spectrum matrix metalloproteinase inhibition, but not the inhibition of MMP2 or MMP9, as well as partial blockage of Fn-collagen interaction further hampers completion of the myofibroblast reversal. Understanding how ECM gradients regulate tissue growth processes and stimulate the transition of myofibroblasts into quiescent fibroblasts behind the growth front as the tissue matures is crucial to develop novel treatment strategies in wound healing, fibrosis and cancer.

4.2 Introduction

Immense heterogeneity is intrinsic to life, from the morphological, transcriptional, translational, and functional heterogeneities of single cells up to the organ level, where distinct cellular organization held together by highly heterogeneous extracellular microenvironments enables tightly regulated organ functions. During tissue homeostasis, ongoing cell-driven assembly and disassembly of extracellular matrix (ECM) is necessary to maintain organ-specific features and physiological functions [1]. In parallel, matrix production, cell proliferation and tissue contraction are central elements of tissue growth, maturation and repair [2], which, if not coordinated sufficiently well and with the necessary speed, cannot win the “race against the clock” upon tissue damage [3] and lead to major impairment of tissue function, or even death of the organism [4-6]. ECM proteins are expressed in a time-dependent fashion during repair and can thus serve as valuable region- and time-specific biomarkers indicative for tissue health and disease [3,7,8]. But how is heterogeneity during embryogenesis formed, and later maintained during tissue homeostasis, and what factors drive pathological transformations?

ECM assembly and maintenance are indispensable for life and orchestrate many outside-in signals to cells that go far beyond providing physical support alone [9,10].

Furthermore, information provided by the ECM can persist long after the cells that initially deposited the ECM have migrated, (de)differentiated or died, and thus 'outlive' paracrine or direct cell to cell signalling [11]. As such, this ECM memory can guide tissue repair and regeneration over time periods of days to months, but at the same time become problematic if a dysregulated repair process has been established as a result of chronic or severe trauma. In such cases, a 'bad neighborhood' ECM can persist and continue to drive a fibrotic repair program. The ECM is composed of approximately 300 proteins/glycoproteins which vary in function and complexity of assembly [12]. Within the first phases of tissue growth, cellular forces are essential for the assembly of a provisional fibronectin (Fn) matrix [13]. During tissue maturation, the initial Fn matrix is gradually replaced by collagen-I and other ECM components which function as load-bearing structures to release the load on the initial Fn matrix and enhance structural tissue strength [14]. Thus, spatio-temporal gradients of Fn and collagen are created along the axis of tissue growth. However, collagen fiber assembly does not only involve complex post-translational processing [15], but also requires the presence of fibrillar Fn as a template for the initiation of collagen polymerization [16-18]. This necessitates a time-regulated formation and remodelling of ECM gradients during the course of tissue growth and maturation. In contrast to the impact of soluble gradients [19-21], fundamental understanding of how ECM gradients are formed and how they regulate tissue development and repair processes is still missing due to the complexity of the multiple interactions.

In recent years, much attention was given to understanding the importance of soluble factor gradients [21-26] and mechanical forces in tissue growth and remodelling processes [10,27-29]. However, far less is known about how spatio-temporal changes in ECM composition and architecture contribute to the formation and stabilization of cell phenotype gradients. Well designed and tightly controllable model systems are thus essential to gain insights into how spatio-temporal biochemical and physical ECM parameters guide tissue morphogenesis and repair in concert with soluble factors. Much has been learned from cell culture experiments on engineered substrates on how rigidity and topography tune cell differentiation, as well as in 3D polymer matrices on how fibrous 3D environments impact cell migration, proliferation, differentiation and matrix assembly [30-32]. Native ECM fibers though have a far more sophisticated molecular design than any synthetic polymer: each matrix molecule presents a distinct set of molecular recognition sites, some of which can be transiently activated or destroyed by fiber stretching [10]. To make progress towards the understanding of the orchestrating role of ECM in tissue growth and repair and as driver of pathological transformations, complex but controllable model systems incorporating self-assembled ECM to form *de novo* grown tissues are urgently needed. While organoids have been powerful in combination with high-throughput 2D drug development pipelines,

they have their limitations due to significant organoid-to-organoid variabilities [33]. Alternatively, we show here how simpler, yet better shape-controlled *de novo* tissues can be grown in engineered clefts on elastomer scaffolds containing arrays of zig-zag shaped edges (Figure 1). When seeding fibroblasts on scaffolds with single clefts, it was previously shown that *de novo* 3D tissues can be grown, whereby the cells proliferate mostly in the outer growth front [34], while *de novo* ECM is assembled on top of the gradually maturing tissues [14].

Myofibroblasts play a particularly important role in tissue morphogenesis and repair as they are more contractile than fibroblasts and produce significantly more ECM [2,35,36]. 2D cell culture experiments revealed that various stimuli (e.g. mechanical tension, PDGF, TGF- β , EDA-Fibronectin) can induce a differentiation of fibroblasts into myofibroblasts, showing an elevated expression of alpha smooth muscle actin (α SMA) [37]. Myofibroblasts under healthy conditions drive wound closure by applying strong contractile forces to reduce the wound size before they are cleared from the wound [38]. Under impaired conditions, such as in inflammation, diabetes, fibrotic transformations or cancer, myofibroblasts remain constitutively active over extended periods of time [36]. Myofibroblasts are also the prevalent cell phenotype in the growth front of our *de novo* grown μ Tissues in engineered clefts [34]. A myofibroblast-to-fibroblast transition (M-F-T) occurs as the μ Tissues mature, whereby the maturing tissues mainly contain fibroblasts predominantly surrounded by a collagen-rich ECM [34]. But what are the central drivers that orchestrate the M-F-T during tissue maturation and what happens under pathological conditions?

To address these questions, we took advantage of our arrays of *de novo* grown μ Tissues and asked how the provisional fibronectin ECM in the growth front is remodelled into the mechanically stabilized collagen-rich matrix in the maturing tissue core. A process of a few days taking place over a spatial distance of less than 100 μ m. We thereby focused our study on the spatiotemporal expression, assembly and degradation of two very interesting candidates: Tenascin-C (TNC) and tissue transglutaminase (TG2). TNC and TG2 are both reported to be quickly upregulated at the boarder of healing wounds and other sites of ECM remodelling [3,39,40], mechanical stress [41-44], as well as during embryonic development, wound healing or pathological conditions of fibrosis or cancer [45-51]. TNC is a star-shaped hexameric matricellular glycoprotein and best known for its mainly anti-adhesive function when binding to Fn matrices [52] and competing with cell surface syndecan-4 binding to the Fn Hep II domain [53-55]. In contrast, TG2 catalytically crosslinks a number of different substrates including fibronectin and collagen [56] via formation of ϵ -(γ -glutamyl)lysine bonds in a calcium-dependent manner [57,58]. Far less well understood are TG2's multiple non-enzymatic functions (reviewed in [59-64]) as TG2 can non-enzymatically stabilize cell adhesions as integrin- and syndecan-binding coreceptor for Fn [59]. As it also remains elusive whether and how TG2 and TNC functionally interact with each other, we exploited various well characterized pharmaceutical inhibitors. We also studied the impact of MMP inhibitors on

tissue growth and maturation, since cleavage of TNC by matrix metalloproteinases (MMP) can lead to a reduction of TNC levels, exposure of cryptic binding sites, release of cell adhesion mediating domains [65,66] and the modulation of ECM binding sites (e.g. for Fn) [67,68]. MMPs are the main enzymes facilitating proteolytic ECM degradation, especially in sites of matrix remodelling [1]. On the other hand, enzymatic cross-linking by transglutaminase, a suggested “reverse proteinase”, partially protects the ECM from proteolytic degradation [69], leading to reduced ECM turnover [60,70]. Thus, we utilized a catalytic site inhibitor to investigate the relevance of TG2 enzymatic activity on the formation of ECM gradients and subsequent tissue maturation.

In summary, our findings suggest a functional dependency between TNC and TG2, where TNC conveys early ECM stabilization and is cleared over time when enzymatic cross-linking via TG2 takes over. Furthermore, TGF- β might be an important player in accelerating tissue maturation. Taken together, our study sheds new insights on tissue growth and remodelling mechanisms that are of major significance to cell biologists, bioengineers and the medical community.

4.3 Results

μ Tissue maturation in engineered PDMS clefts is characterised by a reversible fibroblast-to-myofibroblast transition and steep ECM gradients

De novo μ Tissues were formed by seeding normal human dermal fibroblast onto PDMS scaffolds containing millimetre-sized clefts with a cleft angle of 45° (Fig. 1A). Once the cells had formed a confluent layer on top of the scaffolds after approximately two days, 3D μ Tissues started to grow in the corners of the clefts, gradually filling the cleft over a duration of 12 days (Fig. 1B-C). Typically, the cells at the upper and lower scaffold surfaces organized themselves independently from each other to initiate μ Tissue growth before they started fusing after a few days (Fig. 1B). As the μ Tissues were growing outwards, the tissue gradually matured in its core region positioned at the inner corner of the cleft (Fig. 1B and 1F). In *de novo* grown μ Tissues, fibroblast proliferation occurs mostly in the growth front at the tissue edge [34], while the inner tissue gradually matured as seen by a major change in ECM composition in the central horizontal z-planes (Fig. 1D-I, more samples in Fig. S01). The angular cleft geometry and its gradual filling thus allows the interpretation of spatial information as time imprint of tissue maturation. What is seen as a concave growth front actually represents a thin layer of highly proliferative cells that covers the entire μ Tissue (Fig. 1F) and extends across the PDMS scaffold (Fig. S10). Even though fibroblasts were initially seeded on the scaffold, the proliferative growth front is rich in myofibroblasts as indicated by high levels of α SMA expression (Fig. 1G), while few myofibroblasts are seen in the interior of the tissue away from the growth front. The decline of the α SMA signal from the tissue surface to the interior suggests a reversible fibroblast-to-myofibroblast- (F-M-T) and myofibroblast-to-fibroblast-transition (M-F-T) as the tissues mature [34]. The growth front is rich in a fibrillar Fn matrix, with both the Fn fibers as well as the myofibroblasts aligned tangentially to the growth front (Fig. 1I). In contrast, the μ Tissue interior consists mostly of randomly oriented fibroblasts surrounded by a far less ordered collagen-rich ECM (Fig. 1G) sparsely interdispersed with Fn fibers (Fig. 1I), in agreement with previous observations [34]. Cells arrange ECM fibers and especially load-bearing collagen fibers along the axis of main force transmission. In the pseudo-coloured fiber orientation plot, the SHG signal appears both aligned with the growth front but also along the long axis of the μ Tissue parallel to the bisector angle, suggesting force transmission over long range (Fig. 3E, more samples in Fig. S05). The ratio of Fn to SHG visualized collagen fibers declines sharply within the first 10 μ m from the outer front of the tissue (Fig. 1L). However, the absolute growth front width varies between tissues (Fig. S01). Taken together, F-M-T occurs within the growth front of *de novo* grown μ Tissues without supplementation of TGF- β and myofibroblasts disappear again as the tissue matures, whereby the steep Fn/collagen gradient co-localizes with the rapidly declining α SMA signal (Fig. 1L, more samples in Fig. S01).

4 Tenascin-C and tissue transglutaminase transiently orchestrate tissue growth enabling the transition towards tension-dependent tissue maturation

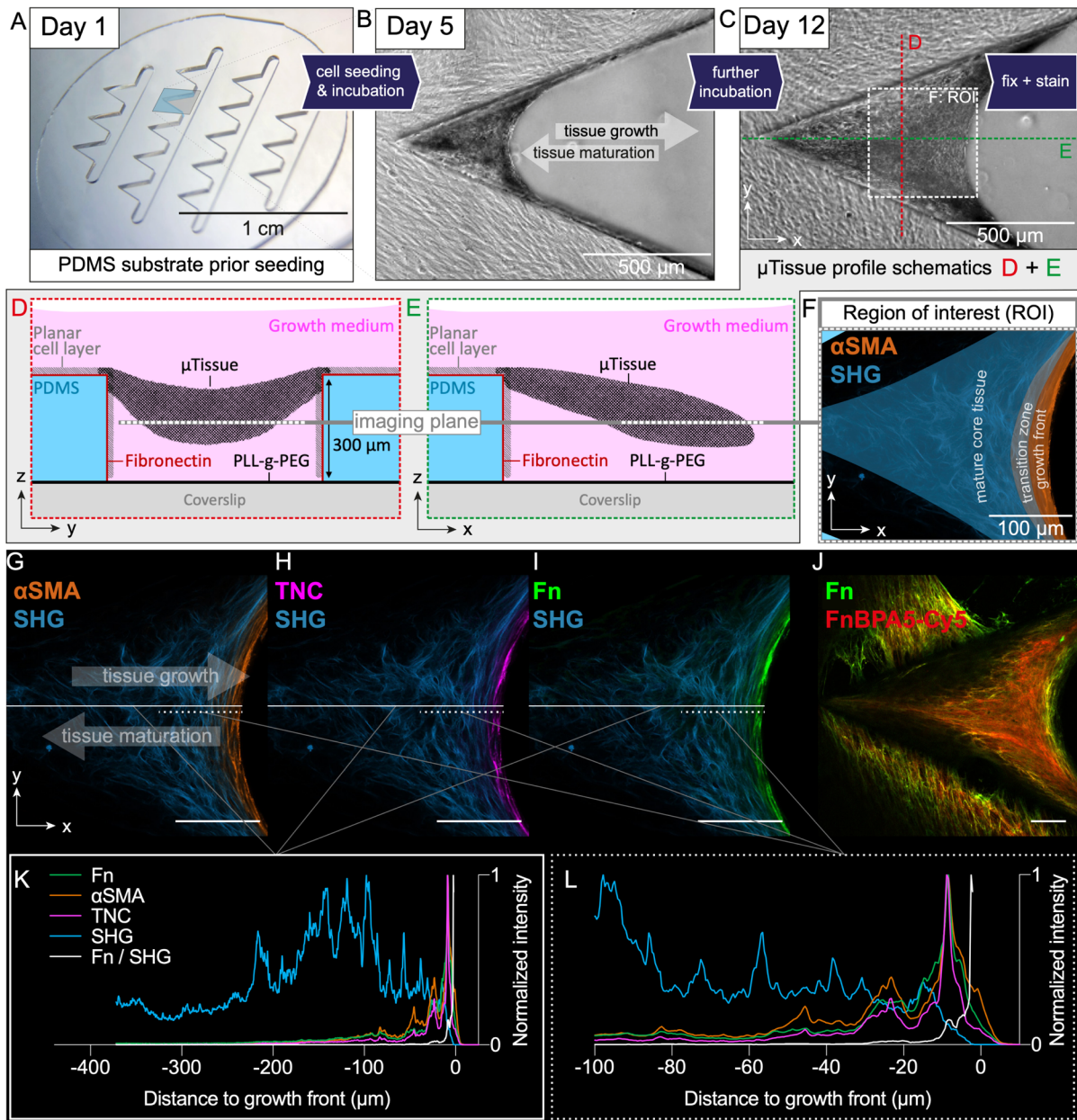


Fig. 1 Experimental setup of *de novo* tissue growth with spatiotemporal resolution in microfabricated PDMS substrates. **(A)** Microfabricated PDMS substrate (diameter: 18 mm, thickness: 300 μm) with array of 16 acute-angled clefts. Cells form in each cleft (light blue colour) *de novo* μTissue over time. **(B)** Phase-contrast image of a cleft with assembled tissue at day 5. The $\mu\text{Tissues}$ grow towards the open angle whereas tissue maturation occurs over time and is directed in the reverse direction (gray arrows). **(C)** $\mu\text{Tissues}$ are fixed and stained at day 12. **(D)** YZ-section of the red dashed line in (C) represents a μTissue freely spanned between the adhesion sites of the functionalized PDMS structures. **(E)** XZ-section of the green dashed line in (C) represents a growing μTissue along the bisector angle of the cleft. **(F)** Magnification of the white boxed region in (C). Focal planes of interest (white dashed line in (D-E)) were chosen for each sample such as to capture the maximum of mature-to-young-tissue-gradient and acquired with 2-photon and confocal laser scanning microscopy. Tissue growth occurs in a layer-by-layer manner in which the structure is preserved over time [14], thus, cross-sectioning here allows to correlate temporal from spatial information. **(G-I)** Overlay of the second harmonic generation (SHG, cyan) signal and αSMA (orange, G), TNC (magenta, H), Fn (green, I) after 12 days. Scale bar 100 μm . **(J)** Overlay of Fn (green) and FnBPAS (red) after 12 days. Scale bar 100 μm . **(K)** Normalized intensity line profile over distance to growth front and along the white line in (G-I) and the respective stains. **(L)** Normalized intensity line profile along the growth front of the dashed white line in (G-I) and the respective stains.

Tensed fibronectin fibers in the growth front stabilize the myofibroblast phenotype

While we previously found that fibronectin fibers are highly stretched in the growth front using a Fn-FRET probe [34], we here utilized our recently developed bacterial adhesin-derived tension probe (FnBPA5) which binds Fn in the relaxed tensional state with higher affinity [71-74]. The μ Tissue interior showed much higher FnBPA5 signal compared to the growth front, indicating structurally relaxed or enzymatically cleaved Fn fibers in the interior and stretched and partially unfolded Fn fibers in the growth front (Fig. 1J).

To ask whether the M-F-T and F-M-T are triggered by soluble factors, ECM composition or mechanical stimuli, such as stretched Fn fibers, we decellularized the μ Tissue such that their ECM remained intact with a modified Cukierman protocol [75-77]. We then re-seeded native fibroblasts or TGF- β stimulated myofibroblasts (Fig. 2A-B), whereby the re-seeded cells were marked with a cell tracker, which was detected as multifocal cytoplasmic accumulations. Within 24 h, the re-seeded cells (both fibroblast and myofibroblast) repopulated the entire decellularized μ Tissue as indicated by a homogenous distribution of the cell tracker (Fig. 2B-C). In contrast, the reseeded fibroblasts do not show any α SMA signal in full dynamic range without and only unstructured noisy signal with contrast enhancement (Fig. 2B). Re-seeded α SMA positive myofibroblasts predominantly located within the decellularized growth front after 24 h incubation, but not in the core μ Tissue region even though the core was filled with cell tracker positive cells. After four days of re-seeding myofibroblast, the α SMA positive cells occupy a wider region at the growth front compared to 24 h incubation (compare left columns of Fig. 2C and Fig. 2B). After four days of incubation, only a very mild intracellular α SMA signal could be detected in re-seeded fibroblasts aligned within the growth front area (indicated by arrows in Fig. 2C, right column). Taken together, the relative differences of ECM composition and architecture, with a tensed fibronectin fiber environment in the growth front of *de novo* grown μ Tissue, seem to not only stabilize the myofibroblast phenotype independent of soluble morphogen stimulation (after 24 h, Fig. 2B), but also trigger the onset of F-M-T (Fig. 2C, right column).

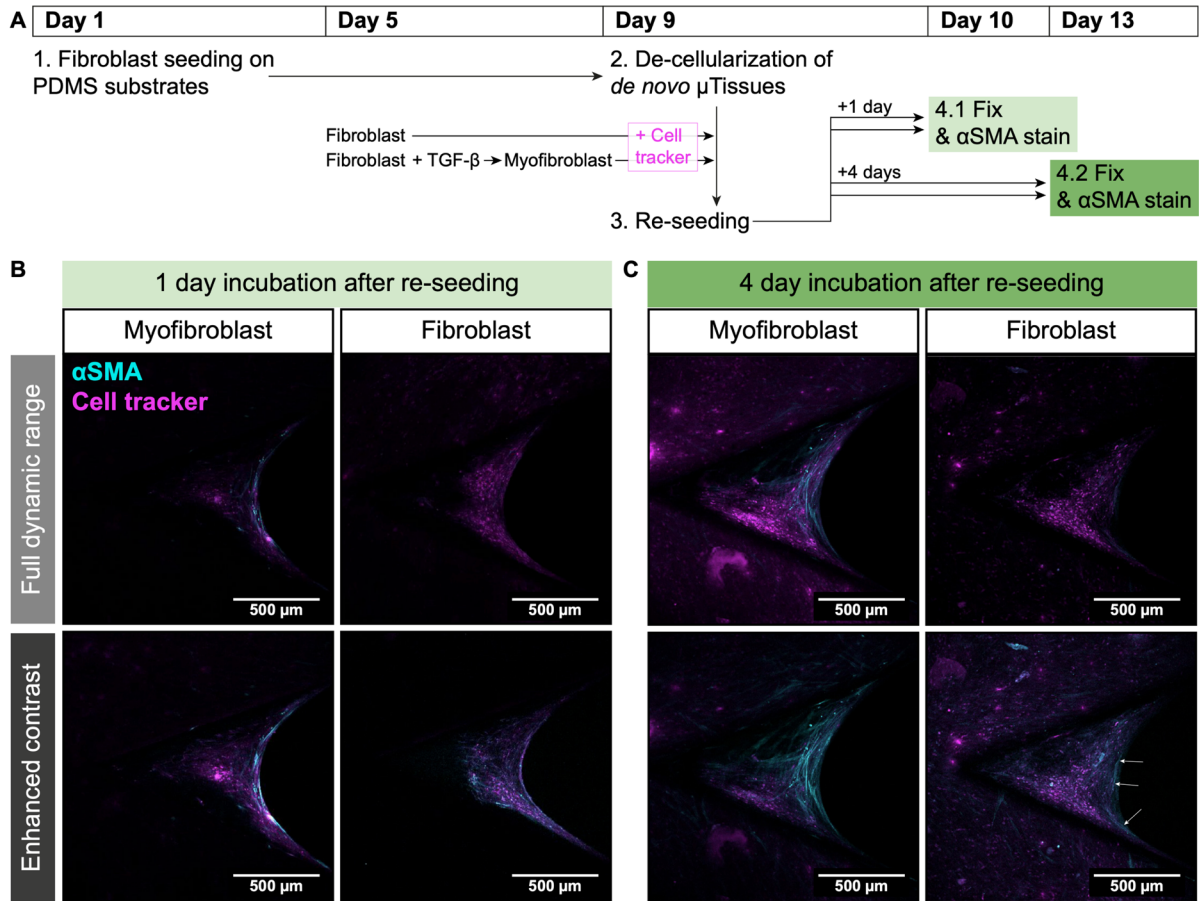


Fig. 2 Re-seeding of decellularized μ Tissues. (A) μ Tissues were decellularized and reseeded with normal fibroblasts or TGF- β 1 stimulated myofibroblasts. All cells were incubated with cell tracker prior to reseeded. μ Tissues were fixed and stained one and four days after reseeded. (B) Central imaging plane of the μ Tissues fixed after one day and visualized for fibroblasts and myofibroblasts. To allow intensity comparison across different μ Tissues as well as visualization of the intra- μ Tissue distribution and morphology, region of interest is shown with full dynamic range (upper row) and with enhanced contrast (lower row) to the same relative number of saturated pixels (1%). Myofibroblasts predominantly localize in the growth front. In fibroblast reseeded μ Tissues no clear α SMA fibers are visible. (C) Central imaging plane of the μ Tissues fixed after four days and visualized for fibroblasts and myofibroblasts. Myofibroblasts populate a wider region in the growth front. In the enhanced contrast images a very dim α SMA signal is visible in the growth front of fibroblast seeded cells (arrows), indicating a starting F-M-T of the seeded fibroblasts. Scale bar 500 μ m.

TNC decorates Fn fibers in the growth front, but gets rapidly degraded as the tissues matures

To ask which ECM players could support the formation of this opposing Fn/Col gradient, we next stained for possible candidates normally found in growing tissue [45,78,79]. TNC as an acute indicator of ECM remodelling is rapidly upregulated in mechanically stressed tissues [42,43,80] or at injury sites [47,81], and gets degraded by many different proteases [66,67,82-87]. Interestingly, immunostaining revealed that TNC decorates only the Fn fibers in the growth front (Fig. 1H). As a polyclonal anti-TNC antibody recognizing full length TNC also did not detect a signal in the back part of the μ Tissue, we concluded that TNC disappeared presumably due to proteolytic degradation (Fig. 1H and Fig. S09).

The TNC signal typically peaked slightly shifted towards core tissue regions, e.g., slightly delayed, in comparison to the α SMA- and Fn-peaks in the profile plots (compare sample 1-4 in Fig. S01). As TNC has

a variety of epitopes that might get masked upon ECM binding, we confirmed the TNC gradient with different antibodies. In addition to the monoclonal antibody BC-24, which is used as standard throughout the study, we also used a polyclonal TNC and another monoclonal TNC B28.13, confirming that TNC mainly accumulated within the early growth region and thus defines immature regions of the control μ Tissue (Fig. S09). Little TNC is left in tissue regions where collagen fibers, visible in SHG, had been assembled (Fig. 3A, more samples in Fig. S01). This suggests that TNC might play a central role in the swift formation of proliferative ECM gradients.

Since each interventional condition is required to be compared with the respective control of the respective staining as reference, those need to be grouped together in Fig. 3 and Fig. 4. To not violate this coherence, the figures cannot be called out in numerical order in the following section.

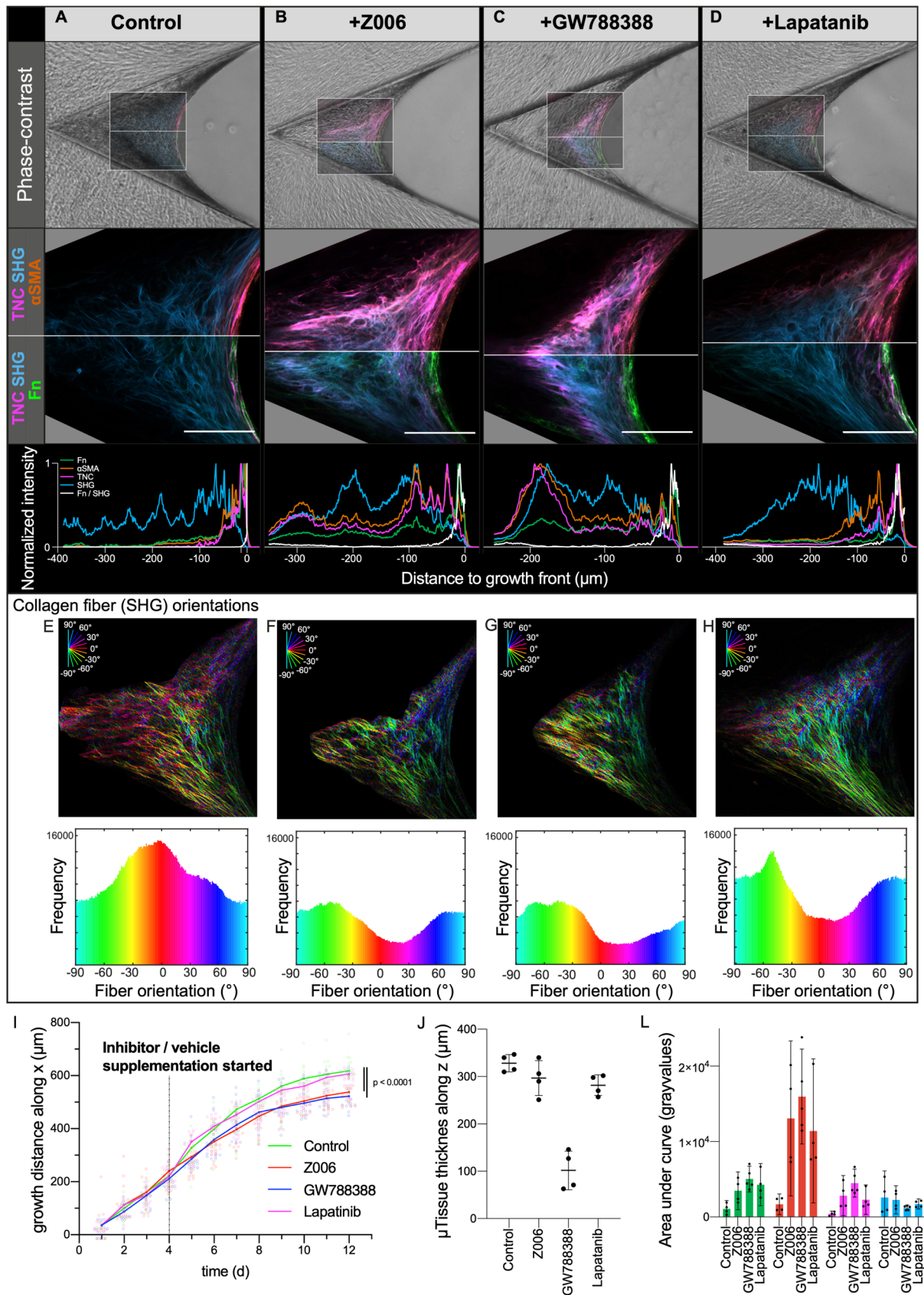


Fig. 3 μTissue interventions with various inhibitors. (A-D, upper row) Representative $\mu\text{Tissues}$ imaged with 2P and CLSM (ROI) and overlaid with the respective phase-contrast image of the following conditions: Control (DMSO, A), the specific inhibition of the enzymatic TG2 activity (Z006, B), the inhibition of TGF- β receptor signalling (GW788388, C) and inhibition of ErbB signalling (Lapatinib, D). (A-D, middle row) Close-up of the respective ROI in the upper row. Since the μTissue grow in their x-profile in approximation symmetric, the CLSM+2P data is depicted with two different sets of look up table (top LUT: αSMA

(orange), TNC (magenta), SHG (cyan); bottom LUT: Fn (green), TNC (magenta), SHG (cyan). Scale bars 100 μm . **(A-D, lower row)** Respective normalized intensity profile of the channel in the middle row is shown parallel to the cleft bisector angle, e.g. main x-growth-direction of tissue here from left to right (cf. Fig. 1B+C). At each distance, the mean of 100 vertically accumulated pixels (50px above and 50px underneath the straight line) is plotted over the distance to growth front. Normalized Fn / SHG ratio is plotted additionally. See supplementary figures S01 – S04 for more data including separated channels and enlarged profile plots. **(E-H, upper row)** Collagen fiber (SHG) orientations depicted as pseudo-coloured ROI. See also supplementary Fig. S05. **(E-H, lower row)** Collagen fiber (SHG) orientations depicted as histogram. **(I)** Growth distances along cleft bisector angle between tip of the cleft to the μTissue -medium-interface measured with phase-contrast images. Data were compared with an unpaired two-tailed Mann-Whitney test. **(J)** μTissue thickness along the z-axis depicted in describe the graph type. **(L)** Integral of profile plots (A-D) in absolute intensities. Mean (n=4) with 95% CI.

Fn-collagen-binding, followed by collagen assembly, precedes the formation of steep Fn-, TNC- and αSMA -gradients and enables tissue maturation

Since collagen assembly requires the presence of Fn fibers (17-19), we next asked how the inhibition of Fn-Col interactions impacts the onset of the tissue maturation processes. We hypothesized that the steep Fn, TNC and αSMA gradients that we see to occur in the transition zone (Fig. 1F) require collagen binding in order to induce its polymerization into an independent collagen fiber network. To test this hypothesis, the bacterial-adhesin-derived R1R2 peptide [88,89] that partially inhibits Fn-collagen interaction through competitive binding was supplemented to the medium. Even though a pronounced growth front rich in Fn, TNC and αSMA is formed in the presence of the R1R2 peptide, indicating that the early F-M-T is not disturbed, TNC-Fn-degradation and partial replacement by a collagen rich matrix is not happening (Fig. 4H, more samples in Fig. S06B). This suggests that either the TNC and Fn degradation is significantly reduced or expression of both matrix molecules is largely increased. Overall, tissue maturation is incomplete and myofibroblast to fibroblast transition is delayed but still occurs, suggesting that the Fn-Col-interaction is essential for prompt clearance of myofibroblasts and subsequent tissue maturation (Fig. 4H). Furthermore, many tissues show detachment and rupture under inhibition of Fn-collagen interaction, indicating a strongly reduced mechanical stability.

Taken together, this suggests that Fn-collagen binding is required for tissue maturation and thus the formation of a steep Fn, TNC and αSMA -gradient. As relaxed Fn is templating subsequent collagen assembly [18], a shift from highly to less stretched Fn fibers is necessary to initiate the μTissue maturation process.

4 Tenascin-C and tissue transglutaminase transiently orchestrate tissue growth enabling the transition towards tension-dependent tissue maturation

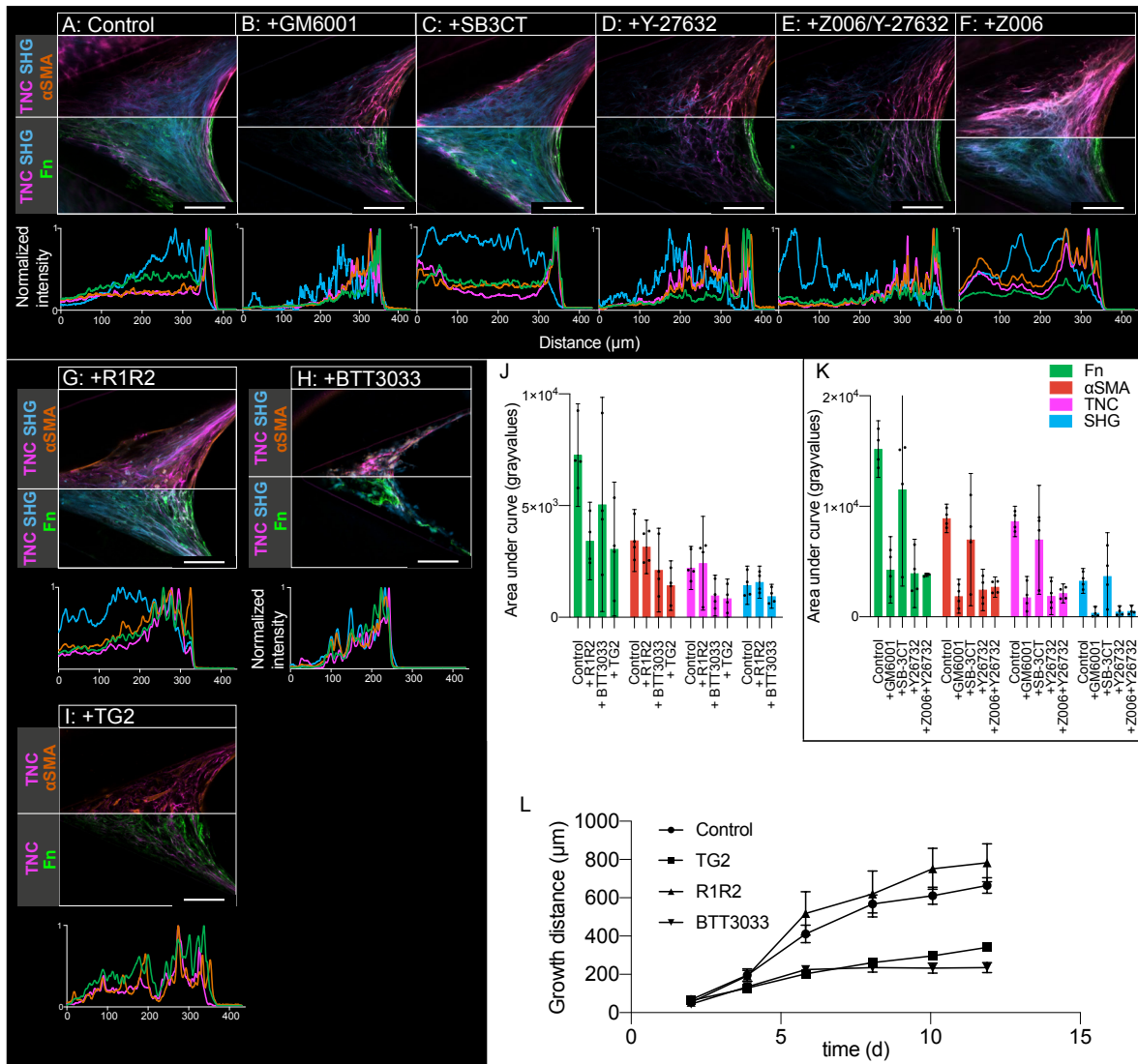


Fig. 4 TNC stain of μ Tissue interventions with various inhibitors and supplementation of TG2. **(A-I, upper row)** Representative ROI of μ Tissues imaged with 2P and CLSM of the control (DMSO, A), the broad spectrum inhibition of MMPs (GM6001, B), the specific inhibition of MMP-2/-9 (SB3CT, C), the inhibition of the Rho-associated kinase (ROCK, Y-27632, D), a combination of inhibition with Y-27632 and Z006 (E), Z006 (F), partial inhibition of collagen-Fn (R1R2, G), inhibition of $\alpha 2\beta 1$ -integrin (BTTT3033, H), and the supplementation of exogenous TG2 (I). The CLSM+2P data is depicted with two different sets of look up table: top LUT: α SMA (orange), TNC (magenta), SHG (cyan); bottom LUT: Fn (green), TNC (magenta), SHG (cyan). Scale bars 100 μ m. See also supplementary figure S06. **(A-I, lower row)** Respective normalized intensity profile of the channel in the middle row is shown parallel to the cleft bisector angle, e.g. main x-growth-direction of tissue here from left to right (cf. Fig. 1B+C). At each distance, the mean of 100 vertically accumulated pixels (50px above and 50px underneath the straight line) is plotted over the distance to growth front. **(J)** Integral of profile plots (G-I) in absolute intensities. Mean (n=4) with 95% CI. **(K)** Integral of profile plots (A-E) in absolute intensities. Mean (n=4) with 95% CI **(L)** Growth distance is defined as distance from cleft tip along bisector angle to growth, here plotted over time. Mean (n=4) with 95% CI.

Inhibition of $\alpha 2\beta 1$ -integrin mediated cell-collagen binding hampers tissue growth and maturation

Since not only Fn, but particularly $\alpha 2\beta 1$ -integrins are required for collagen polymerization and for dense collagen network formation [17,90], we next investigated μ Tissues treated with BTT3033, an $\alpha 2\beta 1$ -integrin inhibitor. Within 12 days, tissue formation was delayed upon exposure to BTT3033 with a

largely reduced growth front (Fig. 4I+L). The variability over different tissues was high (Fig. S06A). All growth front markers were distributed over the entire tissue, and the precise spatial transition, from growth front to a mature core region was lost.

MMP activity is required to degrade TNC and to convert myofibroblasts back to fibroblasts

Once myofibroblasts define and stabilize the growth front, what triggers the conversion M-F-T in these μ Tissues and subsequent tissue maturation? It was previously reported, that the broad-spectrum MMP inhibitor, GM6001, which inhibits MMP1-3, 7-9, 12, 26, also blocks TNC degradation *in vitro* [91]. For GM6001-treated μ Tissues, myofibroblasts accumulated normally in the growth front but TNC degradation was prolonged and tissue maturation was delayed (Fig. 4B, more samples Fig. S07A). Most importantly, α SMA positive cells were present in the core tissue regions, Fn fiber deposition remained upregulated and only few mature collagen fibers were detectable with SHG (Fig. 4B). It appears that the MMP inhibitor blocked either collagen expression/fibril formation and / or Fn expression or interaction with collagen. Since we showed above, that Fn fibers are highly tensed in the growth front, but that a reduced Fn fiber tension is necessary to template the nucleation of collagen fibers, MMP activity might cleave some Fn fibers which can then initiate collagen polymerization. In consequence the deposition of TNC may be hampered which is dependent on Fn-collagen-interaction as shown above with the R1R2 peptides.

Under GM6001, across the entire μ Tissue profile, the absolute intensity of Fn, α SMA, TNC and SHG signal was greatly reduced, and almost no mature collagen fibers were detectable (Fig. 4B+K, more samples Fig. S07A). Together, this suggests that broad-spectrum MMP activity is not only needed for TNC degradation, but also for expression of collagen and Fn. Speculatively, there could be feedback loops involved which hinder further protein accumulation when matrix degradation fragments are no longer detected. Unlike under broad-spectrum MMP inhibition (Fig. 4B), selectively inhibiting MMP-2 and MMP-9 with SB3CT [92] had little effect. Collagen fibers formed normally and the total fluorescence intensities were similar to the control (Fig. 4A,C+K). It neither resulted in alterations of the Fn-TNC-gradient slope, nor in F-M-T-/M-F-T-alterations. This is particularly interesting since MMP-2 and MMP-9, beside many other functions, were also reported to increase the bioavailability of TGF- β in 2D experiments [93,94]. Surprisingly, SB3CT had hardly any effect on the steepness of the gradient between growth front and tissue interior and resembled the control morphology and distribution (Fig. 4C, more samples Fig. S07B). Taken together, reducing bioavailability of TGF- β by selectively inhibiting specifically MMP-2 and MMP-9 did not impact tissue gradients. However, broad spectrum MMP activity is required to form sharp TNC and α SMA gradients and mature collagen fibers in the core region. This indicates, that MMP-1/-3/-7/-8/-12/-26 are more relevant for the described GM6001 effect. All those MMP molecules target a variety of different substrates in the ECM, including Fn, different collagens and other

ECM components, which creates great opportunity for future studies to investigate their individual roles.

Upregulated tissue transglutaminase is a key player to form the sharp ECM gradient

ECM is partially protected from proteolytic degradation through enzymatic cross-linking by transglutaminases [69]. Immunostaining showed TG2 accumulation in the growth front, with a very similar distribution to TNC (compare TG2 in Fig. 5A with TNC in Fig. 3A or Fig. 4A), and likewise, progressively disappeared in the mature μ Tissue core (Fig. 4J). To investigate whether TG2 is a timer regulating the sharpness of the transition from the growth front to maturing tissues, we next supplemented TG2 exogenously. This resulted in reduced μ Tissue growth rates and a redistribution of growth front markers to the core μ Tissue regions, while the absolute α SMA, Fn and TNC intensities decreased along the full μ Tissue profile (Fig. 4J-L). The accumulation of growth front markers in deeper regions indicates continuous ECM remodelling in all regions instigated by the supplemented TG2. As TG2 colocalized with α SMA, we conclude that cells with a myofibroblast (but not normal fibroblast) phenotype express TG2 that largely impacts TNC expression in the μ Tissue. Likely, exogenously added TG2 enhances TNC stability.

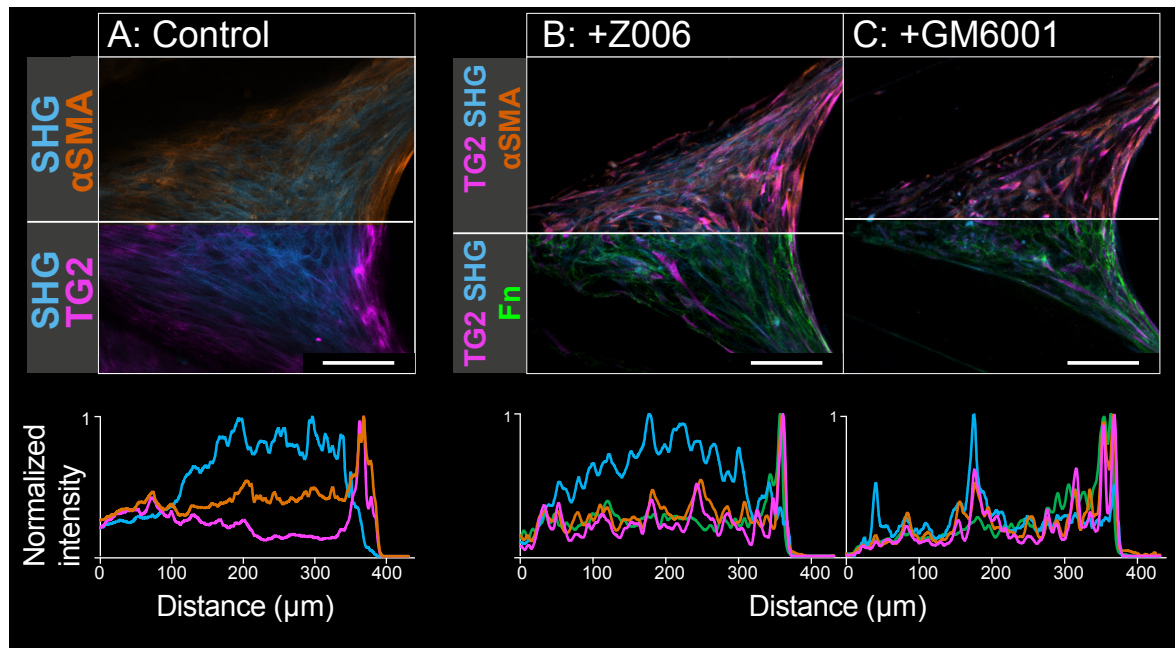


Fig. 5 TG2 stain of μ Tissue interventions with various inhibitors. (A-C, upper row) Representative ROI of μ Tissues imaged with 2P and CLSM of the control (DMSO, A), inhibition with Z006 (B), and inhibition with GM6001 (C). The CLSM+2P data is depicted with two different sets of look up table; top LUT: α SMA (orange), SHG (cyan); bottom LUT: TG2 (magenta), Fn (green), SHG (cyan). Scale bars 100 μ m. See also supplementary figure S08. **(A-C, lower row)** Respective normalized intensity profile of the channel in the middle row is shown parallel to the cleft bisector angle, e.g. main x-growth-direction of tissue here from left to right (cf. Fig. 1B+C). At each distance, the mean of 100 vertically accumulated pixels (50px above and 50px underneath the straight line) is plotted over the distance to growth front.

Inhibition of enzymatic TG2 activity leads to incomplete tissue maturation

To investigate if cross-linking of TG2 is required to form steep TNC gradients, we next inhibited the enzymatic TG2 activity using the specific inhibitor Z006 [95], which blocked TGF- β 1 mediated myofibroblast differentiation in 2D cell culture (Fig. S11). In μ Tissues, TG2 inhibition resulted in strongly reduced ECM maturation in the tissue core (Fig. 3B, more samples in Fig. S02). In contrast to the controls, the onset of tissue maturation was compromised in TG2 inhibited μ Tissues (Fig. 3B). The intensity plots revealed that Fn still showed a widened, but distinct peak at the growth front (Fig. 3B, profile plot), as well as TNC and α SMA, but that all markers are also present in the core. The Fn/col gradient was thus flattened following inhibition of TG2 cross-linking, but was still steeper than the corresponding α SMA and TNC gradients (Fig. 3B, profile plot). Also, the TG2 accumulation peak at the growth front was narrower compared to the control (Fig. 5B, profile plot). Altogether, these results suggest that the myofibroblasts did not fully transition back into fibroblasts and TNC was either less degraded or more produced in the core upon TG2 inhibition.

Not just TG2 inhibition, but also inhibition of TGF- β receptors with GW788388, a TGF- β receptor I/II inhibitor, hampered μ Tissue maturation and resulted in similarly slowed M-F-T as upon TG2 inhibition (Fig. 3C). The presence of myofibroblasts in the μ Tissue core, however, is highly remarkable. As in planar 2D cell culture, we confirmed that GW788388 specifically blocked TGF- β 1 mediated differentiation of fibroblasts into myofibroblast (Fig. S11) as reported before [96]. In 3D μ Tissues, there are apparently other factors (e.g. tension, integrin signalling) in addition to TGF- β 1 signalling that contribute to the myofibroblast phenotype.

Interestingly, when downstream signalling of TGF- β receptor was inhibited with GW788388, μ Tissues still grew but with significantly reduced tissue growth rates (Fig. 3I), tissue heights (Fig. 3J) and the projected area of the region of interest (Fig. 3C). However, inhibition of TG2 enzymatic activity did not affect the tissue height, but also reduced the growth kinetics (Fig. 3I). The combination of cellular contractile forces and ECM stabilization are needed to allow a tissue to advance in space during growth. TGF- β receptor signalling mediates, besides many other functions, increased cellular contractility. Lower force transmission can also be seen in the SHG fiber orientation plots both in TG2 and TGF- β receptor inhibition: while the collagen fibers in the control tissues showed long-range alignment with respect to each other (Fig. 3E), TG2 and TGF- β receptor inhibition resulted in a shorter-range alignment, suggesting a shorter force transmission range (dominated in regions from about 30° to 60° and -30° to -60°, Fig. 3F-G). In summary, both inhibitions appear to reduce the effect of cellular forces: TGF- β receptor inhibition might be associated with reduced contractility, while enzymatic TG2 inhibition results in a less cross-linked and more compliant ECM that cannot counterbalance the same level of contractile forces as a more rigid matrix.

Cellular recognition of fibronectin fiber strain via epidermal growth factor receptor signalling is necessary to drive the myofibroblast-to-fibroblast transition

To next ask if Fn fiber tension plays a role in myofibroblast stabilization and whether it might regulate the M-F-T back-conversion, we took advantage of our previous observation that mesenchymal stem cells show an upregulated osteogenic differentiation on stretched, but not on structurally relaxed Fn fibers, and that this sensitivity to Fn fiber strain is lost in the presence of Lapatanib, a broad epidermal growth factor (EGF) receptor (ErbB) inhibitor [97]. Whether the cellular detection of Fn fiber strain is required for either F-M-T or M-F-T has never been tested. Under ErbB inhibition, F-M-T was not affected and myofibroblasts accumulated within the growth front (Fig. 3D, more samples in Fig. S04). However, the myofibroblasts reverted back to fibroblast much later, leading to a delayed, but not fully inhibited tissue maturation (Fig. 3D). Surprisingly, the width of the Fn-growth front was still narrow compared to the control, and only the TNC and α SMA regions were widened. This finding suggests that ErbB signalling is required for Fn fiber strain sensing and plays a role in the mechanically triggered myofibroblast-to-fibroblast-transition. As Fn fiber tension in 2D cell culture is regulated by cell contractility in a RhoA dependent manner [98], we next asked how RhoA inhibition might change the morphology of our μ Tissues. Either RhoA inhibition alone (Fig. 4D) or in combination with TG2 inhibition both compromised tissue maturation and showed a trabeculated tissue structure, as if parts of it had collapsed (Fig. 4E). The MFT was hampered, resulting in a widened growth front not only of α SMA, but also of TNC signal (Fig. 4E). Interestingly, the short-range SHG fiber orientation under ErbB signalling inhibition indicates a similar force transmission pattern as for the blocking of TG2 enzymatic activity and TGF- β RI signalling (Fig. 3F-H). However, neither the growth distances in xy-plane nor the μ Tissue thickness in ErbB inhibition were reduced (Fig. 3I-J). Together our data suggests that cellular recognition of Fn fiber strain is required to drive M-F-T in a timely manner and, if missing, force transmission distance is reduced while tissue growth seems not disturbed.

Ruptured tissues are partially repaired during tissue growth

During tissue growth, some μ Tissues spontaneously ruptured and initiated repair processes. Interestingly, regions around tissue ruptures showed an accumulation of the growth front markers TNC, α SMA and Fn as in the actual growth front (Fig. 6). For tissue growth, it is essential that repair and subsequent formation of relevant gradients occur rapidly to outcompete rupture events. Our μ Tissue platform allowed us to investigate tissue discontinuity over time. While most of the observed μ Tissues showed a distinct directionality of the upregulated growth front markers (Fn, α SMA, TNC) towards the open cleft (compare Fig. 1), there were also some μ Tissues that showed additional upregulation of the same markers in regions facing towards the cleft edges. Those tissues also showed a loss of internal tissue continuity in those regions (Fig. 6A). Surprisingly, the initiated repair processes appeared in the profile plot in very similar distributions as the growth front itself (Fig. 6C). Just the kinetics might vary,

4 Tenascin-C and tissue transglutaminase transiently orchestrate tissue growth enabling the transition towards tension-dependent tissue maturation

which was visible in a different spatial distribution of the profile intensities (Fig. 6C). Taken together, this μ Tissue platform also allows to investigate spontaneous tissue ruptures and subsequent repair processes.

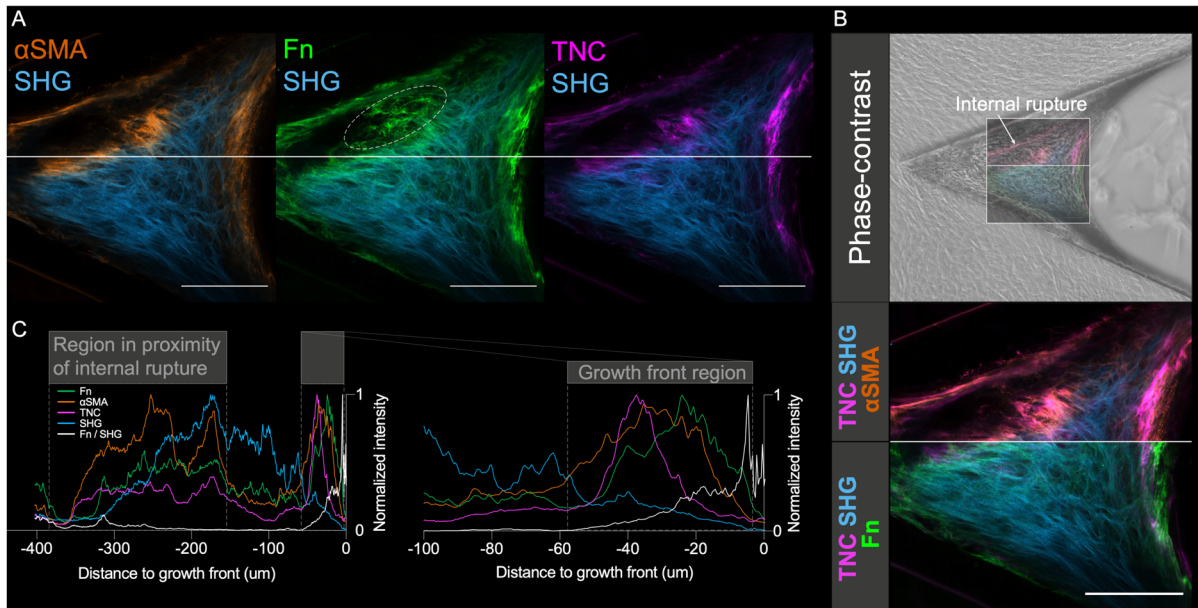


Fig. 6 Internal tissue dissociation and ruptures of μ Tissues. (A) Representative ROI of μ Tissues with spontaneous ruptures imaged with 2P and CLSM after 12 days. The CLSM+2P data is stained for α SMA (orange), SHG (cyan), Fn (green) and TNC (magenta). The early onset of repair can be seen in the Fn channel, where newly Fn matrix was assembled in between the ruptured void (white dashed line). Scale bars 100 μ m. (B) Representative μ Tissue with spontaneous rupture imaged with 2P and CLSM (ROI) and overlaid with the respective phase-contrast (upper row) and the close-up of the ROI (lower row). The CLSM+2P data is depicted with two different sets of look up table (top LUT: α SMA (orange), SHG (cyan); bottom LUT: TNC (magenta), SHG). Scale bars 100 μ m. (C) Intensity profile plots along horizontal line as column average of 100 px indicate the similarity between the growth front markers and the pattern at regions in proximity of internal rupture.

4.4 Discussion

In this study we used *de novo* grown μ Tissues in engineered PDMS cleft arrays (Fig. 1A-C) to investigate what transient roles TNC and TG2 play to initiate tissue maturation and how the spatio-temporal changes in the ECM composition contribute to the transition and stabilization of cell phenotype gradients. While initially seeding fibroblasts onto the scaffolds, we find that the much more contractile myofibroblasts define the growth front, aligned tangentially to the tissue edge (Fig. 1G+I) and assemble highly tensed Fn fibers. TNC, as well as TG2, show both a transient and spatio-temporal upregulation in the growth front and disappear from the ECM in regions where SHG-positive bundles of collagen indicate tissue maturation. Our data suggest a tightly timed functional complementarity between the actions of TNC and TG2 enabling the transition from the provisional to a maturing tissue never described before, where TNC conveys early ECM stabilization and is cleared over time when enzymatic cross-linking via TG2 is active. While gradients of soluble morphogens are typically thought to be primary factors driving tissue growth and gradient formation, we find that the ECM composition is the major driver stabilizing the cell phenotype. Even in the absence of soluble morphogens: when reseeding either fibroblasts or myofibroblast into our cleft-grown decellularized μ Tissues (Fig. 2A), myofibroblast predominantly relocated within the growth front region within the first 24 h (Fig. 2B). We therefore propose that the subsequent steps are essential to create a proliferative, highly tensed growth front, while at the same time promote the maturation and mechanical stabilization of the *de novo* growing tissue beneath.

At the growth front, the highly contractile myofibroblasts start to assemble Fn fibers at the cell culture medium interface (Fig. 1I). These early Fn fibers get progressively bundled by cell generated forces and thus are mostly aligned tangential to the growth front [99,100]. Fn fibers get stretched by cell generated forces to multiple times their equilibrium length, leading to the partial unfolding of Fn type III modules [10], and a similar force-dependent unfolding of TNC has been reported [101,102]. Myofibroblasts in the growth front secrete TNC, which appears to be spatially shifted with respect to the first appearance of Fn (Fig. 3A and Fig. S1, profile plots) and accumulates in the highly tensed growth front (Fig. 3A and Fig. S1, ROI). TNC with its hexameric starlike arms, each arm ranging from 220 to 280 kDa and possessing a Fn binding site, is then prone to organize and crosslink early Fn fibers by acting as crosslinking spacers [103], thereby enhancing the mechanical stability of this very first provisional matrix. It is not known whether TNC in the μ Tissue growth front is still in starlike form, but our additional investigations for different TNC epitopes, including for full length TNC (Fig. S09) suggest, that most of the structure is intact and can form networks. Furthermore, TNC might induce a motile phenotype in the growth front by reducing cell adhesion to Fn [53,54]. TNC is known to suppress RhoA and FAK activities [53,104], which

enhances cell migration while reducing inappropriate matrix contraction and both is advantageous within this newly formed tissue region. Further μ Tissue growth into the open cleft is then driven by myofibroblast proliferation [34]. Layers of cells and matrix are added on top of the tissues while the previously formed growth front moves into the interior [14]. In order to withstand the high tensile forces created by myofibroblasts, mechanical maturation of the provisional Fn matrix is now required. It is thus not surprising that not only TNC, but also the ECM crosslinker TG2 shows a high presence in the growth front and is mostly degraded as the tissue matures (Fig. 5A). TG2 can enzymatically crosslink Fn fibers only if they are pulled already into physical contact [57]. Our data furthermore suggest that the rapid clearance of TNC, and thus the formation of steep TNC gradients, requires the presence of TG2 activity, since inhibition of enzymatic TG2 activity leads to accumulation of TNC until deep into the core tissue regions (Fig. 3B and L). To support this conclusion, exogenously supplemented TG2 results in complete gradient disappearance (Fig. 4J) and significant reduction of the total TNC levels (Fig. 4K). Reduction of total TNC levels seems at first sight counterintuitive, since TG2 might also crosslink TNC and protect it from degradation. However, it was suggested that TG2 can bind to an intermediate of MMP-2 and thus regulate MMP-2 activity [105]. Our data indicate that MMP-2 is not relevant for TNC degradation, but a similar mechanism might exist for other MMPs as well. Interestingly, it was shown that MMP-2 expression in fibroblast were inversely related to the α SMA expression [106]. This could explain why MMP-2 inhibition did not show a difference here, since TNC is expressed within the α SMA positive growth front (Fig. 4C). TNC, Fn and α SMA signals are found throughout the tissue under exogenous supplementation of TG2, which suggests that a time-dependent regulation of TG2 is required for formation of steep ECM gradients and thus timely tissue maturation (Fig. 4J). This is remarkable, as no literature is available so far describing a functional dependency between TNC and TG2, even though few studies identified the presence of both TG2 and TNC *in vitro* and *in vivo* [107-115]. For example, TNC gradients play an important role at the edge of healing wounds, as well as Fn gradients [39].

While the Fn fibers are under high tension in the growth front, they are under far less tension once interdispersed with collagen fibers within the maturing tissues (Fig. 1J) [34]. Does the highly tensed Fn matrix play a role in the stabilization of the myofibroblast phenotype in the growth front, as Fn is known to promote cell proliferation [116,117]? Our finding here that myofibroblasts reseeded into our decellularized μ Tissues rapidly accumulated in the old growth front, in contrast to reseeded fibroblasts (Fig. 2B+C), suggests that this is indeed the case. But it is not just the presence of Fn, but the high tension of Fn fibers in the growth front that stabilize the myofibroblasts. As the tensional state of Fn fibers regulates the exposure of binding sites, mesenchymal stem cells in a previous study lost their ability to recognize the tensional state of Fn fibers when EGF-receptor signalling, i.e. ErbB signalling was blocked [97]. Taken our finding that ErbB signalling inhibition hampers the back-conversion of myofibroblasts to

fibroblasts (Fig. 3D) together with the finding that the predominant accumulation of reseeded myofibroblast in the growth front suggests that the loss of Fn fiber tension actually facilitates the transition of myofibroblasts to fibroblasts.

But how can a growth front rich in highly tensed Fn matrix assembled by α SMA-positive myofibroblasts be converted within a few micrometres into the tissue interior rich in fibroblasts and collagen? The steepness of the ECM gradient is particularly striking when the signals are shown as normalisation over collagen (SHG) (Fig. 1K and L and Fig. S01, lowest row). TG2 conveys in addition plenty of non-enzymatical functions and almost all cell-membrane bound TG2 forms 1:1 complexes with integrins [64,118,119]. TG2 is thus an integrin and syndecan-binding adhesion coreceptor for Fn and by stabilizing the complex, might counterbalance the above described de-adhesive properties of TNC in the growth front (Fig. 5A). Enzymatic cross-linking of TG2 is further reported to protect the ECM from proteolytic degradation [69], to promote the build-up of TGF- β reservoir in the ECM [120,121] and to rigidify the ECM [60,122], which in turn was suggested to facilitate TGF- β mechanical release by stretching the latent complex [123]. Tissue maturation is hampered if downstream TGF- β receptor signalling is inhibited (Fig. 3C), or if either TG2 enzymatic activity is inhibited (Fig. 3B) or if TG2 is exogenously supplemented (Fig. 4J). Tissue remodelling often involves MMP activity [1], and MMP inhibition prevents the degradation of TNC (Fig. 4B) and TG2 (Fig. 5C), in agreement with the literature [60,85,105,124,125]. While we thus identified various ECM factors that regulate the rapid remodelling of the growth front into maturing tissue, which factors drive the rapid conversion of myofibroblasts to fibroblasts? Again, we find here that this conversion is not completed if TGF- β receptors are inhibited (Fig. 3C) or when the timely regulated TG2 activity is disturbed by either inhibition of exogenous supplementation of TG2 (Fig. 3B).

The transition from a motile to a sessile phenotype is essential for later tissue maturation stages, as cellular movement is high in the Fn-dominated growth, but fewer cells are seen to migrate in the collagen-rich core tissue regions. While full-length TNC conveys de-adhesive functions, cleavage of TNC with MMP-2 or memprins was shown to generate cryptic binding sites which could permit interactions with heparan sulfated side-chains of syndecan-4 promoting α 5 β 1 integrin clustering and cell spreading, suggesting a protease-dependent time-switch function of TNC [65,87]. However, in contrast to broad spectrum MMP inhibition (Fig. 4B), selective MMP-2/-9 inhibition (Fig. 4C) did neither alter TNC degradation nor delayed tissue maturation. This suggests that other adhesive functions of TNC fragments might be induced by MMP other than MMP-2. Note here that the effect described by Saito et al. was not screened over a broad MMP spectrum, but targeted only MMP-2 based on previous reported MMP-2 evidence. It is known that research around the two gelatinases MMP-2/-9 tends to be

overrepresented due to the technical fact that historical zymograms were the first way to represent MMP activity, of which gelatin zymography is the easiest to perform [126]. Furthermore, fragments of TNC, TNfn1-8 and the FBG domains, but not full-length TNC, inhibited the assembly of a dense Fn fibrillar matrix within less than 1 day of incubation with temporally and spatially distinct effects [67]. Within similar time period the μ Tissues advance during the final incubation day roughly 25 μ m towards the open cleft (Fig. 3I). Within similar distances, the early Fn peak declines (Fig. 3A and Fig. S01), while the Fn peak appears much wider under broad spectrum MMP inhibitor treatment (Fig. 4B and Fig. S07A). Very recently, also autophagy associated proteasomal degradation of TNC was reported which could in addition also lead to TNC clearance in the deep tissue region [127]. To interrogate a potential link of TNC disappearance to proteolytic or autophagic degradation, specific blocking of these processes (proteasome inhibitor e.g. ALLN) or autophagy inhibitors (3-methyladenine (3-MA) that blocks early steps of autophagosome formation) are suggested for future studies. However, our broad spectrum MMP data together with the literature indicate that the MMP-induced, degradation-dependent time-switch function of TNC likely is key to promote tissue maturation by regulating the transition of the motile to a sessile phenotype, perhaps by inhibiting further Fn fibril assembly in locations of TNC degradation, which subsequently might disturb further collagen fibril assembly during maturation.

As the tissue matures, the older tissue interior shows less cellular movement and is rich in more rounded fibroblasts [34] surrounded by more aligned collagen fibers (Fig. 3E). Tissue maturation is hampered when Fn-collagen-binding is blocked [18], here by the peptide R1R2 (Fig. 4H), which is not surprising as collagen fiber polymerization is initiated by the presence of Fn fibers [16,17]. Also the inhibition of cell-collagen binding via α 2 β 1 integrin, which is reported to be essential for collagen fiber assembly [17,90], hinders tissue growth and maturation (Fig. 4I+L). But what is finally required for the collagen fiber networks to mature into mechanically stabilized tissues? Both broad spectrum MMP- and ROCK-inhibited μ Tissues show decreased levels of absolute signal intensities in Fn as well as in TNC and α SMA, and a reduction in mature collagen fibers. They also show similar internal ECM morphology (compare GM6001- with Y-27632-data in Fig. 4B,D+M, Fig. S06D and Fig. S07A). In contrast, with ROCK inhibition, cellular contractility forces are inhibited directly, which in turn results in a trabeculated morphology, decreased levels of mature collagen fibers, and reduced tissue maturation. Interestingly, once ROCK activity is inhibited, TG2 inhibition does not lead to the earlier reported delay of tissue maturation (compare Fig. 3B and Fig. 4D-E), while TG2 itself is also accumulating in the core tissue regions under enzymatic TG2 inhibition (Fig. 5B). Broad spectrum MMP inhibition lead to reduced collagen fiber network contraction *in vitro* [128,129], *in vivo* wound models associated impaired wound contraction with reduced MMP levels [130,131], and impaired collagen cleavage was reported to retard early wound healing [132]. Taken together, this suggests that the compensatory mechanisms ensuring tissue growth even under inhibition of enzymatic cross-linking activity require cell contractility.

A mechanically stable collagen ECM is needed to maintain mechanical integrity as cells pull on their environment, but how does this relate to the hampered tissue maturation seen under inhibition of enzymatic TG2 activity (Fig. 3B), TGF- β receptor signalling (Fig. 3C) and ErbB signalling (Fig. 3E)? Cells arrange ECM fibers and especially high load bearing collagen fibers along the axis of main force transmission, and mechanical forces regulate ECM synthesis and assembly of collagen fibers [133,134], thus the orientation of collagen fibers allows to estimate main direction of internal matrix stress. Given the height of our PDMS scaffold, μ Tissues start growing separately from both vertical cleft edges (Fig. 1A). After 1-2 days they fuse and form a continuous μ Tissue advancing towards the open cleft. The collagen fiber orientation in the horizontal plane of the ROI indicates thus cumulative force vectors of the continuous μ Tissue. Interestingly, the fiber orientation in the control μ Tissue suggests long-range force transmission towards the tip in addition to the one towards the cleft edges (Fig. 3E, more data see Fig. S05), while all three compared interventions (inhibition of ErbB signalling, TG2 enzymatic activity and TGF- β RI signalling, Fig. 3F-H) suggest a shorter force range transmission oriented towards the cleft edges. It is established in the literature that tissue tension regulates tissue growth [135-140], thus the fiber orientation could reflect the orientation of the surface stress at the time of deposition. Combined with the literature, our data suggest that mechanical force transmission over longer distances (compare Fig. 3E) might be needed for tissue integrity and for steep gradient formation, and in part also for tissue growth. Particularly interesting, since in clinical wound treatment, the redistribution of forces can reduce scar formation around the wound [141,142], and the direction of force can influence scar growth [143]. The collagen fiber alignment visualization could thus be correlated with the parameters of growth kinetics and ECM gradient slope to estimate whether an intervention might support successful closure of the wound or whether the respective force transmission suggests alteration in scar formation.

Our findings of TNC-, Fn- and α SMA-gradients in the *de novo* grown μ Tissues are in agreement with the data from skin wounds, as TNC was reported to regulate migration and proliferation of myofibroblasts and is upregulated in the granulation tissue at wound margins [39,144]. Furthermore, the distribution of the here identified actors can be found in spontaneous ruptures of control μ Tissues (Fig. 6A-C). This underlines the eminent relevance of the aforementioned formation of steep TNC-Fn- α SMA-gradients for healing and bridging those local sites with loss of tissue cohesions.

Life quality of patients will gain from the availability of platforms that closely mimic ECM of target tissue, which not only allows fundamental understanding of mechanisms in health and disease, but also contributes to the translation of such knowledge into clinics [145]. The complexity of the μ Tissue growth system is a great advantage to test mechanisms that otherwise cannot be tested *in vivo* or with even more simple 2D *in vitro* approaches. However, to achieve a complex structure of the controlled 3D

tissues, relatively long incubation times are needed, which can be a great challenge in running large interventional studies. For future follow-up investigations, we recommend combining our method with other animal-free and simplified methods of higher throughput to ultimately build a sequential test bank. Furthermore, to better distinguish between cause and correlation of the outlined accumulated TNC regions, further investigations are needed with TNC-KO/KD cells or supplementation of isolated TNC. It is also important to note that the morphological differences in terms of trabeculated structure observed in immunostaining could be a secondary effect of decreased serial and lateral adhesion strengths which might lead to micro-collapses of the internal tissue despite extremely gentle sample handling during washing steps.

Our *de novo* grown μ Tissues can be used in the future to test 2D cell culture-based hypotheses and might thus contribute as intermediate system prior to animal studies. For example, we demonstrated here that, despite the many reports of TG2 accumulation in processes of fibrosis or cancer [48,50,146,147], the ECM stabilisation mediated by enzymatic active TG2 is an essential requisite to achieve tissue maturation. However, non-covalent crosslinks, as here carried out by TNC, are much weaker than TG2-mediated covalent cross-links and provide fast enough dissociation rates to relax stresses [32]. Targeting tissue transglutaminase as therapy option was suggested as a promising approach to reduce both scar stiffening and ECM binding of LTBP-1, which results in a reduction of TGF- β 1 ECM storage [148]. Our data now suggest that this might not be the best option to go, as supplementation of TG2 inhibitors as well as exogenous TG2 supplementation and TGF- β receptor inhibition all resulted in increased α SMA expression and thus increased cell contractility. This path should be thoroughly reinvestigated further *in vitro*, so that subsequent animal experiments and clinical trials are only carried out if they comply with *in vitro* concepts that allow a sufficient degree of transferability.

It was recently shown that in an oral squamous cell carcinoma (OSCC) context, ECM gradients are present in the tumors where tumor matrix tracks (TMT) are matrix rich and separate tumor cell nests that are largely devoid of matrix [149]. Moreover, investigations of OSCC in a TNCKO setting revealed that TNC is a major regulator of the matrix composition and organisation in the TMT. Thus, results from the current study may be relevant to better understand the establishment and function of the TMT.

Indications are also accumulating that TNC, Fn and TG2 can be targeted for both diagnostic and therapeutic purposes [150-154], but little is known how they orchestrate tissue growth and repair processes in synchrony. Several of our discoveries made in the *de novo* grown μ Tissues significantly go beyond, and in part even contradict conclusions drawn from 2D cell culture. For example, our data

suggest a time-dependent mechanical ECM-stabilization by TNC, which get cleared rapidly when enzymatic TG2 cross-linking function is active and not perturbed. TG2 and TNC have thus been identified here as complementary co-regulating actors, required to form steep ECM gradients which allows both timely tissue maturation and clearance of myofibroblast. This suggests a remarkable functional dependency between TNC and TG2 which has not been reported before. However, it needs to be further investigated how and whether the functional dependency is TG2- or cross-linking specific, since cross-linking can in addition be mediated by other enzymes as well (e.g. LOX). While in 2D cell culture, both inhibition of enzymatic TG2 and TGF- β receptor signalling blocked F-M-T, they hampered tissue maturation in μ Tissues with increased overall F-M-T and even reduced myofibroblast clearance. This illustrates that methods to investigate tissue growth, control matrix production and fabricate tissue scaffolds are urgently needed to advance the fields of tissue engineering and regenerative medicine. ECM composition, and as we discovered here, the tensional state of their ECM fibers, are the major drivers stabilizing the cell phenotype, and rapid MMP dependent clearance of TNC and TG2 is required to achieve full tissue maturation. We propose further that the tissue stabilizing function of TNC is in part capable of compensating missing enzymatic TG2 crosslinking activity, allowing for reduced, but still substantial tissue growth. Furthermore, we identified TG2 enzymatic activity, broad spectrum MMP activity, TGF- β receptor signalling, Fn strain detection and Fn-collagen binding as key actors required to complete tissue maturation, which is defined by the M-F-T and the collagen dominated core ECM. Furthermore, we found that spontaneous ruptures in our *de novo* grown μ Tissue are rapidly bridged and healed under accumulation as earlier identified markers: TNC, α SMA and Fn. Future studies are essential to shed light on many open questions that can be raised in such *de novo* grown μ Tissue. Here, of particular interest is to further investigate the role of TGF- β , since this work indicates alternative functionality than reported in planar 2D cell culture and better understanding is needed. This is particularly important since a not well understood crosstalk between TNC and TGF- β receptor signalling exists. Finally, this study illustrates the importance and requirements of steep ECM gradients and how they influence myofibroblast plasticity, tissue maturation and ultimately tissue growth. μ Tissue platforms create new opportunities for *in vitro* research to systematically tune parameters that cannot be easily studied in reductionist 2D setups or in animal models. In the future, our platform may help to also study personalized factors influencing ECM gradients and screening tissue growth, when combined with fibroblast harvested from patients. Such knowledge can contribute to the development of novel diagnostic and treatment strategies with relevance also in cancer. In summary, tissue growth is delicately organized like a well-orchestrated symphony, where plenty of different actors are required, but each of their individual actions needs to be precisely initiated and tuned in time.

4.5 Materials and methods

Rationale for substrate design and fabrication method

Polydimethylsiloxane (PDMS) substrates were fabricated by replica molding of negative SU8-master structures, improving the previously published protocol [34]. To avoid residual membrane formation, a custom build compression device was applied as described below (Fig. S13, A-C). In order to reduce μ Tissue-to- μ Tissue variability, the cleft edges were smoothed with a photomask of higher resolution and each cleft is separated, so that the grown μ Tissues are not in direct contact with each other. Each substrate consists of a cluster of 16 clefts arranged in arrays. The arrangement of multiple cluster replicas on one master mold allowed a higher production throughput. Since it was shown that geometry can coordinate tissue growth [138], the cleft angle of 45° was chosen to reduce incubation times and still achieve sufficient tissue growth.

Master fabrication

A master mold was fabricated by standard lithography of multiple layers of SU8-3050 photoresist (MicroChem, USA) (Fig. S13, D). In brief, a 4" silicone wafer was dehydrated at 120°C for 10 min. For the first layer, 2 ml of SU8-3050 was dispensed and spin-coated at 500 rpm for 10 s with acceleration 100 rpm/s followed by 1000 rpm for 45 s with acceleration 500 rpm/s. After spin coating, a soft bake at 65°C for 7 min and at 95°C for 15 min was performed. After cooling down to room temperature (RT), spin coating was repeated twice with 4 ml of photoresist each resulting in a ~350 μ m thick resist layer. Samples were stored at RT for 24 hours prior to exposure. For exposure, a photolithography mask with a resolution of 32,000 dpi (Zitzmann GmbH, Germany) and a MA6 mask aligner (Karl Suss, Germany) were used and the samples were exposed with a total dose of 400 mJ/cm² (λ = 365 nm) divided in 4 runs with 60 s pause in between exposures. Post exposure bake was performed at 65°C for 3 min and 95°C for 10 min. Due to the thickness of the resist, all heating and cooling steps were performed at slow ramp. The resist was developed using mr-Dev 600 developer (Microresist Technologies, Germany) under ultrasound for 20 min, followed by a wash with fresh developer and isopropanol, each for 10 s. Master molds were passivated with 20 μ l of Trichloro(1H, 1H, 2H, 2H - Perfluorooctyl)Silane (Sigma 448931) under vacuum for 1 hour.

Microfabrication of PDMS scaffolds

PDMS scaffolds with open cleft free of residual membranes were replica-molded from the master mold using a custom-built compression device (Fig. S13, A-C). PDMS was mixed in a standard ratio of 10:1 base to curing agent (Sylgard 184, Dow Corning, USA), degassed at 70 mbar for 30 min, poured on the master mold placed in the custom-built compression device and degassed at 70

mbar max. 45 min until all air bubbles were removed. Afterwards, a 2 mm thick polymethyl methacrylate (PMMA) lid was placed on the top at a slight angle preventing the formation of any air bubbles (Fig. S13, B). Finally, the top piece of the compression device was mounted and all 4 screws were tightened in crossed manner with a maximum torque of 4 Nm (Fig. S13, C). After the PDMS was cured at 80°C overnight, each substrate was cut out with a 18 mm diameter punch (Fig. 13, E), cleaned in 70% ethanol ultrasonic bath for 20 min and stored in 70 % ethanol.

Functionalization and mounting of PDMS scaffolds

Fibronectin was covalently bound to the surface of the PDMS scaffolds using a heterobifunctional cross-linker (Sulfo-SANPAH, 0.5 mg/ml in PBS (1x, adjusted to pH 8.5 with NaOH), Thermo Fisher Scientific) as described previously [34,57]. The functionalized substrates were attached with optical glue NOA-61 (Norland Optical adhesive 61, Norland) to an uncoated polymer-bottom dish (μ -Dish 35mm, No. 81151, ibidi) that had previously been passivated using PLL(poly-L-lysine)(20)-g[3.5]-PEG(polyethylene glycol)(5) (0.1 mg/ml in HEPES2 (HEPES + 150 mM NaCl), SuSoS) (Fig. S13, F). After assembling the cell culture system, it was washed once with PBS and UV treated for 15 min. Prior to cell seeding, the surface was equilibrated with α -minimum essential medium (α MEM, Biowest SAS) supplemented with 10 % fetal bovine serum at 37°C for at least 1 hour.

μ Tissue growth experiments

Cell culture

Primary normal dermal human fibroblast (NHDF, passage numbers 6 to 10, Lonza) were maintained in α -minimum essential medium (α MEM, Biowest SAS) supplemented with 10 % fetal bovine serum and 1 % penicillin-streptomycin and exchanged every 2-3 days. All experiments were conducted at 37°C in a humidified atmosphere with 5 % CO₂. The cells were trypsinized and seeded on the PDMS substrates at a density of 2×10^5 cells per substrate. For μ Tissue experiments, the cell culture medium was supplemented with 100 μ M L-Ascorbic Acid 2-phosphate sesquimagnesium salt hydrate (A8960-5G, Sigma) and 0.05 mg/ml fibronectin in PBS. Fibronectin was isolated from human plasma as previously described [155]. For interventional experiments, the cell culture medium was further supplemented with 0.1 % DMSO and the following components from day 5 of μ Tissue growth: inhibition of enzymatic TG2 activity with Z006 (100 μ M, Zedira GmbH), inhibition of TGF- β RI with GW788388 (20 μ M, 3264, Tocris), inhibition of epidermal growth factor (EGF) receptor (ErbB) with Lapatanib (1 μ M, GW572016, Axon Medchem), inhibition of broad spectrum MMP with GM6001 (25 μ M, ab120845, Abcam), inhibition of MMP-2/-9 with SB-3CT (5 μ M, ab141579, Abcam), inhibition of ROCK with Y-27632 (10 μ M, No 1254, Tocris Bioscience), inhibition of α 2 β 1-integrin with BTT3033 (10 μ M, No 4724, Tocris), guinea pig liver transglutaminase

(30 µg/ml, T006, Zedira GmbH), inhibition of Fn-collagen interaction with R1R2 as previously described [18] (2.5 µM, amino sequence GLNGENQKEPEQGERGEAGPPLSGLSGNNQG RPSLPGLNGENQKEPEQGERGEAGPP manufactured by GenScript).

In order to assess the αSMA response on Z006 and GW788388 we performed a TGF-β1 stimulation test on 2D Fn coated glass. Primary normal dermal human fibroblast (NHDF, passage numbers 6 to 10, Lonza) were cultured routinely in normal growth medium composed of α-minimum essential medium (αMEM, Biowest SAS) supplemented with 10% fetal bovine serum and 1% penicillin-streptomycin. Once at optimal confluency, the fibroblasts were trypsinized and seeded separately in triplicates in 8-well labtek chambers at 4.500×10^3 cells/cm² in normal growth medium. After 24 h, medium was replaced with and without TGF-β1 (5ng/ml, 100-21C, PeptroTech). Each condition was combined with GW788388 (20 µM, 3264, Tocris), Z006 (100 µM, Zedira GmbH) and 0.1% DMSO and cultured further for additional 3 days including a media exchange at day 3.

In order to assess the potential toxicity of the different inhibitor treatments on the cellular viability and metabolic activity, a WST-1 test was performed on primary normal dermal human fibroblasts cultured in 2D cell culture. Primary normal dermal human fibroblast (NHDF, passage numbers 6 to 10, Lonza) were cultured routinely in normal growth medium composed of α-minimum essential medium (αMEM, Biowest SAS) supplemented with 10% fetal bovine serum and 1% penicillin-streptomycin. Once at optimal confluency, the fibroblasts were trypsinized and seeded separately in triplicates in 96-well plates at 4.500×10^3 cells/cm² in normal growth medium. After 4 hours, the cells were exposed to the following inhibitors treatments: Z006 (100 µM, Zedira GmbH), GW788388 (20 µM, No 3264, Tocris), GM6001 (25 µM, ab120845, Abcam), SB-3CT (5 µM, ab141579, Abcam), Y-27632 (10 µM, No 1254, Tocris Bioscience), BTT3033 (10 µM, No 4724, Tocris). Cells cultured in normal growth medium and in growth medium supplemented with 0.1 % DMSO were used as control as all inhibitors were reconstituted in DMSO. After 24 h, tetrazolium salts-containing WST-1 reagent (1:10, No 05015944001, Roche) was added to the cells and incubated for 90 min at 37°C, 5 % CO₂. During this time, metabolically active cells cleave the tetrazolium salts contained in the WST-1 reagent into formazan, which has a higher absorbance than the tetrazolium salts. For all conditions tested, the absorbance of the medium was then measured with a plate reader (Tecan M200). Absorbances values were further normalized by that of the control with 0.1 % DMSO condition and reported in Figure S11.

Decellularization and re-seeding

Samples were decellularized following a modified Cukierman protocol [75 – 77]. µTissues were washed twice with pre-warmed HBSS (+ Ca, + Mg) and once with cold Sodium Deoxycholate (0.5 % (w/v), Sigma-Aldrich) in PBS. Cell membranes were removed during two incubation on ice for 10

min with cold Sodium Deoxycholate (0.5 % (w/v), Sigma-Aldrich) in PBS. After three times PBS wash, samples were stored at 4°C during preparation of cell suspension for re-seeding. For tracking the re-seeded cells, cell tracker (10 µM, CellTracker™ Red CMTPX Dye, Thermo Fisher Scientific) in serum-free α -minimum essential medium (α MEM, Biowest SAS) and Insulin-Transferin-Selin (ITS, 41400-04, Thermo Fisher Scientific) as serum replacement was replaced with the cells medium and incubated at 37°C with 5 % CO₂ for 30 min. The dye-containing solution was then removed by incubating the cells with the serum free medium for 5 min three times, followed by a wash with PBS. The stained cells were trypsinized and seeded in 2 ml of α -minimum essential medium (α MEM, Biowest SAS) supplemented with 100 µM L-Ascorbic Acid 2-phosphate sesquimagnesium salt hydrate (A8960-5G, Sigma) and 1 % penicillin-streptomycin onto the pre-warmed decellularized matrices at density of 0.5 Mio cells/ml.

Fixation and immunofluorescence

After 12 days of total incubation, Samples were washed twice with pre-warmed HBSS (+ Ca, + Mg) and fixed with 4 % PFA for 15 min. The cell membrane was permeabilized with 1 % Triton X-100 (T8787-50ML, Sigma-Aldrich) for 20 min followed by 60 min incubation in blocking solution (2 % BSA (w/v) (05470-5G, Sigma-Aldrich) and 5 % donkey serum (v/v) (ab7475, Abcam)). μ Tissues depicted in Fig. 1, 3, 4 and 6 were immunostained against TNC and μ Tissues depicted in Fig. 5 were immunostained against TG2. TNC antibody (1:100, BC-24, MA1-26779, Thermo Fisher Scientific) was combined with Fn (C-20) antibody (1:100, sc6952, Santa Cruz) and were supplemented in blocking solution to the respective μ Tissues and incubated for 1 hour at RT. After washing three times in PBS for 5 min each, samples were incubated with anti-goat Alexa Fluor 488 (1:200, ab260129, abcam), anti-mouse Alexa Fluor 647 (1:100, ab150107, Abcam) in blocking solution for 1 hour at RT. After Three additional PBS washes, α SMA was stained with Alexa Fluor 594-conjugated anti- α -smooth muscle actin antibody (1:100, ab202368, Abcam) in blocking solution for 1 hour at RT followed by three PBS washes. In addition to the described staining protocol, we tested different TNC antibodies in μ Tissues depicted in Supplement Fig. S09. In addition to the monoclonal antibody BC-24 (epitope EGF repeats; MA1-26779, Thermo Fisher Scientific) used as standard TNC stain in this study, we tested different epitopes by using a polyclonal TNC antibody (produced in rabbit, provided by G. Orend) counterstained with anti-rabbit Alexa Fluor 555 (1:100, A21429, Thermo Fisher Scientific) and another monoclonal TNC B28.13 (epitope constant Fn-III repeat 6 or 7 (Ambort et al. 2010), produced in mice, kindly provided by G. Orend) counterstained with anti-mouse Alexa Fluor 647 (1:100, ab150107).

In the samples shown in Fig. 5A, primary TG2 antibody (1:100, CUB 7402, ab2386, Abcam) was supplemented in blocking solution, incubated for 1 hour at RT and after washing three times in PBS

for 5 min each, counterstained with anti-mouse Alexa Fluor 647 (1:100, ab150107, Abcam). After washing three times in PBS for 5 min each, α SMA was stained with Alexa Fluor 594-conjugated anti- α -smooth muscle actin antibody (1:100, ab202368, Abcam) in blocking solution for 1 hour at RT followed by three PBS washes following the above protocol. Staining of samples Fig. 5B+C followed the same protocol with addition of with Fn (C-20) antibody (1:100, sc6952, Santa Cruz) counterstained with anti-goat Alexa Fluor 488 (1:200, ab260129, abcam).

The re-seeded μ Tissues in Fig. 2 were fixed, permeabilized and blocked as described above and afterwards stained with Alexa Fluor 594-conjugated anti- α -smooth muscle actin antibody (1:100, ab202368, Abcam) in blocking solution for 1 hour at RT followed by three PBS washes.

Microscopy and image analysis

Image acquisition

Phase-contrast images of the μ Tissues were acquired using a Zeiss Axiovert 200 M inverted microscope with 5x objective. Confocal fluorescence imaging was performed using a Leica TCS SP8 MP inverted multiphoton laser scanning microscope with a 25x objective (0.95NA L Water HCX IRAPO). Fluorophores were directly excited in single photon mode. Mature collagen fibers were imaged by second harmonic generation (SHG) in multiphoton laser scanning mode with open pinhole. Second harmonic was generated with a Mai Tai XF (Spectra-Physics) femtosecond Ti-sapphire pulsed laser tuned at 880nm and signal emitted from collagen fibers was detected at 440 nm.

Image analysis

Growth distances

Growth distances were measured between the angle tip of the cleft and the μ Tissue-medium interphase along the bisector angle axis in the phase-contrast images of the respective timepoints.

Visualization and profile intensity plots

All images were rotated such that the angle tip of the cleft is oriented left-handed and the bisector angle of the cleft is parallel to the x-axis of the image. Since the μ Tissues do not form symmetrically along the bisector angle (parallel to x-axis), a representative symmetry axis was visually assessed such that it represents the young-to-mature-gradient in each μ Tissue. Profile intensities were assessed along this symmetry axis by column intensity average of 100 pixels equally distributed around the symmetry axis at each x-position. Profile intensity data used for plots was normalized by the respective maximum level of each channel, which allows relative comparison on an inter-channel and inter-tissue level. For orientation and comparison of the absolute intensities, the

integral of the curve of each raw intensity profile is plotted (Fig. 3L, Fig. 4K and M). To determine the distance to growth front (e.g. Fig. 1K and L), all channels were cumulated and the boundaries of the μ Tissue was defined at the x position where cumulative signal intensity was greater than the threshold of 25% of maximum intensity at the tissue-medium interphase. The signal ratios over SHG (e.g. Fn/SHG) is only plotted for distances $< 0 \mu\text{m}$. The overview visualizations with split look-up-tables were created by a custom build FIJI script and split at the y-position of the earlier determined symmetry axis used for profile plot.

Fiber orientation

Fiber orientation analysis was carried out using a custom-written MATLAB script provided by T. Yamashita. Orientation of the fibrous structure found in the SHG images was analyzed based on a filtering method using a custom-written MATLAB script (2020a, Mathworks, MA, USA). We here utilized a 5x5 basic operator H_x optimized by Kroon and H_y being the transposition of H_x :

$$H_x = \begin{pmatrix} 0.0007 & 0.0052 & 0.0370 & 0.0052 & 0.0007 \\ 0.0037 & 0.1187 & 0.2589 & 0.1187 & 0.0037 \\ 0 & 0 & 0 & 0 & 0 \\ -0.0037 & -0.1187 & -0.2589 & -0.1187 & -0.0037 \\ -0.0007 & -0.0052 & -0.0370 & -0.0052 & -0.0007 \end{pmatrix}$$

(1)

$H_{xx}=H_x \cdot H_x$, $H_{yy}=H_y \cdot H_y$ and $H_{xy}=H_x \cdot H_y$, where the dot product represents a sequential application of the basic operators to the image, were applied to the pre-processed SHG images to obtain the second order image derivatives I_{xx} , I_{yy} and I_{xy} , respectively. These outcomes were processed using a Gaussian filter with 4 pixel sigma, resulting in smoothed image derivatives I_{xx}^* , I_{yy}^* and I_{xy}^* . The pixel-level local orientation φ was then computed as follows:

$$\varphi(i, j) = 0.5 \arctan \frac{-2I_{xy}^*(i, j)}{I_{xx}^*(i, j) - I_{yy}^*(i, j)}$$

(2)

Statistical analysis

Unpaired two-tailed Mann-Whitney test was performed with GraphPad Prism software to test for statistical significance. Error bars represent 95% confidence intervals (CI). In WST-experiments (Fig. S11), statistical significance between the normalized absorbances of the different conditions tested and that of the control was assessed with a student t-test ($\alpha < 0.05$).

4.6 Acknowledgements

We gratefully thank Marcel Graetz for his contribution in phase-contrast image acquisition and him and Giulia Ammirati for assistance in quantifying growth kinetics, Kathrin Laxhuber for her contribution with WST control experiments, Dr. Isabel Gerber and Chantel Spencer for technical support, the Scientific Center for Optical and Electron Microscopy (ScopeM, ETH Zurich) and Dr. Justine Kusch for her support with multiphoton image acquisition.

4.7 References

1. Bonnans C, Chou J, Werb Z. Remodelling the extracellular matrix in development and disease. *Nat Rev Mol Cell Biol*; 2014 Dec;15(12):786–801.
2. Rodrigues M, Kosaric N, Bonham CA, Gurtner GC. Wound Healing: A Cellular Perspective. *Physiol Rev*; 2019 Jan;99(1):665–706.
3. Midwood KS, Williams LV, Schwarzbauer JE. Tissue repair and the dynamics of the extracellular matrix. *Int J Biochem Cell Biol*; 2004 Jun;36(6):1031–7.
4. Rybinski B, Franco-Barraza J, Cukierman E. The wound healing, chronic fibrosis, and cancer progression triad. *Physiol Genomics*; 2014 Apr;46(7):223–44.
5. Cox TR, Ertler JT. Molecular Pathways: Connecting Fibrosis and Solid Tumor Metastasis. *Clin Cancer Res*; 2014 Jul;20(14):3637–43.
6. Urban ML, Manenti L, Vaglio A. Fibrosis--A Common Pathway to Organ Injury and Failure. *N Engl J Med*; 2015 Jul 2;373(1):95–6.
7. Walker C, Mojares E, del Río Hernández A. Role of Extracellular Matrix in Development and Cancer Progression. *Int J Mol Sci*; 2018 Oct;19(10):3028.
8. Theocharis AD, Manou D, Karamanos NK. The extracellular matrix as a multitasking player in disease. *FEBS J*; 2019 Aug;286(15):2830–69.
9. Hynes RO. The Extracellular Matrix: Not Just Pretty Fibrils. *Science*; 2009 Nov;326(5957):1216–9.
10. Vogel V. Unraveling the Mechanobiology of Extracellular Matrix. *Annual Reviews*; 2018 Feb 12;80(1):353–87.
11. Pakshir P, Hinz B. The big five in fibrosis: Macrophages, myofibroblasts, matrix, mechanics, and miscommunication. *Matrix Biol*; 2018 Aug;68-69:81–93.
12. Hynes RO, Naba A. Overview of the Matrisome--An Inventory of Extracellular Matrix Constituents and Functions. *Cold Spring Harb Perspect Biol*. 2012 Jan;4(1):a004903–3.
13. Dzamba BJ, Peters DM. Arrangement of cellular fibronectin in noncollagenous fibrils in human fibroblast cultures. *J Cell Sci*; 1991 Nov;100(3):605–12.
14. Bidan CM, Kollmannsberger P, Gering V, Ehrig S, Joly P, Petersen A, Vogel V, Fratzl P, Dunlop JWC. Gradual conversion of cellular stress patterns into pre-stressed matrix architecture during *in vitro* tissue growth. *J R Soc Interface*; 2016 May;13(118):20160136.
15. Mouw JK, Ou G, Weaver VM. Extracellular matrix assembly: a multiscale deconstruction. *Nat Rev Mol Cell Biol*; 2014 Dec;15(12):771–85.
16. McDonald JA, Kelley DG, Broekelmann TJ. Role of fibronectin in collagen deposition: Fab' to the gelatin-binding domain of fibronectin inhibits both fibronectin and collagen organization in fibroblast extracellular matrix. *J Cell Biol*. 1982 Jan;92(2):485–92.
17. Sottile J, Hocking DC. Fibronectin polymerization regulates the composition and stability of extracellular matrix fibrils and cell-matrix adhesions. Schwartz M, editor. *Mol Biol Cell*. 2002 Oct;13(10):3546–59.
18. Kubow KE, Vukmirovic R, Zhe L, Klotzsch E, Smith ML, Gourdon D, Luna S, Vogel V. Mechanical forces regulate the interactions of fibronectin and collagen I in extracellular matrix. *Nat Commun*; 2015

Aug;6(1):8026.

19. Nelson CM, VanDuijn MM, Inman JL, Fletcher DA, Bissell MJ. Tissue Geometry Determines Sites of Mammary Branching Morphogenesis in Organotypic Cultures. *Science*; 2006 Oct;314(5797):298–300.
20. Yan D, Lin X. Shaping morphogen gradients by proteoglycans. *Cold Spring Harb Perspect Biol*. 2009 Sep;1(3):a002493.
21. Wu W, Tholozan FM, Goldberg MW, Bowen L, Wu J, Quinlan RA. A gradient of matrix-bound FGF-2 and perlecan is available to lens epithelial cells. *Exp Eye Res*; 2014 Mar;1(120):10–4.
22. Wang Y, He G, Wang F, Zhang C, Ge Z, Zheng X, Deng H, Yuan C, Zhou B, Tao X, Zhang J, Tang K. Aspirin inhibits adipogenesis of tendon stem cells and lipids accumulation in rat injury tendon through regulating PTEN/PI3K/AKT signalling. *J Cell Mol Med*; 2019 Nov;23(11):7535–44.
23. Hubka KM, Carson DD, Harrington DA, Farach-Carson MC. Perlecan domain I gradients establish stable biomimetic heparin binding growth factor gradients for cell migration in hydrogels. *Acta Biomater*; 2019 Oct;97:385–98.
24. Thotakura S, Basova L, Makarenkova HP. FGF Gradient Controls Boundary Position Between Proliferating and Differentiating Cells and Regulates Lacrimal Gland Growth Dynamics. *Front Genet*; 2019 May; 28(10):543.
25. Ishida-Ishihara S, Akiyama M, Furusawa K, Naguro I, Ryuno H, Sushida T, Ishihara S, Haga H. Osmotic gradients induce stable dome morphogenesis on extracellular matrix. *J Cell Sci*; 2020 Jul; 133(14):jcs243865.
26. Shimizu A, Goh WH, Itai S, Karyappa R, Hashimoto M, Onoe H. ECM-based microfluidic gradient generator for tunable surface environment by interstitial flow. *Biomicrofluidics*; 2020 Jul; 14(4):044106.
27. Lampi MC, Reinhart-King CA. Targeting extracellular matrix stiffness to attenuate disease: From molecular mechanisms to clinical trials. *Sci Transl Med*; 2018 Jan;10(422):eaao0475.
28. Harn HIC, Ogawa R, Hsu CK, Hughes MW, Tang MJ, Chuong CM. The tension biology of wound healing. *Exp Dermatol*; 2019 Apr;28(4):464–71.
29. Ambrosi D, Ben Amar M, Cyron CJ, DeSimone A, Goriely A, Humphrey JD, Kuhl E. Growth and remodelling of living tissues: perspectives, challenges and opportunities. *J R Soc Interface*; 2019 Aug;16(157):20190233.
30. Yamada KM, Sixt M. Mechanisms of 3D cell migration. *Nat Rev Mol Cell Biol*; 2019 Dec;20(12):738–52.
31. Xi W, Saw TB, Delacour D, Lim CT, Ladoux B. Material approaches to active tissue mechanics. *Nat Rev Mat*; 2019 Jan 1;4(1):23–44.
32. Chaudhuri O, Cooper-White J, Janmey PA, Mooney DJ, Shenoy VB. Effects of extracellular matrix viscoelasticity on cellular behaviour. *Nature*; 2020 Aug;584(7822):535–46.
33. Kim J, Koo B-K, Knoblich JA. Human organoids: model systems for human biology and medicine. *Nat Rev Mol Cell Biol*; 2020 Oct;21(10):571–84.
34. Kollmannsberger P, Bidan CM, Dunlop JWC, Fratzl P, Vogel V. Tensile forces drive a reversible fibroblast-to-myofibroblast transition during tissue growth in engineered clefts. *Sci Adv*; 2018 Jan;4(1):eaao4881.
35. Shook BA, Wasko RR, Rivera-Gonzalez GC, Salazar-Gatzimas E, López-Giráldez F, Dash BC, Muñoz-Rojas AR, Aultman KD, Zwick RK, Lei V, Arbiser JL, Miller-Jensen K, Clark DA, Hsia HC, Horsley V.

Myofibroblast proliferation and heterogeneity are supported by macrophages during skin repair. *Science*; 2018 Nov;362(6417):eaar2971.

36. Pakshir P, Noskovicova N, Lodyga M, Son DO, Schuster R, Goodwin A, Karvonen H, Hinz B. The myofibroblast at a glance. *J Cell Sci*; 2020 Jul;133(13):jcs227900.
37. Tomasek JJ, Gabbiani G, Hinz B, Chaponnier C, Brown RA. Myofibroblasts and mechano-regulation of connective tissue remodelling. *Nat Rev Mol Cell Biol*; 2002 May;3(5):349–63.
38. Van De Water L, Varney S, Tomasek JJ. Mechanoregulation of the Myofibroblast in Wound Contraction, Scarring, and Fibrosis: Opportunities for New Therapeutic Intervention. *Adv Wound Care*; 2013 May;2(4):122–41.
39. Mackie EJ, Halfter W, Liverani D. Induction of tenascin in healing wounds. *J Cell Biol*; 1988 Jan 1;107(6 II):2757–67.
40. Simon DD, Niklason LE, HUMPHREY JD. Tissue Transglutaminase, Not Lysyl Oxidase, Dominates Early Calcium-Dependent Remodeling of Fibroblast-Populated Collagen Lattices. *Acta Anatomica*; 2015 Jul 1;200(2):104–17.
41. Huelsz-Prince G, Belkin AM, vanBavel E, Bakker ENTP. Activation of Extracellular Transglutaminase 2 by Mechanical Force in the Arterial Wall. *J Vasc Res*; 2013;50(5):383–95.
42. Chiquet M, Renedo AS, Huber F, Flück M. How do fibroblasts translate mechanical signals into changes in extracellular matrix production? *Matrix Biol*; 2003 Mar;22(1):73–80.
43. Fluck M, Tunc-Civelek V, Chiquet M. Rapid and reciprocal regulation of tenascin-C and tenascin-Y expression by loading of skeletal muscle. *J Cell Sci*; 2000 Oct;113(20):3583–91.
44. Webb CMB, Webb CM, Zaman G, Zaman G, Mosley JR, Mosley JR, Tucker RP, Tucker RP, Lanyon LE, Lanyon LE, Mackie EJ, Mackie EJ. Expression of tenascin-C in bones responding to mechanical load. *J Bone Miner Res*; 1997 Jan;12(1):52–8.
45. Chiquet-Ehrismann R, Mackie EJ, Pearson CA, Sakakura T. Tenascin: an extracellular matrix protein involved in tissue interactions during fetal development and oncogenesis. *Cell*; 1986 Oct 10;47(1):131–9.
46. Orend G, Chiquet-Ehrismann R. Tenascin-C induced signaling in cancer. *Cancer Lett*; 2006 Dec 8;244(2):143–63.
47. Midwood KS, Orend G. The role of tenascin-C in tissue injury and tumorigenesis. *J Cell Commun Signal*; 2009 Dec;3(3-4):287–310.
48. Olsen KC, Sapinoro RE, Kottmann RM, Kulkarni AA, Iismaa SE, Johnson GVW, Thatcher TH, Phipps RP, Sime PJ. Transglutaminase 2 and Its Role in Pulmonary Fibrosis. *Am J Resp Crit Care Med*. 2011 Sep 15;184(6):699–707.
49. Bhattacharyya S, Wang W, Morales-Nebreda L, Feng G, Wu M, Zhou X, Lafyatis R, Lee J, Hinchcliff M, Feghali-Bostwick C, Lakota K, Budinger GRS, Raparia K, Tamaki Z, Varga J. Tenascin-C drives persistence of organ fibrosis. *Nat Commun*; 2016 Jun;7(1):ncomms11703.
50. Wang Z, Stuckey DJ, Murdoch CE, Camelliti P, Lip GYH, Griffin M. Cardiac fibrosis can be attenuated by blocking the activity of transglutaminase 2 using a selective small-molecule inhibitor. *Cell Death Dis*; 2018 Apr 27;9(6):45.
51. Eckert RL. Transglutaminase 2 takes center stage as a cancer cell survival factor and therapy target. *Mol Carcinog*; 2019 Jun 1;58(6):837–53.

52. Midwood KS, Chiquet M, Tucker RP, Orend G. Tenascin-C at a glance. *J Cell Sci*; 2016 Dec 1;129(23):4321–7.
53. Huang W, Chiquet-Ehrismann R, Moyano JV, Garcia-Pardo A, Orend G. Interference of Tenascin-C with Syndecan-4 Binding to Fibronectin Blocks Cell Adhesion and Stimulates Tumor Cell Proliferation. *Cancer Res*; 2001 Dec 1;61(23):8586–94.
54. Orend G, Huang W, Olayioye MA, Hynes NE, Chiquet-Ehrismann R. Tenascin-C blocks cell-cycle progression of anchorage-dependent fibroblasts on fibronectin through inhibition of syndecan-4. *Oncogene*; 2003 Jun 19;22(25):3917–26.
55. Williams SA, Schwarzbauer JE. A shared mechanism of adhesion modulation for tenascin-C and fibulin-1. *Mol Biol Cell*; 2009 Feb;20(4):1141–9.
56. Wang Z, Collighan RJ, Gross SR, Danen EHJ, Orend G, Telci D, Griffin M. RGD-independent cell adhesion via a tissue transglutaminase-fibronectin matrix promotes fibronectin fibril deposition and requires syndecan-4/2 $\alpha 5\beta 1$ integrin co-signaling. *J Biol Chem*; 2010 Dec 17;285(51):40212–29.
57. Griffin M, Wilson J. Detection of epsilon(gamma-glutamyl) lysine. *Mol Cell Biochem*; 1984;58(1-2):37–49.
58. Griffin M, Casadio R, Bergamini CM. Transglutaminases: nature's biological glues. *Biochem J*. 2002 Dec 1;368(Pt 2):377–96.
59. Zemskov EA, Janiak A, Hang J, Waghray A, Belkin AM. The role of tissue transglutaminase in cell-matrix interactions. *Front Biosci*; 2006;11:1057–76.
60. Nurminskaya MV, Belkin AM. Cellular functions of tissue transglutaminase. *Int Rev Cell Mol Biol*; 2012;294:1–97.
61. Gundemir S, Colak G, Tucholski J, Johnson GVW. Transglutaminase 2: A molecular Swiss army knife. *Biochim Biophys Acta Mol Cell Res*; 2012 Feb;1823(2):406–19.
62. Kanchan K, Fuxreiter M, Fésüs L. Physiological, pathological, and structural implications of non-enzymatic protein–protein interactions of the multifunctional human transglutaminase 2. *Cell Mol Life Sci*; 2015 May 6;72(16):3009–35.
63. Katt WP, Antonyak MA, Cerione RA. Opening up about Tissue Transglutaminase: When Conformation Matters More than Enzymatic Activity. *Med one*; 2018;3(6).
64. Benn MC, Weber W, Klotzsch E, Vogel V, Pot SA. Tissue transglutaminase in fibrosis — more than an extracellular matrix cross-linker. *Curr Opin Biomed Eng*; 2019 Jun 1;10:156–64.
65. Saito Y, Imazeki H, Miura S, Yoshimura T, Okutsu H, Harada Y, Ohwaki T, Nagao O, Kamiya S, Hayashi R, Kodama H, Handa H, Yoshida T, Fukai F. A peptide derived from tenascin-C induces beta1 integrin activation through syndecan-4. *J Biol Chem*; 2007 Nov 30;282(48):34929–37.
66. Ambort D, Brellier F, Becker-Pauly C, Stöcker W, Andrejevic-Blant S, Chiquet M, Sterchi EE. Specific processing of tenascin-C by the metalloprotease meprin beta neutralizes its inhibition of cell spreading. *Matrix Biol*; 2010 Jan;29(1):31–42.
67. To WS, Midwood KS. Cryptic domains of tenascin-C differentially control fibronectin fibrillogenesis. *Matrix Biol*; 2010 Sep;29(7):573–85.
68. To WS, Midwood KS. Identification of Novel and Distinct Binding Sites within Tenascin-C for Soluble and Fibrillar Fibronectin. *J Biol Chem*; 2011 Apr;286(17):14881–91.
69. Greenberg CS, Birckbichler PJ, Rice RH. Transglutaminases: multifunctional cross-linking enzymes that

- stabilize tissues. *FASEB J*; 1991 Dec;5(15):3071–7.
70. Larreta-Garde V, Berry H. Modeling extracellular matrix degradation balance with proteinase/transglutaminase cycle. *J Theo Biol*; 2002 Jan;217(1):105–24.
 71. Chabria M, Hertig S, Smith ML, Vogel V. Stretching fibronectin fibers disrupts binding of bacterial adhesins by physically destroying an epitope. *Nat Commun*; 2010 Dec;1(9).
 72. Hertig S, Chabria M, Vogel V. Engineering Mechanosensitive Multivalent Receptor-Ligand Interactions: Why the Nanolinker Regions of Bacterial Adhesins Matter. *Nano Lett*; 2012 Oct;12(10):5162–8.
 73. Arnoldini S, Moscaroli A, Chabria M, Hilbert M, Hertig S, Schibli R, Béhé M, Vogel V. Novel peptide probes to assess the tensional state of fibronectin fibers in cancer. *Nat Commun*; 2017 Dec 1;8(1):1793.
 74. Fonta CM, Arnoldini S, Jaramillo D, Moscaroli A, Oxenius A, Béhé M, Vogel V. Fibronectin fibers are highly tensed in healthy organs in contrast to tumors and virus-infected lymph nodes. *Matrix Biol*; 2020 Jan;1:100046.
 75. Remedios Castelló-Cros EC. Stromagenesis during tumorigenesis: characterization of tumor-associated fibroblasts and stroma-derived 3D matrices. *Meth Mol Biol*; 2009;522(19):275–305.
 76. Kubow KE, Klotzsch E, Smith ML, Gourdon D, Little WC, Vogel V. Crosslinking of cell-derived 3D scaffolds up-regulates the stretching and unfolding of new extracellular matrix assembled by reseeded cells. *Integr Biol*; 2009 Dec;1(11-12):635–48.
 77. Wang K, Eguiluz RCA, Wu F, Seo BR, Fischbach C, Gourdon D. Stiffening and unfolding of early deposited-fibronectin increase proangiogenic factor secretion by breast cancer-associated stromal cells. *Biomaterials*; 2015 Jun 1;54:63–71.
 78. Grumet M, Hoffman S, Crossin KL, Edelman GM. Cytotactin, an extracellular matrix protein of neural and non-neural tissues that mediates glia-neuron interaction. *Proc Natl Acad Sci*; 1985 Dec 1;82(23):8075–9.
 79. Mackie EJ, Tucker RP, Halfter W, Chiquet-Ehrismann R, Epperlein HH. The distribution of tenascin coincides with pathways of neural crest cell migration. *Development*; 1988 Jan;102(1):237–50.
 80. Lutz R, Sakai T, Chiquet M. Pericellular fibronectin is required for RhoA-dependent responses to cyclic strain in fibroblasts. *J Cell Sci*; 2010 May 1;123(9):1511–21.
 81. Griffiths DR, Jenkins TM, Addington CP, Stabenfeldt SE, Lifshitz J. Extracellular matrix proteins are time-dependent and regional-specific markers in experimental diffuse brain injury. *Brain Behav*; 2020 Jul 23;33(13):A76.
 82. Mai JX, Sameni M, Mikkelsen T, Sloane BF. Degradation of extracellular matrix protein tenascin-C by cathepsin B: An interaction involved in the progression of gliomas. *Biol Chem*. 2002 Sep;383(9):1407–13.
 83. Tews DS, Nissen A. Expression of Adhesion Factors and Degrading Proteins in Primary and Secondary Glioblastomas and Their Precursor Tumors. *Invas Metast*; 2000 Mar 1;18(5-6):271–84.
 84. Latijnhouwers M, Bergers M, Veenhuis RT, Beekman B, Ankersmit-Ter Horst M, Schalkwijk J. Tenascin-C degradation in chronic wounds is dependent on serine proteinase activity. *Arch Dermatol Res*; 1998 Sep;290(9):490–6.
 85. Siri A, Knäuper V, Veirana N, Caocci F, Murphy G, Zardi L. Different susceptibility of small and large human tenascin-C isoforms to degradation by matrix metalloproteinases. *J Biol Chem*; 1995 Apr 14;270(15):8650–4.

86. Imai K, Kusakabe M, Sakakura T, Nakanishi I, Okada Y. Susceptibility of tenascin to degradation by matrix metalloproteinases and serine proteinases. *Febs Lett*; 1994 Sep 26;352(2):216–8.
87. Giblin SP, Midwood KS. Tenascin-C: Form versus function. *Cell Adh Migr*; 2015;9(1-2):48–82.
88. Lindmark H, Guss B. SFS, a novel fibronectin-binding protein from *Streptococcus equi*, inhibits the binding between fibronectin and collagen. *Infect Immun*; 1999 May;67(5):2383–8.
89. Sottile J, Shi F, Rublyevska I, Chiang HY, Lust J, Chandler J. Fibronectin-dependent collagen I deposition modulates the cell response to fibronectin. *Am J Physiol Cell Physiol*; 2007 Oct 3;293(6):C1934–46.
90. Velling T, Risteli J, Wennerberg K, Mosher DF, Johansson S. Polymerization of Type I and III Collagens Is Dependent On Fibronectin and Enhanced By Integrins $\alpha 11\beta 1$ and $\alpha 2\beta 1$. *J Biol Chem*; 2002 Sep 27;277(40):37377–81.
91. Wallner K, Li C, Shah PK, Wu K-J, Schwartz SM, Sharifi BG. EGF-Like Domain of Tenascin-C Is Proapoptotic for Cultured Smooth Muscle Cells. *Arterioscler Thromb Vasc Biol*; 2004 Aug 1;24(8):1416–21.
92. Brown S, Bernardo MM, Li Z-H, Kotra LP, Tanaka Y, Fridman R, Mobashery S. Potent and Selective Mechanism-Based Inhibition of Gelatinases. *J Am Chem Soc*; 2000 Jul;122(28):6799–800.
93. Dallas SL, Rosser JL, Mundy GR, Bonewald LF. Proteolysis of Latent Transforming Growth Factor- β (TGF- β)-binding Protein-1 by Osteoclasts. *J Biol Chem*; 2002 Jun 7;277(24):21352–60.
94. Yu Q, Stamenkovic I. Cell surface-localized matrix metalloproteinase-9 proteolytically activates TGF-beta and promotes tumor invasion and angiogenesis. *Genes Dev*; 2000 Jan 15;14(2):163–76.
95. Schaertl S, Prime M, Wityak J, Dominguez C, Munoz-Sanjuan I, Pacifici RE, Courtney S, Scheel A, Macdonald D. A Profiling Platform for the Characterization of Transglutaminase 2 (TG2) Inhibitors. *J Biomol Screen*; 2010 Jun;15(5):478–87.
96. Lagares D, García-Fernández RA, Jiménez CL, Magán-Marchal N, Busnadiego O, Lamas S, Rodríguez-Pascual F. Endothelin 1 contributes to the effect of transforming growth factor $\beta 1$ on wound repair and skin fibrosis. *Arthritis & Rheumatism*; 2010 Feb 25;62(3):878–89.
97. Li B, Moshfegh C, Lin Z, Albuschies J, Vogel V. Mesenchymal stem cells exploit extracellular matrix as mechanotransducer. *Sci Rep*; 2013;3(1):2425.
98. Baneyx G, Baugh L, Vogel V. Fibronectin extension and unfolding within cell matrix fibrils controlled by cytoskeletal tension. *Nat Acad Sci*; 2002 Apr 16;99(8):5139–43.
99. Peleg O, Savin T, Kolmakov GV, Salib IG, Balazs AC, Kröger M, Vogel V. Fibers with Integrated Mechanochemical Switches: Minimalistic Design Principles Derived from Fibronectin. *Biophys J*; 2012 Nov 7;103(9):1909–18.
100. Schoen I, Pruitt BL, Vogel V. The Yin-Yang of Rigidity Sensing: How Forces and Mechanical Properties Regulate the Cellular Response to Materials. *Annual Reviews*; 2013 Jul 5;43(1):589–618.
101. Oberhauser AF, Marszalek PE, Erickson HP, Fernandez JM. The molecular elasticity of the extracellular matrix protein tenascin. *Nature*; 1998 May 14;393(6681):181–5.
102. Imanaka-Yoshida K, Aoki H. Tenascin-C and mechanotransduction in the development and diseases of cardiovascular system. *Front Physiol*; 2014 Jul 29;5:154.
103. Lundell A, Olin AI, Mörgelin M, al-Karadaghi S, Aspberg A, Logan DT. Structural basis for interactions between tenascins and lectican C-type lectin domains: evidence for a crosslinking role for tenascins. *Structure*; 2004 Aug;12(8):1495–506.

104. Midwood KS, Schwarzbauer JE. Tenascin-C modulates matrix contraction via focal adhesion kinase- and Rho-mediated signaling pathways. Schwartz M, editor. *Mol Biol Cell*; 2002 Oct;13(10):3601–13.
105. Belkin AM, Zemskov EA, Hang J, Akimov SS, Sikora S, Strongin AY. Cell-Surface-Associated Tissue Transglutaminase Is a Target of MMP-2 Proteolysis. *Biochemistry*; 2004 Sep;43(37):11760–9.
106. Howard EW, Crider BJ, Updike DL, Bullen EC, Parks EE, Haaksma CJ, Sherry DM, Tomasek JJ. MMP-2 expression by fibroblasts is suppressed by the myofibroblast phenotype. *Exp Cell Res*; 2012 Aug 1;318(13):1542–53.
107. Gratchev A, Kzhyshkowska J, Utikal J, Goerdts S. Interleukin-4 and dexamethasone counterregulate extracellular matrix remodelling and phagocytosis in type-2 macrophages. *Scand J Immunol*; 2005 Jan;61(1):10–7.
108. Harvey A, Yen T-Y, Aizman I, Tate C, Case C. Proteomic analysis of the extracellular matrix produced by mesenchymal stromal cells: implications for cell therapy mechanism. *PLOS ONE*; 2013;8(11):e79283.
109. Mižiková I, Morty RE. The Extracellular Matrix in Bronchopulmonary Dysplasia: Target and Source. *Front Med*; 2015;2(3):91.
110. Ohe R, Aung NY, Meng H, Kabasawa T, Suto A, Tamazawa N, Yang S, Kato T, Yamakawa M. Localization of collagen modifying enzymes on fibroblastic reticular cells and follicular dendritic cells in non-neoplastic and neoplastic lymphoid tissues. *Leuk. Lymphoma*; 2015 Dec 24;57(7):1687–96.
111. Pang KL, Parnall M, Loughna S. Effect of altered haemodynamics on the developing mitral valve in chick embryonic heart. *J Mol Cell Cardiol*; 2017 Jul 1;108:114–26.
112. Goddard ET, Hill RC, Nemkov T, D'Alessandro A, Hansen KC, Maller O, Mongoue-Tchokote S, Mori M, Partridge AH, Borges VF, Schedin P. The Rodent Liver Undergoes Weaning-Induced Involution and Supports Breast Cancer Metastasis. *Cancer Discov*; 2017 Feb 1;7(2):177–87.
113. Tomko LA, Hill RC, Barrett A, Szulczewski JM, Conklin MW, Eliceiri KW, Keely PJ, Hansen KC, Ponik SM. Targeted matrisome analysis identifies thrombospondin-2 and tenascin-C in aligned collagen stroma from invasive breast carcinoma. *Sci Rep*; 2018 Aug 28;8(1):646.
114. Solano EC, León C, Díaz F, García FG, García M, Escámez MJ, Aspizua SG, Conti CJ, Mencía Á, Santamaría LM, Llamas S, Pévida M, Caballero JC, Butillé JAP, Maseda R, Puig S, de Lucas R, Baselga E, Larcher F, Dopazo J, del Río M. Fibroblast activation and abnormal extracellular matrix remodelling as common hallmarks in three cancer-prone genodermatoses. *Br J Dermatol*; 2019 Sep 1;181(3):512–22.
115. Yan Z, Yin H, Brochhausen C, Pfeifer CG, Alt V, Docheva D. Aged Tendon Stem/Progenitor Cells Are Less Competent to Form 3D Tendon Organoids Due to Cell Autonomous and Matrix Production Deficits. *Front Bioeng Biotechnol*; 2020 May 5;8:1060.
116. Sottile J, Hocking DC, Langenbach KJ. Fibronectin polymerization stimulates cell growth by RGD-dependent and -independent mechanisms. *J Cell Sci*; 2000 Dec 1;113(23):4287–99.
117. Sottile J, Hocking DC, Swiatek PJ. Fibronectin matrix assembly enhances adhesion-dependent cell growth. *J Cell Sci*; 1998 Oct;111 (Pt 19):2933–43.
118. Akimov SS, Krylov D, Fleischman LF, Belkin AM. Tissue transglutaminase is an integrin-binding adhesion coreceptor for fibronectin. *J Cell Biol*; 2000 Feb 21;148(4):825–38.
119. Wang Z, Collighan RJ, Pytel K, Rathbone DL, Li X, Griffin M. Characterization of heparin-binding site of tissue transglutaminase: its importance in cell surface targeting, matrix deposition, and cell signaling. *J Biol Chem*; 2012 Apr 13;287(16):13063–83.
120. Nunes I, Gleizes PE, Metz CN, Rifkin DB. Latent transforming growth factor-beta binding protein

- domains involved in activation and transglutaminase-dependent cross-linking of latent transforming growth factor-beta. *J Cell Biol*; 1997 Mar 10;136(5):1151–63.
121. Klingberg F, Chau G, Walraven M, Boo S, Koehler A, Chow ML, Olsen AL, Im M, Lodyga M, Wells RG, White ES, Hinz B. The fibronectin ED-A domain enhances recruitment of latent TGF- β -binding protein-1 to the fibroblast matrix. *J Cell Sci*; 2018 Mar 1;131(5):jcs201293.
 122. Delaine-Smith R, Wright N, Hanley C, Hanwell R, Bhome R, Bullock M, Drifka C, Eliceiri K, Thomas G, Knight M, Mirnezami A, Peake N. Transglutaminase-2 Mediates the Biomechanical Properties of the Colorectal Cancer Tissue Microenvironment that Contribute to Disease Progression. *Cancers*; 2019 May;11(5):701.
 123. Buscemi L, Ramonet D, Klingberg F, Formey A, Smith-Clerc J, Meister J-J, Hinz B. The single-molecule mechanics of the latent TGF- β 1 complex. *Curr Biol*. 2011 Dec 20;21(24):2046–54.
 124. Imai K, Kusakabe M, Sakakura T, Nakanishi I, Okada Y. Susceptibility of tenascin to degradation by matrix metalloproteinases and serine proteinases. *FEBS Lett*; 1994 Sep 26;352(2):216–8.
 125. Chiao YA, Zamilpa R, Lopez EF, Dai Q, Escobar GP, Hakala K, Weintraub ST, Lindsey ML. In vivo Matrix Metalloproteinase-7 Substrates Identified in the Left Ventricle Post-Myocardial Infarction Using Proteomics. *J Proteome Res*; 2010 May 7;9(5):2649–57.
 126. Lindsey ML, Zamilpa R. Temporal and spatial expression of matrix metalloproteinases and tissue inhibitors of metalloproteinases following myocardial infarction. *Cardiovasc Ther*; 2010 Jul 14;30(1):31–41.
 127. Li ZL, Zhang HL, Huang Y, Huang JH, Sun P, Zhou NN, Chen YH, Mai J, Wang Y, Yu Y, Zhou LH, Li X, Yang D, Peng XD, Feng GK, Tang J, Zhu XF, Deng R. Autophagy deficiency promotes triple-negative breast cancer resistance to T cell-mediated cytotoxicity by blocking tenascin-C degradation. *Nat Commun*; 2020 Jul 30;11(1):169–19.
 128. Sheridan CM, Occlleston NL, Hiscott P, Kon CH, Khaw PT, Grierson I. Matrix metalloproteinases: a role in the contraction of vitreo-retinal scar tissue. *Am J Pathol*; 2001 Oct;159(4):1555–66.
 129. Olaso E, Lin H-C, Wang L-H, Friedman SL. Impaired dermal wound healing in discoidin domain receptor 2-deficient mice associated with defective extracellular matrix remodeling. *Fibrogenesis Tissue Repair*; 2011 Feb 2;4(1):5.
 130. Agren MS, MERTZ PM. Are excessive granulation tissue formation and retarded wound contraction due to decreased collagenase activity in wounds in tight-skin mice? *Br J Dermatol*; 1994 Sep;131(3):337–40.
 131. Bullard KM, Lund L, Mudgett JS, Mellin TN, Hunt TK, Murphy B, Ronan J, Werb Z, Banda MJ. Impaired Wound Contraction in Stromelysin-1-Deficient Mice. *Annals Surg*; 1999 Aug 1;230(2):260–5.
 132. Beare AHM, O'Kane S, Ferguson MWJ, Krane SM. Severely Impaired Wound Healing in the Collagenase-Resistant Mouse. *J Inv Dermatol*; 2003 Jan 1;120(1):153–63.
 133. Wilson SL, Haj El AJ, Yang Y. Control of Scar Tissue Formation in the Cornea: Strategies in Clinical and Corneal Tissue Engineering. *J Funct Biomater*; 2012 Sep;3(3):642–87.
 134. Mousavizadeh R, Hojabrpour P, Eltit F, McDonald PC, Dedhar S, McCormack RG, Duronio V, Jafarnejad SM, Scott A. β 1 integrin, ILK and mTOR regulate collagen synthesis in mechanically loaded tendon cells. *Sci Rep*; 2020;10(1):1620.
 135. Rumpler M, Woesz A, Dunlop JWC, van Dongen JT, Fratzl P. The effect of geometry on three-dimensional tissue growth. *J R Soc Interface*; 2008 Oct 6;5(27):1173–80.

136. Bidan C, Kommareddy K, Manjubala I, Rumpler M, Fratzl P, Dunlop J. Geometric Control of Tissue Growth. *Bone*; 2010 Mar;46:S47–8.
137. Dunlop JWC, Fischer FD, Gamsjäger E, Fratzl P. A theoretical model for tissue growth in confined geometries. *J Mech Phys Solids*; 2010 Aug;58(8):1073–87.
138. Bidan CM, Kommareddy KP, Rumpler M, Kollmannsberger P, Bréchet YJM, Fratzl P, Dunlop JWC. How Linear Tension Converts to Curvature: Geometric Control of Bone Tissue Growth. *PLOS ONE*; 2012 May 11;7(5):e36336.
139. Bidan CM, Kommareddy KP, Rumpler M, Kollmannsberger P, Fratzl P, Dunlop JWC. Geometry as a Factor for Tissue Growth: Towards Shape Optimization of Tissue Engineering Scaffolds. *Adv Healthc Mater*; 2013 Jan 1;2(1):186–94.
140. Gamsjäger E, Bidan CM, Fischer FD, Fratzl P, Dunlop JWC. Modelling the role of surface stress on the kinetics of tissue growth in confined geometries. *Acta Biomater*; 2013 Mar;9(3):5531–43.
141. Gurtner GC, Dauskardt RH, Wong VW, Bhatt KA, Wu K, Vial IN, Padois K, Korman JM, Longaker MT. Improving Cutaneous Scar Formation by Controlling the Mechanical Environment: Large Animal and Phase I Studies. *Ann Surg*; 2011 Aug 1;254(2):217–25.
142. Januszyk M, Wong VW, Bhatt KA, Vial IN, Paterno J, Longaker MT, Gurtner GC. Mechanical offloading of incisional wounds is associated with transcriptional downregulation of inflammatory pathways in a large animal model. *Organogenesis*; 2014 Apr 16;10(2):186–93.
143. Ogawa R. Mechanobiology of scarring. *Wound Repair Regen*; 2011 Jul 27;19((P):s2–s9.
144. Brellier F, Martina E, Chiquet M, Ferralli J, van der Heyden M, Orend G, Schittny JC, Chiquet-Ehrismann R, Tucker RP. The Adhesion Modulating Properties of Tenascin-W. *Int J Biol Sci*; 2012;8(2):187–94.
145. Kim Y, Ko H, Kwon IK, Shin K. Extracellular Matrix Revisited: Roles in Tissue Engineering. *Int Neurourol J*; 2016 May;20(Suppl 1):S23–9.
146. Szondy Z, Korponay-Szabó I, Király R, Sarang Z, Tsay GJ. Transglutaminase 2 in human diseases. *BioMedicine*; 2017 Sep 1;7(3):15.
147. Tatsukawa H, Otsu R, Tani Y, Wakita R, Hitomi K. Isozyme-specific comprehensive characterization of transglutaminase-crosslinked substrates in kidney fibrosis. *Sci Rep*; 2018 May 9;8(1):7306.
148. Hinz B. The extracellular matrix and transforming growth factor- β 1: Tale of a strained relationship. *Matrix Biol*; 2015 Sep 1;47:54–65.
149. Spenlé C, Loustau T, Murdamoothoo D, Erne W, Beghelli-de la Forest Divonne S, Veber R, Petti L, Bourdely P, Mörgelin M, Brauchle E-M, Cremel G, Randrianarisoa V, Camara A, Rekima S, Schaub S, Nouhen K, Imhof T, Hansen U, Paul N, Carapito R, Pythoud N, Hirschler A, Carapito C, Dumortier H, Mueller CG, Koch M, Schenke-Layland K, Kon S, Sudaka A, Anjuère F, Van Obberghen-Schilling E, Orend G. Tenascin-C Orchestrates an Immune-Suppressive Tumor Microenvironment in Oral Squamous Cell Carcinoma. *Cancer Immunol Res*; 2020 Sep;8(9):1122–38.
150. Page TH, Charles PJ, Piccinini AM, Nicolaidou V, Taylor PC, Midwood KS. Raised circulating tenascin-C in rheumatoid arthritis. *Arthritis Res Ther*; 2012;14(6):R260.
151. Jacobson O, Yan X, Niu G, Weiss ID, Ma Y, Szajek LP, Shen B, Kiesewetter DO, Chen X. PET Imaging of Tenascin-C with a Radiolabeled Single-Stranded DNA Aptamer. *J Nucl Med*; 2015 Apr 1;56(4):616–21.
152. Sundquist E, Kauppila JH, Veijola J, Mroueh R, Lehenkari P, Laitinen S, Risteli J, Soini Y, Kosma V-M, Sawazaki-Calone I, Macedo CCS, Bloigu R, Coletta RD, Salo T. Tenascin-C and fibronectin expression divide early stage tongue cancer into low- and high-risk groups. *Br J Cancer*; 2017 Feb 1;116(5):640–8.

153. Ni WD, Yang ZT, Cui CA, Cui Y, Fang LY, Xuan YH. Tenascin-C is a potential cancer-associated fibroblasts marker and predicts poor prognosis in prostate cancer. *Biochem Biophys Res Commun*; 2017 May;486(3):607–12.
154. Gritti G, Gianatti A, Petronzelli F, De Santis R, Pavoni C, Rossi RL, Cattaneo L, Spagnoli LG, Ferrari S, Rossi A, Barbui AM, Rambaldi A. Evaluation of tenascin-C by tenatumomab in T-cell non-Hodgkin lymphomas identifies a new target for radioimmunotherapy. *Oncotarget*; 2018 Jan 3;9(11):9766–75.
155. Smith ML, Gourdon D, Little WC, Kubow KE, Eguiluz RA, Luna-Morris S, Vogel V. Force-Induced Unfolding of Fibronectin in the Extracellular Matrix of Living Cells. *PLOS Biol*; 2007 Oct 2;5(10):e268.

5 Eliciting insights how tissue tension impacts tissue growth processes

Parts of this chapter I presented in oral presentation at the 8th World Congress of Biomechanics in Dublin in July 2018 in the session “Biomechanical microengineering of tissue mimics for human disease modelling”.

The work presented in this chapter is currently under preparation and will be submitted for publication in the near future.

Mario C. Benn, Philip Kollmannsberger, Tadahiro Yamashita, Marcel Graetz, Viola Vogel. *Eliciting insight how tissue tension impacts tissue growth processes.*

M.C.B. and V.V. designed the research; V.V. and P.K. supervised the project; **M.C.B.** designed the μ Tissue platform; **M.C.B.** microfabricated master structures and PDMS scaffolds; **M.C.B.** performed all cell culture experiments; **M.C.B.** performed confocal (CLSM) and 2-photon (2P) laser scanning microscopy; M.G. and **M.C.B.** performed live phase-contrast imaging; M.G. scripted a python code to automatically detect growth parameter in phase-contrast data; M.G. and **M.C.B.** analyzed growth distances and growth curvature in phase-contrast data; **M.C.B.** performed data visualization and analysis of CLSM-, 2P- and live phase-contrast-data; T.Y. provided code for fiber analysis; **M.C.B.** and T.Y. analyzed the SHG fiber orientation; **M.C.B.**, P.K., T.Y. and V.V. interpreted the results wrote the manuscript.

5.1 Abstract

We took advantage of our μ Tissue platform to independently tune key parameters, i.e. tissue tension as function of cleft angle, combined with the presence of supplemented pharmaceutical inhibitors, thus parameters which are technically challenging to be tuned independently in a living system. As expected, reducing cellular contractility through myosin II inhibition reduces tissue tension and thus increases the growth front curvature. Increased cellular contractility through TGF- β 1 supplementation resulted in increased tissue volume and narrowed growth front width in all different cleft angle geometries, which underlines the prominent role of cellular contractility for tissue growth and maturation. Furthermore, TGF- β 1 supplementation did not prevent the reverse myofibroblast-to-fibroblast transition as the tissue matured. Inhibition of fibronectin-collagen-interaction leads to more reduced tissue maturation in tissues grown in narrower clefts and subject to higher tissue tension while reducing the mechanical stability as witnessed by an increased tissue rupture probability. Taken together, we here show that tissue tension can be systematically tuned in *de novo* μ Tissue growth in arrays of microengineered clefts. Our data show that tissue tension together with cellular contractility are key parameters which regulates phenotype conversion with subsequent tissue maturation and tissue growth without indications to affect the sequence in which the spatiotemporal upregulation of TNC and TG2 orchestrate ECM remodelling and the myofibroblast-to-fibroblast transition.

5.2 Introduction

Mounting evidence underlines the eminent relevance of mechanobiological dependencies in health and disease [1-5]. Mechanical signalling plays a prominent role in health and disease and many novel therapeutical approaches in the emerging field of mechanomedicine have been proposed [6]. Tissue tension is especially in skin wounds of outstanding importance [7]. While there is a full body of literature how tensional homeostasis is understood across the length scales [8], it remains completely elusive how tissue tension affects tissue growth and tissue maturation processes. Despite substantial research efforts, we are lacking *in vitro* testing platforms that allow us to investigate mechanobiological parameters like tension at the tissue level, and at the same time provide good transferability of the knowledge towards the clinics [9,10]. Reaching sufficient degree of transferability is a huge challenge, because many 3D tissue platforms are typically based on scaffold biomaterials that introduce non-physiological biointerfaces. Scaffold-free 3D systems such as spheroids or organoids emerged increasingly, however tuning mechanical properties in such systems is extremely difficult [11]. On the cellular side, transformation of fibroblasts into myofibroblasts that display significantly upregulated cell contractility is a central physiological process enabling tissue repair [12], typically promoted in 2D cell culture by TGF- β 1 supplementation [13]. Whether a reversal back to fibroblasts is happening in living tissues once an inflammation has subsided or a wound been repaired is controversial, even though such a fibroblast-myofibroblast transition and a reversal has been observed in *de novo* grown μ Tissues without the supplementation of TGF- β 1 [14]. A deregulation of these processes drives fibrosis and carcinogenesis [15].

To shed light into these questions how tissue tension and cell contractility drive tissue growth processes, we took advantage of a newly engineered angle array platform of *de novo* grown μ Tissues that allows us to tune tissue tension through microfabrication of different cleft geometries. Previous work in a similar assay using osteoblasts and made from hydroxyapatite material showed that tissue growth starts in the cleft corners and is progressively filling the angular clefts, whereby the cleft angle tunes the tissue curvature [16]. Cell contractility thereby drives the effect of scaffold geometry on tissue growth [17-19]. In *de novo* tissues grown from fibroblasts, a reversible fibroblast-to-myofibroblast transition was found to occur at the growth front, exhibiting the typical upregulated myofibroblast characteristics (proliferation, α smooth muscle actin (α SMA) contractility, YAP-signalling), while the myofibroblasts transitioned back to fibroblasts in the maturing tissue [14]. The emergence of steep spatial gradients of cell phenotypes and of extracellular matrix composition, from the fibronectin-rich growth front to the collagen-rich tissue

interior, is fine-tuned by the spatially well-orchestrated appearance and disappearance of other ECM components, including tenascin-C (TNC) and tissue transglutaminase (TG2) (Benn et al. in preparation, Chapter 4). Since a detailed analysis of the interplay of cell phenotype and ECM composition, and thus the mechanobiological characterization of the emerging respective spatiotemporal gradients was done at a fixed cleft angle [14](Benn et al. in preparation, Chapter 4), we are asking here how the tissue tension as tuned by the cleft angle affects tissue growth processes.

Accordingly, we engineered here a microfabricated angle array platform by which we can tune tissue tension as a function of the cleft angle in the PDMS scaffold. Tissue tension can be modified via two approaches in our platform, the cleft angle as provided by our self-engineered scaffold geometry and cell contractility using pharmaceutical inhibitors. Cellular contractility was decreased when myosin II activity was inhibited with blebbistatin, and increased by supplementation of exogenous TGF- β 1 [20]. We further applied a chemical compound, GW788388, which is a TGF- β type I and II receptor inhibitor with proven decreasing effects in fibrosis, which is a disease state in which myofibroblast are the key effector cells [21-23]. Further, GW788388 was shown to diminish SMAD phosphorylation [24] and inhibiting TGF- β downstream signalling effects like α SMA expression in dermal fibroblast [25]. Since it is known that upregulated α SMA expression correlates positively with fibroblast contractility [13], we hypothesized to reduce cellular contractility mediated through endogenously produced TGF- β with GW788388, to inhibited TGF- β downstream signalling. Furthermore, we also asked how inhibitors that hamper Fn-induced collagen maturation impact the overall tissue maturation process. While blebbistatin, TGF- β and TGF- β receptor signalling inhibitor address the cellular side, we also asked what might happen if we interfere with the maturation of the ECM. The growth front is rich in highly stretched fibronectin fibers [14], which is subsequently remodelled by interlacing a network of collagen fibers to enhance the mechanical stability of the maturing tissue. Since fibronectin fibers are essential to nucleate the polymerization of the first collagen fibers and act as template [26,42], we next explored how the partial blocking of fibronectin-collagen interactions by the well characterized R1R2 bacterial-adhesin-derived peptide [27,28] might interfere with the ECM maturation process (Benn et al. in preparation, Chapter 4), and whether this interference is dependent on tissue tension of the growth front. We hypothesized that inhibition of Fn and collagen interaction with R1R2 peptide hampers tissue maturation, reduces tissue stability, and thus leads to higher levels of tissue ruptures (Benn et al. in preparation, Chapter 4). We investigate here to what extent tissue growth processes are

dependent on Fn and collagen interaction and tissue tension using R1R2 peptides during *de novo* μ Tissue growth in our angle array.

By independently tuning key parameters, i.e. tissue tension as function of cleft angle or in the presence of supplemented pharmaceutical inhibitors, which are technically challenging to tune independently in a living system, we explored their interrelationships. We found that the build-up of sufficient tissue tension is required for tissue growth and maturation, as mediated by cellular contractility and that fibronectin(Fn)-collagen-interactions play a key role in tension-dependent tissues maturation processes. These findings are significant to understand the underpinning mechanobiology of tissue growth processes, but also learn how to interfere more efficiently using pharmaceutical approaches to modulate tissue tension and subsequently tissue growth and maturation in wounds.

5.3 Results

Widening of cleft angle leads to reduced growth front curvature and tissue growth

Since previous reports show that tissue growth results from enhanced cell proliferation in the growth front, while cell proliferation is neglectable in the tissue interior [14], we first quantified how the cleft angle might affect tissue growth processes. PDMS substrate with cleft arrays of 22.5°, 45° and 90° angles were seeded with normal human dermal fibroblast (NHDF), and *de novo* μ Tissue formed within 12 days (see Video S01 and Fig. 1A). The time-lapse video demonstrates the highly dynamic and collective process of tissue growth. After seeding, primary normal human dermal fibroblasts (NHDF) adhered to the FN-crosslinked scaffold surfaces, but not to the passivated well bottom, and started to proliferate until a dense monolayer had formed on all sides, including on the vertical cleft walls. After typically 1-2 days, the corners of the clefts started to fill with a thick 3D tissue. After 12 days the μ Tissues were fully grown. Tissue growth in wider clefts resulted in reduced tissue growth and vice versa (Video S01, Fig. 1A+F). This correlation was also confirmed in a second data set of slightly different cleft angle arrays (Fig. S09A). Since tissue growth increases with higher growth front curvature [16-18], we quantified the growth front curvature and found that tissue growth and curvature correlated negatively with the cleft angle (Fig. 2). For larger cleft angles, the tissues were curved less and grew slower than for the narrow angles (Fig. 3 and Fig. S90) in agreement with the literature [16-19]. When plotting the growth front curvature over growth distance, the data points for each cleft angle can be fitted by a straight line (Fig. 3). Taken together, we can conclude that our tissues grown in the scaffold with large cleft angles exhibit lower growth front curvature and reduced tissue growth.

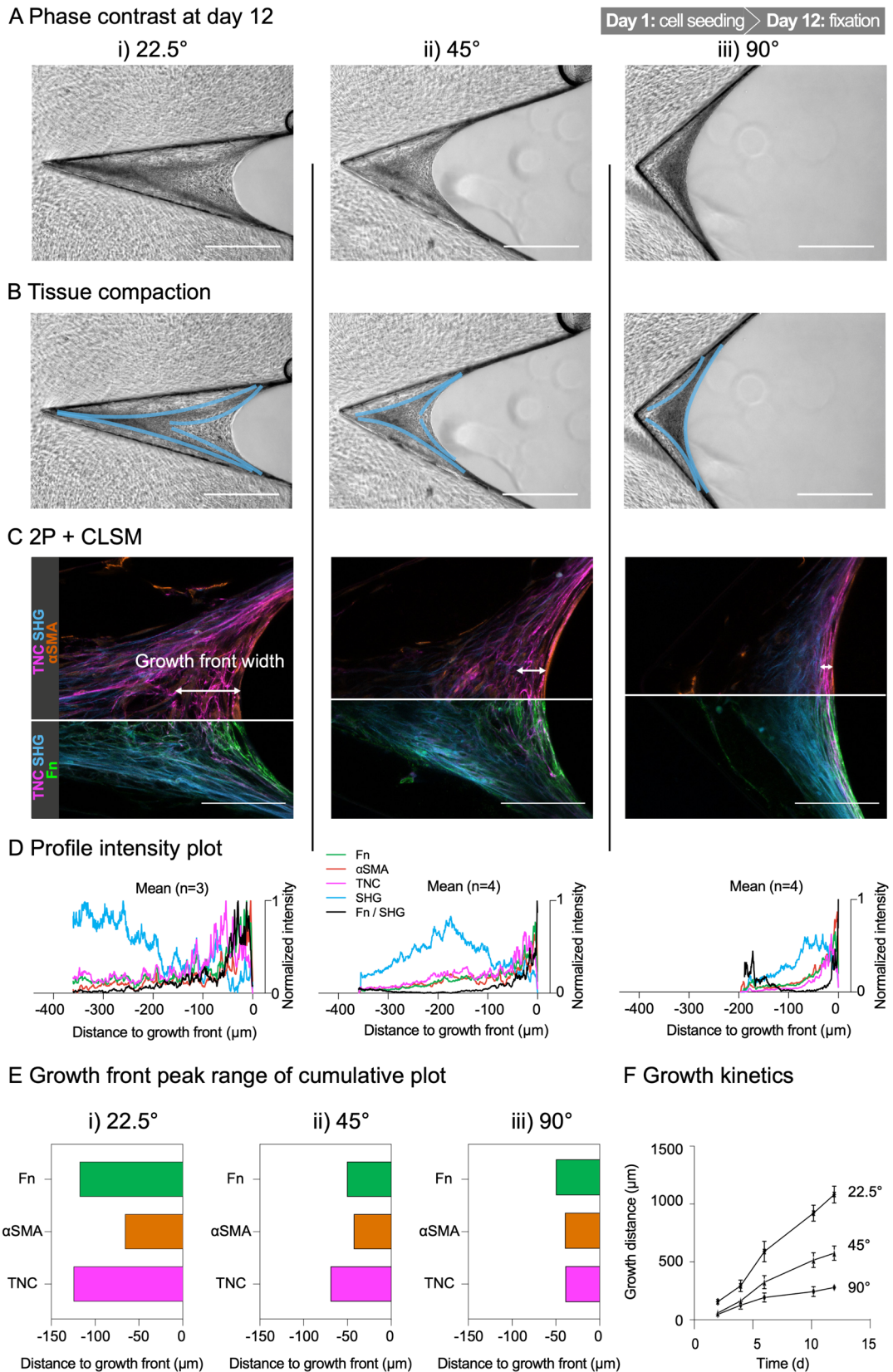


Fig. 1 *De novo* μTissue growth in clefts with varying angle. (A) Phase-contrast images of μTissues assembled by human dermal fibroblast in 22.5°(i)-, 45°(ii)- and 90°(iii)-clefts over 12 days of incubation. Scale bar = 500 μm. (B) Areas of compaction visible in phase-contrast images are outlined with light blue lines in 22.5°, 45° and 90° clefts. Scale bar 500 μm. (C) 2-photon microscopy (2P) and confocal laser scanning microscopy (CLSM) of representative μTissues in 22.5°(i)-, 45°(ii)- and 90°(iii)-clefts and imaged for αSMA (orange), Fn (green) TNC (magenta) and SHG (cyan). White

arrows indicate the growth front width. Scale bar = 100 μm . See Fig. S05 for more samples. **(D)** Normalized intensity plots along distance to growth front as mean over multiple $\mu\text{Tissues}$ in 22.5°, 45°- and 90°-clefs. **(E)** Growth front peak range (width) measured in cumulative profile intensity plot (D) at 25 % threshold and plotted in distance to growth front at tissue-liquid interface. **(F)** Growth distances along cleft bisector angle between tip of the cleft to the μTissue -medium-interface measured with phase-contrast images. For more data see Fig. S06.

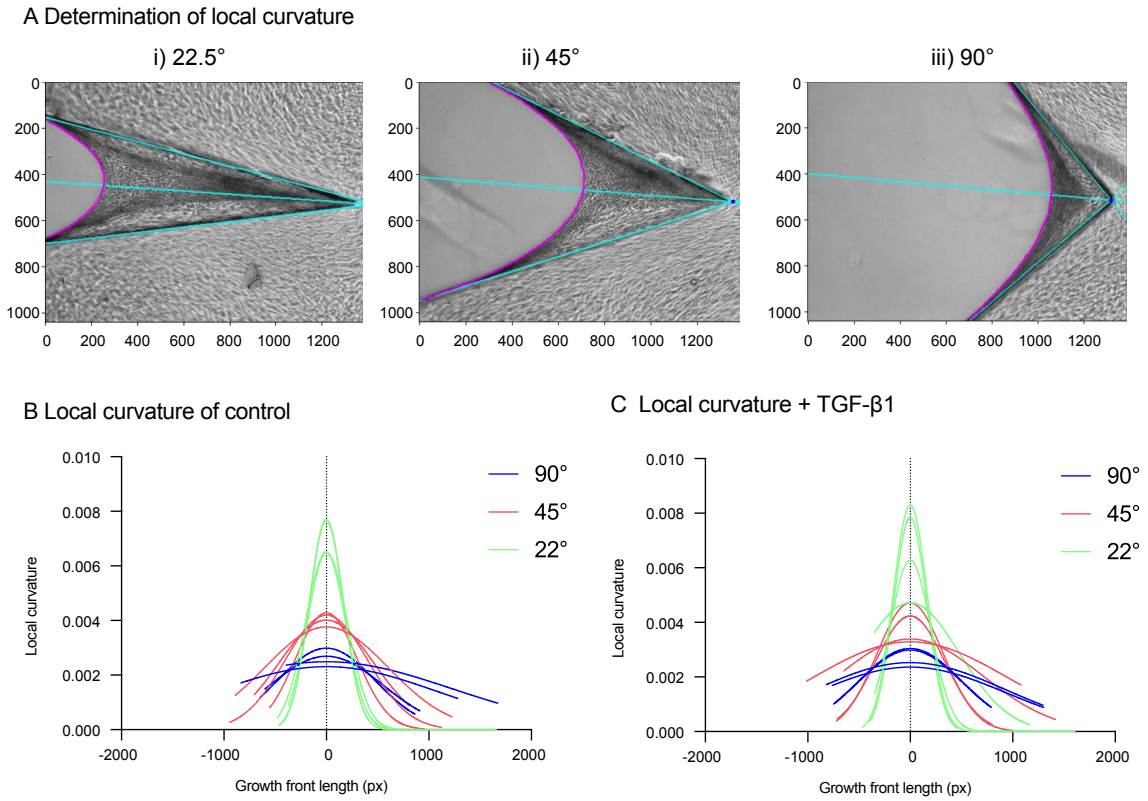


Fig. 2 Local tissue curvature of $\mu\text{Tissues}$ with varying angles and supplementation of TGF- β . **(A)** The local tissue curvature was determined by fitting a sampling radius along the tissue growth front using a previously introduced algorithm [17]. Gaussian fits of each cleft angle ($n=4$) are depicted over the distance of the growth front length. See Fig. S09 for individual data plots. **(B)** Control and **(C)** + TGF- β 1 for $\mu\text{Tissues}$ with a cleft angle of 22.5° (green), 45° (red) and 90° (blue). px = pixel.

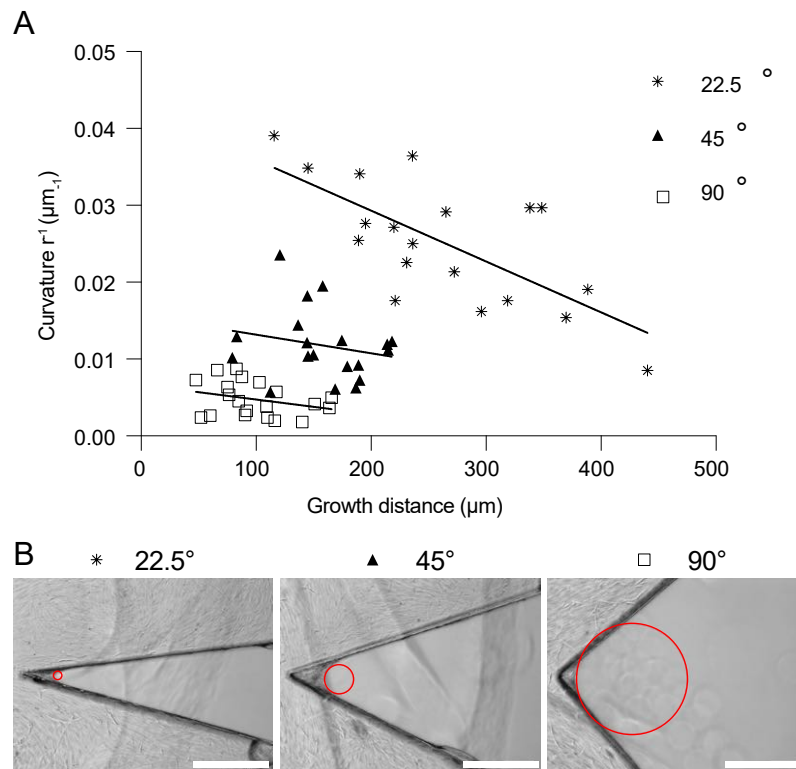


Fig. 3 Growth front curvature varies over cleft angles (A) Curvature of growth front over growth distance at day 4 for μ Tissues with a cleft angle of 22.5° (asterisk), 45° (triangle) and 90° (quadrat). Same cleft angles under different conditions were fitted with a simple linear regression (black line). **(B)** Curvature of central growth front region was determined for μ Tissues with different cleft angles by inversion of the radius (red circle) that was fitted in three points in equidistant sectors on the growth front region. Scale bar = 500 μm .

Reduced cell contractility via myosin II inhibition increases the growth front curvature

Increased growth front curvature was identified to cause increased tissue tension which drives tissue growth towards the open cleft [16-19]. To prove that growth front curvature and tissue tension are in our system correlated, we next inhibited cell contractility by 10 μM blebbistatin and it resulted in reduced tissue deposition (Fig. 4, Fig. 9D and Fig. S03). Ehrig et al. demonstrated that control tissues and tissues with increased cellular contractility both minimized their total surface area in a liquid-like behaviour, whereas blebbistatin treated tissues deviated significantly from this Laplace-Young law predictions [19]. Thus, we next asked how tissue tension, as varied via the cleft angle in synergy with reduced cellular contractility with blebbistatin, affects the tissue growth processes. Tissues grown at first normally for 5 days and then getting exposed to 10 μM blebbistatin for 7 days did not show much further growth (Fig. S03). The growth front curvature increased under Blebbistatin (Fig. 4).

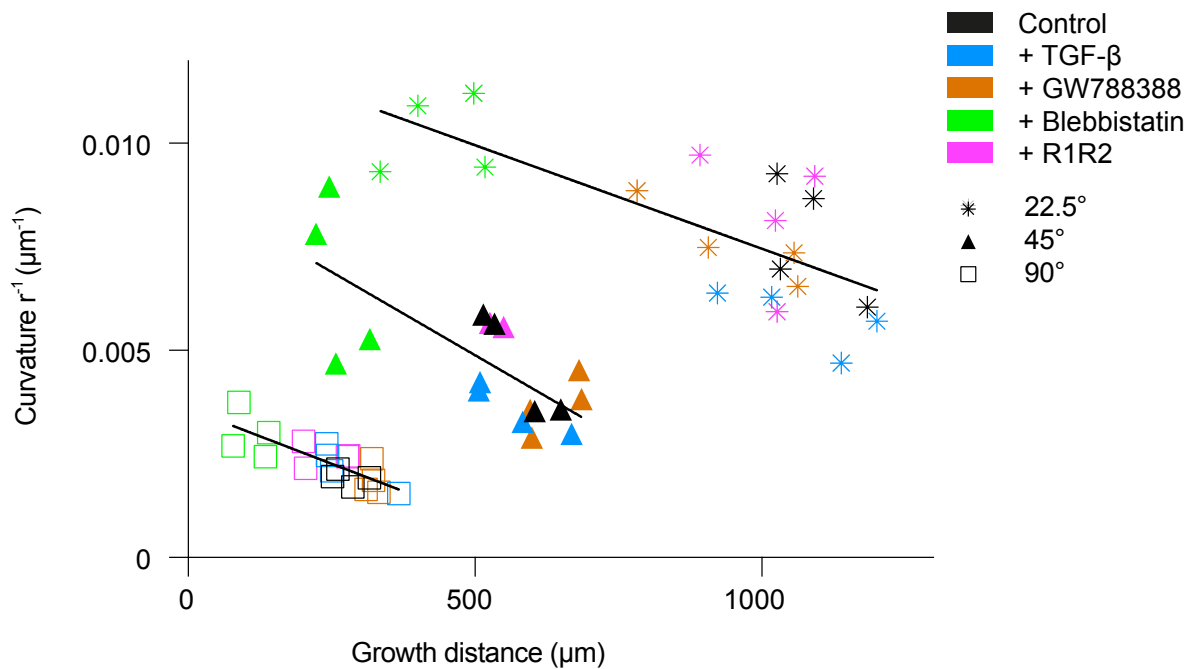


Fig. 4 Correlation between growth front curvature and growth distance of μ Tissues with varying angles fixed after 12 days. Curvature of growth front over growth distance was determined as in Fig. 1 for μ Tissues with a cleft angle of 22.5° (asterisk), 45° (triangle) and 90° (quadrat). μ Tissues were treated with GW788388 (orange), Blebbistatin (green) or R1R2 (magenta) or TGF- β was supplemented (blue) vs. the control sample (black). Same cleft angles under different conditions were fitted with a simple linear regression (black line). Same conditions with different cleft angles were clustered in their respective color.

The cleft angle does not impact the sequence of emerging ECM components and their degradation as tissue matures, but the steepness of the gradients

Since we recently found that steep spatiotemporal gradients of the ECM components are required for timely tissue maturation with Fn fibers appearing first, followed transiently by TNC and TG2 before the appearance of SHG-positive collagen fiber bundles can be detected (Benn et al. in preparation, Chapter 4), we next asked how varying tissue tension influences tissue maturation processes. During maturation, a sharp transition from a myofibroblast dominated growth front to a SHG positive collagen matrix in the interior occurs. Behind the growth front of each μ Tissue, a fibroblast-to-myofibroblast transition emerges without supplementation of TGF- β , visible in α SMA signal at the growth front (Fig. 6), and Fn and TNC accumulate within this early ECM (Fig. 1C). Tissues grow towards the open cleft and gradually mature as myofibroblasts, Fn and TNC get cleared. This leads to mature tissue found in the core that is dominated by collagen ECM, mature enough to be detected by second harmonic generation [29,30], and separated from the α SMA positive growth front (Fig. 6). Fibroblasts in the tissue interior are thus responsible for the organization and remodelling of the SHG-positive collagen bundles (Fig. 6). Especially the Fn / SHG

ratio (black) indicates a strikingly flattened gradient in 22.5°-clefs, while it was steepest in 90° (Fig. 1D). However, also in direct comparison of all channels identifying the immature growth front (α SMA, TNC, Fn) this cleft-angle difference can be seen nicely. To visualize this, the growth front peak width to the tissue-medium interface is plotted per channel as 'growth front peak range' (Fig. 1E). After 12 days of incubation, the width of the growth front region varies in different cleft angles (Fig. 1A), whereby the smallest cleft angle results in growth front width $102.7 \pm 32.06 \mu\text{m}$, while the tissues within the largest cleft angle shows a width of $42.59 \pm 6.14 \mu\text{m}$ (Fig. 1C, white double-headed arrows in fluorescence data, and Fig. 1D-E). Similar correlations were also seen in a second set of experiments with slightly different cleft angles (Fig. S09). Taken together, increased tissue growth in smaller cleft angles, corresponding to higher tissue tension, results in growth front widening and thus higher spatiotemporal resolution of the gradients of young-to-mature tissue conversion.

The collagen fibers in the interior align parallel to the geometrical tissue constrains with intersecting fibers that enhance mechanical stability

Since the architecture of collagen fiber networks determines the mechanical stability of tissues [31], we next looked at the collagen architecture as function of the cleft angle. Collagen fibers appear as interwoven fabric (Fig. 7A). In each tissue, there is a dominance of collagen fibers running parallel to the cleft wall, typically with a few much shorter intersecting fibers at skewed angles. Along the growth front, compacted bundles of fibers run parallel to the outer edge. As the collagen fibers get aligned by the contracting cells [31], which apply the strongest forces along their long axis, we thus expect that the cells at the tissue-scaffold edges are aligned parallel to the edge, as confirmed by the phase contrast images (Fig. 1A+B) and immunostainings of the central plane (Fig. 1C and Fig. 6). In the growth front, the cells are aligned tangentially with the highly tensed fibronectin fibers (Fig. 1C).

As the tissue matures, time lapse movies of the μ Tissue show the build-up of tissue compaction regions that run parallel to the cleft walls (Video S01 and Fig. S02B), and this process is associated with collagen fiber compaction (Fig. 1A-C and Fig. S04). Depending on the cleft angle, compaction occurs in different patterns (Fig. 1B). In small clefs, the inner compaction margins do not align with the growth front, whereas in 90°-clefs they align beautifully with the growth front (Fig. S02A, orange lines). In contrast, major tissue compaction did not occur if cellular contractility was inhibited with Blebbistatin after 7 days in culture (compare overviews of full arrays in Fig. S04). Taken together, the co-localizing effects of fiber alignment and tissue compaction are likely reciprocal events caused by tissue tension, since both are increased in smaller cleft angles.

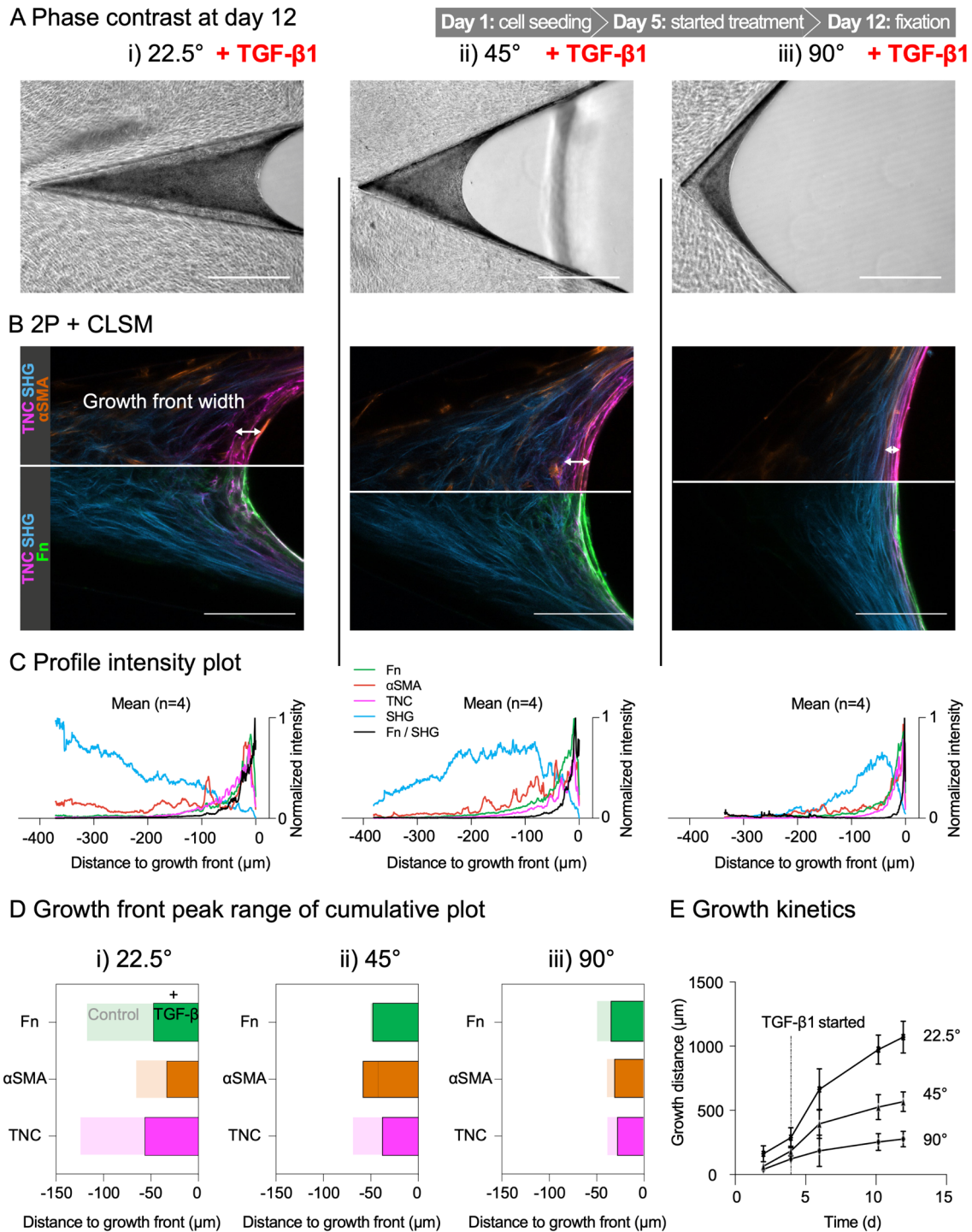
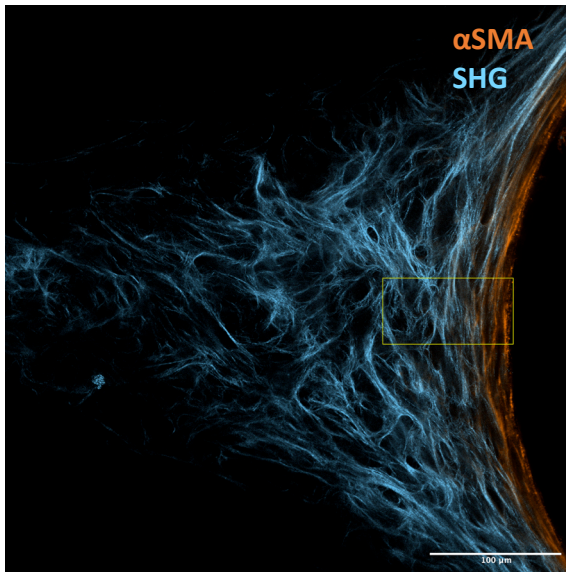


Fig. 5 *De novo* μ Tissue growth in clefts with varying angle and TGF- β 1 supplementation from day 5. **(A)** Phase-contrast images of μ Tissues assembled by human dermal fibroblast in 22.5°(i)-, 45°(ii)- and 90°(iii)-clefts over 12 days of incubation. Scale bar = 500 μ m. **(B)** 2-photon microscopy (2P) and confocal laser scanning microscopy (CLSM) of representative μ Tissues in 22.5°(i)-, 45°(ii)- and 90°(iii)-clefts and imaged for α SMA (orange), Fn (green), TNC (magenta) and SHG (cyan). White arrows indicate the growth front width. Scale bar = 100 μ m. **(C)** Normalized intensity plots along distance to growth front as mean over multiple μ Tissues in 22.5°(i)-, 45°(ii)- and 90°(iii)-clefts. **(D)** Growth front peak range (width) measured in cumulative profile intensity plot (D) at 25 % threshold and plotted in distance to growth front at tissue-liquid interface. Bar graphs of the control are overlaid in transparent. **(E)** Growth distances along cleft bisector angle between tip of the cleft to the μ Tissue-medium-interface measured with phase-contrast images. For more data see Fig. S06.

A: grown over 12 days



B: grown over 35 days

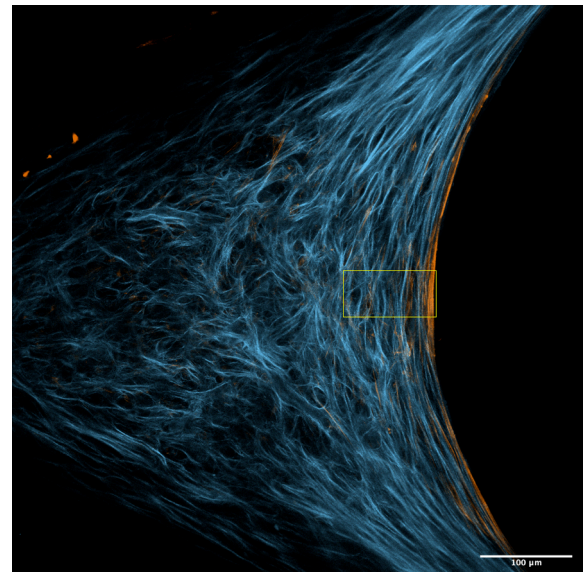
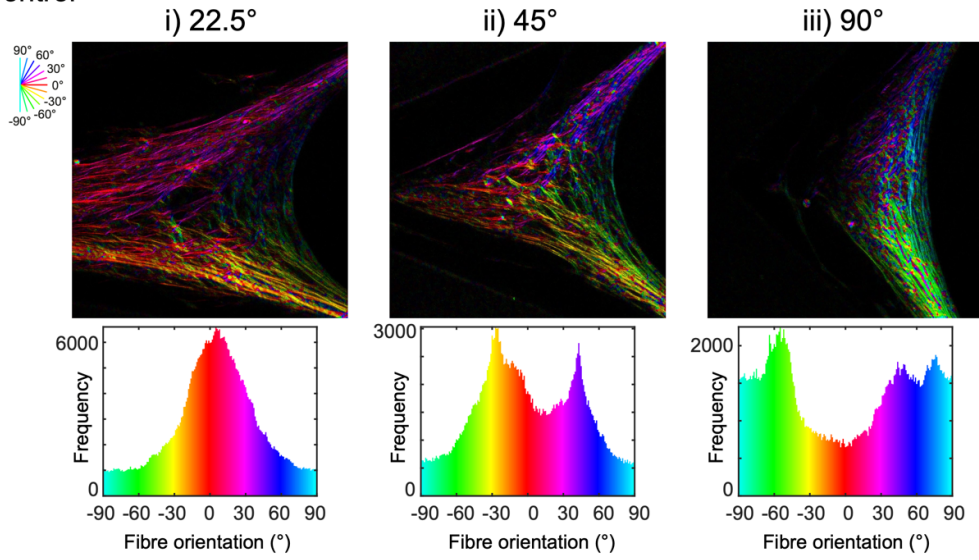
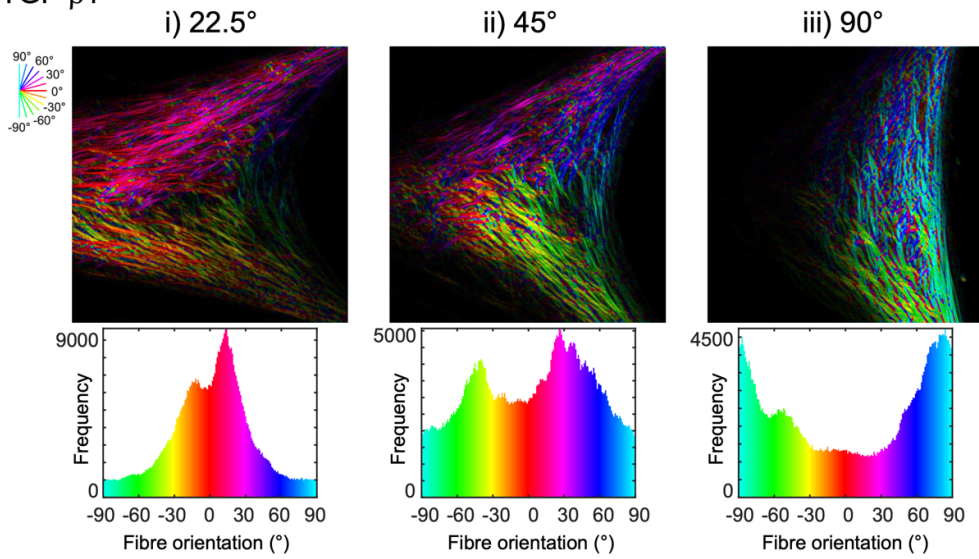


Fig. 6 Tissue maturation in shorter (12d) and longer time periods (35d) (A) μ Tissue incubated over 12 days and (B) μ Tissue incubated over 35 days. Both show different width of their growth front marker α SMA and varying organisation and density in mature SHG detectable fibers. Yellow box (100 μ m x 50 μ m) indicates the transition from growth front to interior. Scale bar = 100 μ m.

A Control



B +TGF- β 1



C +GW788388

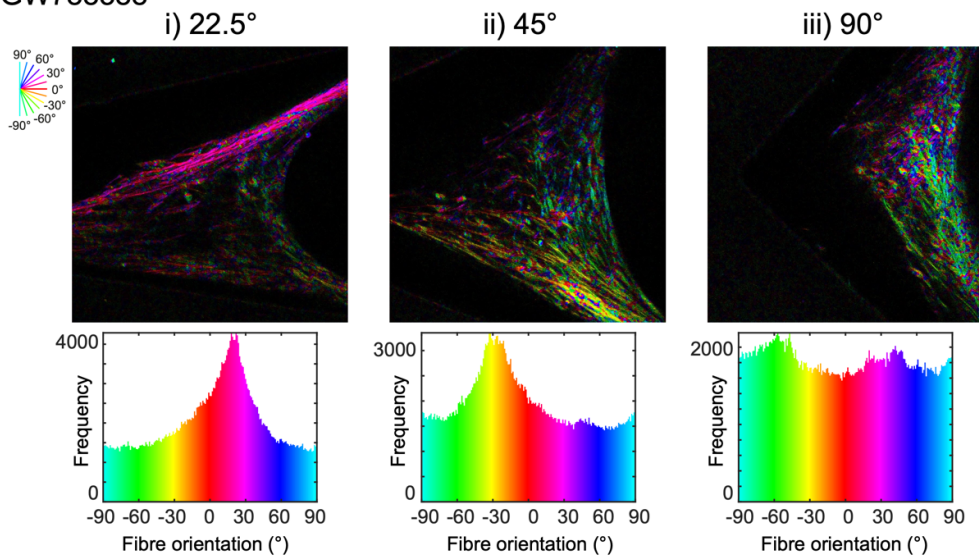


Fig. 7 continues on next page

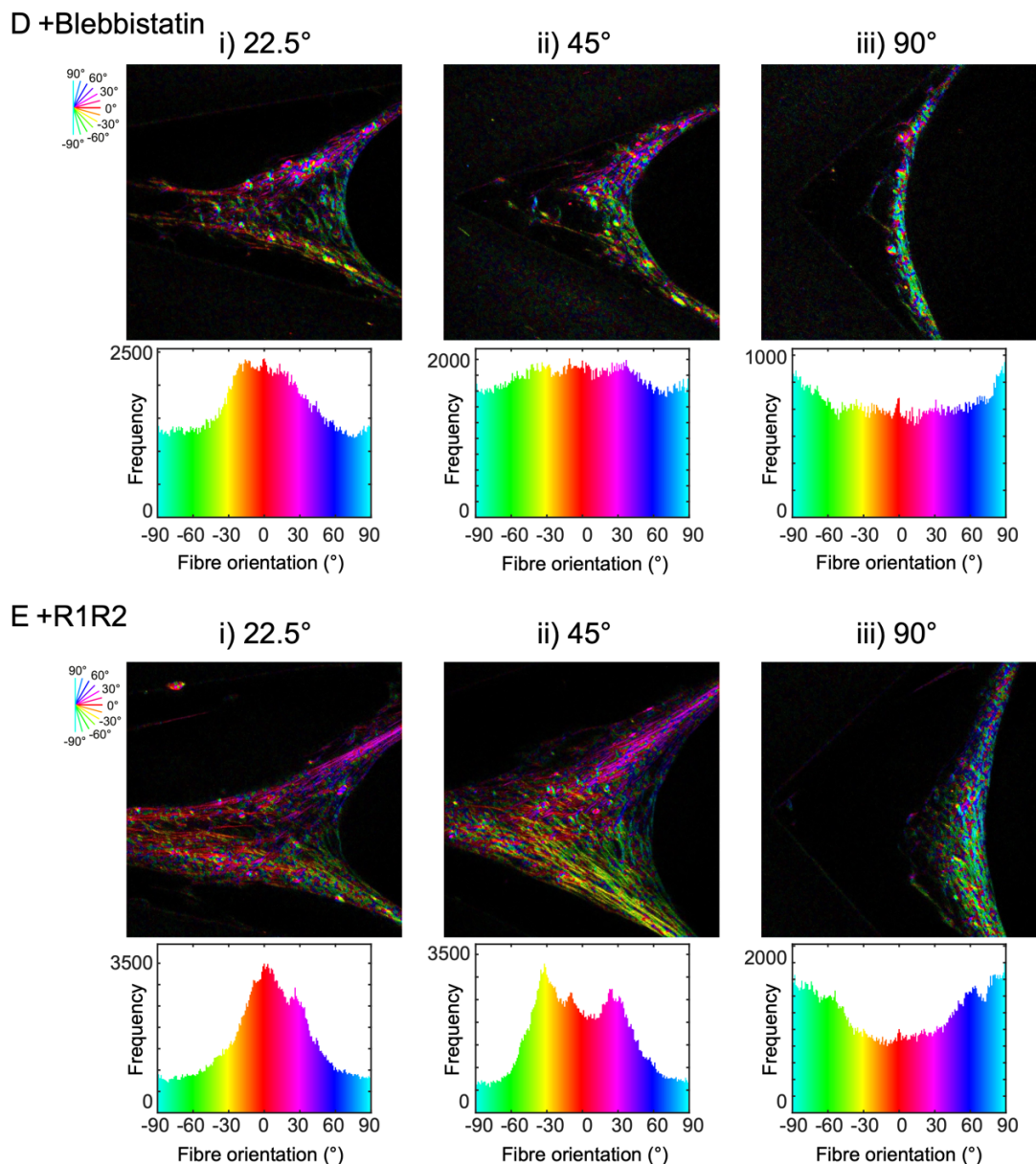


Fig. 7 Analysis of the collagen fiber (SHG) orientation for μ Tissues with different cleft angles under various conditions. (A) Fiber orientation analysis was carried out using a custom-written MATLAB script for representative μ Tissues with cleft angles of 22.5°(i), 45° (ii) and 90° (iii). The orientation of the SHG-signal is color-coded from blue ($\pm 90^\circ$) to red (0) and the frequency distribution of the respective μ Tissue is depicted below the pseudo-coloured 2P micrographs. Further information about the image analysis are provided in the method section. **(B-E)** The same fiber orientation analysis was done for μ Tissues supplemented with TGF- β 1 (B), GW788388 (C), Blebbistatin (D) or R1R2 (E). For more data see Fig. S08.

Exogenous TGF- β 1 supplementation narrows the growth front and does not prevent the myfibroblast-to-fibroblast transition as the tissue matures towards the interior

To investigate the role of TGF- β 1 signalling on tissue processes as a function of tissue tension, we supplemented TGF- β 1 in our array of tuned μ Tissue growth. While the growth front width is decreasing with wider cleft angles under control conditions, this difference becomes less prominent under TGF- β 1 stimulation (compare Fig. 1D and Fig. 5C). Since it is known that upregulated α SMA expression correlates positively with fibroblast contractility [13], the overall

higher levels in α SMA indicate the increase in cellular contractility (Fig. S05), while the myofibroblast-to-fibroblast transition in most of the tissues seems not disturbed in agreement with Kollmannsberger et al. 2018 [14] (Fig. S06B). In addition, both the overall signal intensity of all detected channels varies as a function of cleft angle (Fig. S05), as well as the region of interest (ROI) width in each angle varies as function of cleft angle (Fig. S06). Therefore, we assessed the signal density over the full width of the sample region of interest (Fig. 7).

The signal density of all channels decreases with wider clefts in control samples (Fig. 8, first row). Interestingly, the signal density of all channels in TGF- β 1 supplemented tissues show fewer differences over the different cleft angles (Fig. 8, second row). Here, especially wider clefts show increased Fn and α SMA signal densities (Fig. 8, second row), while the growth front width is decreased (Fig. 5C+D). This could indicate that the local density of Fn and α SMA positive myofibroblast is much increased in the growth front of the 90°-clefts compared to the interior (Fig. 8, second row and Fig. S11, second row). In addition, TGF- β 1 significantly increases total SHG intensity (Fig. 8 and Fig. S05, second row) and the collagen fibers that run parallel to the growth front, which agrees with our observation that the growth front is narrower (Fig. 5B). We furthermore found that more ruptures occurred in samples supplemented with TGF- β 1 (Fig. S07). TGF- β 1 was supplemented at day 5 (compare video S01 with S03, TGF- β 1 was supplemented at timestamp = 114.5h).

TGF- β 1 supplementation further resulted in much increased tissue volumes, which can be seen in the much more optically dense tissues in phase contrast (Fig. S04) and the fact that there is no difference in compaction area between the different angles (Fig. 1B and Fig. S04). The significant increase in tissue volume can also be estimated in the XZ/YZ-profiles (Fig. 8) and is in agreement with previous reports [14,19].

The curvature to tissue growth correlation under TGF- β 1 supplementation shows a slight trend towards decreased curvature in smaller angles (Fig. 2B and Fig. 4), however due to low sample number this trend needs to be confirmed in future studies. Taken together, while the different tensional states in the control μ Tissue, as tuned by the cleft angle, induce a change of growth front width and compaction area, our data suggest that increasing cellular contractility by TGF- β 1 seems to balance those tensional state differences.

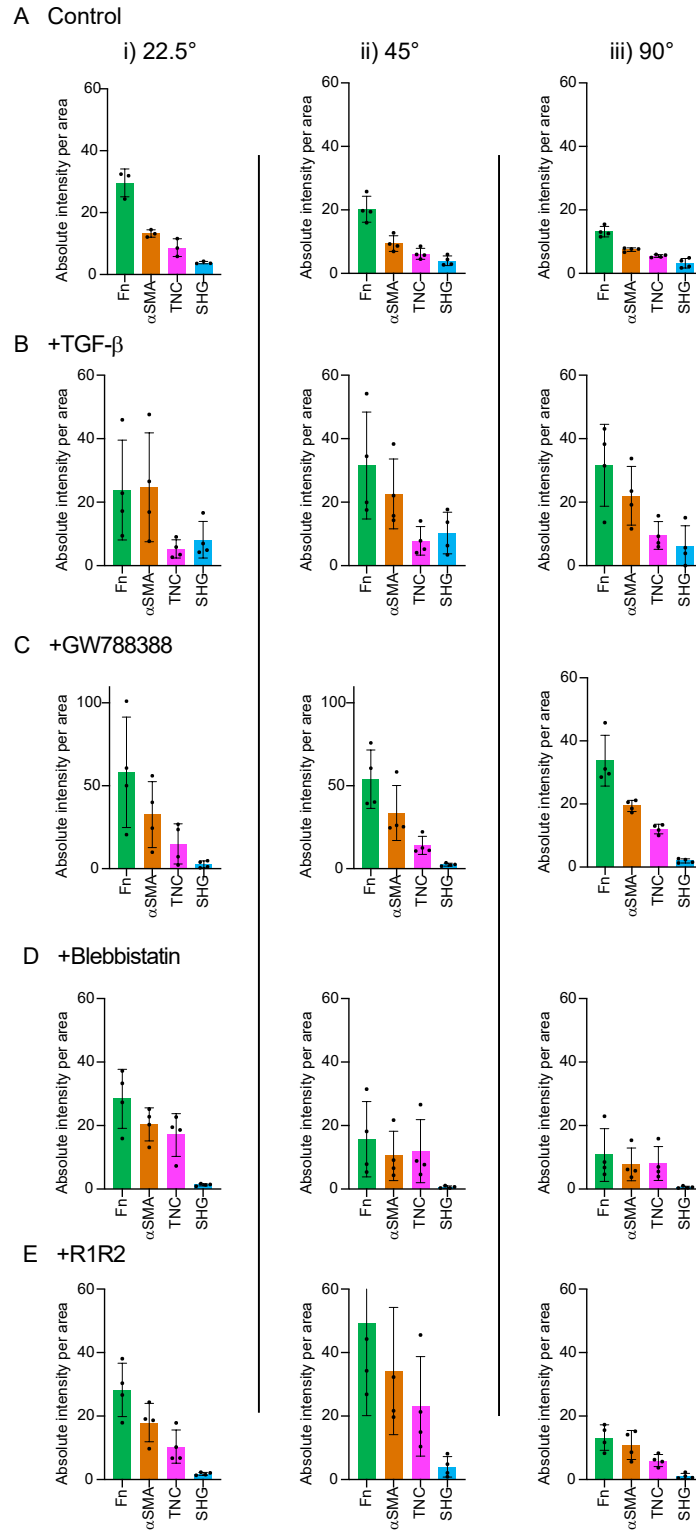
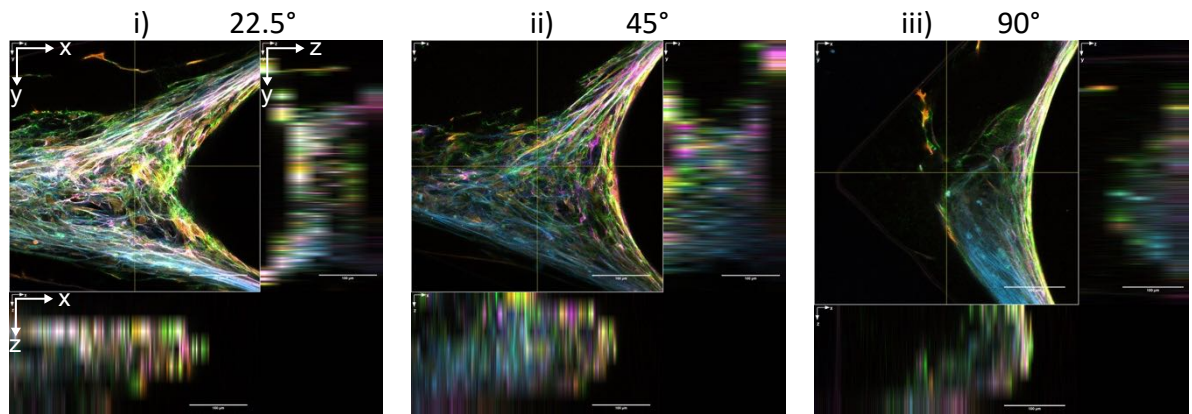
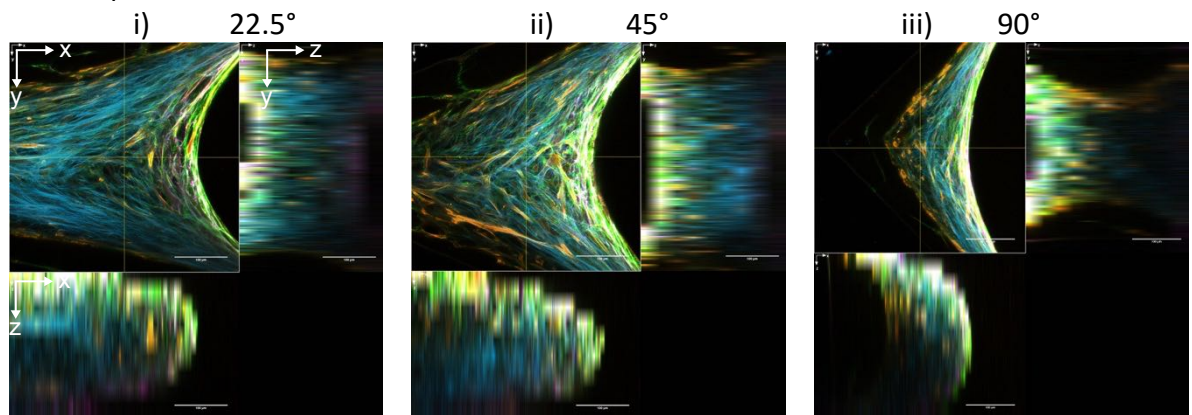


Fig. 8 Fluorescence and SHG signal density over full region of interest width with different angles under various conditions. (A-E) Both ROI width (Fig. S05) and absolute intensities (Fig. S10) are varying per left angle. For comparison, the ratio of absolute signal intensity as integral of profile plots (e.g. Fig. 1D) over the sampled area along the profile plot axis is depicted as absolute intensity per area in bar graphs. Absolute intensity per area was calculated for μ Tissues with left angles of 22.5°(i), 45° (ii) and 90° (iii) of the control (A), supplemented with TGF- β 1 (B), GW788388 (C), Blebbistatin (D) or R1R2 (E).

A Control



B + TGF- β



C + GW788388

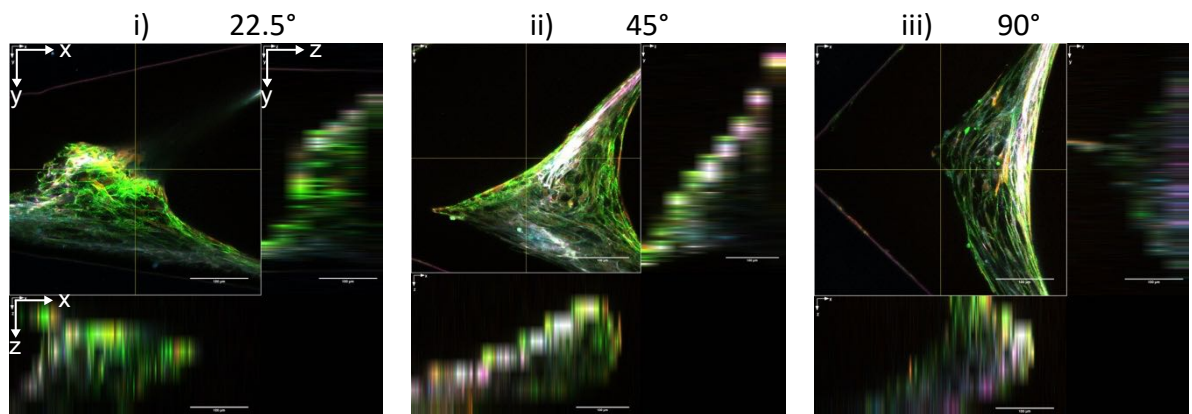


Fig. 9 continues on next page

D + Blebbistatin

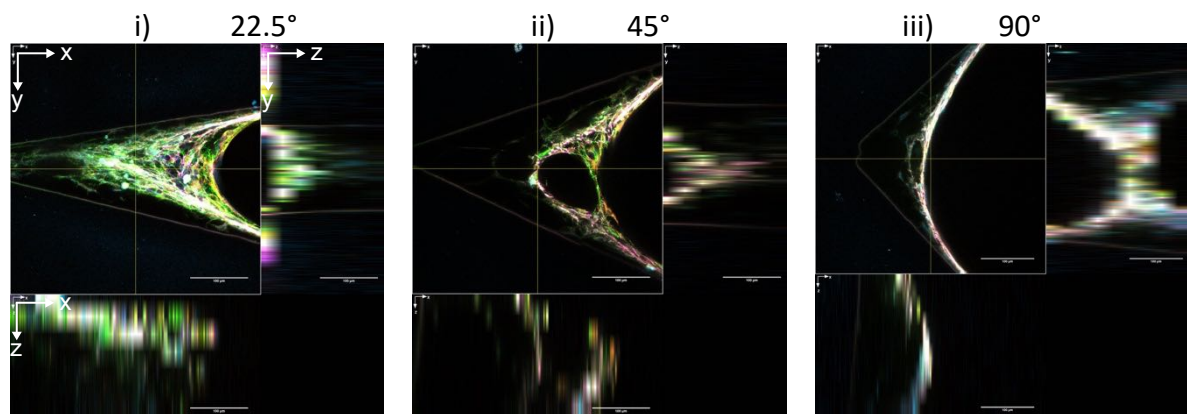


Fig. 9 XZ- and YZ-profiles for μ Tissues with different cleft angles under various conditions. Multi-channel composite images of representative μ Tissues imaged with 2P and CLSM for α SMA (orange), Fn (green), TNC (magenta) and SHG (cyan). Each image shows central XY-profile on top-left, ZY-profiles on top-right and ZX-profile on bottom-left. Scale bars 100 μ m. **(A-D)** Z-profiles of μ Tissues with cleft angles of 22.5°(i), 45° (ii) and 90° (iii) of the control (A) and supplemented with TGF- β 1 (B), GW788388 (C) or Blebbistatin (D).

Inhibition of TGF- β receptors hampers tissue maturation, reduces bundling of collagen fibers and their alignment and reduces tissue volume

As previously described, GW788388 inhibits downstream signalling of TGF- β receptor I and II [22]. To investigate the relative impact of GW788388 on endogenously produced TGF- β , conveying auto- or paracrine functionality [32], we tested the inhibitor for α SMA response with and without TGF- β supplementation in 2D planar experiments. We showed in 2D planar inhibitor that GW788388 is capable to significantly reduce α SMA expression with and without exogenous TGF- β supplementation (Fig. 10), in agreement with the literature [25]. Since it is known that upregulated α SMA expression correlates positively with fibroblast contractility [13], we applied GW788388 in our *de novo* μ Tissue to reduce cellular contractility mediated presumably by endogenous TGF- β . However, the results need to be discussed with caution, since TGF- β downstream signalling effects many additional functions, of which many are not fully understood [33-39]. By targeting TGF- β receptors, we investigated whether TGF- β receptor signalling via endogenously produced TGF- β , or perhaps even independently of TGF- β , might play a role in the tissue-tension dependent growth processes. Inhibition of downstream TGF- β receptor signalling with GW788388 resulted in much less optically dense tissues (Fig. 11A and Fig. S04) with milder tissue compaction and decreased tissue volume in their XZ/YZ-profiles (Fig. 9C) compared to the untreated controls. While treatment with GW788388 showed slightly reduced appearance of myofibroblasts in the growth front, tissue maturation was hampered as signal of α SMA, TNC and Fn also distributes in the interior (Fig. 10B and Fig. S06), which is in agreement with our previous findings (Benn et al. in preparation, Chapter

4). Furthermore, the density of SHG positive collagen fibers was greatly reduced (Fig. 7), as a much smaller fraction of fibers is running in tight bundles along the tissue edges and the existing collagen fibers are much more interwoven by intersecting fibers (Fig. 6). Since GW788388 is inhibiting TGF- β receptor I and II and since there were physical interactions between TGF- β receptor I and $\alpha 2\beta 1$ -integrins reported [40], the observed delay in maturation could in parts also due to perturbed $\alpha 2\beta 1$ -integrin signalling, which is one of the main collagen binding integrins and required for polymerization of collagen fibers [41]. In the discussion this interaction is described in more detail. Interestingly, reduced effects on tissue maturation are more prone in 22.5°- and 45°-clefts, while 90°-clefts show more intense growth fronts with steeper maturation gradients (Fig. 11B and Fig. S06). Taken together, under supplementation of GW788388 only tissues with reduced growth front curvature, thus reduced tension, show enhanced tissue maturation, while in tissues of increased growth front curvature tissue maturation is delayed.

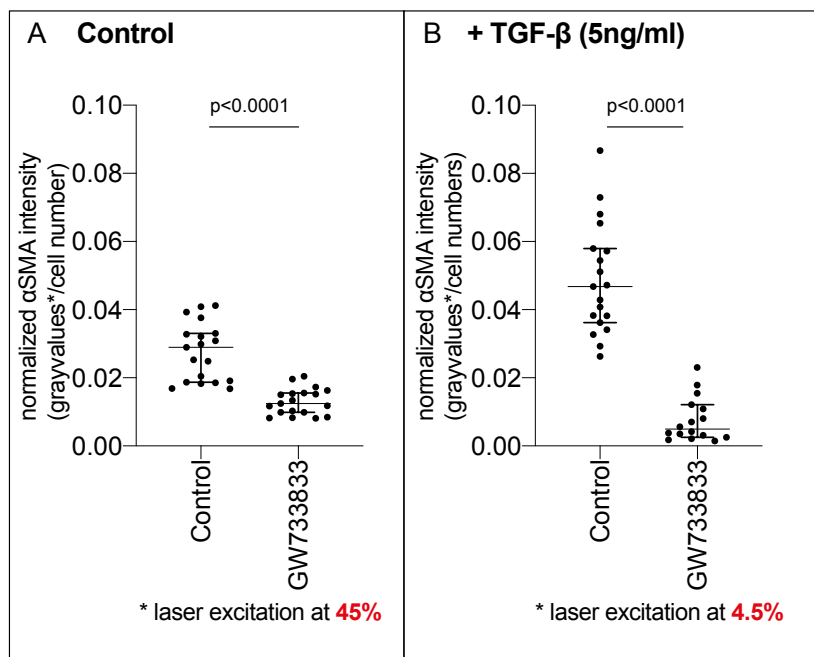
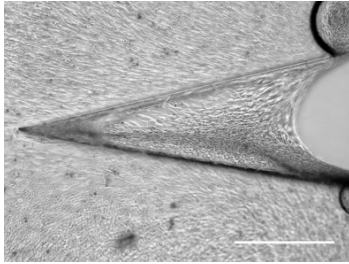


Fig. 10 α SMA response to GW788388 on planar glass substrates (A) without and (B) with TGF- β 1 supplementation was tested on 2D planar Fn coated glass with and without supplementation of GW788388. The glass substrates were physioadsorbed with Fn (50 μ g/ml in PBS) for 1 h at room temperature. Cell number per region of interest was determined by nucleus count of DAPI channel. Overall intensity of α SMA was a magnitude of approximately 10 higher under TGF- β 1 stimulation, thus the laser excitation energy was adapted from 45% (A) to 4.5% (B) intensity to allow signal detection with sufficient sensitivity in both conditions, i.e. assuring appropriate signal-to-noise ratio while avoiding pixel saturation. Data were compared with an unpaired two-tailed Mann-Whitney. Error bars represent 95% confidence intervals (CI).

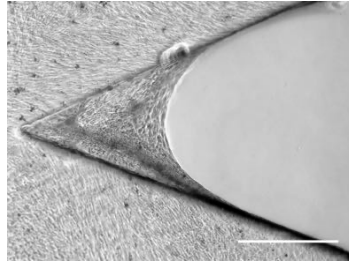
A Phase contrast

Day 1: cell seeding > Day 5: started treatment > Day 12: fixation

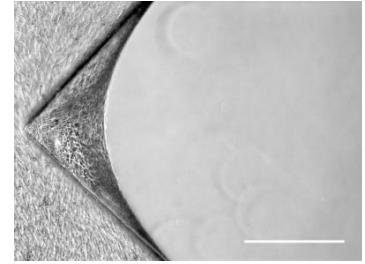
i) 22.5° + GW7888388



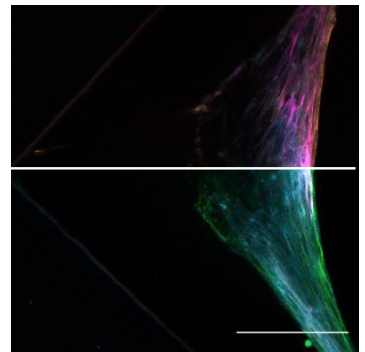
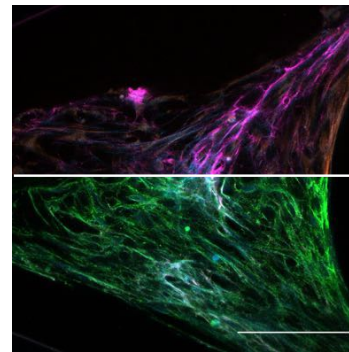
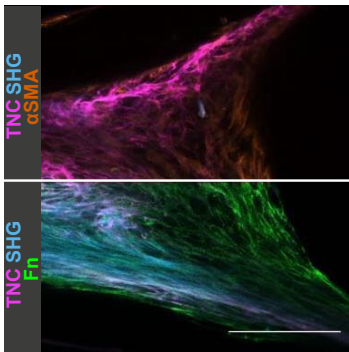
ii) 45° + GW7888388



iii) 90° + GW7888388



B 2P + CLSM



C Profile intensity plot

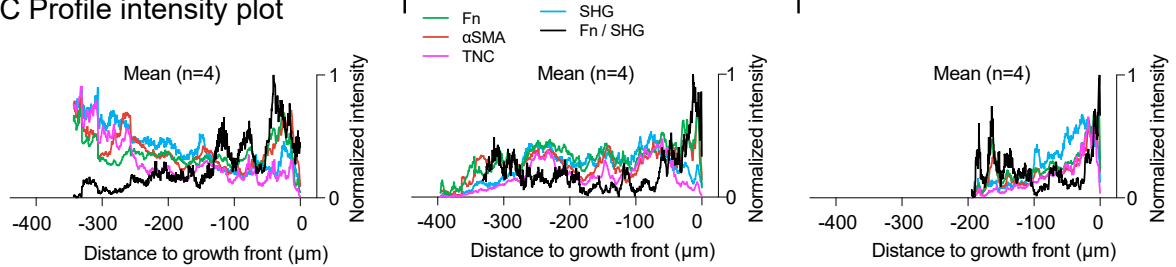


Fig. 11 *De novo* μ Tissue growth in clefts with varying angle and GW7888388 treatment from day 5. **(A)** Phase-contrast images of μ Tissues assembled by human dermal fibroblast in 22.5°(i)-, 45°(ii)- and 90°(iii)-clefts over 12 days of incubation. Scale bar = 500 μ m. **(B)** 2-photon microscopy (2P) and confocal laser scanning microscopy (CLSM) of representative μ Tissues in 22.5°(i)-, 45°(ii)- and 90°(iii)-clefts and imaged for α SMA (orange), Fn (green) TNC (magenta) and SHG (cyan). Scale bar = 100 μ m. **(C)** Normalized intensity plots along distance to growth front as mean over multiple μ Tissues in 22.5°(i)-, 45°(ii)- and 90°(iii)-clefts. For more data see Fig. S06.

Partial inhibition of Fn-collagen-interaction hampers maturation of μ Tissues in 22.5°- and 45°-clefts, while 90°-cleft tissues are much less perturbed

The nucleation of collagen polymerization is templated by the provisional fibronectin fibers, whereby only locations of structurally relaxed but not stretched Fn can serve as template [42]. While we found already in Chapter 4 that partial inhibition of Fn and collagen interaction with R1R2 peptide hampers tissue maturation and leads to higher levels of tissue ruptures, we next asked whether and how this relates to μ Tissues tension. μ Tissues grown in all cleft angles under supplementation of R1R2 show Fn, α SMA and TNC markers in the core tissue (Fig. 10B+C), indicating hampered tissue maturation in agreement with previous findings (Benn et al. in preparation, Chapter 4). The tissue morphology appears in the confocal slice similar to the effects seen with blebbistatin (compare Fig. 12B with Fig. 13B). Under R1R2 treatment the steepest maturation gradient is visible with a 90°-cleft angle (Fig. 12B-C), while the SHG signal is reduced (Fig. 7E). Interestingly, the correlation of curvature to growth indicates a trend that 90° μ Tissues show similar curvatures with slightly reduced growth (Fig. 5). Interestingly, full tissue ruptures occur mainly in 45°- μ Tissues (see Fig. S04, lowest row and Video S05, R1R2 supplemented at timestamp = 114.5[h]). However, early tissue ruptures after R1R2 supplementation occur in all cleft angles (Fig. S07). Inhibition of fibronectin-collagen interaction using R1R2 resulted in reduced collagen fiber bundling (Fig. 7). This suggests together with the high occurrence of rupture events that R1R2 treatment results in tissues of reduced stability.

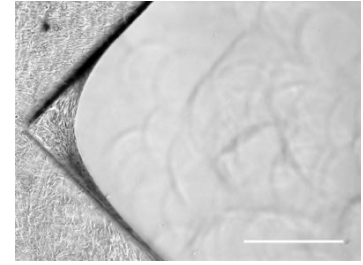
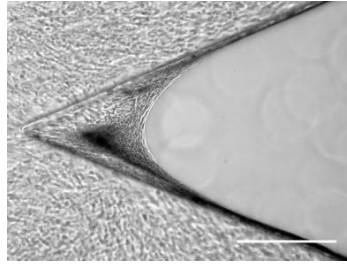
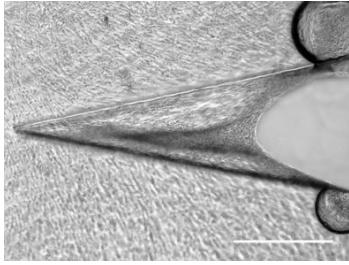
A Phase contrast

Day 1: cell seeding > Day 5: started treatment > Day 12: fixation

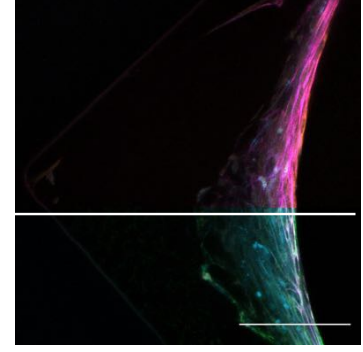
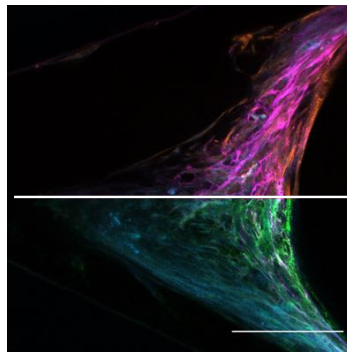
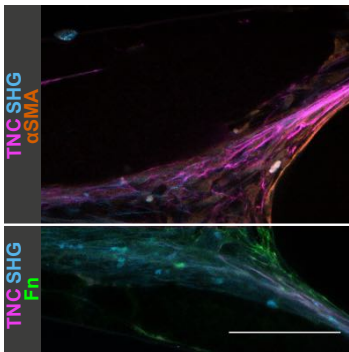
i) 22.5° + R1R2

ii) 45° + R1R2

iii) 90° + R1R2



B 2P + CLSM



C Profile intensity plot

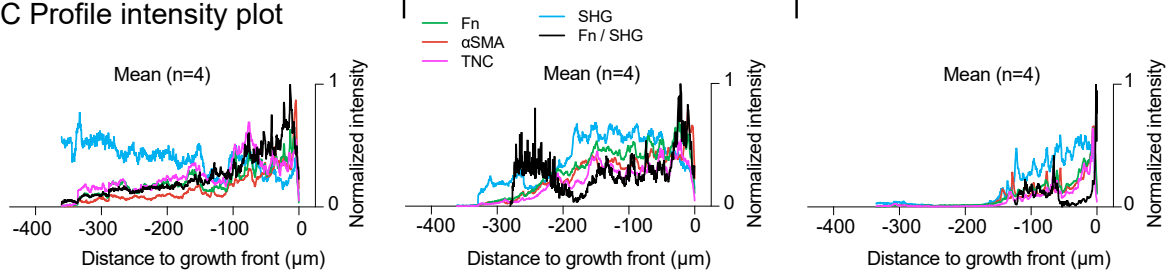


Fig. 12 *De novo* μ Tissue growth in clefts with varying angle and R1R2 treatment from day 5. **(A)** Phase-contrast images of μ Tissues assembled by human dermal fibroblast in 22.5°(i)-, 45°(ii)- and 90°(iii)-clefts over 12 days of incubation. Scale bar = 500 μ m. **(B)** 2-photon microscopy (2P) and confocal laser scanning microscopy (CLSM) of representative μ Tissues in 22.5°(i)-, 45°(ii)- and 90°(iii)-clefts and imaged for α SMA (orange), F_n (green) TNC (magenta) and SHG (cyan). Scale bar = 100 μ m. **(C)** Normalized intensity plots along distance to growth front as mean over multiple μ Tissues in 22.5°(i)-, 45°(ii)- and 90°(iii)-clefts. For more data see Fig. S06.

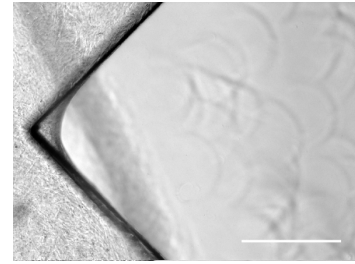
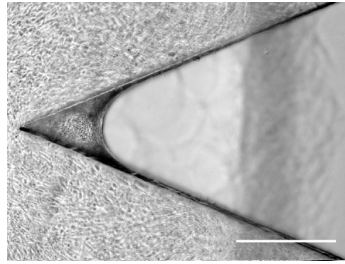
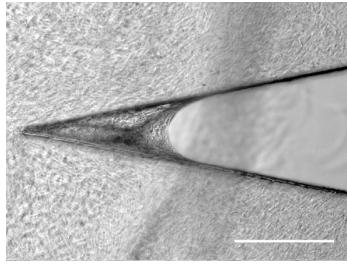
A Phase contrast at day 12

Day 1: cell seeding > Day 5: started treatment > Day 12: fixation

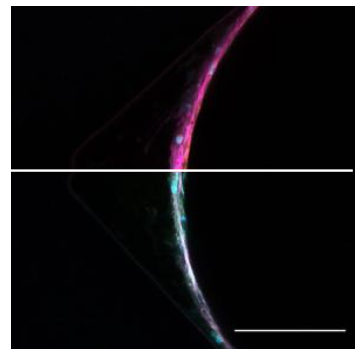
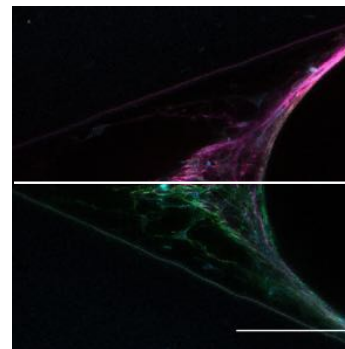
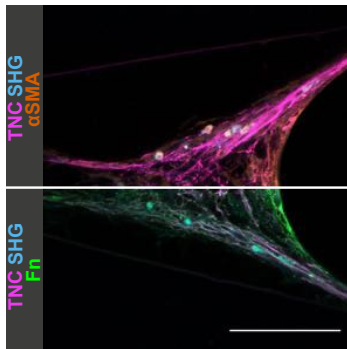
i) 22.5° + Blebbistatin

ii) 45° + Blebbistatin

iii) 90° + Blebbistatin



B 2P + CLSM



C Profile intensity plot

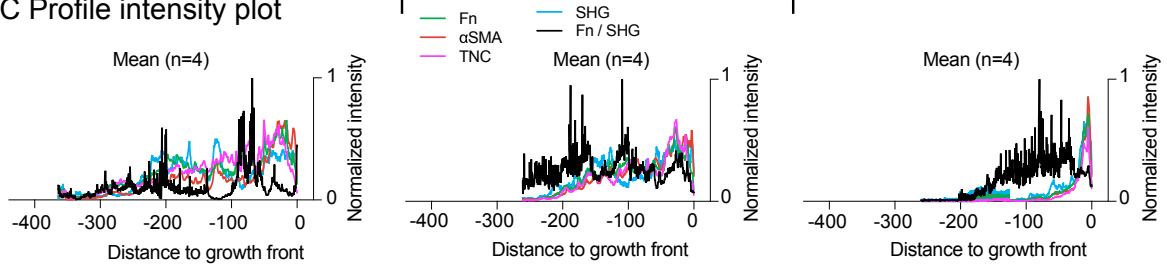


Fig. 13 *De novo* μTissue growth in clefts with varying angle and blebbistatin treatment from day 5. **(A)** Phase-contrast images of μTissues assembled by human dermal fibroblast in 22.5°(i)-, 45°(ii)- and 90°(iii)-clefts over 12 days of incubation. Scale bar = 500 μm. **(B)** 2-photon microscopy (2P) and confocal laser scanning microscopy (CLSM) of representative μTissues in 22.5°(i)-, 45°(ii)- and 90°(iii)-clefts and imaged for αSMA (orange), Fn (green) TNC (magenta) and SHG (cyan). Scale bar = 100 μm. **(C)** Normalized intensity plots along distance to growth front as mean over multiple μTissues in 22.5°(i)-, 45°(ii)- and 90°(iii)-clefts. For more data see Fig. S05.

5.4 Discussion

Here we provide a novel μ Tissue model by advancing our microfabricated PDMS platform and integrated an array of different cleft angle that allowed us to tune the growth curvature and thus tissue tension of the fibroblast *de novo* grown μ Tissues. We found that widening of the cleft angle leads to reduced growth front curvature and tissue growth (Fig. 1A, Fig. 2 and Fig. 3). In our model, tissue tension can be modified via cleft angle and cell contractility. Reducing cellular contractility with Blebbistatin resulted in increased growth front curvature, underlining the importance of residual ECM tension in tensional homeostasis (Fig. 4). Interestingly, increased cellular contractility through TGF- β 1 supplementation reduced the prominent differences in μ Tissues grown in different cleft angle geometries, which underlines the prominent role of cellular contractility on tissue growth and maturation (Fig. 5). Furthermore, inhibition of TGF- β receptor signalling with GW788388 hampered tissue maturation in μ Tissues of high tensional states, but disturbed only mildly tissue maturation in 90°-clefts with low tissue tension (Fig. 11). In addition, sufficient tissue stability is required to prevent tissue rupture. We found that fibronectin-collagen-interaction is important for both tissue maturation and tissue stabilization (Fig. 12 and Fig. S07). Mechanical tissue stability is further enhanced by collagen fibers in the interior that align parallel to the geometrical tissue constrains with intersecting fibers (Fig. 7).

In our cleft angle arrays, we observed in wider clefts reduced tissue growth as well as reduced growth front curvature (Fig. 4). Decreased substrate and growth front curvature was reported to decrease tissue tension and reduce tissue growth towards the open cleft [16-19]. Since the μ Tissue fuses from the confluent layer of the two-merging vertical cleft walls, the 90°-cleft provides lowest curvature from the beginning of growth. The tissue then grows into the open cleft in a seamlessly sequential process [44] and the already assembled tissue with the newly advanced growth front provides the geometrical guidance as curvature for the next 'layer'. Our finding is thus in agreement with the literature, that larger curvature correlate with reduced tissue growth. Taken together with the literature we can conclude, that μ Tissues in smaller clefts contain increased tissue tension compared to the wider clefts.

Our finding that inhibition of myosin II contraction lead to increased growth front curvature can be explained with tensional homeostasis of ECM where the total amount of cellular forces are counterbalanced by ECM tensions [45]. Disturbed equilibrium here will result in alteration either of the cells or the ECM. Accordingly, it was shown that a short 20 μ M blebbistatin pulse on *de novo* grown tissues resulted in an immediate reduction in tissue volume [44]. Thus, the release of cellular

contractility leads to a passive retraction of the in-between-the-cleft-spanned tissue due to residual tension stored in the ECM, which explains why growth front curvature increases as soon as cellular contractility is inhibited. α SMA positive myofibroblasts are visible less prominently under blebbistatin treatment (Fig. 13).

In agreement with previous suggestions that sufficient cellular contractility is required to generate the surface stress required for tissue growth [19], here we also show that treatment with the myosin II inhibitor blebbistatin resulted in reduced tissue growth. While Ehrig et al. demonstrated that both control and TGF- β 1 supplemented tissues minimized their total surface area in a liquid-like behaviour, blebbistatin treated tissues deviated significantly from the Laplace-Young law predictions [19]. Our experiments show in agreement that blebbistatin not only significantly decreased tissue growth, but also resulted in a significant pattern shift when all angles of all conditions are combined in a plot of curvature over tissue growth (Fig. 4). Taken together, μ Tissue treated with inhibition of cellular contractility is in agreement with the described effects in the literature and the decreased tissue tension results in decreased tissue growth is inhibited.

When the contractile forces generated by cells exceed the matrix resistance, an inward compaction of the fibrillar network combined with partial de-adhesion from cleft walls is the result (Fig. 1B, Video S01 and Fig. S02). The fact that the cells pull not against the PDMS scaffold walls which can be seen by the main SHG fiber orientation (Fig. 7), is not surprising as the Fn-functionalized but still smooth PDMS walls do not allow the cells to anchor firmly. In the tissue interior away from the tissue edges, the network is organized such that the fibers connect the edge regions. They are pulling at intermittent angles and the fibers are less compacted. Under GW788388 treatment the collagen fibers are much more tightly woven, with a smaller fraction of fibers running in tight bundles along the tissue edges, and thus an increased fraction of fibers pulling along the 0° -axis of the μ Tissues. Addition of TGF- β 1 significantly increases the collagen fibers that run parallel to the growth front, which agrees with the observation that the growth front is narrower (Fig. 7 and Fig. 5). The Laplace equation describes how surface curvature depends on surface energy which then predicts the shape of water droplets. The surface energy of water is high due to the attractive interactions of water molecules. Similarly, attractive interactions of cells lead to tissue surface tension, a concept that has been applied in Biology to predict shapes across length scales [46]. A series of studies from Dunlop and colleagues has shown that the growth speed of μ Tissues on surfaces is proportional to the local curvature of the μ Tissue-fluid interface [16], which can be explained by a physical model considering the accumulation of local mechanical stress at the growing front [47]. Our experimental results of the μ Tissue growth kinetics (Fig. 1F and Fig. 4) show

a similar trend to the conventional description. From a biological viewpoint, such geometry-dependent growth of μ Tissue generates residual strain inside the μ Tissue balanced by the cellular contractility and the ECM network [44]. In our system, more aligned fibers were observed along the growth front as the cleft angle increased (Fig. 7A), and this trend was enhanced by addition of exogenous TGF- β 1 (Fig. 7B). These observations, together with the conventional findings on ECM networks inside μ Tissues, imply that the difference in cleft angle shifts the distribution of residual strain inside the growing μ Tissue.

Supplementation of GW788388 and blebbistatin both reduced collagen fiber assembly (Fig. 8), despite the fact that their effects have totally different causes. However, a physical interaction between integrin α 2 β 1 and TGF- β receptor I (also known as ALK5) was described to induce Smad phosphorylation with downstream signal propagation, without TGF- β ligand participation [40]. This reported physical interaction between α 2 β 1-integrins and TGF- β receptors could potentially also stabilize α 2 β 1-integrins and result in an increased force transmission. Since GW788388 inhibits TGF- β receptor I and II [22], the inhibitor might also alter its interaction with α 2 β 1 integrins and could interfere with α 2 β 1 collagen binding, which is in turn required for collagen polymerization [41]. This could in addition explain reduced collagen fiber assembly under GW788388 treatment. Furthermore, it was shown that cellular tension regulates the spatial distribution of TGF- β receptor I and II, since they organize in integrin-rich focal adhesions [48], through which the cells form tensional homeostasis with the ECM via Rho/ROCK-dependent mechanisms [49]. It was furthermore described, that RhoA signalling can convert the response of TGF- β to promote proliferation [50]. Taken our data together with the literature, those TGF- β independent effects might explain the alterations seen in SHG fiber bundling (Fig. 7).

Interestingly the fiber orientation patterns under R1R2 show some similarity with the GW788388 condition in terms of alignment with the cleft wall and reduced fibers aligned to the growth front (Fig. 7). It is notable that inhibition of fibronectin-collagen interaction using R1R2 did not have a crucial impact on fiber assembly (Fig. 6), because it was formerly shown that relaxed fibronectin works as a template of collagen deposition in a 2D cell-culture environment [42]. Interestingly, the location shift of the aligned fibers from the deep region to the growth front over the increase of cleft angle was kept in the presence of these inhibitors (Fig. 7), which is also in agreement with the compaction patterns (Fig. S02). The cleft angle affects the mechanical environment within the μ Tissue, however, the influence seems to be orthogonal to the effect of biochemical reagents. Further studies are required to elucidate the anteroposterior relationship of the phenotypic change of fibroblast and the ECM maturation in the 3D confinement.

Growth front peak width (Fig. 1E, growth front peak range) correlates with tissue tension, as wider growth front peaks are seen in tissue grown in smaller cleft angles with increased growth front curvature (Fig. 1D-E) and the literature allows translation to tension as outlined above. However, since the tissue compaction in 22.5°- and 45°-clefts is also decreased in areas contributing where the increased growth front width is located (Fig. 1B), it is important to discuss whether there could be also alternative ways to explain growth front width variation.

Growth front width correlates negatively with the cleft angle (Fig. 1E). Growth speed is increased by smaller cleft angles [17,44]. Growth speed is quantified here by growth distance per time, thus spatial to temporal translation within the young-to-mature gradient in central ROI seems to be widened or spread over longer space, when growth speed is increased in smaller cleft angles. Since the main compaction branches in smaller cleft angles are framing the optically less dense growth front area (Fig. 1B, 22.5° and 45°) it is likely that here is again a high local tissue compaction driven by cell contractility in the small growth front area that spreads between the tension bearing tissue compaction branches. Thus, further tissue growth might be directed by new curvatures that are formed during sequential tissue growth with local ruptures and further tissue compaction. Interesting, the SHG fiber alignment co-localizes nicely with the compaction branches (Fig. 1B and Fig. 6, control). Together with the literature and since μ Tissues with increased cellular contractility do neither show angle differences in tissue compaction nor much in growth front width, the factor of tissue tension seems inherently coupled to the system and likely dominates the effect of alterations of growth front width.

TGF- β is known to convey multiple, sometimes even paradox functions as in tumor growth where it switches functionality [37,38]. In 2D planar experiments, TGF- β 1 was reported to induce fibroblast-to-myofibroblast transdifferentiation [59], as we also demonstrated in Fig. 10. Interestingly, in *de novo* grown μ Tissue TGF- β supplementation did not lead to an increase of myofibroblasts in mature core regions which are dominated by fibroblast [14], as expected from 2D experiments [59]. Here we see a mild increase of α SMA positive myofibroblast in the interior, but the dominant appearance is in agreement with the previous *de novo* tissue report (Fig. S06B). TGF- β 1 supplementation is causing higher signal density of α SMA (Fig. 8 and Fig. S05). Higher signal density of α SMA means higher amount of alpha smooth muscle actin per area, which can be correlated with higher contractility [20]. Our data suggest that this leads to an accelerated tissue maturation with faster collagen assembly and faster myofibroblast-to-fibroblast transition, since the growth front peak range is significantly decreased (Fig. 5B-D). The curvature over tissue growth

indicates a trend towards decreased curvature under TGF- β 1 supplementation, indicating higher tissue tension compared to the control (Fig. 4). Our data indicate that while we see a much wider growth front peak range in the control 22.5°-clefts (Fig. 1C-E), more concentrated cellular contractility upon TGF- β 1 supplementation in the growth front allows to equalize the tensional difference seen in the control (Fig. 5B-D). This is in agreement with our finding that more ruptures occur under supplementation of TGF- β 1 (Fig. S07). Since the sample number here is low ($n=4$) and the variation high, follow up experiments with higher sample numbers need to further elucidate these interdependences.

Although TGF- β has many complex biochemical signalling functions, it seems that in tension accelerated growth cell contractility overlays dominantly other regulatory effects. Our data indicates that the process of myofibroblast-to-fibroblast transition and subsequent tissue maturation is accelerated when early high contraction forces are exerted. However, this can also be due to TGF- β independent mechanisms for example through reported physical interaction of TGF- β receptor with α 2 β 1 integrin [40], which could potentially stabilize α 2 β 1 integrin and allow increased force transmission exerted on the ECM. For all these processes, to maintain tissue integrity with tensional homeostasis it is required that all forces are counterbalanced.

We found recently that timely tissue maturation and thus the rapid clearance of myofibroblasts via the conversion to fibroblasts [14] requires TNC and enzymatically active TG2 (Benn et al. in preparation, Chapter 4). Both TG2 and TNC are known to regulate cellular adhesion: TG2 as a Fn- β 1-integrin coreceptor increases adhesion, and TNC – via competitive binding to Snydecin-4 – decreases adhesion [51-54]. However, TNC fragments after MMP degradation were shown to have adhesive functionality as well. Adhesion strength correlates with levels of force cells can exert on their environment [55], and build-up of cell contractility in turn correlates with expression of α SMA [20]. With supplementation of exogenous TGF- β 1, contractility is kept artificially high, which likely perturbs the orchestrated actions of TNC and TG2 in promoting the myofibroblast-to-fibroblast-transition. Accordingly, the growth front peaks are narrower in all angles, but this in turn lead to increased ruptures, as the forces cell generate are not sufficiently counterbalanced by the mechanical strength of the provisional matrix. Both TGF- β 1 supplementation and inhibition of Fn-collagen binding show increased tissue rupture (Fig. S07), which is likely due to increased cellular contractility and decreased tissue stability. Furthermore, Yamashita et al. characterized contractile cell behaviour on curved surfaces using a phase diagram of contractility, adhesion and curvature [56]. Although this was only on short timescales, our observations could be interpreted using an extension of this picture in mind, where the right balance of curvature, contractility and tissue

integrity is required to result in a trajectory through phase space that leads towards a balanced homeostatic outcome, while perturbation of this balance due to insufficient or excessive contractility or by disrupting tissue stability leads to failure.

We here show that tissue tension can be systematically tuned in *de novo* μ Tissue growth in arrays of microengineered clefts. In summary, our study identifies tissue tension together with cellular contractility as key parameter which regulate fibroblast-to-myofibroblast transition and conversion with subsequent tissue maturation and tissue growth. This knowledge can contribute to develop future μ Tissue platforms. Of particular significance is here that the spatiotemporal resolution of the ECM gradients can be tuned in dependence of the tissue tension to investigate future interventions on this platform not only as function of tissue tension, but also with higher spatial separation of the temporal ECM gradient. This increased sensitivity combined with the feature of tunable tissue tension might allow to identify completely novel strategies relevant for diagnostics and treatments in tension-related diseases.

5.5 Materials and methods

Rationale for substrate design and fabrication method

Polydimethylsiloxane (PDMS) substrates were fabricated by replica molding of negative SU8-master structures, improving the previously published protocol [14]. To avoid residual membrane formation, a custom build compression device was applied as described below. In order to reduce μ Tissue-to- μ Tissue variability, the cleft edges were smoothed with a photomask of higher resolution and each cleft is separated, so that the grown μ Tissues are not in direct contact with each other. Each substrate consists of a cluster of 12 clefts (22.5°, 45°, 90°) arranged in arrays. The arrangement of multiple cluster replicas on one master mold allowed a higher production throughput.

Master fabrication

A master mold was fabricated by standard lithography of multiple layers of SU8-3050 photoresist (MicroChem, USA). In brief, a 4" silicon wafer was dehydrated at 120°C for 10 min. For the first layer, 2 ml of SU8-3050 was dispensed and spin-coated at 500 rpm for 10 s with acceleration 100 rpm/s followed by 1000 rpm for 45 s with acceleration 500 rpm/s. After spin coating, a soft bake at 65°C for 7 min and at 95°C for 15 min was performed. After cooling down to room temperature (RT), spin coating was repeated twice with 4 ml of photoresist each resulting in a \sim 350 μ m thick resist layer. Samples were stored at RT for 24 hours prior to exposure. For exposure, a photolithography mask with a resolution of 32,000 dpi (Zitzmann GmbH, Germany) and a MA6 mask aligner (Karl Suss, Germany) were used and the samples were exposed with a total dose of 400 mJ/cm² (λ = 365 nm) divided in 4 runs with 60 s pause in between exposures. Post exposure bake was performed at 65°C for 3 min and 95°C for 10 min. Due to the thickness of the resist, all heating and cooling steps were performed at slow ramp. The resist was developed using mr-Dev 600 developer (Microresist Technologies, Germany) under ultrasound for 20 min, followed by a wash with fresh developer and isopropanol, each for 10 s. Master molds were passivated with 20 μ l of Trichloro(1H, 1H, 2H, 2H - Perfluorooctyl)Silane (Sigma 448931) under vacuum for 1 hour.

Microfabrication of PDMS scaffolds

PDMS scaffolds with open cleft free of residual membranes were replica-molded from the master mold using a custom-built compression device. PDMS was mixed in a standard ratio of 10:1 base to curing agent (Sylgard 184, Dow Corning, USA), degassed at 70 mbar for 30 min, poured on the master mold placed in the custom built compression device and degassed at 70 mbar max. 45 min until all air bubbles were removed. Afterwards, a 2 mm thick polymethyl methacrylate lid (PMMA)

was placed on the top at a slight angle preventing the formation of any air bubbles. Finally, the top piece of the compression device was mounted and all 4 screws were tightened in crossed manner with a maximum torque of 4 Nm. After the PDMS was cured at 80°C overnight, each substrate was cut out with a 18 mm diameter punch, cleaned in 70 % ethanol ultrasonic bath for 20 min and stored in 70 % ethanol.

Functionalization and mounting of PDMS scaffolds

Fibronectin was covalently bound to the surface of the PDMS scaffolds using a heterobifunctional cross-linker (Sulfo-SANPAH, 0.5 mg/ml in PBS (1x, adjusted to pH 8.5 with NaOH), Thermo Fisher Scientific) as described previously [14,57]. The functionalized substrates were attached with optical glue NOA-61 (Norland Optical adhesive 61, Norland) with 1 mm thick PDMS spacer as described in Kollmannsberger et al. [14] into a 12-well culture plate that had previously been passivated using PLL(poly-L-lysine)(20)-g[3.5]-PEG(polyethylene glycol)(5) (0.1 mg/ml in HEPES2 (HEPES + 150 mM NaCl), SuSoS). After assembling the cell culture system, it was washed once with PBS and UV treated for 15 min. Prior to cell seeding, the surface was equilibrated with α -minimum essential medium (α MEM, Biowest SAS) supplemented with 10 % fetal bovine serum at 37°C for at least 1 hour.

μ Tissue growth experiments

Cell culture

Primary normal dermal human fibroblast (NHDF, passage numbers 6 to 10, Lonza) were maintained in α -minimum essential medium (α MEM, Biowest SAS) supplemented with 10 % fetal bovine serum and 1 % penicillin-streptomycin exchanged every 2-3 days. All experiments were conducted at 37°C in a humidified atmosphere with 5 % CO₂. The cells were trypsinized and seeded on the PDMS substrates at a density of 2×10^5 cells per substrate. For μ Tissue experiments, the cell culture medium was supplemented with 100 μ M L-Ascorbic Acid 2-phosphate sesquimagnesium salt hydrate (A8960-5G, Sigma) and 0.05 mg/ml fibronectin in PBS. Fibronectin was isolated from human plasma as previously described [58]. For interventional experiments, the cell culture medium was further supplemented with 0.1% DMSO and the following components from day 5 of μ Tissue growth: recombinant human TGF- β 1 (1 ng/ml, 100-21C, Peptrotech), inhibition of TGF- β RI/II with GW788388 (20 μ M, 3264, Tocris), inhibition of myosin II with blebbistatin (10 μ M, B0560-1MG, Sigma-Aldrich), inhibition of Fn-collagen interaction with R1R2 as previously described [42] (2.5 μ M, amino sequence GLNGENQKEPEQGERGEAGPPLSLGSLGNNQGRPSLPGLNGENQKEPEQG ERGEAGPP manufactured by GenScript).

In order to assess the α SMA response on GW788388 we performed a TGF- β 1 stimulation test on 2D Fn coated glass. Primary normal dermal human fibroblast (NHDF, passage numbers 6 to 10,

Lonza) were cultured routinely in normal growth medium composed of α -minimum essential medium (α MEM, Biowest SAS) supplemented with 10 % fetal bovine serum and 1 % penicillin-streptomycin. Once at optimal confluency, the fibroblasts were trypsinized and seeded separately in triplicates in 8-well labtek chambers at 4.5×10^3 cells/cm² in normal growth medium. After 24 h, medium was replaced with and without TGF- β 1 (5 ng/ml, 100-21C, PeptroTech). Each condition was combined with GW788388 (20 μ M, 3264, Tocris) or with 0.1 % DMSO and cultured further for additional 3 days including a media exchange at day 3.

Fixation and immunofluorescence

After 12 days of total incubation, samples were washed twice with pre-warmed HBSS (+ Ca, + Mg) and fixed with 4% PFA for 15 min. The cell membrane was permeabilized with 1 % Triton X-100 (T8787-50ML, Sigma-Aldrich) for 20 min followed by 60 min incubation in blocking solution (2 % BSA (w/v) (05470-5G, Sigma-Aldrich) and 5 % donkey serum (v/v) (ab7475, Abcam)). μ Tissues depicted in Fig. 1, 3, 4 and 6 were immunostained against TNC and μ Tissues depicted in Fig. 5 were immunostained against TG2. TNC antibody (1:100, BC-24, MA1-26779, Thermo Fisher Scientific) was combined with Fn (C-20) antibody (1:100, sc6952, Santa Cruz) and were supplemented in blocking solution to the respective μ Tissues and incubated for 1 h at RT. After washing three times in PBS for 5 min each, samples were incubated with anti-goat Alexa Fluor 488 (1:200, ab260129, abcam), anti-mouse Alexa Fluor 647 (1:100, ab150107, Abcam) in blocking solution for 1 hour at RT. After Three additional PBS washes, α SMA was stained with Alexa Fluor 594-conjugated anti- α -smooth muscle actin antibody (1:100, ab202368, Abcam) in blocking solution for 1 hour at RT followed by three PBS washes.

Microscopy and image analysis

Image acquisition

Live phase-contrast images of the μ Tissues were acquired every 30 min. using a Zeiss Axiovert 200 M inverted microscope with 5x objective. Confocal fluorescence imaging was performed using a Leica TCS SP8 MP inverted multiphoton laser scanning microscope with a 25x objective (0.95NA L Water HCX IRAPO). Fluorophores were directly excited in single photon mode. Mature collagen fibers were imaged by second harmonic generation (SHG) in multiphoton laser scanning mode with open pinhole. Second harmonic was generated with a Mai Tai XF (Spectra-Physics) femtosecond Ti-sapphire pulsed laser tuned at 880nm and signal emitted from collagen fibers was detected at 440 nm.

Image analysis

Growth distances

Growth distances were measured between the angle tip of the cleft and the μ Tissue-medium interphase along the bisector angle axis in the phase-contrast images of the respective timepoints.

Projected tissue area

Projected tissue area was masked and quantified in a semi-automated way with a custom-built ImageJ script. The outline of the cleft was manually detected. The medium – tissue interface was detected with automated Otsu thresholding after median filter with $\sigma = 2$ was applied.

Curvature analysis

In dataset (Fig. 3, Fig. 4, Fig. S01) growth front curvature was determined by inversion of the radius of a circle, that was fitted in three points. To define the fitting points, the cleft walls were manually identified, and a first angle bisector was calculated to divide the cleft into two equal angles. Two additional angle bisectors were drawn in the upper and lower angle half. The circle for curvature measurement was fitted into the intersection points of all three bisectors with the growth front. In dataset (Fig. 2 and Fig. S09), the local tissue curvature was determined in an automated python script by sliding a circular mask with defined radius along the growth front and determining the overlap with the tissue at each point, as described in Bidan et al. [17].

Visualization and profile intensity plots

All images were rotated such that the angle tip of the cleft is oriented left-handed and the bisector angle of the cleft is parallel to the x-axis of the image. Since the μ Tissues do not form symmetrically along the bisector angle (parallel to x-axis), a representative symmetry axis was visually assessed such that it represents the young-to-mature-gradient in each μ Tissue. Profile intensities were assessed along this symmetry axis by column intensity average of 100 pixels equally distributed around the symmetry axis at each x-position. Profile intensity data used for plots was normalized by the respective maximum level of each channel, which allows relative comparison on an inter-channel and inter-tissue level. For orientation and comparison of the absolute intensities, the integral of the curve of each raw intensity profile is plotted (Fig. 1D). To determine the distance to growth front, all channels were cumulated and the boundaries of the μ Tissue was defined at the x position where cumulative signal intensity was greater than the threshold of 25 % of maximum intensity at the tissue-medium interphase. The signal is only plotted for distances to growth front $< 0 \mu\text{m}$. The overview visualizations with split look-up-tables were created by a custom build FIJI script and split at the y-position of the earlier determined symmetry axis used for profile plot.

Growth front peak range analysis

In the cumulated profile plots the growth front peak width was determined by assessing the x-intersection of the growth front peak with a baseline that was adjusted to 25 % of maximum intensity value per channel. Note, growth front peak range assessment (e.g. Fig. 1E) is only meaningful in samples in which the signal clearly separates of peak and interior.

Fiber orientation

Fiber orientation analysis was carried out using a custom-written MATLAB script provided by T. Yamashita. Orientation of the fibrous structure found in the SHG images was analyzed based on a filtering method using a custom-written MATLAB script (2020a, Mathworks, MA, USA). We here utilized a 5x5 basic operator H_x optimized by Kroon and H_y being the transposition of H_x :

$$H_x = \begin{pmatrix} 0.0007 & 0.0052 & 0.0370 & 0.0052 & 0.0007 \\ 0.0037 & 0.1187 & 0.2589 & 0.1187 & 0.0037 \\ 0 & 0 & 0 & 0 & 0 \\ -0.0037 & -0.1187 & -0.2589 & -0.1187 & -0.0037 \\ -0.0007 & -0.0052 & -0.0370 & -0.0052 & -0.0007 \end{pmatrix}$$

(1)

$H_{xx}=H_x \cdot H_x$, $H_{yy}=H_y \cdot H_y$ and $H_{xy}=H_x \cdot H_y$, where the dot product represents a sequential application of the basic operators to the image, were applied to the preprocessed SHG images to obtain the second order image derivatives I_{xx} , I_{yy} and I_{xy} , respectively. These outcomes were processed using a Gaussian filter with 4 pixel sigma, resulting in smoothed image derivatives I_{xx}^* , I_{yy}^* and I_{xy}^* . The pixel-level local orientation φ was then computed as follows:

$$\varphi(i, j) = 0.5 \arctan \frac{-2I_{xy}^*(i, j)}{I_{xx}^*(i, j) - I_{yy}^*(i, j)}$$

(2)

Statistical analysis

Unpaired two-tailed Mann-Whitney test was performed with GraphPad Prism software to test for statistical significance. Error bars represent 95% confidence intervals (CI).

5.6 Acknowledgements

We gratefully thank Dr. Sebastian Lickert for his contribution with figure editing, Dr. Jens Moeller and Prof. Simon A. Pot for their scientific input, Dr. Isabel Gerber and Chantel Spencer for technical support, the Scientific Center for Optical and Electron Microscopy (ScopeM, ETH Zurich) and Dr. Justine Kusch for her support with multiphoton image acquisition.

5.7 References

1. Phillip JM, Aifuwa I, Walston J, Wirtz D. The Mechanobiology of Aging. *Annu Rev Biomed Eng*; 2015;17(1):113–41.
2. Vining KH, Mooney DJ. Mechanical forces direct stem cell behaviour in development and regeneration. *Nat Rev Mol Cell Biol*; 2017 Nov 8;18(12):728–42.
3. Cole MA, Quan T, Voorhees JJ, Fisher GJ. Extracellular matrix regulation of fibroblast function: redefining our perspective on skin aging. *J Cell Commun Signal*; 2018 Mar 1;12(1):35–43.
4. Hsu CK, Lin HH, Harn HIC, Hughes MW, Tang MJ, Yang CC. Mechanical forces in skin disorders. *J Dermatol Sci*; 2018 Jun 1;90(3):232–40.
5. Vogel V. Unraveling the Mechanobiology of Extracellular Matrix. *Annu Rev*; 2018 Feb 12;80(1):353–87.
6. Tschumperlin DJ, Lagares D. Mechano-therapeutics: Targeting Mechanical Signaling in Fibrosis and Tumor Stroma. *Pharmacol Ther*; 2020 Aug;212:107575.
7. Harn HIC, Ogawa R, Hsu CK, Hughes MW, Tang MJ, Chuong CM. The tension biology of wound healing. *Exp Dermatol*; 2019 Apr 1;28(4):464–71.
8. Stamenović D, Smith ML. Tensional homeostasis at different length scales. *Soft Matter*; 2020;16(30):6946–63.
9. Xi W, Saw TB, Delacour D, Lim CT, Ladoux B. Material approaches to active tissue mechanics. *Nat Rev Mat*; 2019 Jan 1;4(1):23–44.
10. Chaudhuri O, Cooper-White J, Janmey PA, Mooney DJ, Shenoy VB. Effects of extracellular matrix viscoelasticity on cellular behaviour. *Nature*; 2020 Aug 1;584(7822):535–46.
11. Langhans SA. Three-Dimensional *in vitro* Cell Culture Models in Drug Discovery and Drug Repositioning. *Front Pharmacol*; 2018;9:6.
12. Grinnell F. Fibroblasts, myofibroblasts, and wound contraction. *J Cell Biol*; 1994 Feb;124(4):401–4.
13. Hinz B, Celetta G, Tomasek JJ, Gabbiani G, Chaponnier C. Alpha-Smooth Muscle Actin Expression Upregulates Fibroblast Contractile Activity. Matsudaira PT, editor. *Mol Biol Cell*; 2001 Sep;12(9):2730–41.
14. Kollmannsberger P, Bidan CM, Dunlop JWC, Fratzl P, Vogel V. Tensile forces drive a reversible fibroblast-to-myofibroblast transition during tissue growth in engineered clefts. *Sci Adv*; 2018 Jan 1;4(1):eaao4881.
15. Piersma B, Hayward MK, Weaver VM. Fibrosis and cancer: A strained relationship. *Biochim Biophys Acta Rev Cancer*; 2020 Apr 1;1873(2):188356.
16. Rumpler M, Woesz A, Dunlop JWC, van Dongen JT, Fratzl P. The effect of geometry on three-dimensional tissue growth. *J R Soc Interface*; 2008 Oct 6;5(27):1173–80.
17. Bidan CM, Kommareddy KP, Rumpler M, Kollmannsberger P, Bréchet YJM, Fratzl P, Dunlop JWC. How Linear Tension Converts to Curvature: Geometric Control of Bone Tissue Growth. *PLOS ONE*; 2012 May 11;7(5):e36336.
18. Bidan CM, Kommareddy KP, Rumpler M, Kollmannsberger P, Fratzl P, Dunlop JWC. Geometry as a Factor for Tissue Growth: Towards Shape Optimization of Tissue Engineering Scaffolds. *Adv Healthcare Mat*; 2013 Jan 1;2(1):186–94.

19. Ehrig S, Schamberger B, Bidan CM, West A, Jacobi C, Lam K, Kollmannsberger P, Petersen A, Tomancak P, Kommareddy K, Fischer FD, Fratzl P, Dunlop JWC. Surface tension determines tissue shape and growth kinetics. *Sci Adv*; 2019 Sep;5(9):eaav9394.
20. Bhadriraju K, Yang M, Alom Ruiz S, Pirone D, Tan J, Chen CS. Activation of ROCK by RhoA is regulated by cell adhesion, shape, and cytoskeletal tension. *Exp Cell Res*; 2007 Oct;313(16):3616–23.
21. Gellibert F, de Gouville A-C, Woolven J, Mathews N, Nguyen V-L, Bertho-Ruault C, Patikis A, Grygielko ET, Laping NJ, Huet S. Discovery of 4-{4-[3-(Pyridin-2-yl)-1 H-pyrazol-4-yl]pyridin-2-yl}- N-(tetrahydro-2 H- pyran-4-yl)benzamide (GW788388): A Potent, Selective, and Orally Active Transforming Growth Factor- β Type I Receptor Inhibitor. *J Med Chem*; 2006 Apr;49(7):2210–21.
22. Petersen M, Thorikay M, Deckers M, van Dinther M, Grygielko ET, Gellibert F, de Gouville AC, Huet S, Dijke ten P, Laping NJ. Oral administration of GW788388, an inhibitor of TGF- β type I and II receptor kinases, decreases renal fibrosis. *Kidney Int*; 2008 Mar;73(6):705–15.
23. Pakshir P, Hinz B. The big five in fibrosis: Macrophages, myofibroblasts, matrix, mechanics, and miscommunication. *Matrix Biol*; 2018 Aug 1;68-69:81–93.
24. Micha D, Voermans E, Eekhoff MEW, van Essen HW, Zandieh-Doulabi B, Netelenbos C, Rustemeyer T, Sistermans EA, Pals G, Bravenboer N. Inhibition of TGF β signaling decreases osteogenic differentiation of fibrodysplasia ossificans progressiva fibroblasts in a novel *in vitro* model of the disease. *Bone*; 2016 Mar 1;84:169–80.
25. Lagares D, García-Fernández RA, Jiménez CL, Magán-Marchal N, Busnadiego O, Lamas S, Rodríguez-Pascual F. Endothelin 1 contributes to the effect of transforming growth factor β 1 on wound repair and skin fibrosis. *Arthr Rheuma*; 2010 Feb 25;62(3):878–89.
26. Sottile J, Hocking DC. Fibronectin polymerization regulates the composition and stability of extracellular matrix fibrils and cell-matrix adhesions. *Mol Biol Cell*; 2002 Oct;13(10):3546–59.
27. Lindmark H, Guss B. SFS, a novel fibronectin-binding protein from *Streptococcus equi*, inhibits the binding between fibronectin and collagen. *Infect Immun*; 1999 May;67(5):2383–8.
28. Sottile J, Shi F, Rublyevska I, Chiang HY, Lust J, Chandler J. Fibronectin-dependent collagen I deposition modulates the cell response to fibronectin. *Am J Cell Physiology*; 2007 Oct 3;293(6):C1934–46.
29. Zoumi A, Yeh A, Tromberg BJ. Imaging cells and extracellular matrix *in vivo* by using second-harmonic generation and two-photon excited fluorescence. *Proc Natl Acad Sci*; 2002 Aug 12;99(17):11014–9.
30. Chen X, Nadiarynkh O, Plotnikov S, Campagnola PJ. Second harmonic generation microscopy for quantitative analysis of collagen fibrillar structure. *Nat Prot*; 2012 Apr 1;7(4):654–69.
31. Jansen KA, Licup AJ, Sharma A, Rens R, MacKintosh FC, Koenderink GH. The Role of Network Architecture in Collagen Mechanics. *Biophys J*; 2018 Jun;114(11):2665–78.
32. Kojima Y, Acar A, Eaton EN, Mellody KT, Scheel C, Ben-Porath I, Onder TT, Wang ZC, Richardson AL, Weinberg RA, Orimo A. Autocrine TGF-beta and stromal cell-derived factor-1 (SDF-1) signaling drives the evolution of tumor-promoting mammary stromal myofibroblasts. *Proc Natl Acad Sci*; 2010 Nov 16;107(46):20009–14.
33. Roberts AB, LM W. The two faces of transforming growth factor beta in carcinogenesis. *Proc Natl Acad Sci*; 2003 Jul 22;100(15):8621–3.
34. Yingling JM, Blanchard KL, Sawyer JS. Development of TGF- β signalling inhibitors for cancer therapy. *Nat Rev Drug Discov*; 2004 Dec 1;3(12):1011–22.
35. Massagué J. TGF β signalling in context. *Nat Rev Mol Cell Biol*; 2012 Oct;13(10):616–30.

36. Weiss A, Attisano L. The TGFbeta Superfamily Signaling Pathway. *Dev Biol*; 2013 Jan 1;2(1):47–63.
37. Principe DR, Doll JA, Bauer J, Jung B, Munshi HG, Bartholin L, Pasche B, Lee C, Grippo PJ. TGF- : Duality of Function Between Tumor Prevention and Carcinogenesis. *J Natl Cancer Inst*; 2014 Jan 30;106(2):djt369–9.
38. Caja L, Dituri F, Mancarella S, Caballero-Diaz D, Moustakas A, Giannelli G, Fabregat I. TGF- β and the Tissue Microenvironment: Relevance in Fibrosis and Cancer. *Int J Mol Sci*; 2018 May;19(5):1294.
39. Vander Ark A, Cao J, Li X. TGF- β receptors: In and beyond TGF- β signaling. *Cell Signal*; 2018 Dec 1;52:112–20.
40. Garamszegi N, Garamszegi SP, Samavarchi-Tehrani P, Walford E, Schneiderbauer MM, Wrana JL, Scully SP. Extracellular matrix-induced transforming growth factor- β receptor signaling dynamics. *Oncogene*; 2010 Apr 1;29(16):2368–80.
41. Velling T, Risteli J, Wennerberg K, Mosher DF, Johansson S. Polymerization of Type I and III Collagens Is Dependent On Fibronectin and Enhanced By Integrins $\alpha 11\beta 1$ and $\alpha 2\beta 1$. *J BiolChem*; 2002 Sep 27;277(40):37377–81.
42. Kubow KE, Vukmirovic R, Zhe L, Klotzsch E, Smith ML, Gourdon D, Luna S, Vogel V. Mechanical forces regulate the interactions of fibronectin and collagen I in extracellular matrix. *Nat Commun*; 2015 Aug 14;6(1):8026.
43. DuFort CC, Paszek MJ, Weaver VM. Balancing forces: architectural control of mechanotransduction. *Nat Rev Mol Cell Biol*; 2011 May;12(5):308–19.
44. Bidan CM, Kollmannsberger P, Gering V, Ehrig S, Joly P, Petersen A, Vogel V, Fratzl P, Dunlop JWC. Gradual conversion of cellular stress patterns into pre-stressed matrix architecture during *in vitro* tissue growth. *J R Soc Interface*; 2016 May;13(118):20160136.
45. Ingber DE, Wang N, Stamenović D. Tensegrity, cellular biophysics, and the mechanics of living systems. *Rep Prog Phys*; 2014 Apr 1;77(4):046603.
46. Kollmannsberger P, Bidan CM, Dunlop JWC, Fratzl P. The physics of tissue patterning and extracellular matrix organisation: how cells join forces. *Soft Matter*; 2011;7(20):9549–60.
47. Dunlop JWC, Fischer FD, Gamsjäger E, Fratzl P. A theoretical model for tissue growth in confined geometries. *J Mechanics Physics Solids*; 2010 Aug;58(8):1073–87.
48. Rys JP, DuFort CC, Monteiro DA, Baird MA, Oses-Prieto JA, Chand S, Burlingame AL, Davidson MW, Alliston TN. Discrete spatial organization of TGF β receptors couples receptor multimerization and signaling to cellular tension. *eLife Sciences*; 2015 Dec 10;4:e09300.
49. Schoen I, Pruitt BL, Vogel V. The Yin-Yang of Rigidity Sensing: How Forces and Mechanical Properties Regulate the Cellular Response to Materials. *Annu Rev*; 2013 Jul;43(1):589–618.
50. Bhowmick NA, Ghiassi M, Aakre M, Brown K, Singh V, Moses HL. TGF- induced RhoA and p160ROCK activation is involved in the inhibition of Cdc25A with resultant cell-cycle arrest. *Proc Natl Acad Sci*; 2011 May 1;100(26):15548–53.
51. Lightner VA, Erickson HP. Binding of hexabrachion (tenascin) to the extracellular matrix and substratum and its effect on cell adhesion. *J Cell Sci*; 1990 Feb;95 (Pt 2)(2):263–77.
52. Chiquet-Ehrismann R. Anti-adhesive molecules of the extracellular matrix. *Curr Opin Cell Biol*; 1991 Oct 1;3(5):800–4.
53. Zemskov EA. The role of tissue transglutaminase in cell-matrix interactions. *Front Biosci*;

2006;11(1):1057.

54. Radwanska A, Grall D, Schaub S, la Forest Divonne SB-D, Ciais D, Rekima S, Rupp T, Sudaka A, Orend G, Van Obberghen-Schilling E. Counterbalancing anti-adhesive effects of Tenascin-C through fibronectin expression in endothelial cells. *Sci Rep*; 2017 Oct 6;7(1):12762.
55. Geiger B, Spatz JP, Bershadsky AD. Environmental sensing through focal adhesions. *Nat Rev Mol Cell Biol*; 2009 Jan;10(1):21–33.
56. Yamashita T, Kollmannsberger P, Mawatari K, Kitamori T, Vogel V. Cell sheet mechanics: How geometrical constraints induce the detachment of cell sheets from concave surfaces. *Acta Biomater*; 2016 Nov;45:85–97.
57. Trappmann B, Gautrot JE, Connelly JT, Strange DGT, Li Y, Oyen ML, Stuart MAC, Boehm H, Li B, Vogel V, Spatz JP, Watt FM, Huck WTS. Extracellular-matrix tethering regulates stem-cell fate. *Nat Mater*; 2012 Jul 1;11(7):642–9.
58. Smith ML, Gourdon D, Little WC, Kubow KE, Eguiluz RA, Luna-Morris S, Vogel V. Force-Induced Unfolding of Fibronectin in the Extracellular Matrix of Living Cells. *PLOS Biol*; 2007 Oct 2;5(10):e268.
59. Hinz B. The extracellular matrix and transforming growth factor- β 1: Tale of a strained relationship. *Matrix Biol*; 2015 Sep 1;47:54–65.

6 Preliminary study: Integration of *de novo* μ Tissue growth in Geistlich Mucograft® and Geistlich Bio-Gide®

In a preliminary study, I investigated *de novo* μ Tissue growth using clefts cut into scaffold materials of commercial products from Geistlich Pharma AG, Wolhusen, Switzerland in collaboration with PD Dr. med. Birgit Schäfer.

M.C.B., B.S. and V.V. designed the research; V.V. supervised the project; B.S. provided collagen scaffolds; **M.C.B.** designed and fabricated custom built scaffold mount; **M.C.B.** prepared collagen scaffolds and conducted cell culture experiments; **M.C.B.** performed phase-contrast, confocal (CLSM) and 2-photon (2P) laser scanning microscopy; **M.C.B.** performed data visualization and analysis of CLSM-, 2P- and phase-contrast-data; B.S. provided stained histological sections; **M.C.B.** acquired and described brightfield images of histological sections; **M.C.B.** reported the results; V.V. and B.S. revised and edited the report.

6.1 Introduction

In this preliminary study we tested whether commercial collagen scaffolds would support the *in vitro* growth of μ Tissues using primary human dermal fibroblasts. Tissue growth was primarily tested in manually cut clefts on Geistlich Mucograft® scaffold, a 3D non-crosslinked collagen matrix of porcine origin. This scaffold consists of a thick and porous layer, which is composed of native collagen I and III, and a compact thin layer [1,2]. The growth and subsequent integration of *de novo* μ Tissue was compared with Geistlich Bio-Gide®, which represents essentially the low-porose compact thin layer of the Geistlich Mucograft® [2]. Both products were developed to serve as a matrix scaffold and guide tissue regeneration.

We hypothesized, that fibroblast will assemble *de novo* grown μ Tissue in manually cut clefts of both scaffolds. This study allowed us furthermore to explore whether the platform can be adapted to both commercialized scaffold materials and how the growth kinetics compares to our standard approach. Most importantly, with our approach we can learn whether serum fibronectin is initially decorating the scaffolds, whether early fibronectin ECM assembly occurs during tissue growth and how μ Tissue integrates into the scaffolds. Our data provide valuable insights and motivate future studies that will deepen our understanding of the time-dependent actors in tissue growth on commercialized scaffolds, which can contribute to the development of future treatment and diagnostic strategies in wound surgery and beyond.

6.2 Results and discussion

6.2.1 Identified a technical solution to handle the fragile samples

The previously established protocol established for “*de novo* grown μ Tissues in engineered clefts” (Chapter 4) was applied using Geistlich Mucograft® as scaffold material. The technical challenge of handling Geistlich Mucograft® *in vitro* is, that the scaffold dissolves partially over time and thus its dimensions change. For image acquisition it is however required that the scaffold is held in place. To accomplish this, a new cell culture approach had to be developed to keep the Geistlich Mucograft® in place and allow visualization of cells in custom built PDMS bars and mounting device (Fig. 1). Clefts were cut into the Geistlich Mucograft® at the longitudinal edges and Geistlich Mucograft® was pre-incubated with 0.05 mg/ml fibrinogen (F3879, Sigma) for 1 hour followed by 3x gentle PBS washes and loaded with normal human dermal fibroblasts (PromoCell). It could be observed that μ Tissues formed in the clefts similar to the PDMS control with similar structural characteristics.

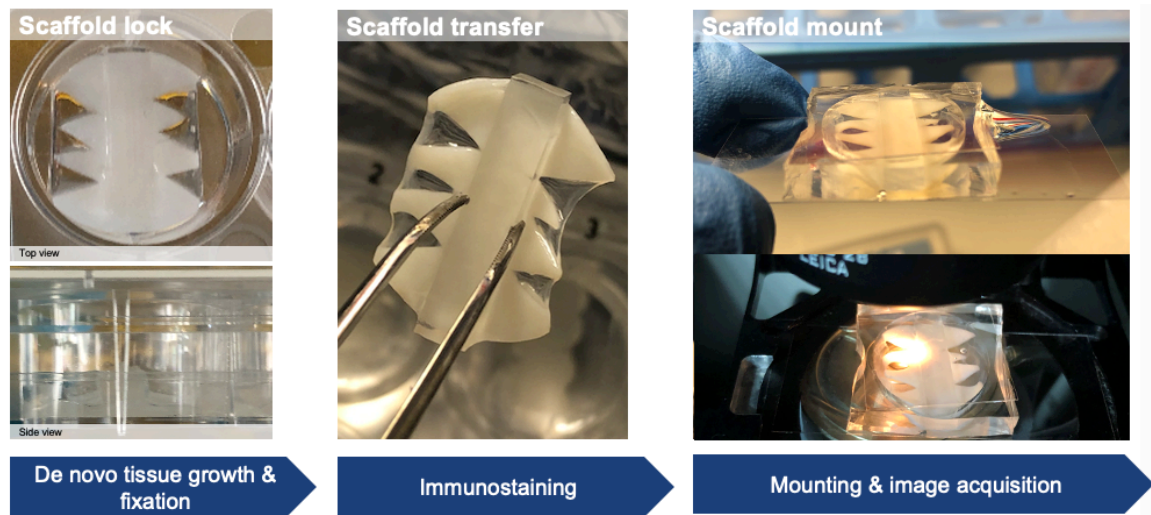


Fig. 1 Technical solution to mount the fragile samples and allow sample handling **(Left)** Custom build side and top PDMS bars keep scaffold at location on standard tissue culture 12-well plate. **(Middle)** The top PDMS bar renders the specimen immobile enabling manipulation (immunostaining and transfer to microscope mount). **(Right)** Samples were mounted in custom build PDMS chamber to allow image acquisition with inverted 2P microscope, Leica SP8.

6.2.2 Growth rate of *de novo* grown μ Tissues *in vitro*

μ Tissues formed in the clefts of both Geistlich Bio-Gide® and Geistlich Mucograft®. Compared to the PDMS control, it was found that fibroblast assembled tissue slower in manually cut clefts immersed in MEM Alpha (L0475-500, Biowest) medium supplemented with 10% FCS, 1% P/S and 100 μ M L-AA2P (L-Ascorbic acid 2-phosphate sesquimagnesium salt hydrate, Sigma-Aldrich) (Fig. 2). This decrease in tissue growth speed is possibly due to the more acidic culture medium introduced by Geistlich Mucograft®. Fibroblast proliferation kinetics are dependent on pH, a shift towards alkaline conditions accelerates fibroblast proliferation, while a shift towards acidic conditions decelerates fibroblast migration, which is essential for tissue growth [3]. Histology of Geistlich Mucograft® samples cultured for 17 days revealed that *fibroblasts grew mainly locally at the more lateral surface of the collagen matrix, and that most of them do not enter into the spongy part of the Geistlich Mucograft®, as there were only few Nuclei seen inside* (Fig. 3). As expected, the locally grown fibroblasts were embedded in a dense ECM (Fig. 3 red box), thus confirming the formation of a “true” μ Tissue observed by transmitting-light brightfield microscopy.

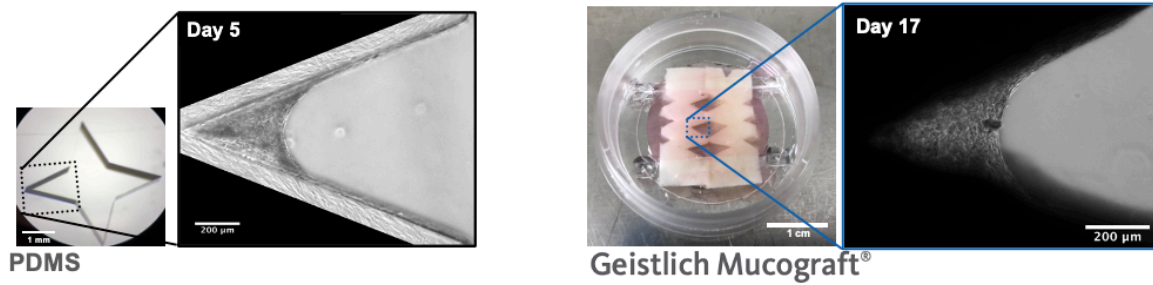


Fig. 2 Tissue growth rate is approximately three- fold slower in Geistlich Mucograft® compared to standard PDMS cleft platforms Regular phase-contrast images were acquired with Axiovert 200 M inverted microscope (Carl Zeiss) to document growth advancements. The growth of the μ Tissue was to similar extend developed after 17 days in Geistlich Mucograft® compared to PDMS after 5 days.

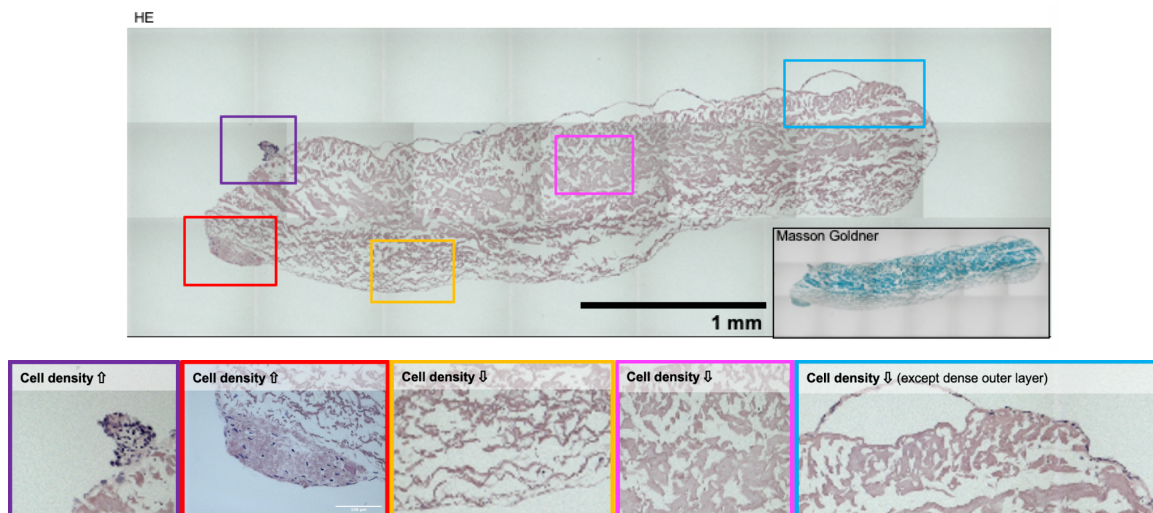


Fig. 3 Histological section of Geistlich Mucograft® scaffold showing bilayer architecture Only few cells reside inside the scaffold, while high densities cell clusters are seen in the outer parts of the dark purple and red box.

6.2.3 Development of a biomimetic approach to promote the ingrowth of fibroblasts

To ask whether fibroblast ingrowth could potentially be stimulated, we next supplemented the medium with plasma fibronectin and observed that it decorated the collagen fibers of Geistlich Mucograft® (Fig. 4). This suggests that the Mucograft® collagen is recognized by the gelatin binding domain of fibronectin. Please note though that a higher binding capacity of fibronectin was observed in Geistlich Mucograft® when compared to Geistlich Bio-Gide® (Fig. 5). Precoating of the Mucograft® collagen with plasma fibronectin indeed promoted fibronectin fibrillogenesis after 4 days in cell culture. Given that fibronectin is essential for the transmigration of fibroblasts from adjacent tissue into the wound site, *we thus propose that binding of plasma fibronectin takes place in vivo and that precoating of Geistlich Mucograft® with fibronectin could significantly promote the ingrowth of fibroblasts also under in vivo conditions.*

Geistlich Mucograft®

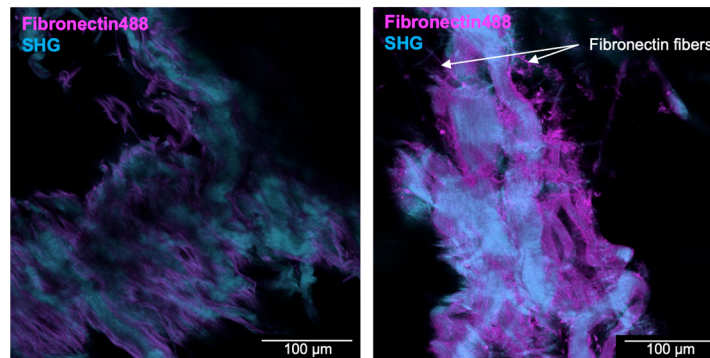


Fig. 4 Fibronectin adsorbs to Geistlich Mucograft® scaffolds in early states (after 4 d), and thereby paves the way for further matrix assembly, tissue growth and ECM maturation. Mucograft® collagen matrices get decorated with supplemented fibronectin that was labeled with Alexa fluorophore 488.

Geistlich Bio-Gide®

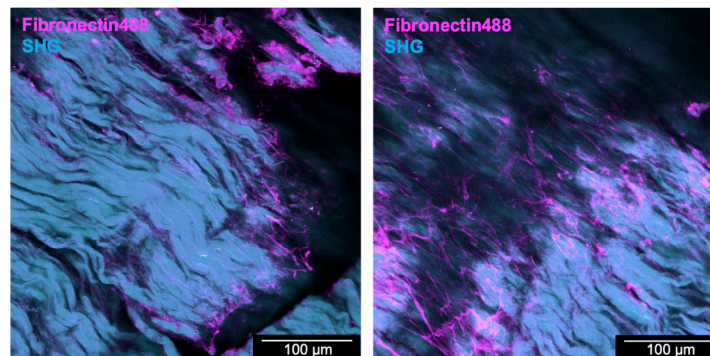


Fig. 5 Geistlich Bio-Gide® promotes more fibronectin fibrillogenesis after 4d. Fibronectin decoration of Geistlich Bio-Gide® scaffolds is reduced compared to Geistlich Mucograft® after 4d, but the fibronectin fibrillogenesis occurred more rapidly compared to Mucograft.

6.2.4 Enhancing the integration of the scaffold material with the *de novo* grown μ Tissue

Next, we ask how the *in vitro* μ Tissue platform can help us understand the integration of *de novo* grown μ Tissue in the initial growth phase directly at the scaffold-tissue interface. After 4 days in culture, we observed that new fibronectin fibers were assembled by cells in close vicinity to the Geistlich Mucograft® collagen fibers. Furthermore, collagen fibers from the less stable porous part of Geistlich Mucograft® were pulled by the cells into the μ Tissue. Since this requires a certain degree of mechanical stability for *de novo* grown μ Tissue to exert forces through tissue tension, we conclude that the *de novo* grown μ Tissue is intimately integrated into the Geistlich Mucograft® matrix. The formation of new fibronectin fibers occurred more rapidly in Geistlich Bio-Gide®, while its collagen had less adsorbed fibronectin after 4 days. *Our data suggest, that the integration of de novo grown μ Tissues leads to a functional entity of μ Tissue and matrix as evidenced by the scaffold*

deformations. Our data further reinforces the earlier suggestion, that sufficient integration of *de novo* μ Tissue at the scaffold-tissue interfaces might be enhanced by the initial Fibronectin coating and early Fibronectin fibrillogenesis.

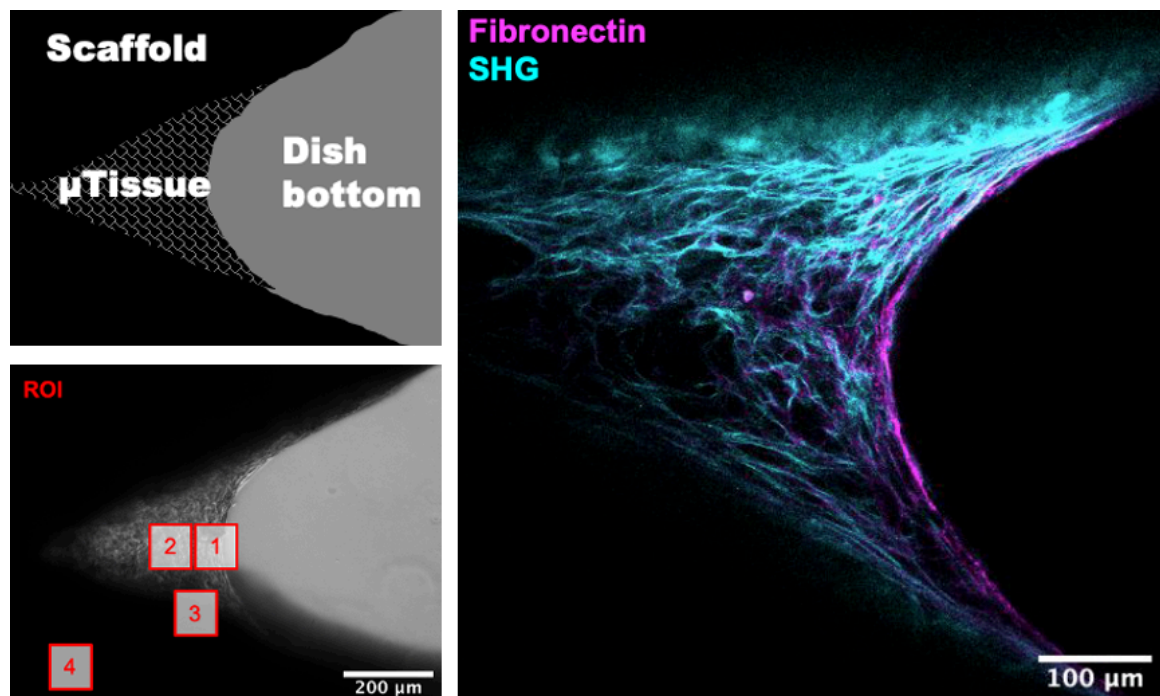


Fig. 6 *de novo* μ Tissue integrates well into Mucograft® and is attached to scaffold via mature collagen fibers after 35 days of incubation. **(top left)** Schematic morphometric classification of phase-contrast image below **(bottom left)** Phase-contrast image and definition of region of interests (ROI). **(right)** Central plane of *de novo* μ Tissue grown in Geistlich Mucograft® scaffold. ROI1: At the growth front fibronectin fibrils form the first provisional ECM that later initiates the polymerization of collagen. ROI2: As the tissue matures, thick fibrous collagen networks emerge. ROI3: At the scaffold/tissue interphase mature collagen fibers interconnect the *de novo* grown μ Tissue with the scaffold. ROI4: Interior scaffold regions are difficult to analyze due to scattering effects of the scaffold. Image acquisition done with 2-photon and confocal laser scanning microscopy with Leica SP8 from ScopeM.

6.2.5 Can the probability of scarring be predicted?

It would be a major milestone if *in vitro* grown tissue could predict the potency of a material to modify the extend of scarring in a wound site. Here we observed that after tissue maturation, some μ Tissues grown in Geistlich Bio-Gide® showed relative high fibronectin signals not only in the young growth front, but also in more mature tissue areas. In contrast, the mature areas of the μ Tissue formed in Geistlich Mucograft® were dominated by the collagen and less so by the fibronectin signal. This finding implies that the type of scaffold has impact on either the μ Tissue composition per se or the kinetics of its formation. Increased fibronectin signals in the interior as observed on Bio-Gide® could indicate, that tissue maturation is not yet completed. Assumingly, the ECM remodelling processes is still ongoing leading to future replacement of the existing fibronectin by collagen. In case of Mucograft® the remodelling of the μ Tissue could be in an already more

advanced status. However, the higher levels of Fn in the core in Geistlich Bio-Gide® was not seen in all tissues and needs to be confirmed in future experiments. In addition, the transient transformation of human dermal fibroblasts into myofibroblasts within the growth front was found to be similar to the PDMS cleft control (Fig. 7). *Taken all findings together, the different ECM compositions could potentially impact proliferation, and potential transmigration of fibroblasts combined with altered new formation of collagen. This data indicates a trend, that Geistlich Mucograft® might show less scarring in vivo than Geistlich Bio-Gide®, but further investigations with higher sample number and screens for proliferation are needed.*

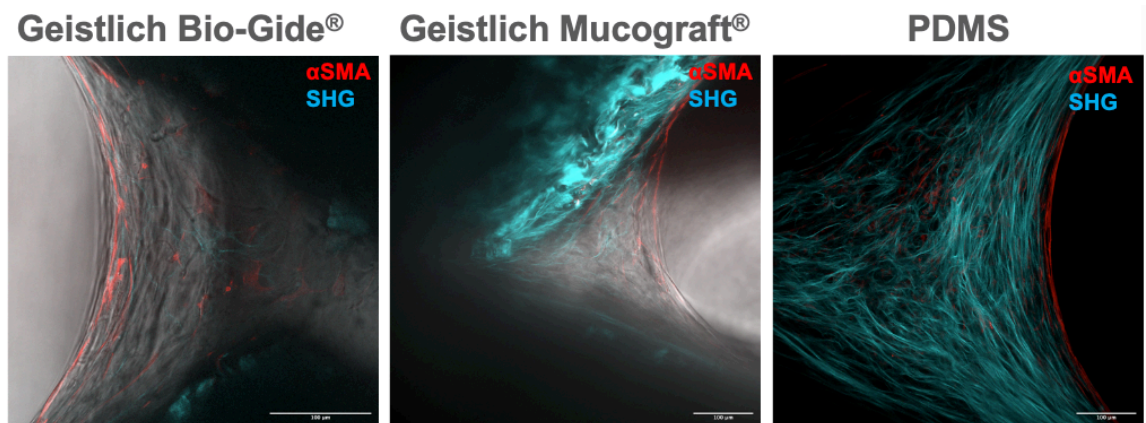


Fig. 7 Transient transformation from fibroblast to myofibroblasts similar across substrates In μ Tissues grown in Geistlich Bio-Gide® and Mucograft® myofibroblast form in the growth front and get cleared during tissue maturation similar to PDMS scaffold. However, since μ Tissue grow faster in PDMS substrates the maturation state is much advanced as the SHG fibers are more dense.

6.2.6 Material shrinkage and healing capacity

Geistlich Mucograft® was found to shrink over 35 days and deform during culture as opposed to Geistlich Bio-Gide®, which provided bigger clefts, with consequently promoted a faster growth of the μ Tissues (Fig. 8). We therefore hypothesize that as soon as initial tissue is formed around the scaffolds in a wound environment, the here observed shrinkage might cause a reduction of wound size, bringing wound edges closer together and thus accelerate wound healing. Furthermore, the shrinkage of scaffolds underlines the importance of the initial fibronectin matrix, since it was shown that fibronectin is required for fibroblast to mediate substrate shrinkage in 3D collagen scaffolds [4]. *Since tissue contraction is required to complete wound healing, we would like to suggest that the enhanced Geistlich Mucograft® contraction described here might be beneficial for wound healing in vivo.*



Fig. 8 Geistlich Mucograft® scaffolds get deformed intensively after 35 days of incubation Cellular Contractile forces deformed and contracted Geistlich Mucograft® scaffolds, compared to the more stable Geistlich Bio-Gide®. Top view of substrates in 12-well-tissue-culture-plate.

6.3 Mechanobiology of wound repair: personalized wound healing

An immense advantage of using a commercially available scaffold already in clinical use is the possibility to correlate *in vivo* data to *in vitro* data and thus judge on the translational power of the mTissue platform. Showcasing that the *de novo* μ Tissue platform technology is applicable on different scaffolds materials is an important milestone towards a standardized 3D *in vitro* test system enabling the comparison of the effectiveness of different scaffolds with regards to early connective tissue formation. The mTissue technology platform may thus in future give rise to a plethora of follow up investigations dealing with the impact of different scaffolds on connective tissue regeneration such as e.g. scaffold - host tissue compatibility, or scaffold - tissue integration. As exemplarily shown, the application of μ Tissue technology on biomedical scaffold relevant for current treatment procedures, like the Geistlich Mucograft® and Bio-Gide®, allows for the investigations of tissue growth and the role of early ECM.

Our preliminary results suggest that fibronectin plays an important role in the tissue integration of scaffolds. Importantly, our results show that the fibronectin induced *de novo* formation of early connective tissue is modified in a scaffold specific mode. Of fundamental importance are our findings on early fibronectin coating and fibrillogenesis promoting the tissue growth in both Geistlich Mucograft® and Bio-Gide® in early phases, as well as the observed differences in initial scaffold decorations with fibronectin, and fibronectin fibrillogenesis. Taken all these findings together we hypothesize that the interaction of fibronectin with collagenous scaffolds is essential for the interaction and integration of the scaffold into the surrounding tissue and will also influence the composition and structure of early and potentially late connective tissue. If this hypothesis can be confirmed our findings might have significant influence on the further development of the scaffolds as well as new clinical application recommendations.

Further work can shed light into identifying a correlation between cut cleft geometries, designs and orientation and their influence on the direction of the scaffold contraction in the presence of fibroblasts. Such knowledge can have a huge impact in treatment of wounds. When closing skin wounds surgically, the applied tension of the surrounding tissue is not equally distributed [5]. Especially keloidal scars, where there is a benign overproduction of collagen fibers, spread beyond boundaries of the initial wound in the direction of mechanical stress [6]. In wounded skin closure, surgeons use static stress maxima lines (Langer's lines) as orientation to reduce scar formation [7-9]. Engineered scaffold with directed contraction could be arranged in the open surgical field of a wound in such a way that the anisotropic forces of the surrounding tissue, estimated by Langer's lines, cancel each other out. In personalized approach, with fibroblasts harvested directly from

patients, the capabilities of exerting contractile forces can furthermore be quantified. This can be used as additional marker to improve characterization and subsequent management of impaired wound healing [10].

In parallel to these macroscopic models, further studies using fibroblast isolated directly from patients could be applied to test to the *de novo* tissue growth in Geistlich Mucograft® or Geistlich Bio-Gide® before surgical implantation. The tissue growth could then be correlated with gene or protein expression. Such knowledge can help to predict the outcome and time course of tissue growth after surgical scaffold implementation and treatment and potentially also have impact on the choice of the most appropriate scaffold for a selected patient.

All these approaches can be combined with different pharmaceutical components and additional treatments, e.g. pre-coating with autologous plasma fibronectin, which might allow to not only diagnose but also develop fast treatment approaches for impaired wound healing, decreased scarring or even suggest specific supplements, which can either be applied in systemically or locally in open field of surgery.

In summary, we demonstrate that fibronectin scaffold decoration and fibronectin fibrillogenesis occurs in early states and may promote fibroblast ingrowth. Coupled with the proof that *de novo* grown μ Tissue technology can be applied on different biomaterials our work sets the stage for an advanced analytical approach and will contribute to the development of novel diagnostic and treatment strategies in wound healing.

6.4 References

1. Ghanaati S, Schlee M, Webber MJ, Willershausen I, Barbeck M, Balic E, Görlach C, Stupp SI, Sader RA, Kirkpatrick CJ. Evaluation of the tissue reaction to a new bilayered collagen matrix *in vivo* and its translation to the clinic. *Biomed Mater*; 2011 Jan;6(1):015010.
2. Willershausen I, Barbeck M, Boehm N, Sader R, Willershausen B, Kirkpatrick CJ, Ghanaati S. Non-cross-linked collagen type I/III materials enhance cell proliferation: *in vitro* and *in vivo* evidence. *J Appl Oral Sci*; 2014 Jan;22(1):29–37.
3. Kruse CR, Singh M, Targosinski S, Sinha I, Sørensen JA, Eriksson E, Nuutila K. The effect of pH on cell viability, cell migration, cell proliferation, wound closure, and wound reepithelialization: *In vitro* and *in vivo* study. *Wound Repair Regen*; 2017 Apr;25(2):260–9.
4. Beyeler J, Katsaros C, Chiquet M. Impaired Contracture of 3D Collagen Constructs by Fibronectin-Deficient Murine Fibroblasts. *Front Physiol*; 2019 Mar;10:1290.
5. Harn HIC, Ogawa R, Hsu CK, Hughes MW, Tang MJ, Chuong CM. The tension biology of wound healing. *Exp Dermatol*; 2019 Apr;28(4):464–71.
6. Ogawa R. Mechanobiology of scarring. *Wound Repair Regen*; 2011 Jul 27;19((P):s2–s9.
7. Edlich RF E, Carl BA. Predicting scar formation: from ritual practice (Langer's lines) to scientific discipline (static and dynamic skin tensions). *J Emerg Med*; 1998 Sep;16(5):759–60.
8. Waldorf JC, Perdakis G, Terkonda SP. Planning incisions. *Operat Tech Gen Surg*; 2002 Sep;4(3):199–206.
9. Deroy C, Destrade M, Alinden AM, Annaidh AN. Non-invasive evaluation of skin tension lines with elastic waves. *Skin Res Tech*; 2017 Aug;23(3):326–35.
10. Atkin L, Bučko Z, Montero EC, Cutting K, Moffatt C, Probst A, Romanelli M, Schultz GS, Tettelbach W. Implementing TIMERS: The race against hard-to-heal wounds. *J Wound Care*; 2019 Jan;23(3):S1–S52.

7 Significance and Outlook

The work presented in this thesis focus on the effect of ECM gradients, tissue tension and cellular phenotype of ECM composition and cellular phenotype on tissue growth and maturation. Tissue growth is essential for multicellular life. This thesis demonstrates the significance of the reciprocal interactions between ECM and cells on the fast formation and stabilization of ECM gradients, which is the fundamental basis to enable tissue growth.

The first project (**Chapter 4**) showed that the emergence of steep spatial gradients of cell phenotypes and extracellular matrix composition, from the fibronectin-rich growth front to the collagen-rich tissue interior, is fine-tuned by the spatially well-orchestrated appearance and disappearance of other ECM components, including tenascin-C and tissue transglutaminase. The environment of *de novo* grown μ Tissues are extremely complex, which might be a good approximation towards biological complexity. Follow up studies with further investigation of various relevant factors are needed. What remains to be elucidated is a closer look at the distribution of collagen, especially for collagen I and collagen III, since collagen III is produced quickly by fibroblast and transiently replaced during maturation by more strong and thick collagen I fibers [1]. In addition, collagen III is a hallmark of fibrotic ECM [2], which could potentially allow further development towards disease models. Of particular interest is further the spatiotemporal distribution of TGF- β , syndecan-4 and various MMP, since they are all involved in the upregulation, functionality and degradation of TNC and TG2. The incomplete tissue maturation demonstrated here upon varying interventions, can form a basis for the development of *de novo* grown μ Tissues towards disease models. Subsequently, this could be combined with pharmaceutical components, co-culture or with cells or body fluids harvested directly from patients in a personalized approach, for example to diagnose tissue maturation speed and quality, which could provide insights for tissue regeneration in clinics.

Even though fibroblast-myofibroblast transition and a reversal has been observed in our *de novo* μ Tissue platform [3], it is controversially discussed whether myofibroblast get cleared from living tissues through reversal back to fibroblast or through extrinsic apoptosis [4]. Since nature has evolved highly complex living tissue, a combination of both mechanisms seems likely, but probably with a strong weighting towards phenotype reversal, which might depend on the prevailing environmental conditions. In a future study, the phenotype gradient in the μ Tissues of our platform could be used for further investigation. Utilizing live tracking techniques with phenotypic or

apoptotic markers in combination with light sheet microscopy could provide novel insights towards assessing the balance of myofibroblast fate, which is currently unknown.

The second project (**Chapter 5**) showed that sufficient tissue tension is required to allow tissue growth and maturation, and cellular contractility is here a key factor. With our study we provide a novel μ Tissue model allowing to tune tissue tension by altering cleft geometries of tissues grown in a self-assembled manner. This knowledge can contribute towards development of novel topical or generalized therapeutic strategies to modulate tissue tension and subsequently tissue growth and also maturation in wounds.

Of particular significance is here that the spatiotemporal resolution of the ECM gradients can be tuned in dependence of the tissue tension to investigate future interventions on this platform not only as function of tissue tension, but also with higher spatial separation of the temporal ECM gradient. This increased sensitivity with our novel μ Tissue model with tuned tissue tension might allow to identify completely novel strategies relevant for diagnostics and treatments in tissue tensional related disease.

In **Chapter 4** we showed that the growth front shows upregulated myofibroblasts, TNC and increased Fn fiber strain. YAP nuclear localization, known to be upregulated in response to mechanical stress [5,6], was previously identified in the growth front together with increased Fn fiber strain detected [3]. What remains to be elucidated, is to investigate both Fn fiber strain and YAP nuclear localization in the *de novo* grown μ Tissue of tuned tissue tension. In combination to that, the tissue tension relevance on the suggested functional complementarity of TG2 and TNC on stabilization of ECM gradients is highly interesting and could be investigate with the angle array. Furthermore, much research was done in cell culture methods under application of external tension, e.g. strain of substrates [7]. While our platform here tune tissue tension internally by alteration of the growth front curvature, it could be interesting to further investigate how this, tissue growth and maturation, relate to externally applied strain as well. In addition, it would be very interesting to perform combinatorial studies of different pharmaceutical components and different tensional states, which is challenging since quite resource demanding, but it might be rewarded with meaningful novel insights.

The preliminary project in commercial scaffolds (**Chapter 6**) showed that tissue growth rate reflected the differential observations made in the clinic. We further found that the preadsorption of fibronectin to the scaffold materials promoted fibronectin fibrillogenesis and tissue growth in both Geistlich Mucograft® and Geistlich Bio-Gide®, which represents a fundamentally new insight. Coupled with the proof that *de novo* grown μ Tissue can be integrated in other surgically relevant

biomaterials sets stage for the development of novel diagnostic and treatment strategies in the mechanobiology of wound healing in combination with approaches in personalized medicine as outlined in Chapter 6.3.

Reaching sufficient degree of transferability is a huge challenge, because many 3D tissue platforms are typically based on scaffold biomaterials that introduce non-physiological biointerfaces. Scaffold-free 3D systems such as spheroids or organoids emerged increasingly, however tuning mechanical properties in such systems is extremely difficult [8]. In our platforms, μ Tissues grow in between macroscopic clefts of structural scaffolds either PDMS (**Chapter 4** and **Chapter 5**) or collagen xenograft (**Chapter 6**) scaffolds. However, the tissues themselves are self-assembled by cells and thus scaffold free. The elucidated mechanisms on such systems carry high potential for good transferability and thus the new knowledge and understanding could be implemented or applied in *in vivo* settings. However, to assess this, future studies need to correlate characteristic markers with *in vivo* biopsies. A suggested approach is, to compare the gradient of *de novo* μ Tissue with the maturation gradient seen in biopsies of wound tissue. The comparison of ECM composition and other relevant markers at different wound healing stages with the μ Tissue gradients might allow to assess the transferability further. In addition to that, the μ Tissue platform can be advanced to co-culture of multiple cell types. A very interesting follow up study towards application of our system is to grow μ Tissues with fibroblasts isolated from patients and supplement it with whole or different autologous blood components to mimic the physiological wound healing situation.

Despite intense efforts in translational research from “bench-to-bedside”, the translational gap between basic research and clinical research remains wide [9]. Our platforms could play relevant roles on the path of bridging translational gaps, not only from 2D to 3D cell culture, but also at the interspecies level. Relevant mechanism could be preliminarily explored with human cells in high-throughput 2D approaches and further investigated in our *de novo* grown μ Tissue. Subsequently, this procedure can be repeated with cells of potential test species candidates for pre-clinical studies. Successful reproduction of the findings will increase probability of good transferability into human. Thus, there is high potential that further utilization of our platform contributes to the 3R concept to refine, reduce and replace animal experiments, while ensuring high animal welfare and high-quality science.

Taken together, our findings on how time-dependent stabilization of ECM gradients and tissue tension together with cell contractility and collagen scaffolds influences tissue growth provide

valuable new insights for biomedical research, crucial to develop novel treatment strategies for wound healing, fibrosis and cancer. Combined with the transferability across different scaffolds materials, our platforms allow a plethora of follow up investigations.

We expect the presented platforms of *de novo* μ Tissue growth together with the outlined follow up studies that go far beyond of the findings in this thesis find intriguing new applications for applied biomedical research.

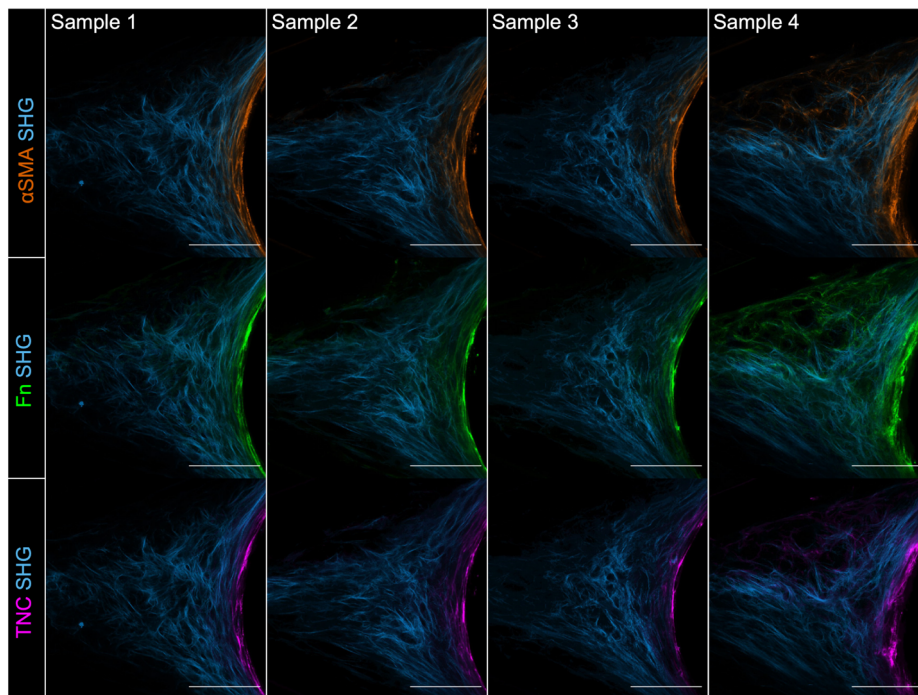
7.1 References

1. Kadler KE, Hill A, Canty-Laird EG. Collagen fibrillogenesis: fibronectin, integrins, and minor collagens as organizers and nucleators. *Curr Opin Cell Biol*; 2008 Oct;20(5):495–501.
2. Herrera J, Henke CA, Bitterman PB. Extracellular matrix as a driver of progressive fibrosis. *J Clin Invest*; 2018 Jan 2;128(1):45–53.
3. Kollmannsberger P, Bidan CM, Dunlop JWC, Fratzl P, Vogel V. Tensile forces drive a reversible fibroblast-to-myofibroblast transition during tissue growth in engineered clefts. *Sci Adv*; 2018 Jan 1;4(1):eaao4881.
4. Pakshir P, Noskovicova N, Lodyga M, Son DO, Schuster R, Goodwin A, Karvonen H, Hinz B. The myofibroblast at a glance. *J Cell Sci*; 2020 Jul;133(13):jcs227900.
5. Nardone G, Oliver-De La Cruz J, Vrbsky J, Martini C, Pribyl J, Skládal P, Pešl M, Caluori G, Pagliari S, Martino F, Maceckova Z, Hajduch M, Sanz-Garcia A, Pugno NM, Stokin GB, Forte G. YAP regulates cell mechanics by controlling focal adhesion assembly. *Nat Commun*; 2017 May;8(1):730–13.
6. Panciera T, Azzolin L, Cordenonsi M, Piccolo S. Mechanobiology of YAP and TAZ in physiology and disease. *Nat Rev Mol Cell Biol*; 2017 Sep;18(12):758–70.
7. Eyckmans J, Chen CS. 3D culture models of tissues under tension. *J Cell Sci*; 2017 Jan 2;130(1):63–70.
8. Langhans SA. Three-Dimensional *in vitro* Cell Culture Models in Drug Discovery and Drug Repositioning. *Front Pharmacol*. 2018;9(1):6.
9. Seyhan AA. Lost in translation: the valley of death across preclinical and clinical divide – identification of problems and overcoming obstacles. *Transl Med Commun*; 2019 Dec;4(1):1–19.

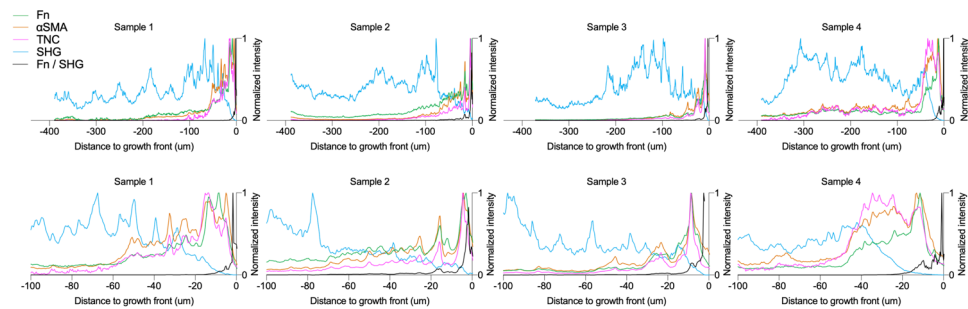
8 Supplementary information

8.1 Supplementary Figures Chapter 4

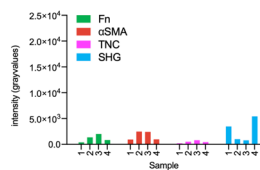
A Control



B Normalized intensity profiles



C Area under the curve



D Normalized intensity profiles SHG-ratios

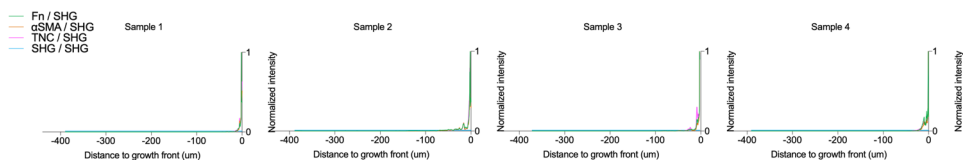


Fig. S01 Supplementary control data (A) Central ROI (cf. Fig. 1 D-F, Chapter 4) of representative μ Tissues imaged with 2P and CLSM for α SMA (orange), Fn (green), TNC (magenta) and SHG (cyan). Scale bar 100 μ m. **(B)** Respective normalized intensity profile over distance to growth front along the bisector angle and the respective stains. **(C)** Absolute signal intensity as integral of profile plots (B) is depicted in bar graphs for all representative samples. **(D)** Respective normalized intensity profile SHG-ratios over distance to growth front along the bisector angle and the respective stains.

A + Z006

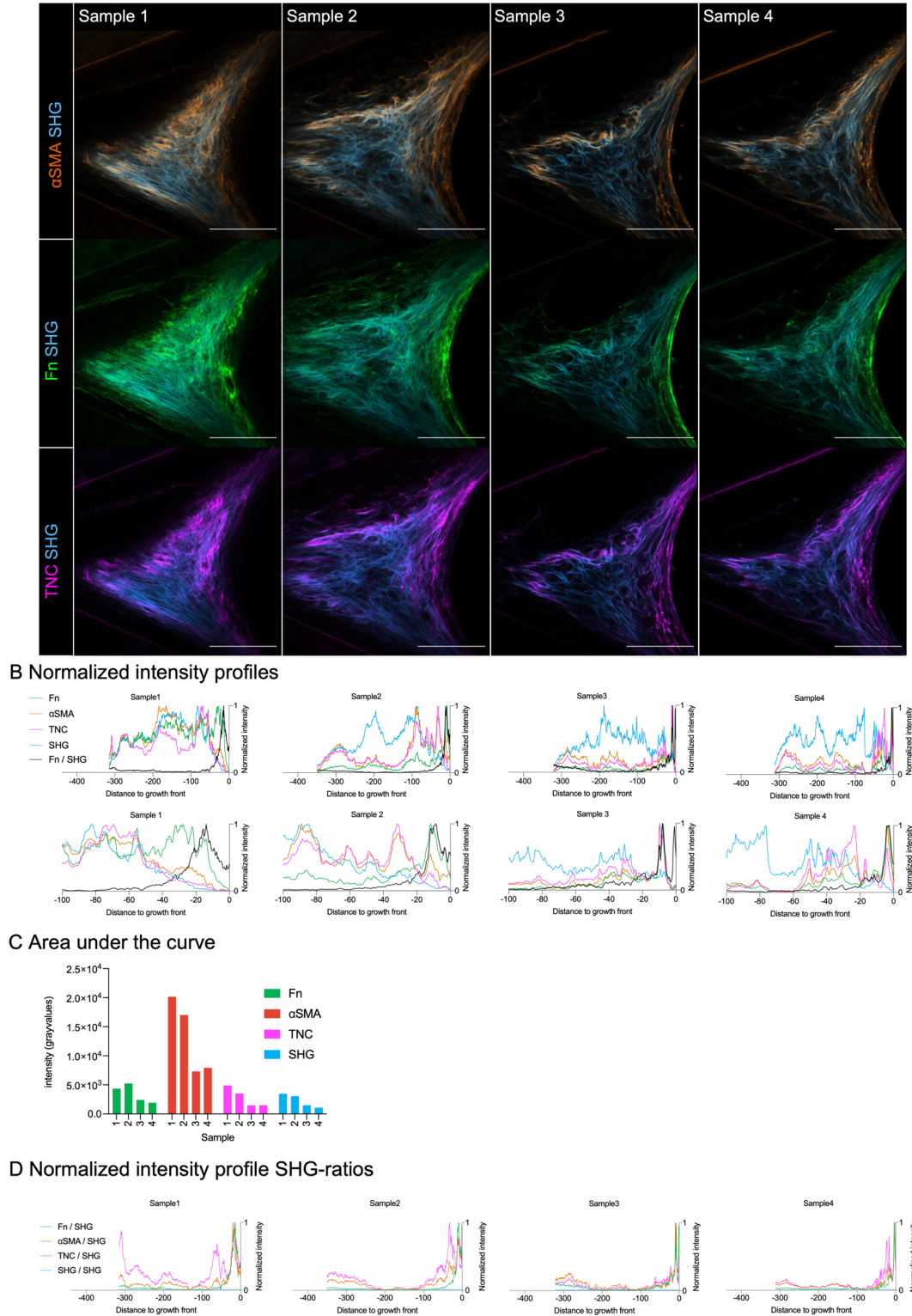
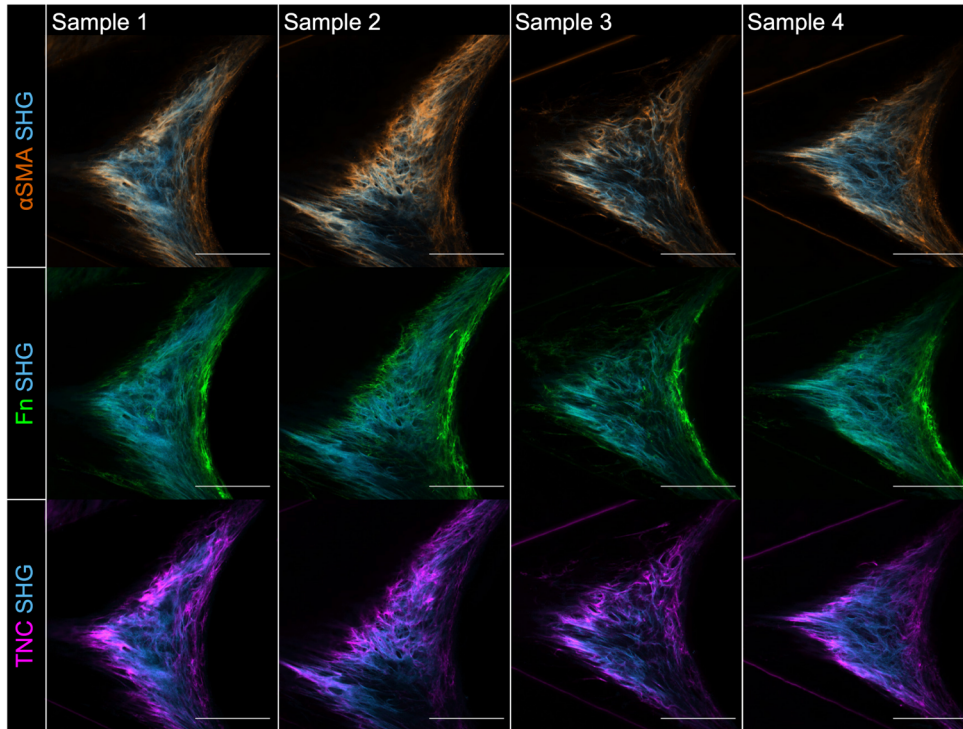
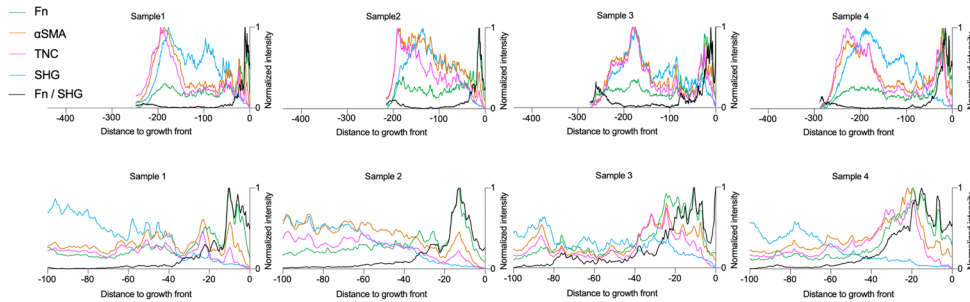


Fig. S02 Supplementary Z006 data (A) Central ROI (cf. Fig. 1 D-F, Chapter 4) of representative μ Tissues imaged with 2P and CLSM for α SMA (orange), Fn (green), TNC (magenta) and SHG (cyan). Scale bar 100 μ m. **(B)** Respective normalized intensity profile over distance to growth front along the bisector angle and the respective stains. **(C)** Absolute signal intensity as integral of profile plots (B) is depicted in bar graphs for all representative samples. **(D)** Respective normalized intensity profile SHG-ratios over distance to growth front along the bisector angle and the respective stains.

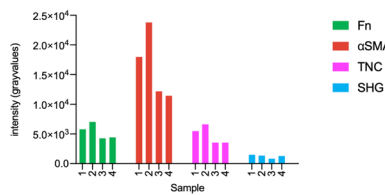
A + GW788388



B Normalized intensity profiles



C Area under the curve



D Normalized intensity profile SHG-ratios

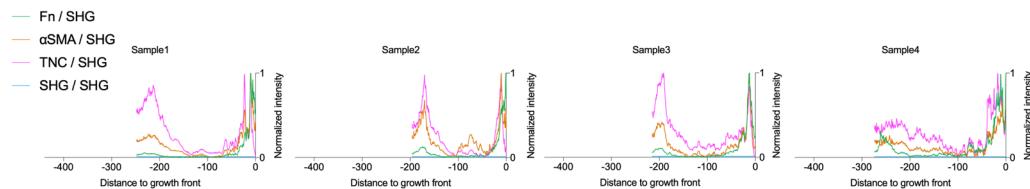


Fig. S03 Supplementary GW788388 data (A) Central ROI (cf. Fig. 1 D-F, Chapter 4) of representative μ Tissues imaged with 2P and CLSM for α SMA (orange), Fn (green), TNC (magenta) and SHG (cyan). Scale bar 100 μ m. **(B)** Respective normalized intensity profile over distance to growth front along the bisector angle and the respective stains. **(C)** Absolute signal intensity as integral of profile plots (B) is depicted in bar graphs for all representative samples. **(D)** Respective normalized intensity profile SHG-ratios over distance to growth front along the bisector angle and the respective stains.

A + Lapatanib

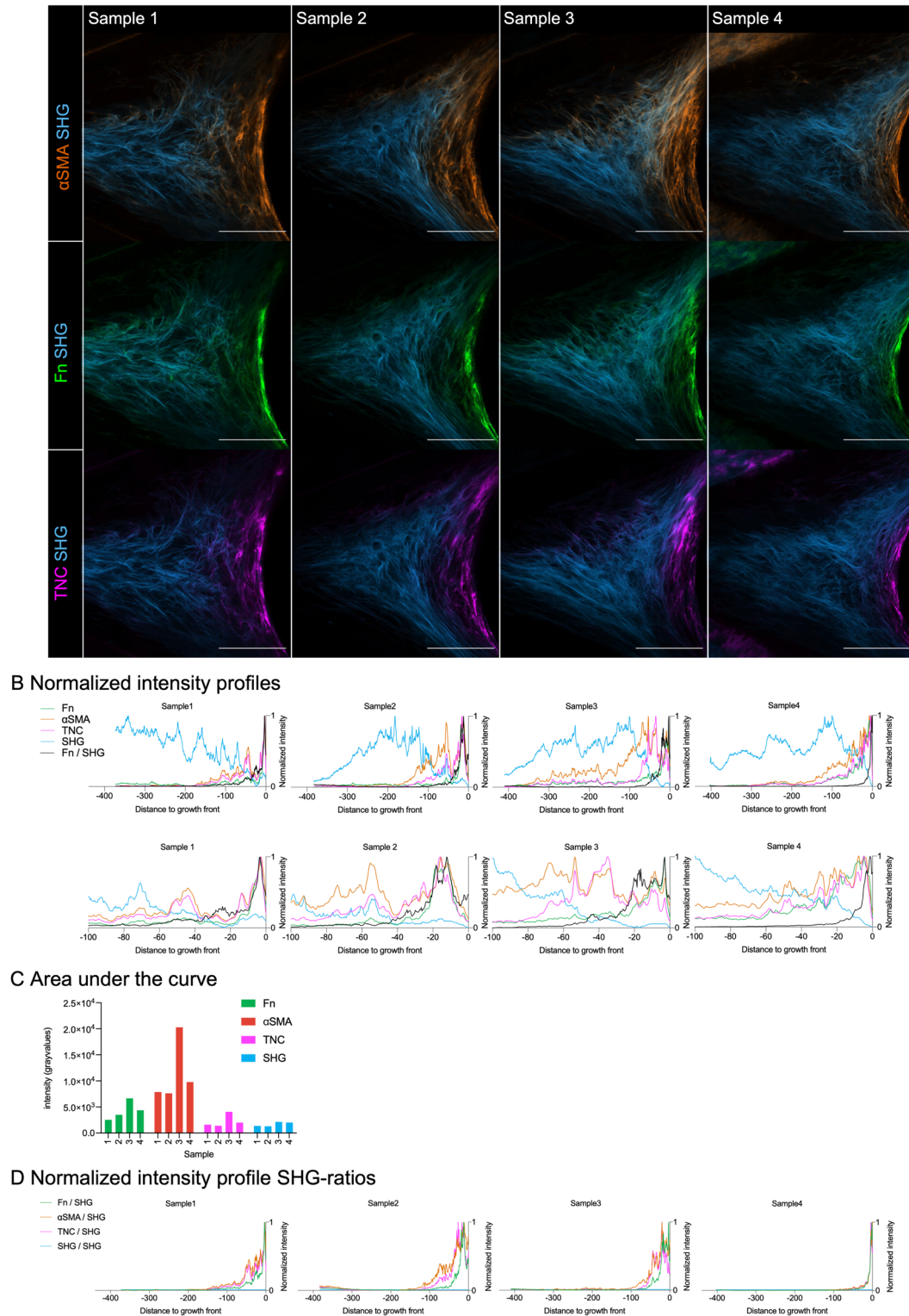
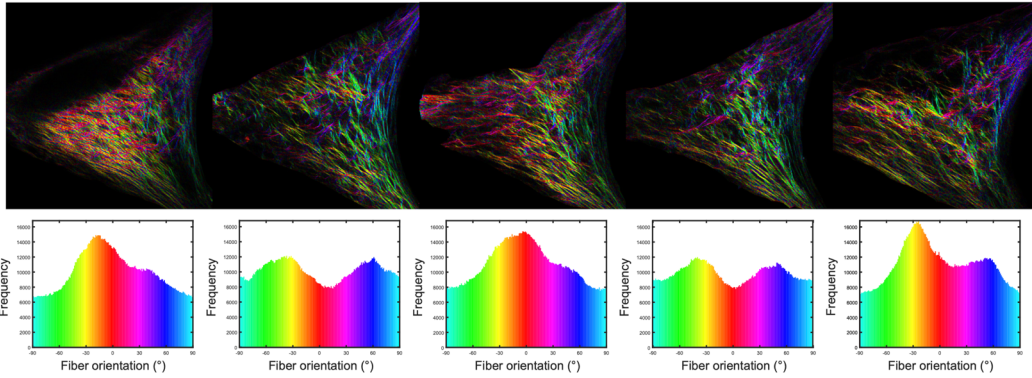
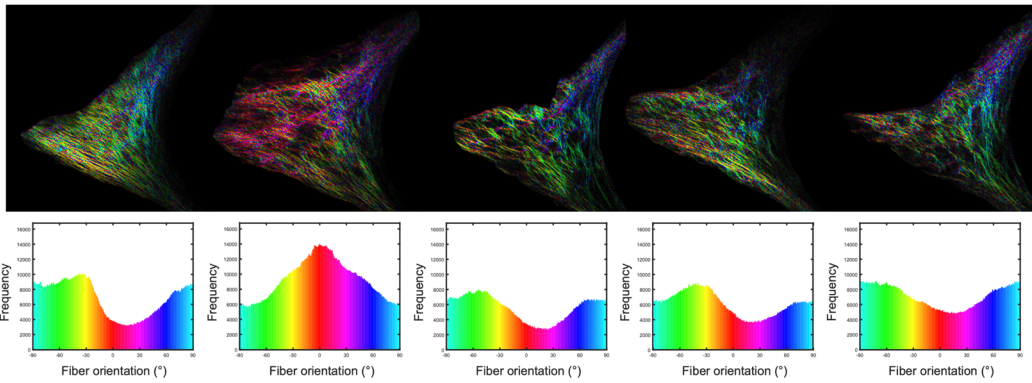


Fig. S04 Supplementary Lapatanib data (A) Central ROI (cf. Fig. 1 D-F, Chapter 4) of representative μ Tissues imaged with 2P and CLSM for α SMA (orange), Fn (green), TNC (magenta) and SHG (cyan). Scale bar 100 μ m. **(B)** Respective normalized intensity profile over distance to growth front along the bisector angle and the respective stains. **(C)** Absolute signal intensity as integral of profile plots (B) is depicted in bar graphs for all representative samples. **(D)** Respective normalized intensity profile SHG-ratios over distance to growth front along the bisector angle and the respective stains.

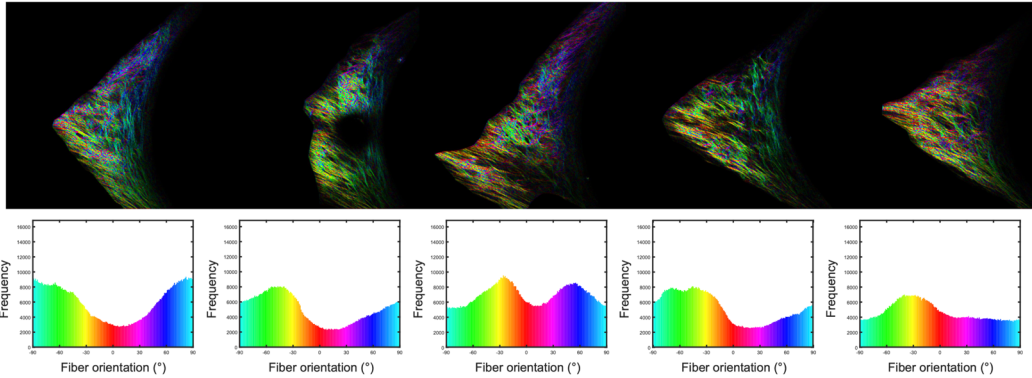
A Control, SHG



B Z006, SHG



C GW788388, SHG



D Lapatanib, SHG

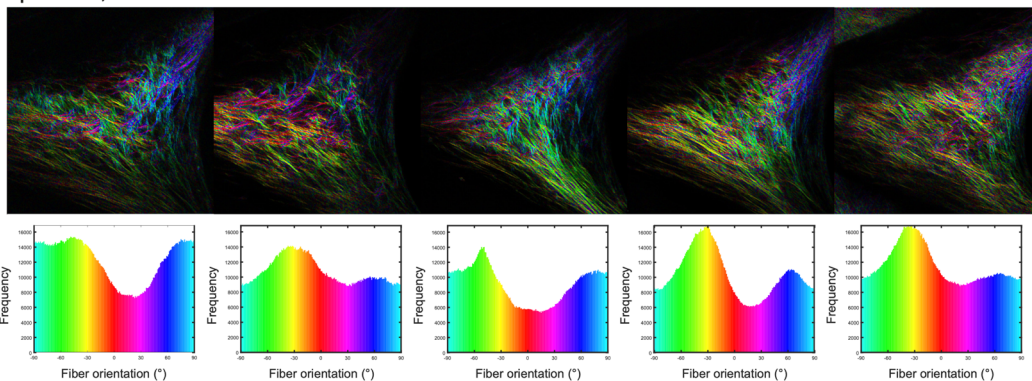


Fig. S05 Supplementary fiber orientation data Collagen fiber (SHG) orientations depicted as pseudo-coloured ROI for supplementary representative μ Tissues. Fiber orientation analysis was carried out using a custom-written MATLAB script for representative μ Tissues of the control (**A**) and supplemented with Z006 (**B**), GW788388 (**C**) and Lapatanib (**D**). The orientation of the SHG-signal is color-coded from blue (± 90) to red (0) and the frequency distribution of the respective μ Tissue is depicted below the pseudo-coloured SP micrographs.

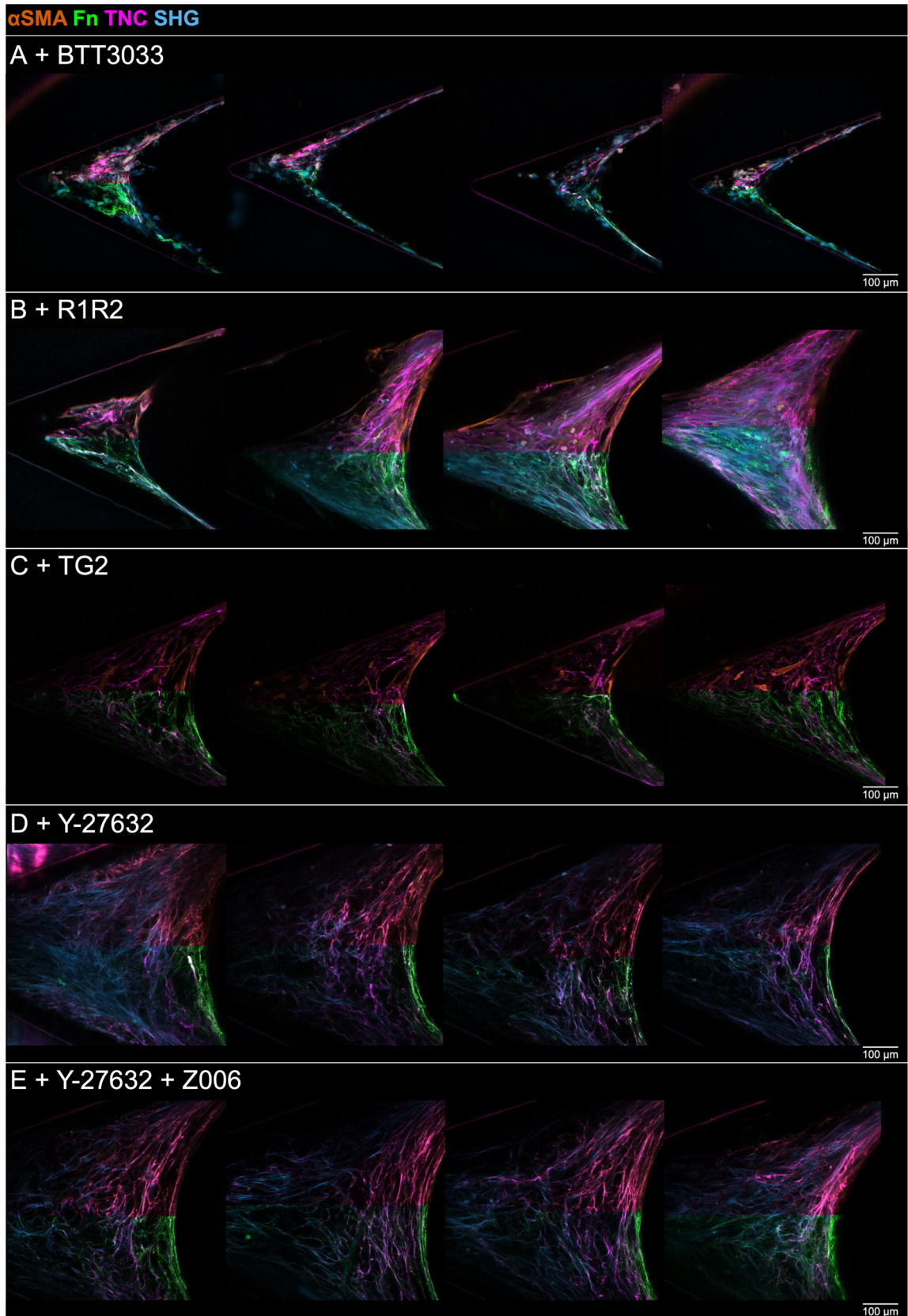


Fig. S06 Supplementary inhibitor data (TNC stain) Representative ROI of μ Tissues supplemented with BTTT3033 (A), R1R2 (B), TG2 (C), Y-27632 (D) and Y-27632 + Z006 (E), and imaged with 2P and CLSM. The data is depicted with two different sets of look up table: top LUT: α SMA (orange), TNC (magenta), SHG (cyan); bottom LUT: Fn (green), TNC (magenta), SHG (cyan). Scale bars 100 μ m.

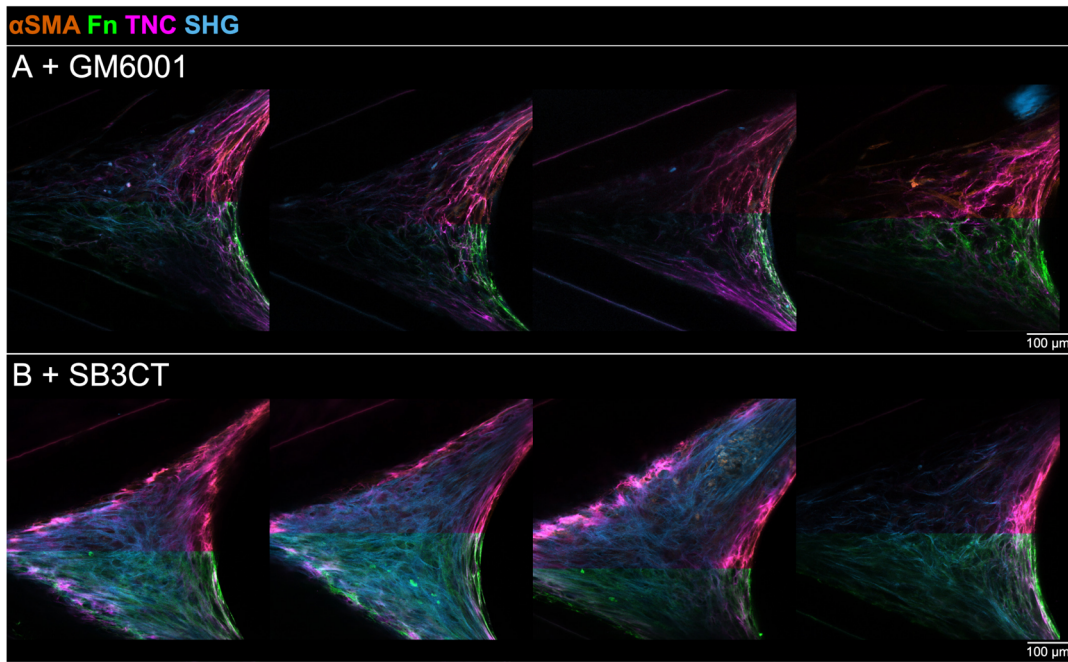


Fig. S07 Supplementary inhibitor data (TNC stain) Representative ROI of μ Tissues supplemented with GM6001 (**A**) and SB3CT (**B**), and imaged with 2P and CLSM. The data is depicted with two different sets of look up table: top LUT: α SMA (orange), TNC (magenta), SHG (cyan); bottom LUT: Fn (green), TNC (magenta), SHG (cyan). Scale bars 100 μ m.

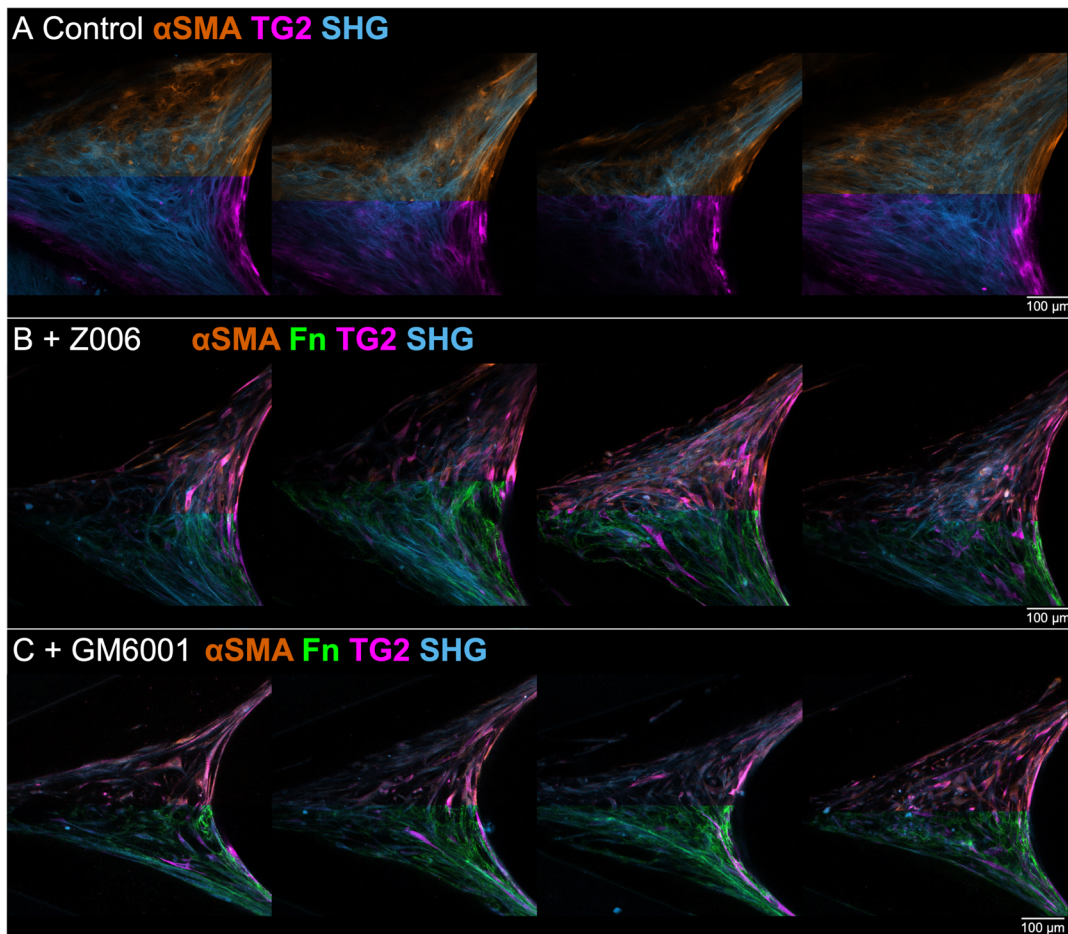


Fig. S08 Supplementary TG2 stained data Representative ROI of control μ Tissues (**A**) and supplemented with Z006 (**B**) and GM6001 (**C**), and imaged with 2P and CLSM. The data is depicted with two different sets of look up table: top LUT: α SMA (orange), SHG (cyan); bottom LUT: Fn (green, not in A), TG2 (magenta), SHG (cyan). Scale bars 100 μ m.

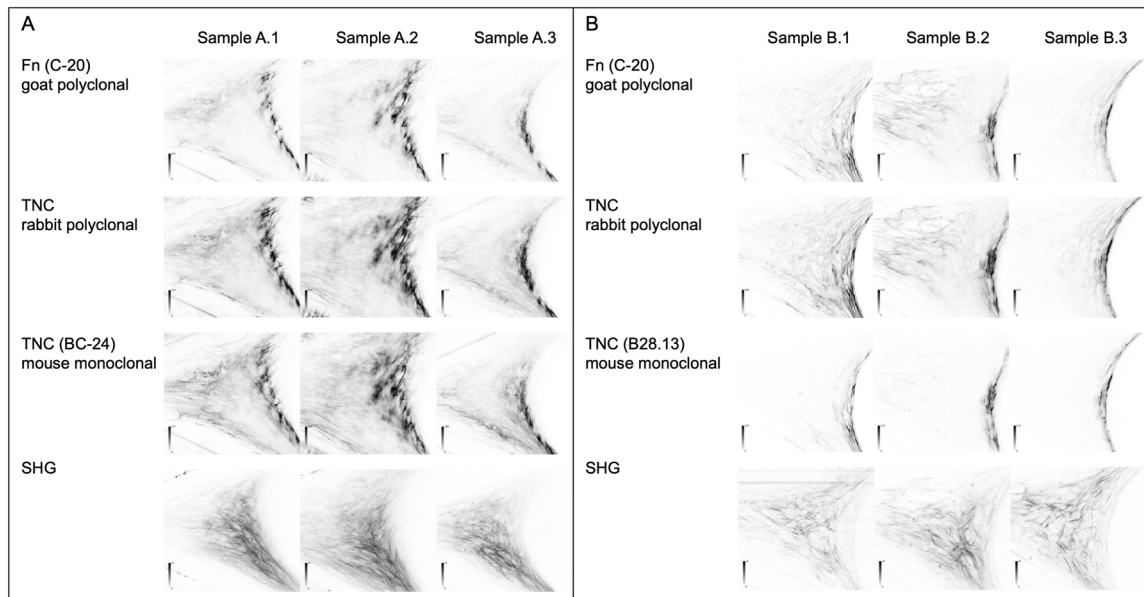


Fig. S09 Supplementary TNC epitope investigation Two independent μ Tissue experiments were run (A and B). In all images the cleft's tip is oriented on the left ($<$). Depicted are z-central and grayscale immunofluorescence images of each μ Tissue with their respective fibronectin and second harmonic generation channels. To ensure that TNC detection is not masked due to cryptic epitopes within the interior of the μ Tissues, we examined newly grown μ Tissues with the monoclonal antibody BC-24 (epitope EGF repeats; MA1-26779, ThermoFisher), which is used as standard throughout the study, the rabbit polyclonal TNC antibody (provided by G. Orend, Spenle et al., 2015, CAM) and the mouse monoclonal TNC B28.13 (epitope constant Fn-III repeat 6 or 7 (67), provided by G. Orend).

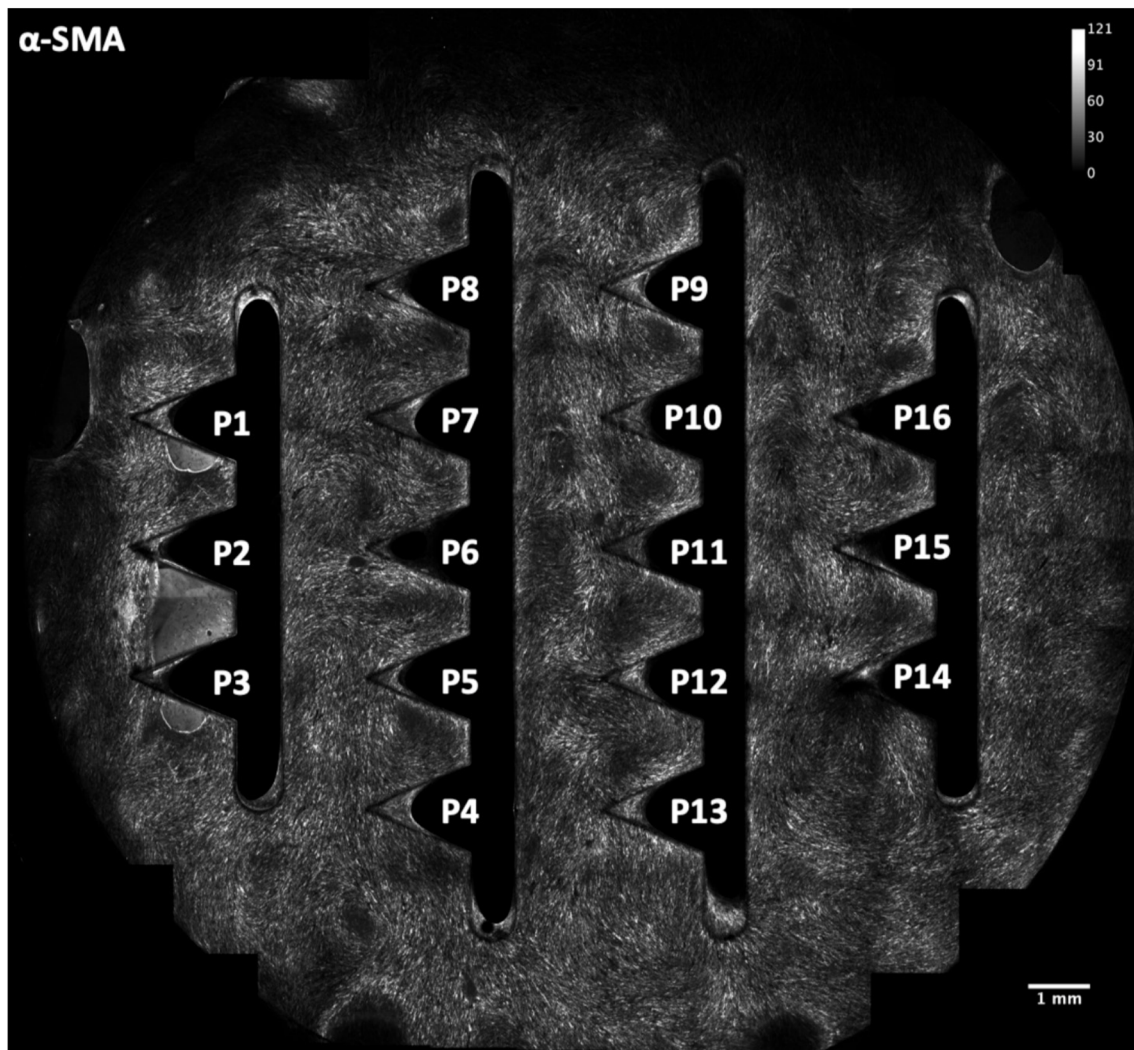


Fig. S10 Overview tile scan of full PDMS after 12 days incubation While myofibroblast appear only within the growth front of the μ Tissues between the clefts, myofibroblast are abundant in the multicellular layer on top of the PDMS substrates after 12 days of incubation. The visualization shows α SMA signal on top of a complete PDMS substrates with 16 different cleft position (P1 – P16), in which μ Tissues are assembled. Note: the focus plane of top layer and each cleft μ Tissue is mismatching due to two different refractive indices of PDMS and PBS.

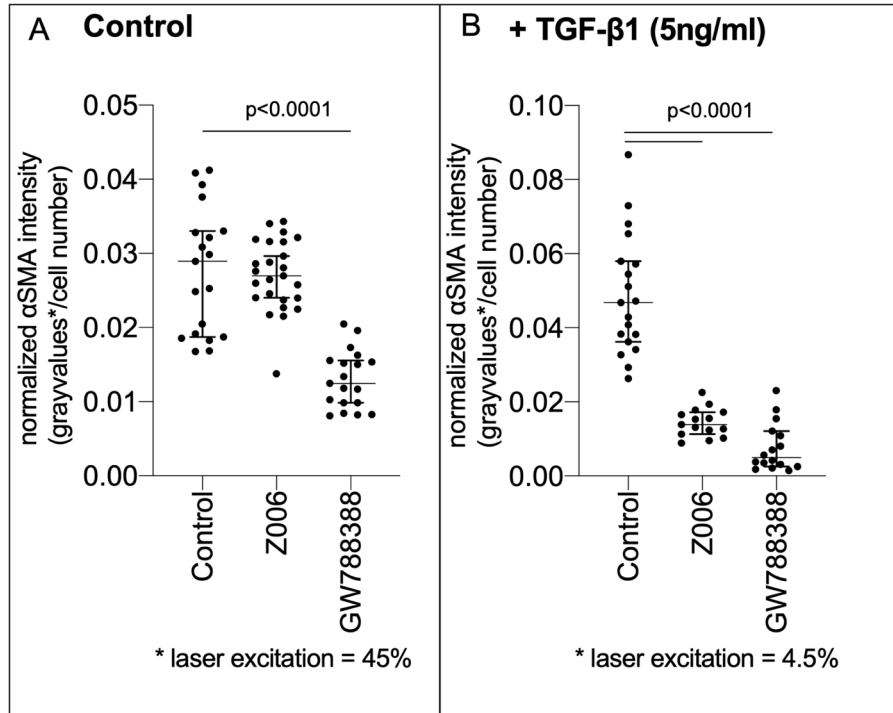


Fig. S11 Fibroblast stimulation with TGF-β1 in planar cell culture Preliminary planar inhibitor test on Fn coated glass with normal human dermal fibroblast. TGF-β1 and inhibitor supplemented 24 h after cell seeding, medium was exchange with fresh supplements every 2 days. Cells were fixed with 4% PFA and stained 4 days after TGF-β1 and inhibitor treatment was started.

Fibroblast metabolic activity measured with WST-1 assay

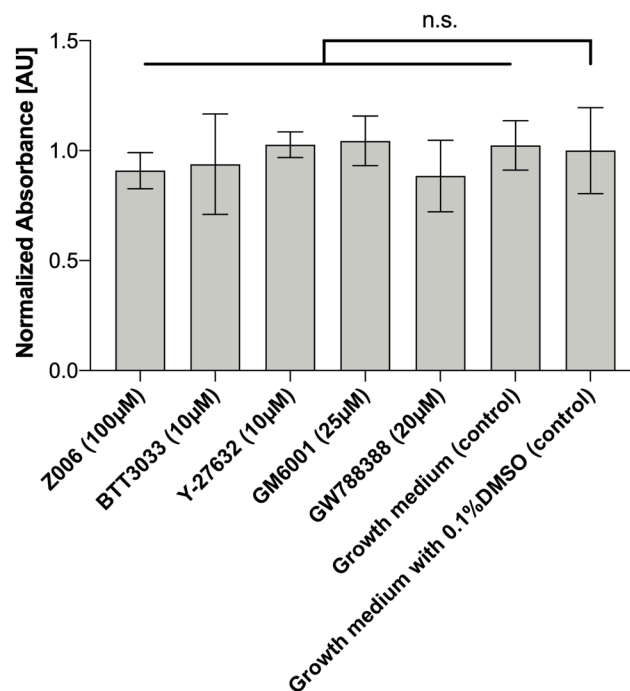


Fig. S12 Fibroblast metabolic activity measured with WST-1 assay

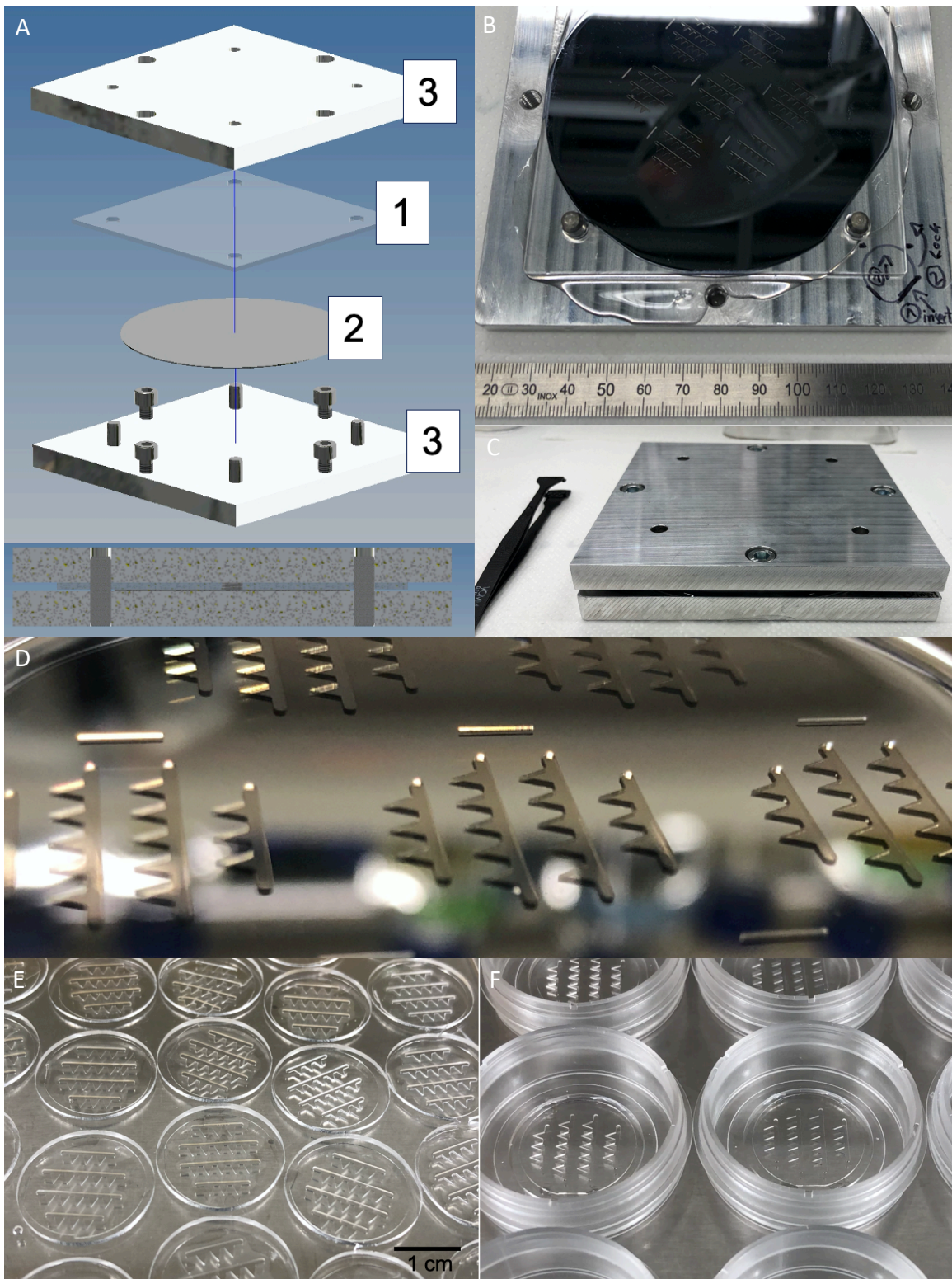


Fig. S13 Custom built compression device (A-C) to produce residual membrane-free polydimethylsiloxane (PDMS) scaffolds by replica molding of negative SU8-master structures. (A) Polymethylmethacrylate (PMMA) lid (1); 4" silicon wafer, SU8-master structures not depicted (2); Aluminum plates (3). **(B)** Wafer mounted with PDMS and PMMA spacer on aluminum plate. **(C)** Fully assembled device under compression. **(D)** Side-angled view on central part of negative master mold on 4" silicon wafer fabricated in cleanroom facility by standard lithography of multiple layers of SU8-3050 photoresist. **(E)** PDMS substrates fabricated by replica molding of negative SU8-master structures using custom built compression device (A-C). **(F)** Mounted PDMS substrates in polymer-bottom ibidi dishes.

8.2 Supplementary Figures Chapter 5

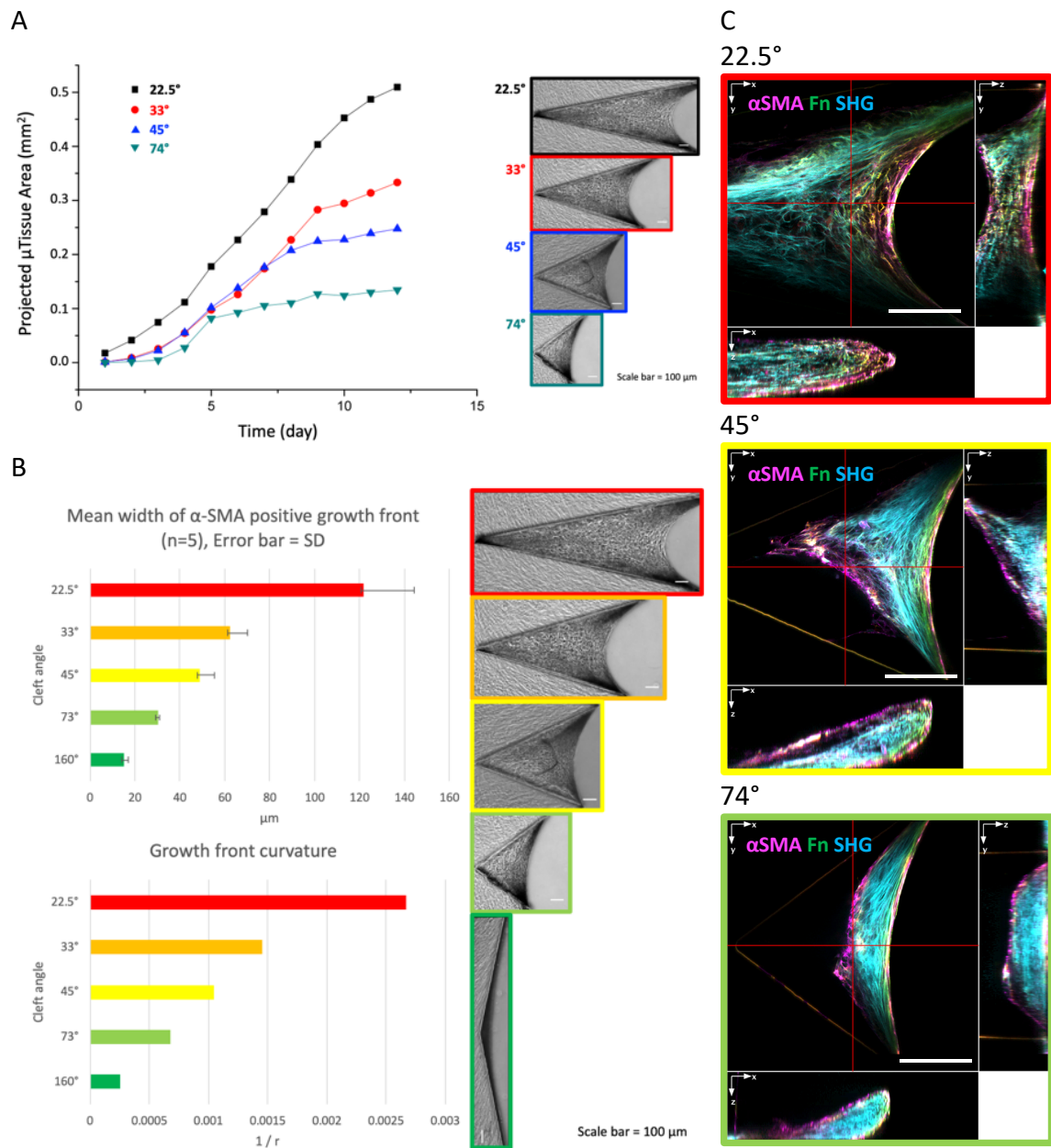


Fig. S01 μ Tissue growth in angle array and comparison of α SMA-positive-growth-front width and growth front curvature
 This data set shown here was done using a differently designed cleft angle array with carrying cleft-sidewall length. **(A)** The μ Tissue growth plateaus at different timepoints is due to the fact that too short sidewall hinder μ Tissue growth. The angle array data in the other figures were acquired with an adapted cleft-array design where sidewall length was the in all clefts the same to allow investigation of the cleft angle effect (Fig. 1A, F). **(B)** μ Tissues formed in smaller cleft angles show a much wider width of the α SMA positive region (C, magenta) and a higher growth front curvature. **(C)** Orthogonal views of representative μ Tissue samples with Fn (green), α SMA (magenta) and second harmonic generation (cyan). Scale bars 100 μm

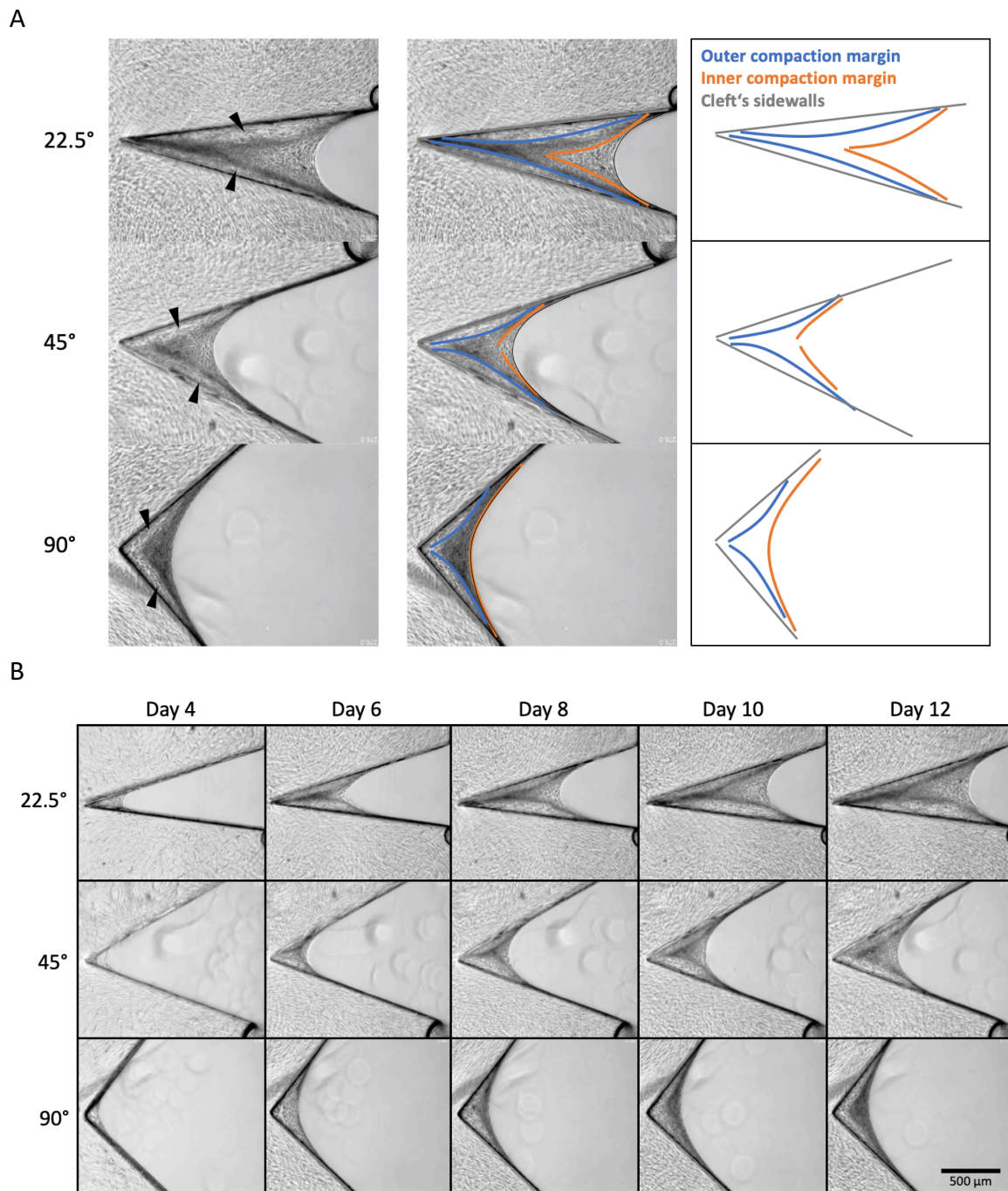


Fig. S02 Comparison of different compaction patterns in phase-contrast images from day 12 (A) Over time μ Tissues partially detach from the PDMS vertical sidewall visible as bright areas in the phase-contrast images located close to each cleft sidewalls (black arrow heads in left column). Furthermore, tissue compaction is seen as darker areas caused by increased light absorption of locally higher tissue density. Tissue compaction occurs in the interior of each tissue over time in different patterns depending on the cleft angle. In μ Tissues grown in 22.5°- and 45°-clefs there are distinct two compaction arms formed with inner compaction margin (orange lines) which do not align with the growth front. For 90° cleft the inner compaction margin aligns completely with the growth front. **(B)** Timelapse series.

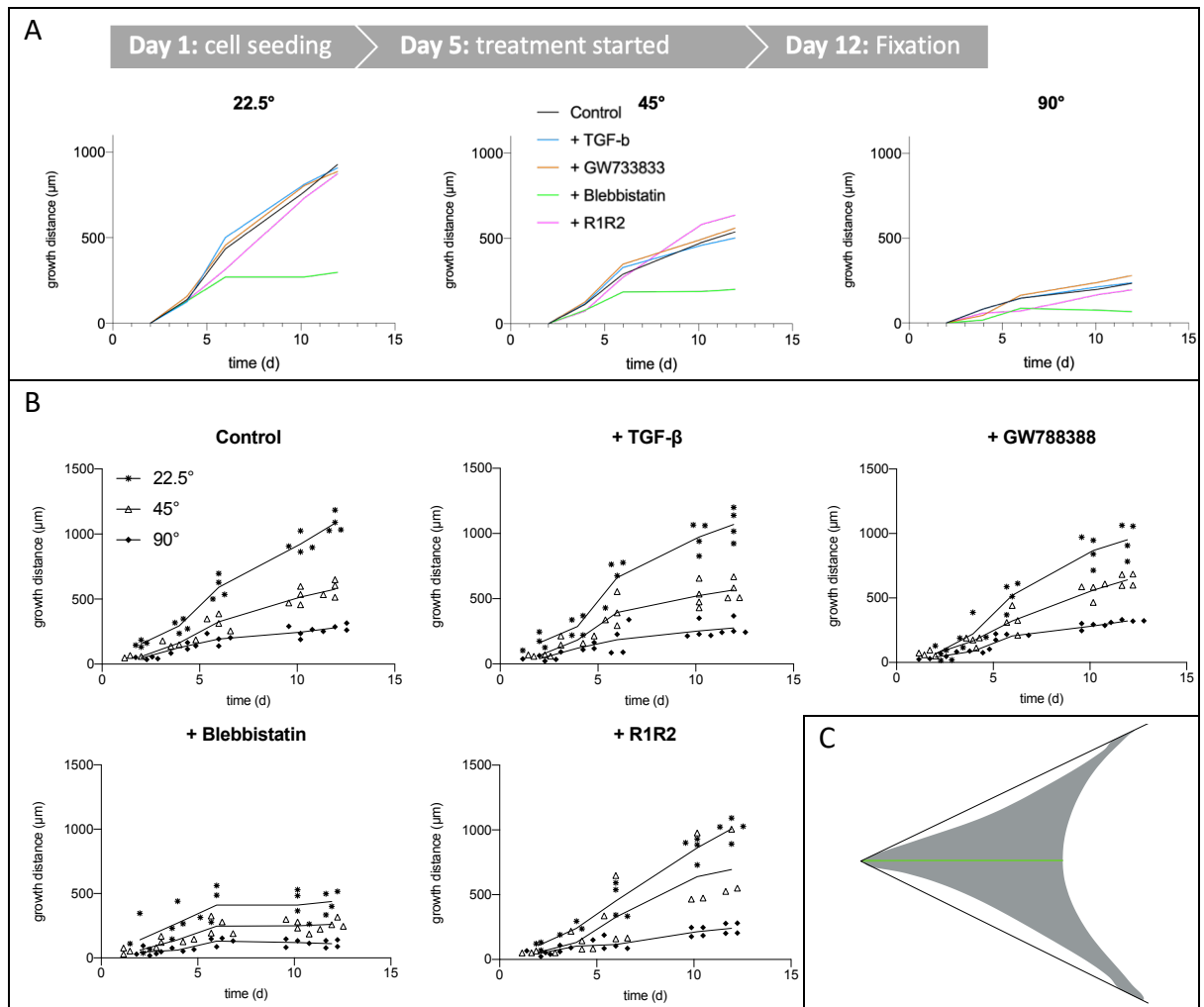


Fig. S03 Quantification of μ Tissue growth and cleft closure (A) During μ Tissue growth, phase-contrast images were frequently taken and growth distance (cf. C, green line) was analyzed along the bisector angle of each cleft. Growth distances are utilized to plot growth kinetics (see Fig. 3B). See Fig. S05 for growth front length and maximum anchor point distance. See also supplementary timelapse videos S01-S05. Inhibitor were supplemented from day 5 on. Data is baseline corrected by growth distance of first data point. **(B)** Data distribution per condition. **(C)** Schematic of projected μ Tissue is depicted as gray area with growth distance as green line and PDMS cleft edges (interface between PDMS and cell culture medium or tissue) as black lines.

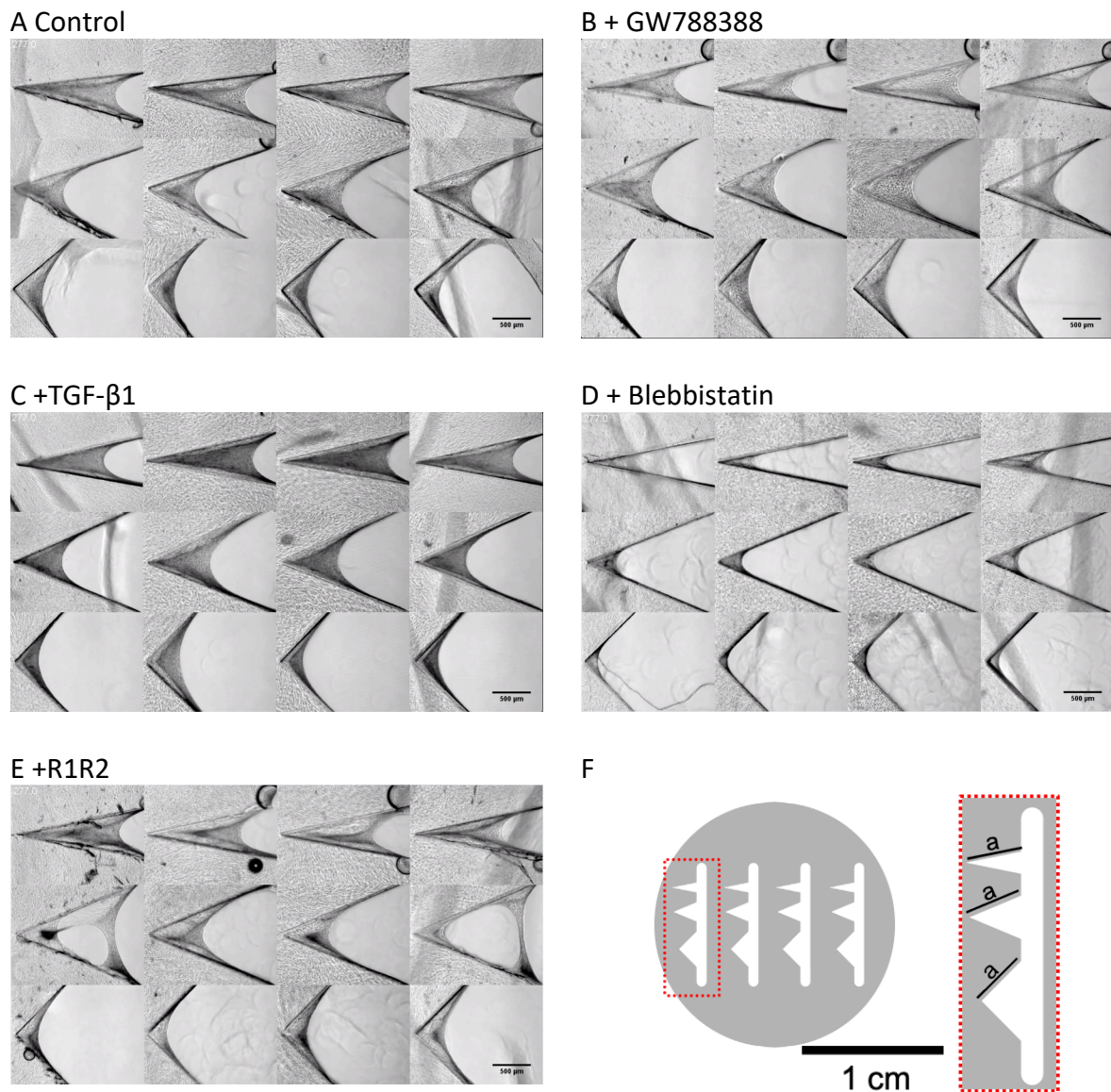


Fig. S04 Comparison of full substrate arrays phase-contrast μ Tissues at day 12. (A-E) The final μ Tissue growth stages prior fixation at day 12 of all four 22.5°, 45°- and 90°-clefs are depicted from each substrate of control (A) and supplementation of GW788388 (B), TGF- β 1 (C), Blebbistatin (D) and R1R2 (E). Scale bars 500 μ m. (F) Scaffold schematic of angle array substrate with equalized inner cleft area by choosing constant sidewall length (a) and PDMS substrate thickness. Scale bar 1 cm.

A Control

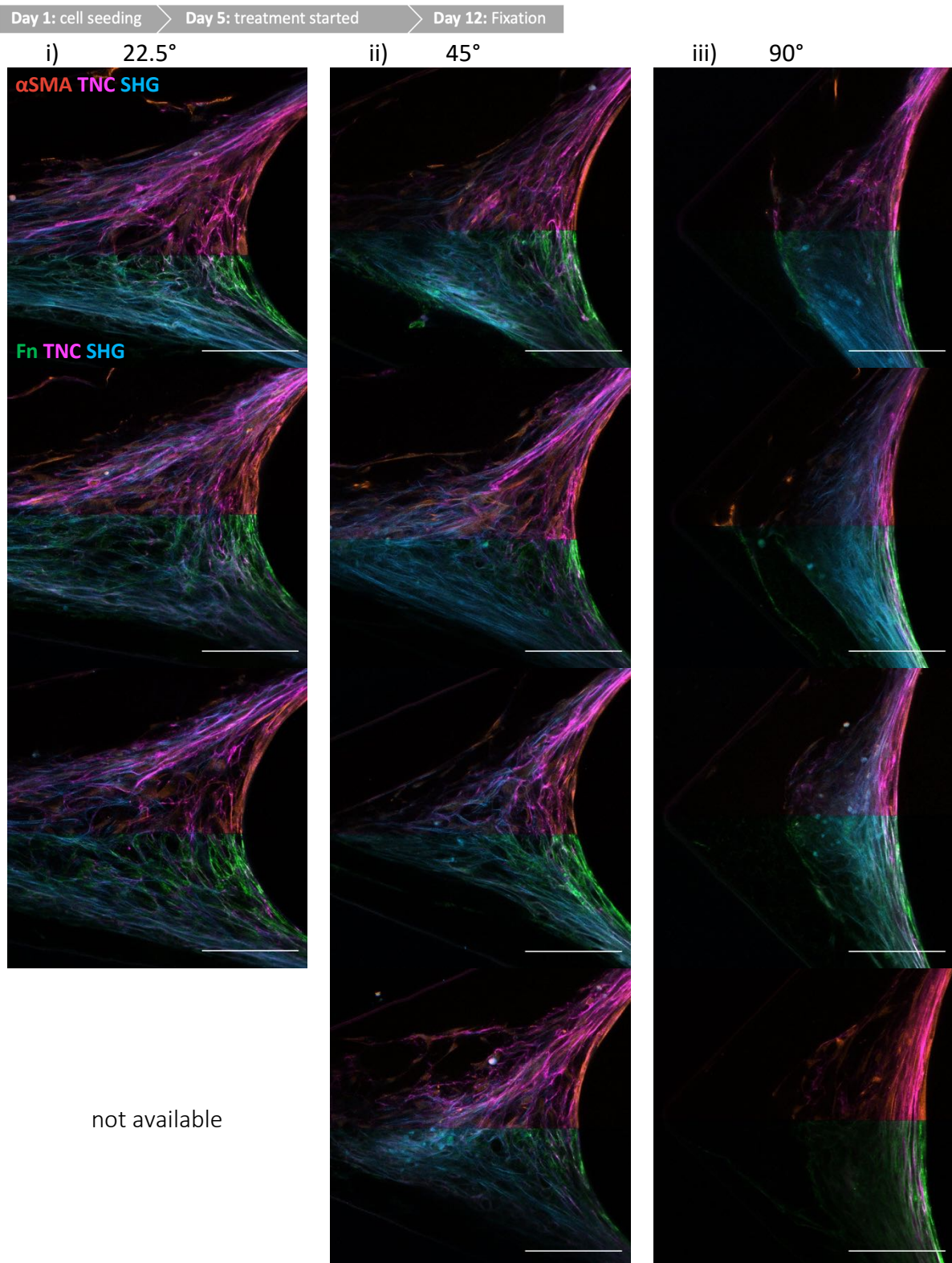


Fig. S06 (A) Central region of interest of supplementary μ Tissues of control condition 2P and CLSM data of representative μ Tissues in 22.5°(i)-, 45°(ii)- and 90°(iii)-clefts and depicted with two different sets of lookup table (LUT); top LUT: α SMA (orange), TNC (magenta), SHG (cyan); bottom LUT: Fn (green), TNC (magenta), SHG (cyan). Scale bar 100 μ m.

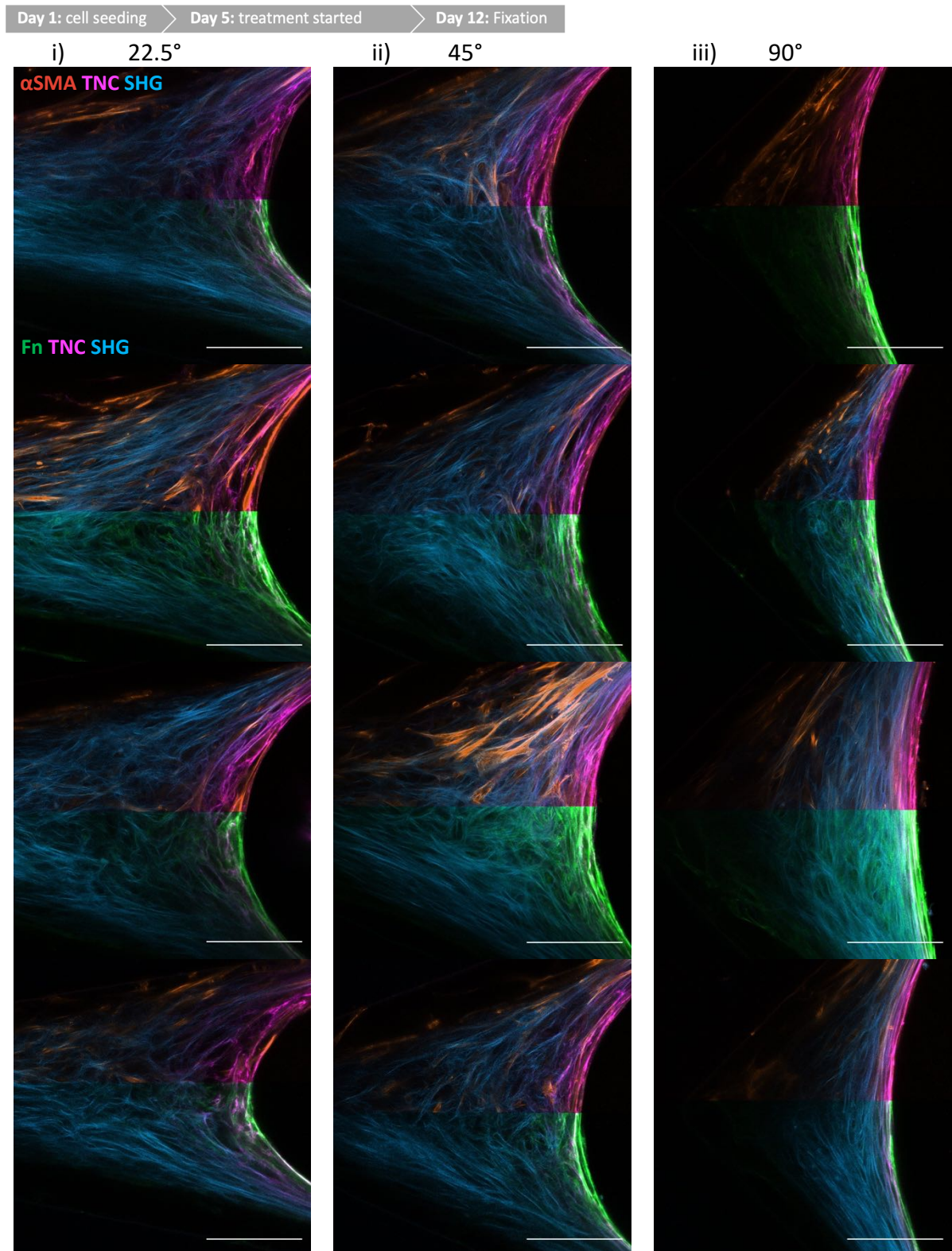
B +TGF- β 

Fig. S06 (B) Central region of interest of supplementary μ Tissues of TGF- β supplemented from day 5 2P and CLSM data of representative μ Tissues in 22.5°(i)-, 45°(ii)- and 90°(iii)-clefts and depicted with two different sets of lookup table (LUT); top LUT: α SMA (orange), TNC (magenta), SHG (cyan); bottom LUT: F_n (green), TNC (magenta), SHG (cyan). Scale bar 100 μ m.

C +GW788388

Day 1: cell seeding Day 5: treatment started Day 12: Fixation

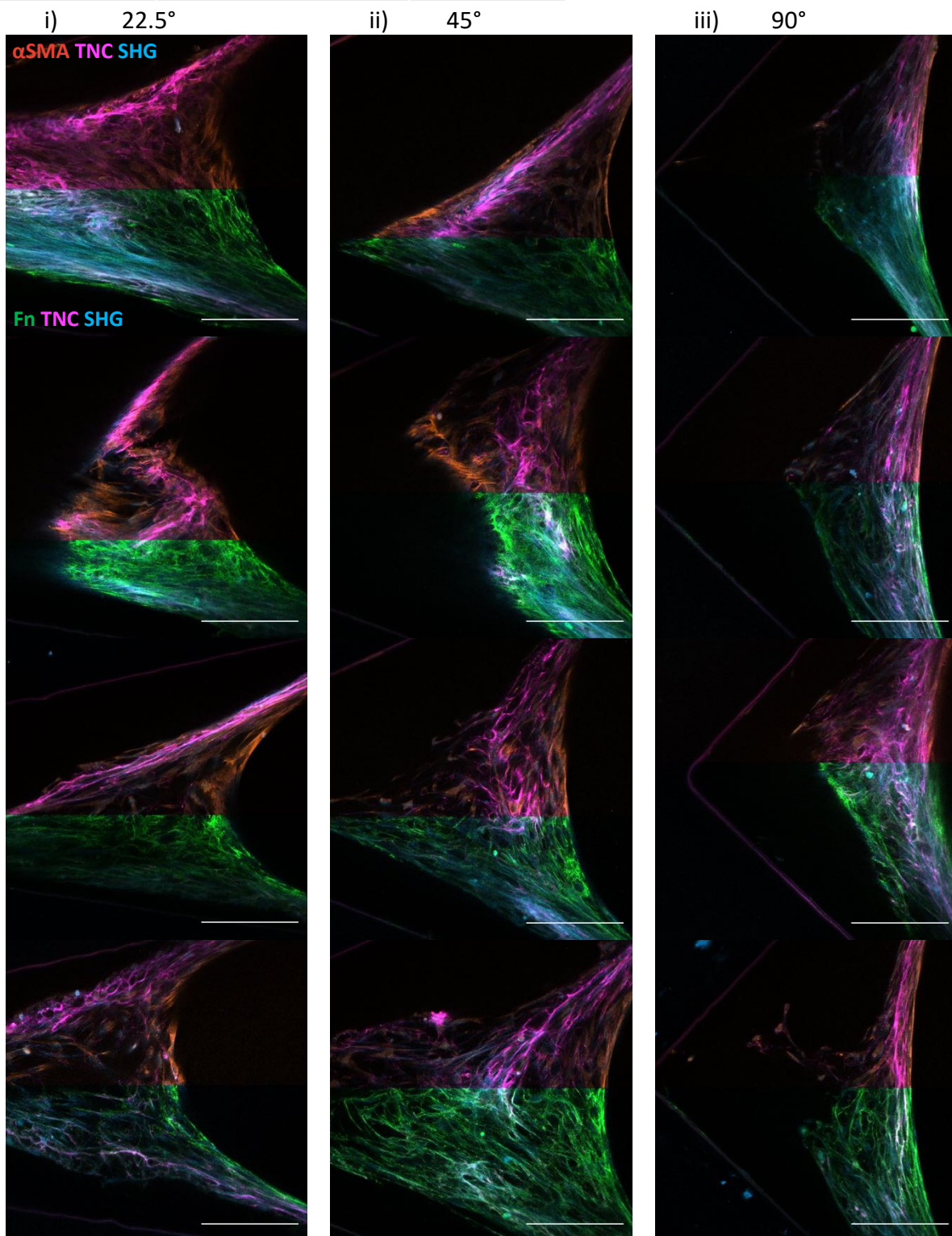


Fig. S06 (C) Central region of interest of supplementary μ Tissues of GW788388 supplemented from day 5 2P and CLSM data of representative μ Tissues in 22.5°(i)-, 45°(ii)- and 90°(iii)-clefts and depicted with two different sets of lookup table (LUT); top LUT: α SMA (orange), TNC (magenta), SHG (cyan); bottom LUT: Fn (green), TNC (magenta), SHG (cyan). Scale bar 100 μ m.

D +R1R2

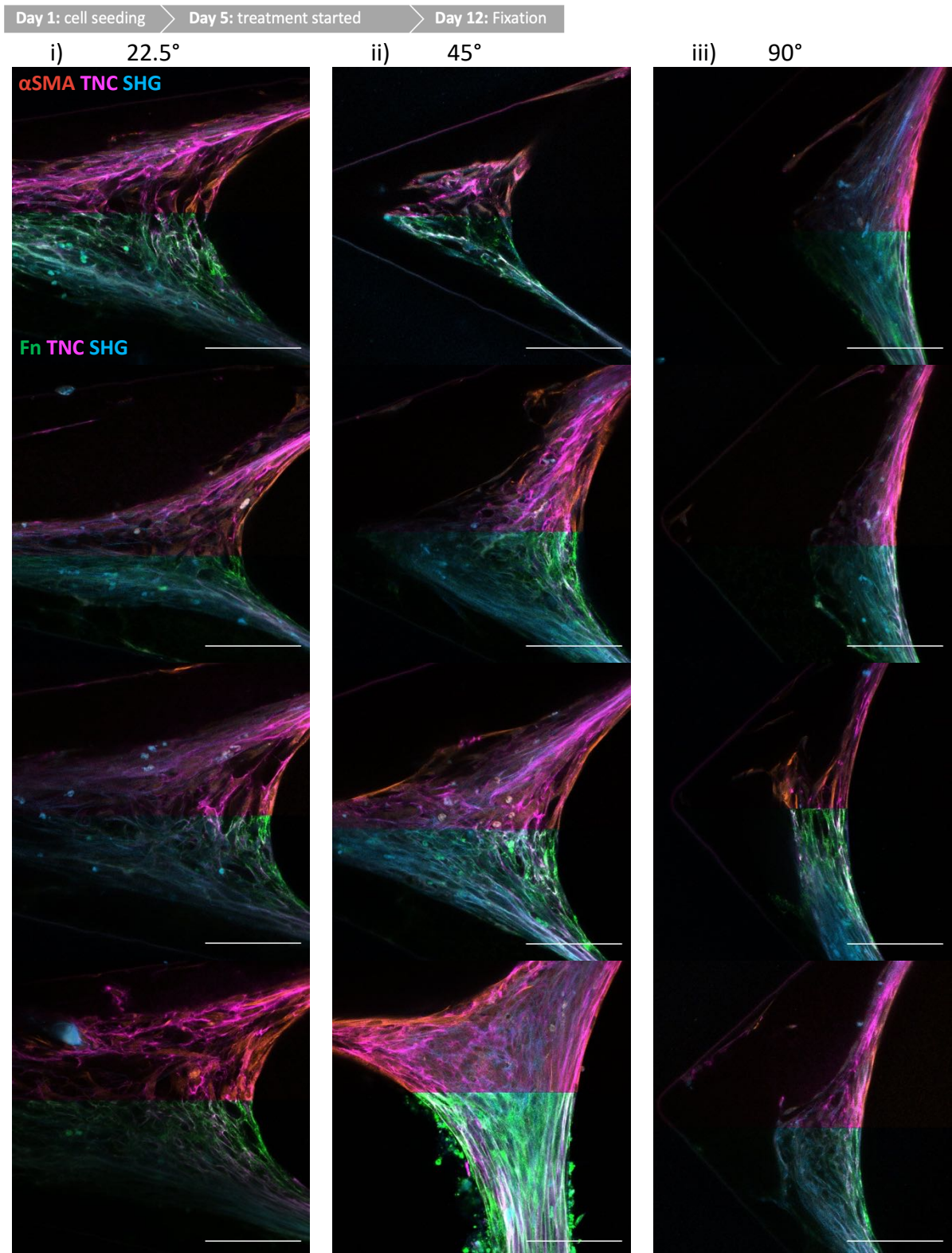


Fig. S06 (D) Central region of interest of supplementary μ Tissues of R1R2 supplemented from day 5 2P and CLSM data of representative μ Tissues in 22.5°(i)-, 45°(ii)- and 90°(iii)-clefts and depicted with two different sets of lookup table (LUT); top LUT: α SMA (orange), TNC (magenta), SHG (cyan); bottom LUT: Fn (green), TNC (magenta), SHG (cyan). Scale bar 100 μ m.

E +Blebbistatin

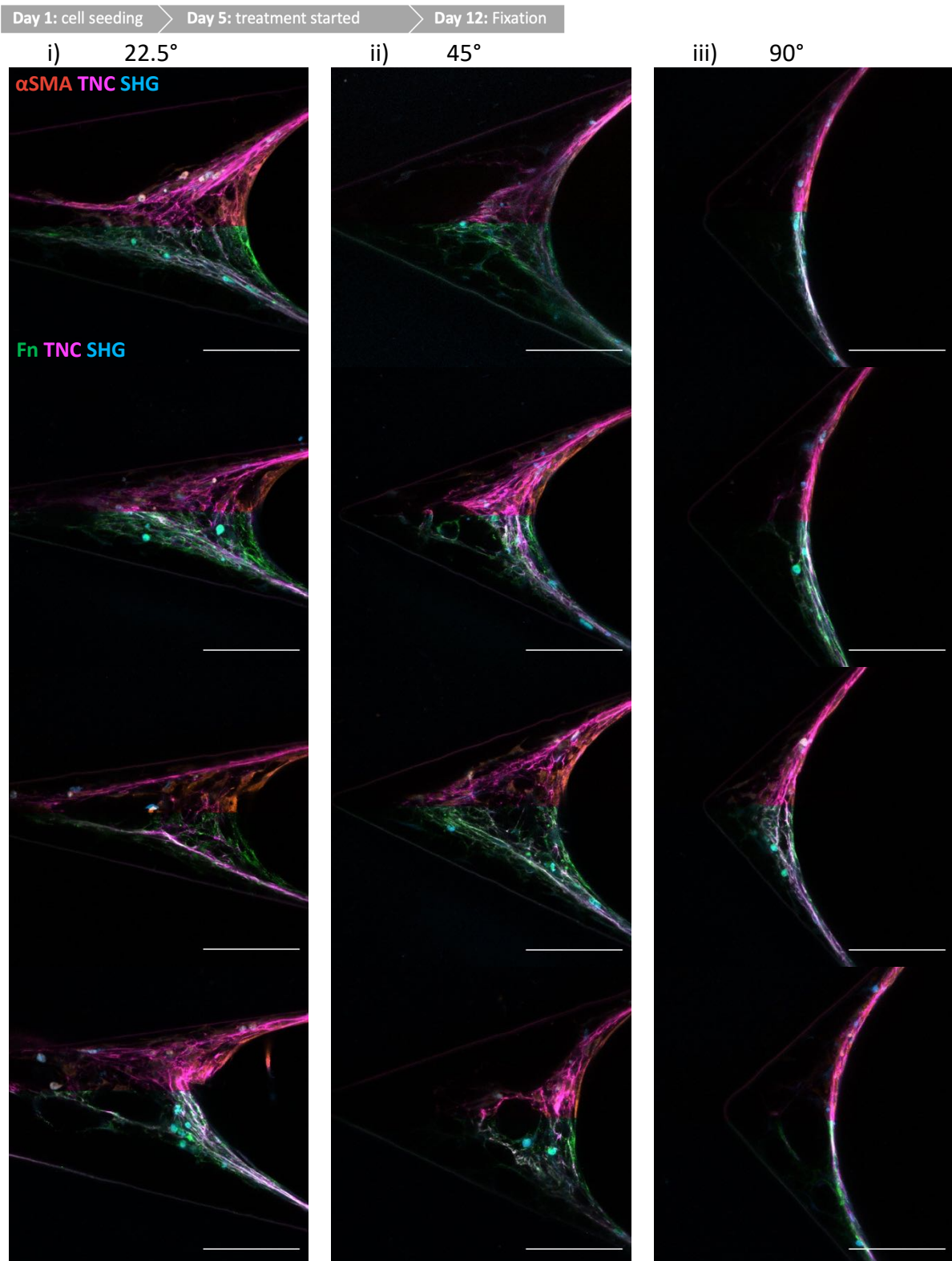


Fig. S06 (E) Central region of interest of supplementary μ Tissues of Blebbistatin supplemented from day 5 2P and CLSM data of representative μ Tissues in 22.5°(i)-, 45°(ii)- and 90°(iii)-clefts and depicted with two different sets of lookup table (LUT); top LUT: α SMA (orange), TNC (magenta), SHG (cyan); bottom LUT: Fn (green), TNC (magenta), SHG (cyan). Scale bar 100 μ m.

A Frames of rupture events before chemical supplementation

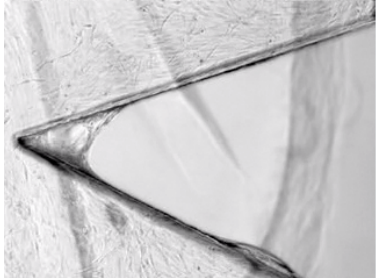
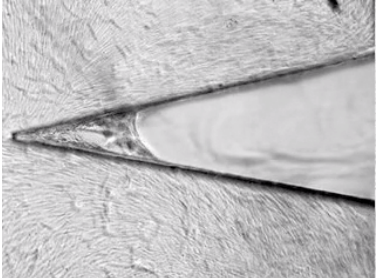
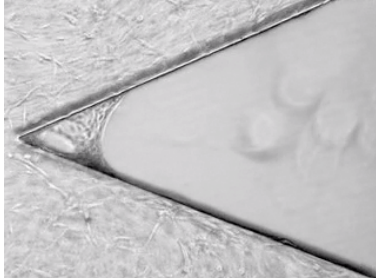
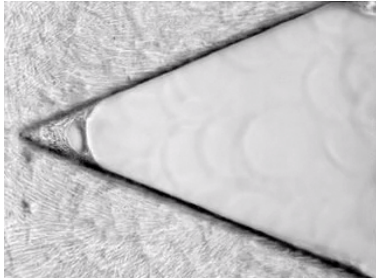
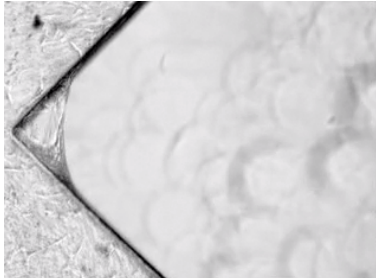
	i) 22.5°	ii) 45°	iii) 90°
Control	none	@111.5 h 	none
later with TGF-β @108 h		@108 h 	none
later with R1R2	none	@112 h 	@100 h 

Fig. S07 continues on next page with B Frames of rupture events after component supplementation.

B Frames of rupture events after component supplementation

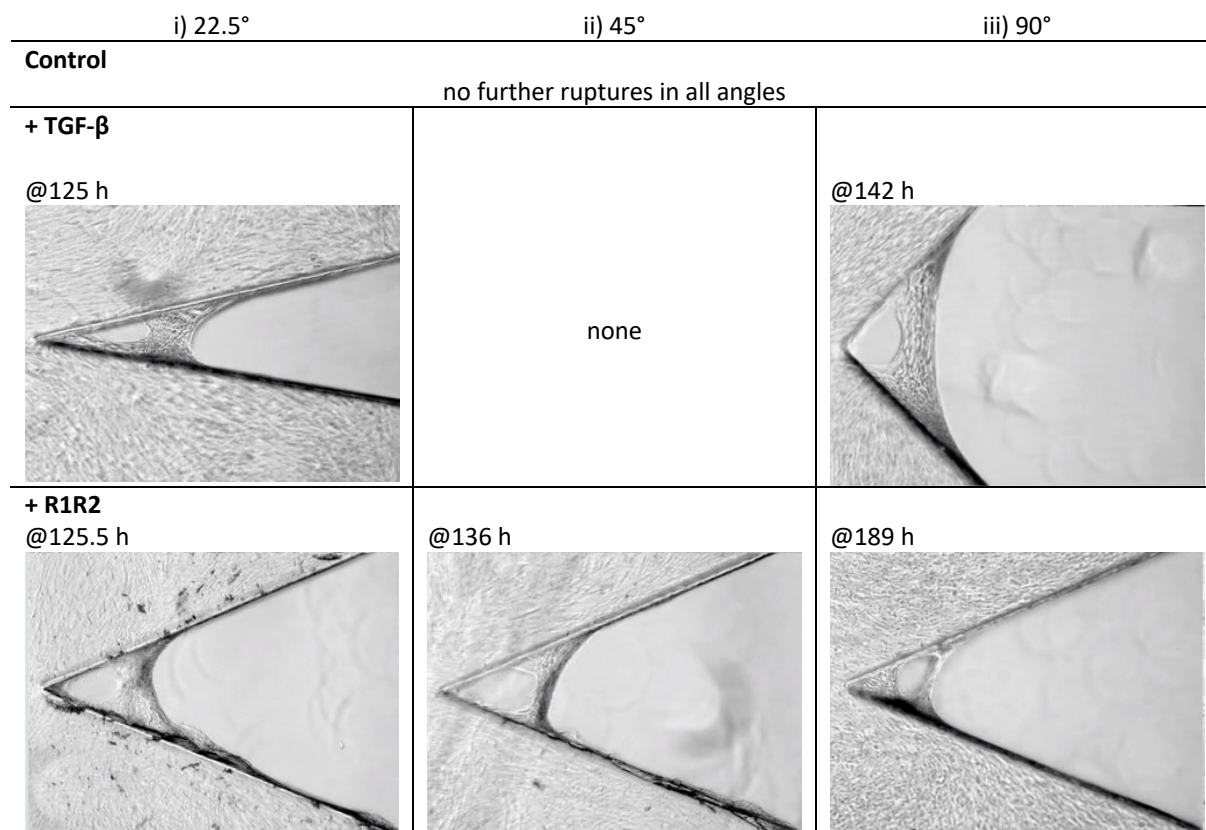


Fig. S07 Comparison of μ Tissue ruptures during tissue growth Supplementary time-lapse videos show phase-contrast images sampled every 0.5 h of tissue growth in all four 22.5°-, 45°- and 90°-clefs from each substrate of control (Video S01) and supplementation with GW788388 (Video S02), TGF- β 1 (Video S03), Blebbistatin (Video S04) and R1R2 (Video S05). Frames depicted here indicate events of tissue rupture that occurred around the incubation time indicated top left. Chemical component supplementation started at day 5 which relates to timestamp 114.5 h. Frames are grouped by tissue rupture events that occurred before (A) and after (B) supplementation of TGF- β 1, GW788388, Blebbistatin and R1R2.

A Control

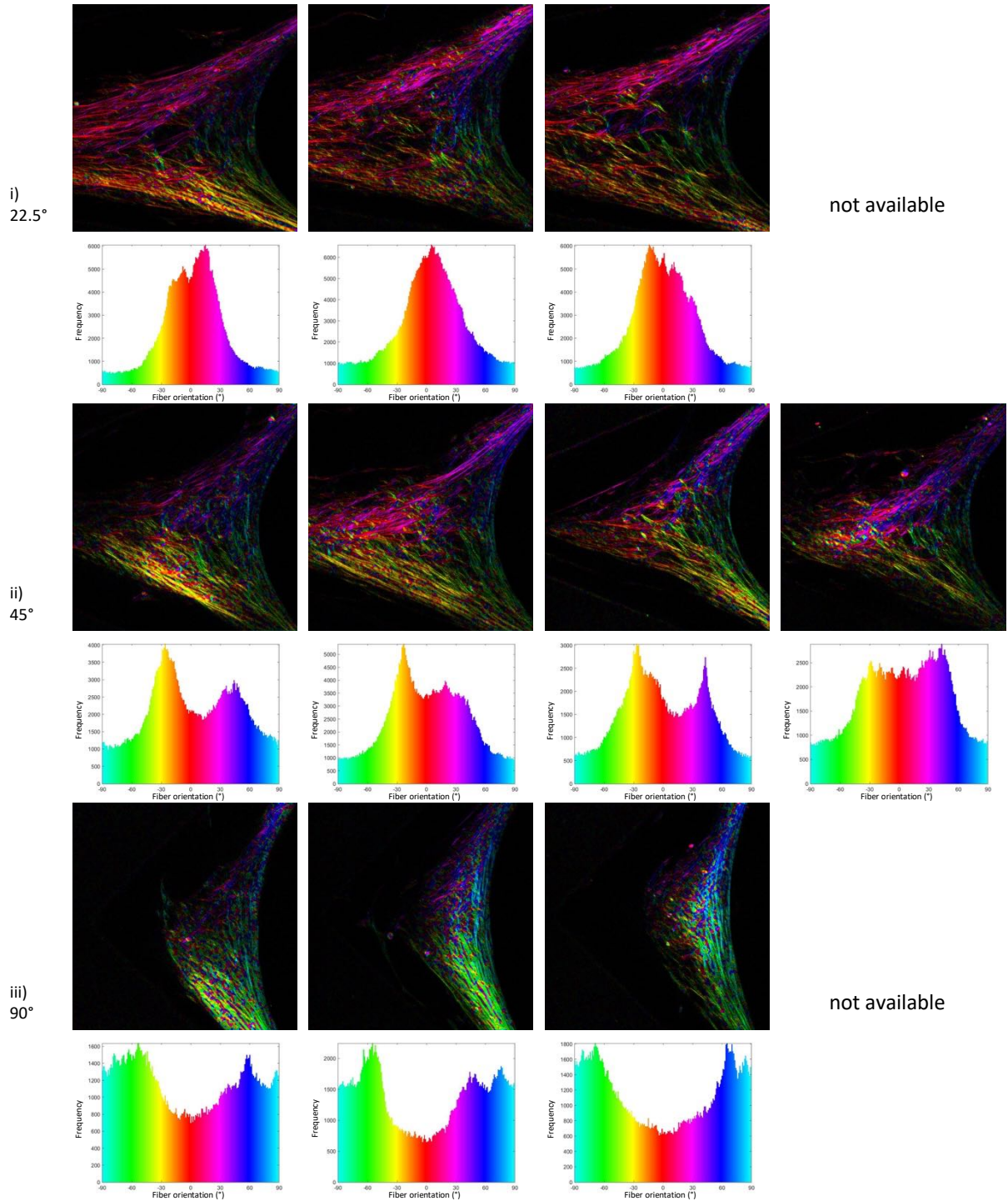


Fig. S08 (A) Analysis of the collagen fiber orientation for μ Tissues with different cleft angles of control condition. Fiber orientation analysis was carried out using a custom-written MATLAB script for SHG data with cleft angles of 22.5°(i), 45°(ii) and 90°(iii). The orientation of the SHG-signal is color-coded from blue ($\pm 90^\circ$) to red (0°) and the frequency distribution of the respective μ Tissue is depicted below the 2P micrographs. Further information about the image analysis is provided in the method section.

B + GW788388

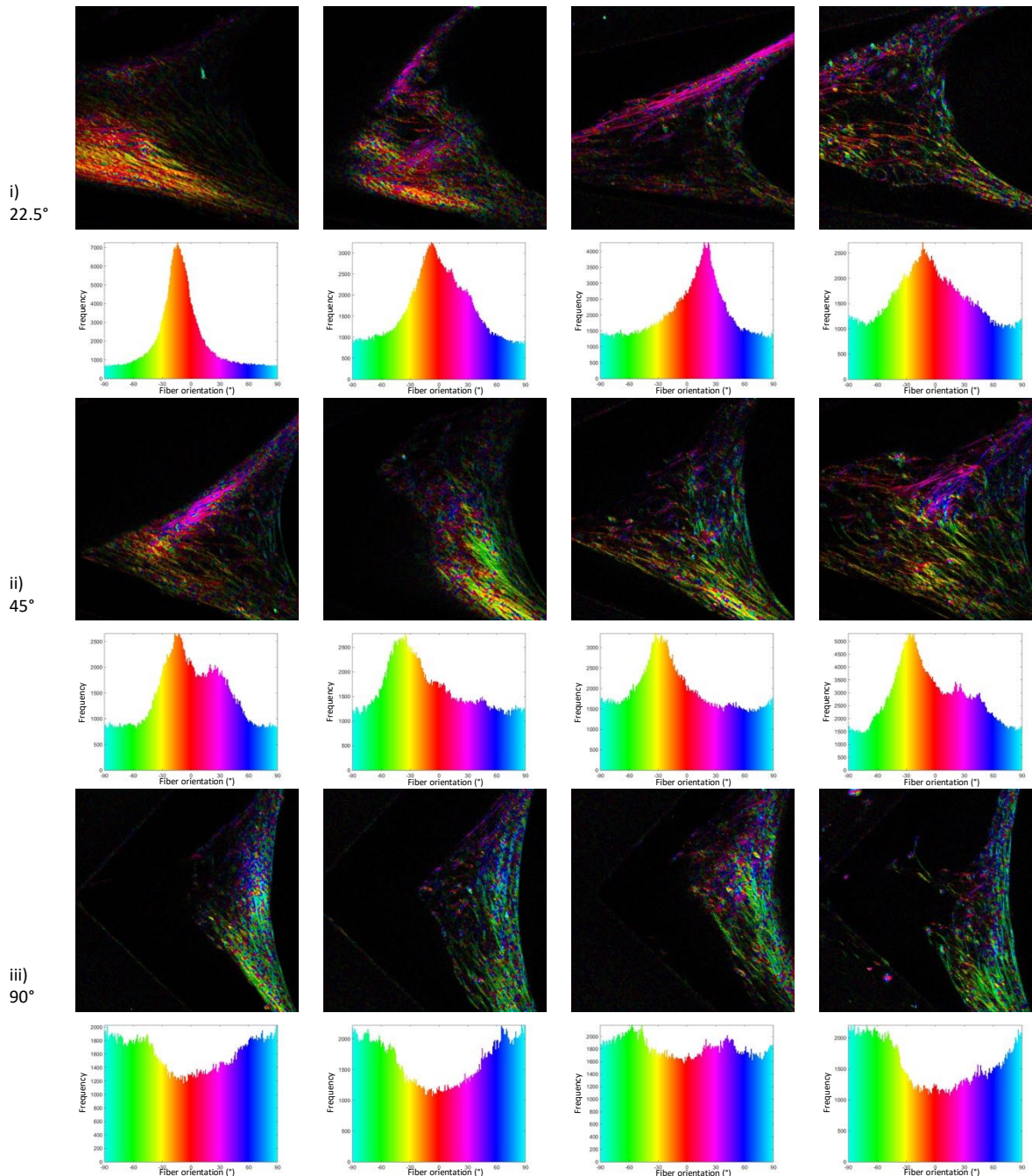


Fig. S08 (B) Analysis of the collagen fiber orientation for μ Tissues with supplementation of GW788388 from day 5. Fiber orientation analysis was carried out using a custom-written MATLAB script for SHG data with cleft angles of 22.5°(i), 45° (ii) and 90° (iii). The orientation of the SHG-signal is color-coded from blue ($\pm 90^\circ$) to red (0°) and the frequency distribution of the respective μ Tissue is depicted below the 2P micrographs. Further information about the image analysis is provided in the method section.

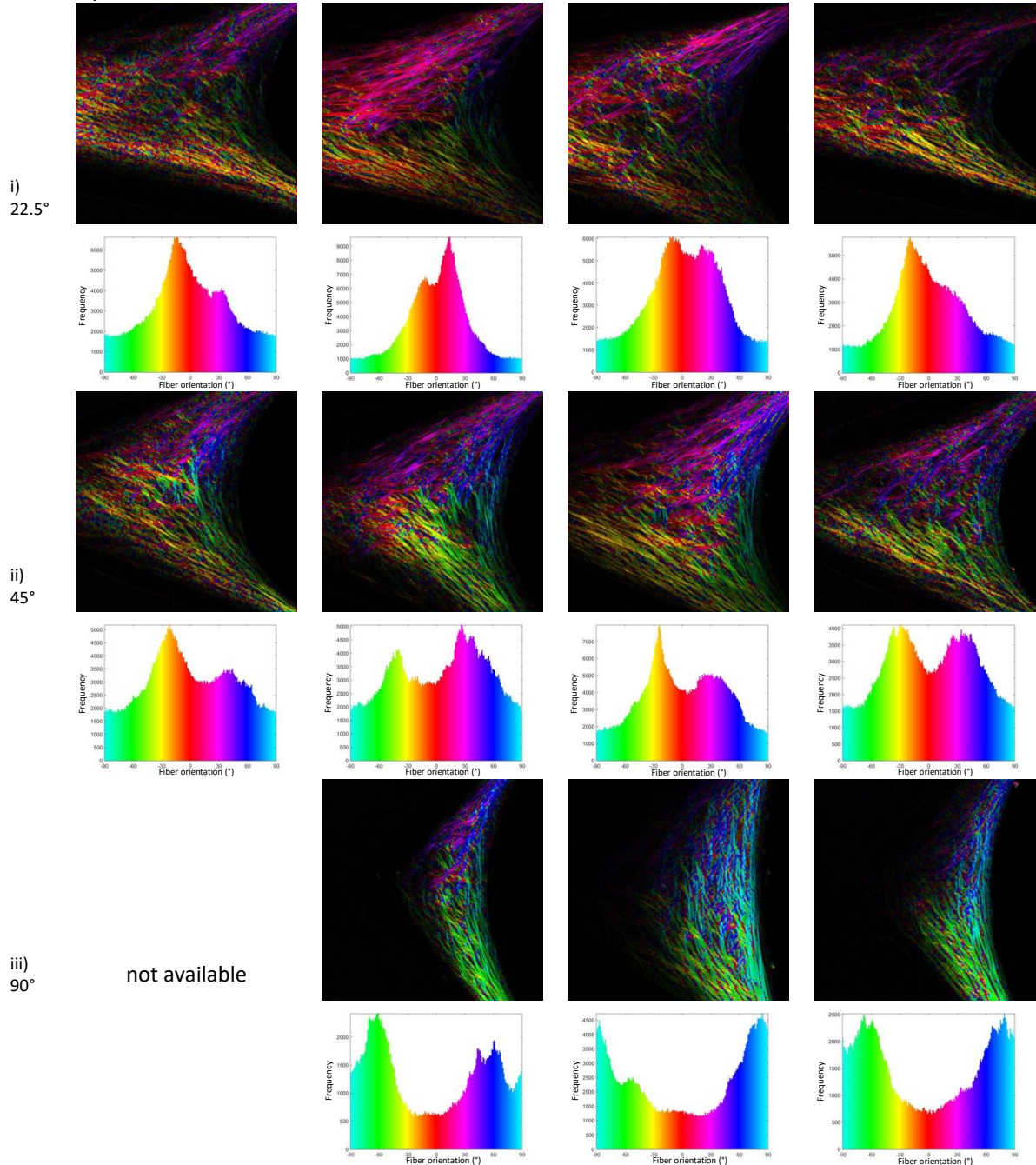
C + TGF- β 

Fig. S08 (C) Analysis of the collagen fiber orientation for μ Tissues with supplementation of TGF- β from day 5. Fiber orientation analysis was carried out using a custom-written MATLAB script for SHG data with cleft angles of 22.5°(i), 45° (ii) and 90° (iii). The orientation of the SHG-signal is color-coded from blue ($\pm 90^\circ$) to red (0°) and the frequency distribution of the respective μ Tissue is depicted below the 2P micrographs. Further information about the image analysis is provided in the method section.

D + Blebbistatin

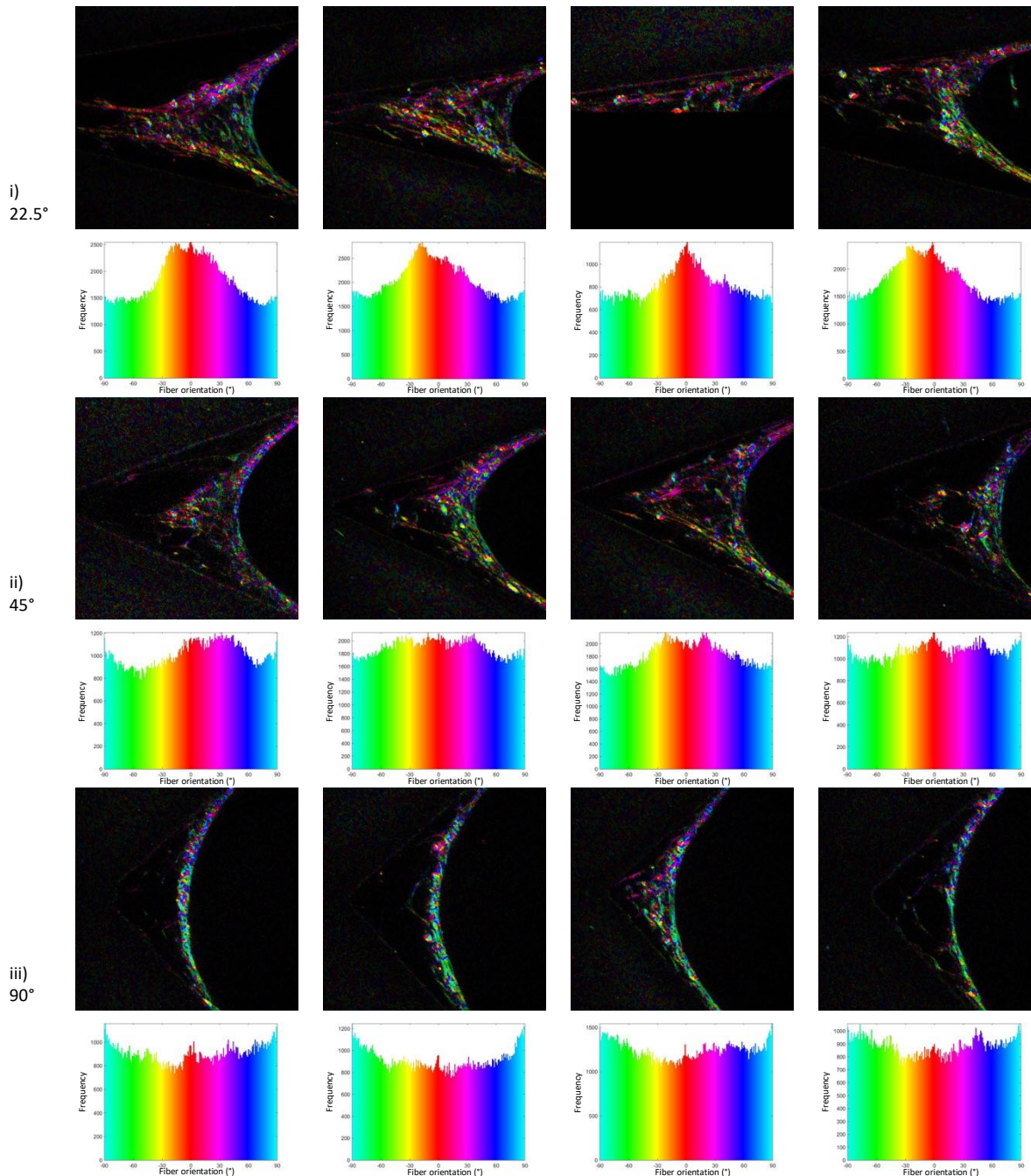


Fig. S08 (D) Analysis of the collagen fiber orientation for μ Tissues with supplementation of blebbistatin from day 5. Fiber orientation analysis was carried out using a custom-written MATLAB script for SHG data with cleft angles of 22.5°(i), 45°(ii) and 90° (iii). The orientation of the SHG-signal is color-coded from blue ($\pm 90^\circ$) to red (0°) and the frequency distribution of the respective μ Tissue is depicted below the 2P micrographs. Further information about the image analysis is provided in the method section.

E + R1R2

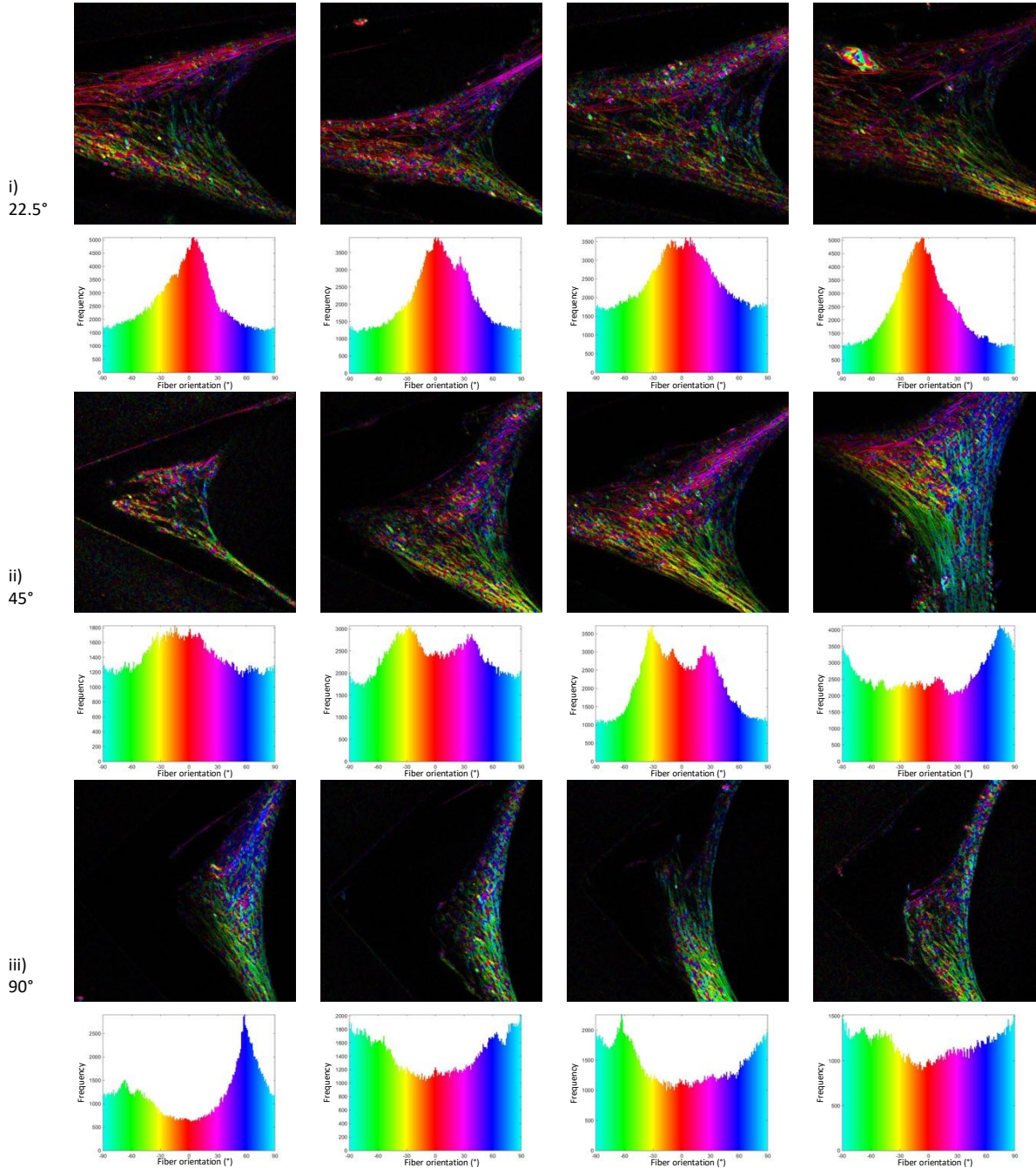
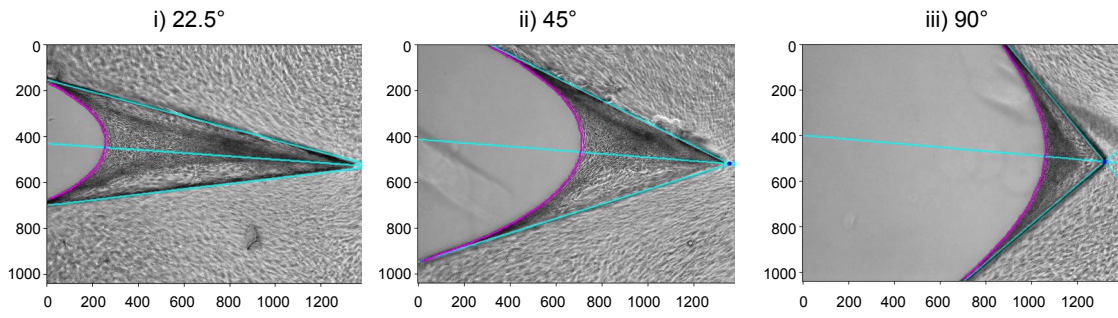
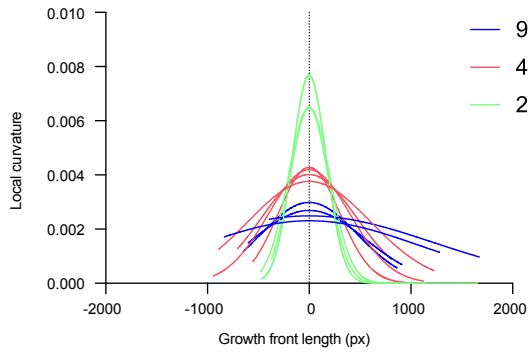


Fig. S08 (E) Analysis of the collagen fiber orientation for μ Tissues with with supplementation of R1R2 from day 5. Fiber orientation analysis was carried out using a custom-written MATLAB script for SHG data with cleft angles of 22.5°(i), 45°(ii) and 90°(iii). The orientation of the SHG-signal is color-coded from blue ($\pm 90^\circ$) to red (0°) and the frequency distribution of the respective μ Tissue is depicted below the 2P micrographs. Further information about the image analysis is provided in the method section.

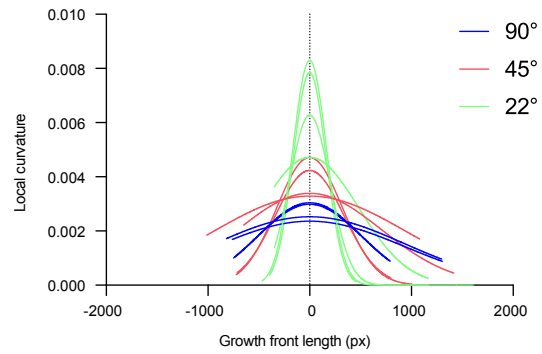
A Determination of local curvature



B Local curvature of control

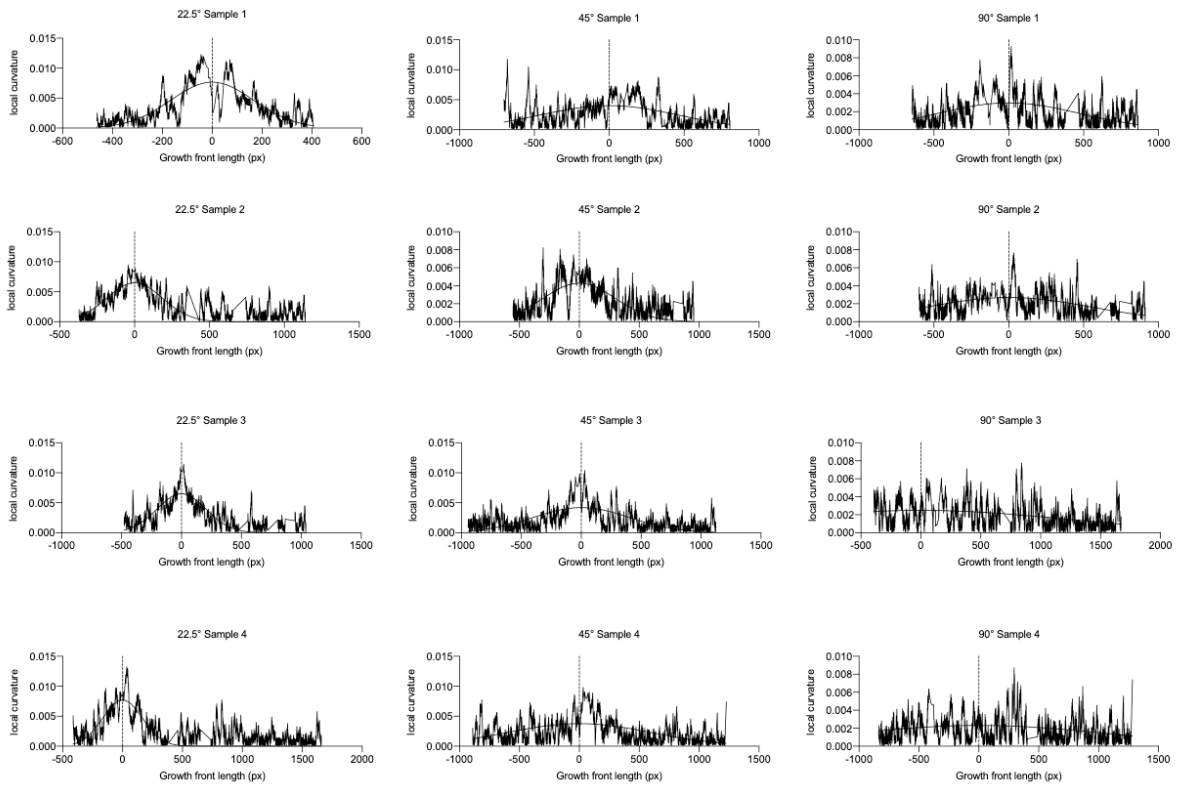


C Local curvature + TGF- β 1



D

Control



E

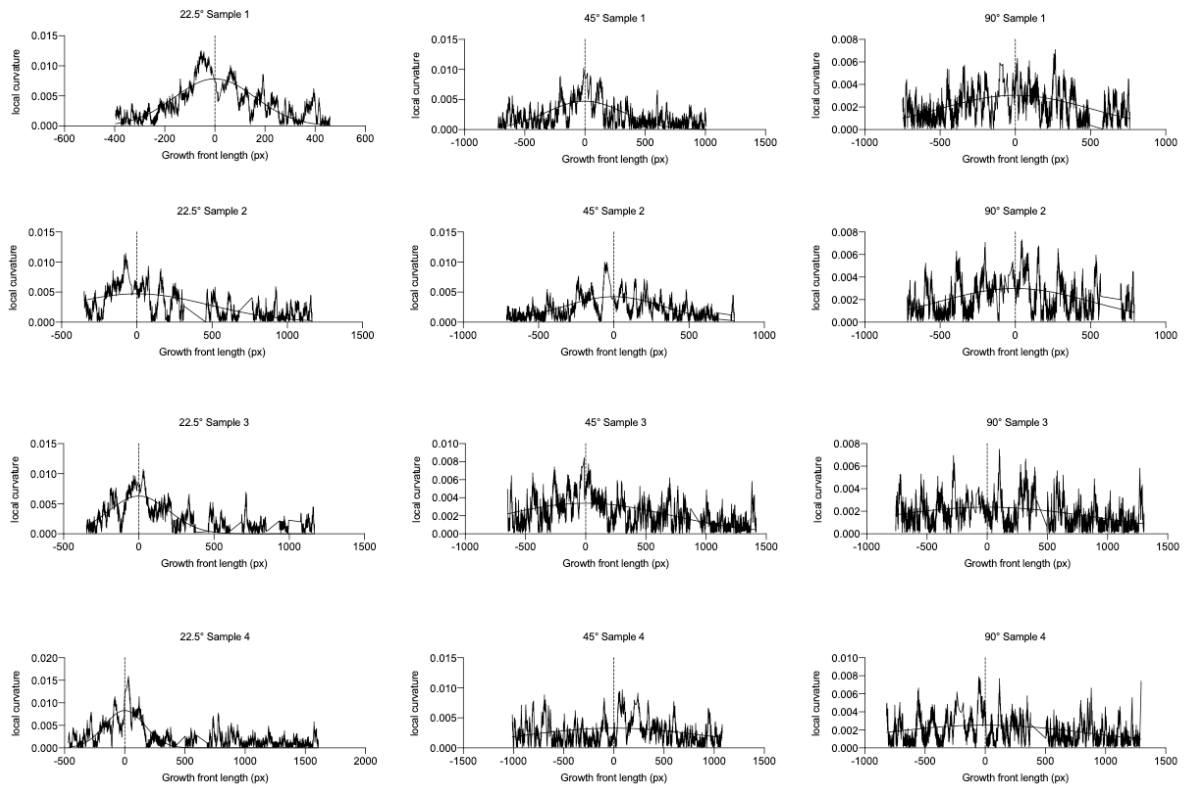
+TGF- β 

Fig. S09 Local Curvature The local tissue curvature was determined by fitting a sampling radius along the tissue growth front using a previously introduced algorithm (Bidan et al. 2012) and here determined by an automated python script written by Marcel Graetz. **(A - C)** Gaussian fits of each cleft angle ($n=4$) are depicted over the distance of the growth front length. **(D and E)** Local curvature distribution data plotted over growth front length of the individual samples.

Abbreviations

2P	Two-photon laser scanning microscopy
α SMA	Alpha smooth muscle actin
α MEM	Alpha minimum essential medium
BSA	Bovine serum albumin
CLSM	Confocal laser scanning microscopy
Col	Collagen
DMSO	Dimethyl sulfoxide
ECM	Extracellular matrix
F-M-T	Fibroblast-to-myofibroblast transition
FBS	Fetal bovine serum
Fn	Fibronectin
Hepes	4-(2-hydroxyethyl)-1-piperazineethanesulfonic acid
LOX	Lysyl oxidase
LUT	Lookup table
M-F-T	Myofibroblast-to-fibroblast transition
μ Tissue	Microtissue
MMP	Matrix metalloproteinase
NHDF	Normal human dermal fibroblast
PBS	Phosphate buffered saline
PDMS	Polydimethylsiloxane
PFA	Paraformaldehyde
PLL- <i>g</i> -PEG	Poly(l-lysine)- <i>graft</i> -poly(ethylene glycol)
PMMA	Polymethyl methacrylate
ROI	Region of interest
RT	Room temperature
SHG	Second harmonic generation
TG2	Tissue transglutaminase
TGF- β	Transforming growth factor-beta
TNC	Tenascin-C

Acknowledgements

To quote Isaac Newton "If I have seen further it is by standing on the shoulders of giants.", I would like to thank all the many giants who let me stand on their shoulders and allowed me to see further.

First of all, I would like to thank my supervisor **Prof. Dr. Dr. h.c. Viola Vogel** for giving me the opportunity to develop myself scientifically and personally in her lab. It is absolutely fascinating how you address and bring together such a diverse research field, and I am deeply grateful to have learned an incredible amount during this time and for all your great support. Thank you for providing me with an extraordinary environment in which I had freedom to grow, allowing me to explore things and, most importantly, learn from my own mistakes. Thank you for stimulating scientific creativity and critical thinking!

Next, I would like to thank **Prof. Dr. Philip Kollmannsberger** who, during the first days of my PhD, introduced me to the exciting world of *de novo* grown μ Tissues, which sparked my curiosity to dive deeper into this fascinating approach. Thank you very much for your extremely helpful support, the many inspiring and insightful discussions, and for taking the time to be my co-examiner.

I also thank **PD Dr. Gertraud Orend** for being my co-examiner and for her highly valuable scientific ideas, advice and feedback during the course of my PhD, which helped me a lot to move the project forward. Further, I appreciate **Prof. Dr. David P. Wolfer** chairing my defense exam. I have also greatly enjoyed the collaboration with Geistlich Pharma AG and I thank especially **PD Dr. Birgit Schäfer** for the fruitful discussions and her helpful feedback on Chapter 6.

During my PhD journey I received fantastic scientific and non-scientific support from many friends inside and outside the lab and I would like to express a few extra portions of gratitude. For teaching me plenty highly relevant and extremely supportive theoretical and practical concepts to propel my projects and me further, often before or while having great times e.g. at the Specialty Restaurant Höngg or at one of the well synchronized last-minute dinner events, for countless advice that helped tremendously on my journey, and for their terrific friendships which make all times much more enjoyable, I deeply thank both **Dr. Jens Möller** and **Prof. Dr. Tadahiro Yamashita**. For knowing how to unravel all sorts of different PhD phases, especially the complicated ones, and how to always turn them and many others into moments of pure joy, for being a superb LICKERT Travel CEO and a truly fantastic friend, I deeply thank **Dr. Sebastian Lickert** – I'm very much looking forward to chasing some gnotschis during our next "Elferli". Together with you and Lukas we created countless memories that will stay forever, of which Cortona alone was quite a blast! Especially for those, but also for sharing the joy of rowing, all the brilliant extra science input and being a wonderful friend, I thank **Dr. Lukas P. Braun**.

Special thanks also go to **Prof. Dr. Simon A. Pot** for his great friendship, many fruitful clinical and scientific powwows, very helpful advice, and highly fun and productive joined writing sessions that contributed to this work. For holding all the ropes together, having a solution for everything and spreading so much joy, I deeply thank **Norma De Giuseppe** – Du bist einfach di Beschi! For a wonderful collaboration, for sharing her cheerful and creative scientific mind and for always having a song in mind to turn all sorts of PhD phases into bright moments that feel good or even better, I deeply thank **Charlotte M. Fonta**. For teaching me many relevant physical concepts, providing extremely helpful ideas and advice, having inspiring discussions and - together with **Dr. Sebastian Lickert** - keeping me motivated to get fit for our yearly SOLA run, I thank **Dr. Ingmar Schön**. For teaching me how to “FRET”, how to elevate my image acquisition quality to much higher levels, and for providing highly valuable advice, I thank **Dr. Daniela Ortiz Franyuti**, whose wonderfully creative and open scientific mind has provided sheer joy during collaborative work. For all the very helpful input, technical support and providing a safe place to work, I greatly thank **Dr. Isabel Gerber** and **Chantel Spencer**. For caring about my project and me and giving me very valuable input, ideas and advice, I thank both **Dr. Nikhil Jain** and **Dr. Lina Aires**. For many inspiring scientific and philosophic discussions, I thank **Dr. Cameron Moshfegh**. For sharing plenty of inspiring and constructive ideas, critical thinking and lots of positive energy, I thank **Dr. Mamta Chabria**! For many valuable insights in the cleanroom facility and with microfabrication, I thank **Prof. Dr. Jau-Ye Shiu**. For being a fabulous DIY geek and saving me plenty of working hours with her marvelous 3D printing experience and creative ideas that are mind-blowing, I thank **Elise A. Aeby**. For extremely efficient and most enjoyable collaborative labwork around TG2 and protein labeling, I thank **Kateryna Selçuk**. For great discussions and quite entertaining exchange, I thank **Prof. Dr. Enrico Klotzsch**. For bringing in exciting ideas for future follow-up paths, I thank **Konstantin Wolf**. Since I can't name all, my sincere gratitude goes to all current and former members of the “**Vogelschar**” for inspiring discussions, an extremely friendly and helpful atmosphere, tremendous fun and creating countless memories that will stay! Special thanks also go to inspiring and fun scientific discussions and great collaborative work with **Dr. Andrea Malandrino**, **Dr. Rolando Vegliante**, **PD Dr. Enni E. Markkanen**, **Dr. Nobuyuki Tanaka**, **Dr. Kae Sato**, **Dr. Masumi Taki** and **Dr. Kathryn Rosowski**. Many thanks to the entire **ScopeM team**, especially to **Dr. Justine Kusch**, to the complete **FIRST team**, to **Martin Elsener** from the D-MATL machine shop and to **Tommy Kovacevic** from our IT group for all their fantastic support. Big thanks to my hard-working students, **Marcel Graetz**, **Kathrin S. Laxhuber** and **Giulia Ammirati** for investing time and energy into their projects; it was and is a pleasure to work with you all! Special thanks for sharing great times with my office mates **Dr. Nikhil Jain**, **Prof. Dr. Jau-Ye Shiu**, **Prof. Dr. Simon A. Pot**, **Dr. Jens Möller** and **Dr. Mamta Chabria**. Thanks to **Prof. Dr. Simon A. Pot**,

Dr. Jens Möller, Prof. Dr. Tadahiro Yamashita, Charlotte M. Fonta, Dr. Sebastian Lickert, Dr. Mamta Chabria, Dr. Nikhil Jain and Dr. Lukas P. Braun for proofreading parts of my thesis.

I would also like to thank Prof. Dr. Brigitte von Rechenberg, who supervised my doctorate in veterinary medicine, for encouraging me to see beyond the classic veterinary path and for having been a wonderful mentor throughout the years. Further, I am extremely thankful for Dr. Flurina C. Clement Frey who taught me the very first steps in the cell culture lab, which sparked in me so much curiosity, and soon turned into a true friend. As we never walk alone, I'm also very grateful for all the additional supporters and friends of which I would like to name especially Dr. Ramon Bucher, Dr. Markus Zimmermann, Dr. Anika Drechsler, Dr. Svende Pfundstein, Dr. Agnieszka A. Carol, Richard S. Lane, David W. Melo Lane, Martina Bär, Stefan Tobler, Dr. Carolin Rommel and Dr. Deniz Danaci.

Finally, I would like to express my deepest gratitude to each and every close and distant member of my entire family who thought of me and supported me during this time. But especially to my parents, Astrid and Manfred Benn, for always believing unconditionally in me. No matter in which situation, your continuous support allowed me to stay curious and deeply influenced my perspective on science and life, for what I am infinitely thankful. Mama and Papa, without you I would not be here today. My brother Luca J. Benn joined us when I was 14 years old and literally brought so much fresh wind in our all lives. Luca, thank you for your wonderfully fresh and critical mind, for fantastic discussions and most enjoyable good times, and for always being there! Oma Gudrun and Opa Dieter Ullrich, thank you for all your very helpful support and for sharing so many valuable experiences which greatly help me on my exciting journey. I further thank my godson Leonard Benn for his curiosity and my godparents, Tante Waltraud and Onkel Horst Benn, for all their great support.

Last but not least, the biggest thanks go to my partner: Raquel Melo Frota, you make the sun shine and you spread endless joy! I am sorry that a large piece of our highly valuable shared time cake has shrunk due to the countless irregular working hours I have imposed on myself for research. Thank you for all your wonderful love and support throughout the years.

Curriculum Vitae

Name	Dr. med. vet. Mario Christian Benn
Address	Laboratory of Applied Mechanobiology ITM, D-HEST, ETH Zurich Vladimir-Prelog-Weg 4 CH-8093 Zurich
E-mail	mbenn@ethz.ch
Place of birth	Hanau, Germany
Date of birth	4 th August 1985
Nationality	German

Professional experience

- 08/2015 - present **Research Assistant** at Laboratory of Applied Mechanobiology, Institute of Translational Medicine, Department of Health Sciences and Technology, ETH Zurich, Switzerland
- 12/2012 - 05/2015 **Veterinarian and Research Assistant** at Musculoskeletal Research Unit (MSRU) and Center for Applied Biotechnology and Molecular Medicine (CABMM), Vetsuisse Faculty, University of Zurich, Switzerland
- 09/2006 - 12/2008 **Paramedic** in emergency care and patient transportation, German Red Cross, Hanau, Germany
- 10/2005 - 09/2006 Voluntary year of social service as **paramedic assistant**, German Red Cross, Hanau, Germany

Education

- 08/2015 - present **Doctor of Sciences (Dr. sc. ETH)** at Laboratory of Applied Mechanobiology, Institute of Translational Medicine, Department of Health Sciences and Technology, supervised by Prof. Dr. Dr. h.c. Viola Vogel, ETH Zurich, Switzerland
- 12/2012 - 09/2015 **Doctor of Veterinary Medicine (Dr. med. vet.)** at Musculoskeletal Research Unit (MSRU) and Center for Applied Biotechnology and Molecular Medicine (CABMM), Vetsuisse Faculty, supervised by Prof. Dr. med. vet. Brigitte von Rechenberg, University of Zurich, Switzerland
- 04/2012 - 07/2012 Training in Surgical Oncology, Alta Vista Animal Hospital, Ottawa, Canada
- 10/2010 - 12/2010 Visiting clinical clerkship and studies, College of Veterinary Medicine, University of Tennessee, Knoxville, USA
- 10/2006 - 03/2012 **Degree in Veterinary Medicine (Staatsexamen)**, Justus-Liebig University Giessen, Germany

- 05/2006 - 09/2006 **Paramedic training**, Landesschule Hessen, German Red Cross, Mühlthal-Trautheim, Germany
- 08/1996 - 07/2005 **High school leading to university entrance qualification (Abitur)**, Franziskanergymnasium Kreuzburg, Grosskrotzenburg, Germany

Publications

1. Benn MC, Pot SA, Moeller J, Yamashita T, Fonta CM, Lickert S, Orend G, Kollmannsberger P, Vogel V. **Tenascin-C and tissue transglutaminase transiently orchestrate tissue growth enabling the transition towards tension-dependent tissue maturation.** *in preparation*
2. Benn MC, Kollmannsberger P, Yamashita T, Graetz M, Vogel V. **Eliciting insight how tissue tension impacts tissue growth processes.** *in preparation*
3. Benn MC, Weber W, Klotzsch E, Vogel V, Pot SA. **Tissue transglutaminase in fibrosis — more than an extracellular matrix cross-linker.** *Current Opinion in Biomedical Engineering.* Elsevier; 2019. <https://doi.org/10.1016/j.cobme.2019.06.003>
4. Meyer DC, Hasler A, Wyss S, Nuss K, Benn MC, Gerber C, Wieser K. **Mechanisms of Suture Integration in Living Tissue: Biomechanical and Histological *In vivo* Analysis in Sheep.** *Orthopedics.* Slack; 2019. <https://doi.org/10.3928/01477447-20190424-09>
5. Flück M, Valdivieso P, Ruoss S, Rechenberg von B, Benn MC, Meyer DC, Wieser K, Gerber C. **Neurectomy preserves fast fibers when combined with tenotomy of infraspinatus muscle via upregulation of myogenesis.** *Muscle & Nerve.* John Wiley & Sons; 2019. <https://doi.org/10.1002/mus.26316>
6. Ruoss S, Möhl CB, Benn MC, Rechenberg von B, Wieser K, Meyer DC, Gerber C, Flück M. **Costamere protein expression and tissue composition of rotator cuff muscle after tendon release in sheep.** *J Orthop Res.* John Wiley & Sons; 2017. <https://doi.org/10.1002/jor.23624>
7. Gerber C, Meyer DC, Flück M, Valdivieso P, Rechenberg von B, Benn MC, Wieser K. **Muscle Degeneration Associated with Rotator Cuff Tendon Release and/or Denervation in Sheep.** *Am J Sports Med.* SAGE Publications; 2017. <https://doi.org/10.1177/0363546516677254>
8. Flück M, Ruoss S, Möhl CB, Valdivieso P, Benn MC, Rechenberg von B, Laczko E, Hu J, Wieser K, Meyer DC, Gerber C. **Genomic and lipidomic actions of nandrolone on detached rotator cuff muscle in sheep.** *J. Steroid Biochem.* Elsevier; 2017. <https://doi.org/10.1016/j.jsbmb.2016.08.005>
9. Gerber C, Meyer DC, Flück M, Benn MC, Rechenberg von B, Wieser K. **Anabolic Steroids Reduce Muscle Degeneration Associated With Rotator Cuff Tendon Release in Sheep.** *Am J Sports Med.* SAGE Publications; 2015. <https://doi.org/10.1177/0363546515596411>
10. Benn MC. **Vergleichende Darstellung des Nandroloneffekts auf die strukturelle Muskelveränderung des M. infraspinatus im Schafmodell für Rotatorenmanschettenruptur zum Zeitpunkt der Ruptur und chirurgischen Reparatur.** University of Zurich, Vetsuisse Faculty; 2015. <https://doi.org/10.5167/uzh-122746>

Oral presentation at international scientific conference

8th World Congress of Biomechanics in Dublin in July 2018, title of presentation “De novo grown 3D microtissues to investigate factors that drive the fibroblast-to-myofibroblast transition and can reverse it (O1751)” in session “Biomechanical microengineering of tissue mimics for human disease modelling”

The image features a dark blue, textured background with a marbled or fibrous appearance. The texture consists of intricate, swirling patterns of lighter blue and white fibers against a darker blue base. In the center of the image, the text "ETH zürich" is displayed in a white, sans-serif font. The "ETH" portion is bold and italicized, while "zürich" is in a regular weight and includes a lowercase 'ü'.

ETH zürich